UNIVERSITY OF ZIMBABWE

Effects of shading on leaf temperature, photosynthesis and water relations of two navel orange [*Citrus sinensis* (L.) Osbeck] cultivars

by

Anywhere Tsokankunku

A thesis submitted in partial fulfilment of the requirements of the degree of Master of Science in Agricultural Meteorology

Supervisors: Mr S. Dzikiti (UZ**)**

Prof. Dr. Franz X. Meixner
(Max Planck Institute for Chemistry, Mainz, Germany; UZ)

Department Chairman/Program coordinator: **Mr. B. Chipindu**

Department of Physics,
Faculty of Science,
University of Zimbabwe,
P.O. Box MP167,
Mount Pleasant,
Harare,
Zimbabwe

June 2007

Many, O LORD my God, are thy wonderful works which thou hast done, and thy thoughts which are to usward
they cannot be reckoned up in order unto thee
if I would declare and speak of them, they are more than can be numbered.
(Psalms 40:5 KJV+)

ABSTRACT

Between January and February 2007, diel variability in carbon dioxide (CO_2) and water vapour (H_2O) exchange with leaf temperature on four potted 5-year-old navel orange trees [*Citrus sinensis* (L.) Osbeck] on an open-air laboratory on the roof of the Physics Department (University of Zimbabwe) was measured. Two of the four trees were of the *Baianinha* variety while the other two were *Navelina*. An automated dynamic chamber (cuvette) was installed sequentially on each of the four trees with flux measurements on a selected branch of each tree typically taking ten days. Out of the ten days on each tree, three days consisted of measurements under full solar radiation, three days under a single layer plastic mesh shade net whose transmittivity was found to be 24 % of full solar radiation, and the remainder of the ten day period under a double layer net (7 % transmittivity). Leaf temperature was measured as well as branch and stem sap flow rates. Results showed that photosynthesis was highest when leaf temperatures were between 25 and 30 °C while transpiration was also increased at such temperatures. There was less than ten percent difference between the two varieties of navel orange trees in terms of net exchange of fluxes. Although the shade nets were able to effectively lower leaf temperature, they also significantly lowered the levels of photosynthetic flux density to levels much less than the level at which photosynthesis saturates in citrus trees (600-700 $\mu mol\ m^{-2}\ s^{-1}$). Photosynthetic water productivity was found to be highest under the unshaded conditions. A model was run in April 2007 on two trees to predict stem sap flow rates under different shading conditions using leaf water potential, branch sap flow and soil water potential as inputs. Data for the model was collected over two days for each tree: first under full solar radiation conditions then with a single layer shade net. The results showed that the model was, to a large extent, able to predict the stem sap flow. Optimization of the model yielded the hydraulic parameters for each tree under the different radiation regimes. Overall, photosynthetic photon flux density was found to be a more important factor than leaf temperature in optimizing photosynthesis and water productivity.

ACKNOWLEDGEMENTS

I would like to thank my supervisor Mr Sebinasi Dzikiti for encouraging me to take up this project, which I never imagined I could do. His amazing work rate was infectious and certainly rubbed off on me, enabling me to complete this thesis. I am also grateful to my co-supervisor, Professor Franz X Meixner for some very productive discussions on the technical aspects of the project as well as his input at the beginning of the project. Professor James R. Milford provided some very useful comments throughout the various times that he edited my manuscript - thank you Prof. I sincerely thank Dr Ivonne Trebs who helped me to set up the LI-COR Infrared Gas Analyzer and to understand how to use it. Her subsequent consistent help with many other aspects of the project helped to make this thesis what it is today.

This MSc project would not have been possible without funding from the Flemish Inter-University Council (VLIR) through their link with the University of Zimbabwe. They provided financial support as well as equipment for the project for which I am thankful. I also thank the Max Planck Institute for Chemistry (Mainz, Germany) who, through Professor Franz X Meixner and Dr Ivonne Trebs provided some additional equipment and accessories which was crucial to the success of my experimental measurements.

The guys in the workshop as well as Mr Butau, the chief technician and all the technicians in the Physics Department deserve mention for their sterling work when they assisted me on several occasions.

I sincerely thank Mr B Chipindu, the MAGM program coordinator and chairman of the Physics Department for tirelessly coordinating the MAGM program and ensuring that all our project requirements were taken care of. His brotherly advice throughout my project was gratefully accepted. I also thank the MAGM members of staff Professor Milford, Dr Nyanganyura, Mr Dzikiti, Mr Mashonjowa and Mr Mhizha. Your friendliness, advice and zest for life made these last two years unforgettable. I also thank all the other members of staff in the Department who made the working environment conducive.

I shall forever cherish the friendly banter as well as the serious discussions that I shared with my colleagues in the MAGM program. You were all unique and I thank you for creating a great, friendly environment throughout the two years that we were together.

To my brothers Patrick and Charles, my sisters Christine and Barbara I say thank for your support and understanding throughout these past two years. I also thank my little niece Gabriella and my little nephew Tanaka for always having the ability to make me laugh whenever I was feeling low. Last but certainly not least, I thank my mother for her kindness, patience and for being the pillar of strength that she is. God bless you all.

TABLE OF CONTENTS

LIST OF SYMBOLS AND ABBREVIATIONS

Abbreviations and acronyms as used in the thesis

14C	carbon-14 isotope
ABA	abscisic acid
AC	alternating current
CO_2	carbon dioxide
DC	direct current
ET	evapotranspiration
GMT	Greenwich mean time
H_2O	water
IRGA	infra-red gas analyzer
LAI	leaf area index
LT	local time
LWP (=Ψ_l)	leaf water potential
MDC	median diel cycle
NIST	(American) National Institute of Standards
PPFD	photosynthetically-active photon flux density
RH	relative humidity of the air
RuBisCO	ribulose bisphosphate carboxylase oxygenase
SPAC	soil-plant-atmosphere continuum
SWP (=Ψ_s)	soil water potential
UV	ultra-violet
VPD	vapour pressure deficit
WUE	water use efficiency
WUE_i	instantaneous water use efficiency

Roman symbols

Symbol	Description	Unit
A	assimilation rate (CO_2)	[µmol m^{-2} s^{-1}]
A_l	leaf area enclosed in the cuvette	[m^2]
C	capacitance of the storage compartment	[kg MPa^{-1}]
c	mixing ratio of carbon dioxide	[mmol mol^{-1}]
c_1, c_2	mole fractions of CO_2	[mmol mol^{-1}]
c_a	CO_2 concentration inside a leaf	[mmol mol^{-1}]
c_e	CO_2 concentration at chamber entrance	[µmol mol^{-1}]
c_o	CO_2 concentration at chamber outlet	[µmol mol^{-1}]
c_p	specific heat capacity of water	[J kg^{-1} K]
E	transpiration flux	[mmol m^{-2} s^{-1}]
F	Sap flow rate	[g h^{-1}]
F	xylem sap flow rate	[g h^{-1}]
F	flux (CO_2 or H_2O)	[µmol m^{-2} s^{-1}]
g_s	stomatal conductance	[µmol m^{-2} s^{-1}]
K_{co}	thermal conductivity of cork substrate	[W mV^{-1}]
K_{sh}	effective thermal sheath conductance	[W mV^{-1}]
K_{sh}	effective thermal sheath conductance	[W mV^{-1}]
K_{st}	thermal conductivity of the stem	[W m^{-1} K^{-1}]
m	mixing ratio of CO_2, H_2O	[µmol mol^{-1}, mmol mol^{-1}]
p_1, p_2	pressure	[kPa]
P_{in}	heat applied to the stem segment	[W]
p_n	net photosynthesis	[µmol m^{-2} s^{-1}]
P_v	pressure in volume V	[kPa]
Q_f	rate of convective heat transport by	[W]
Q_r	rate of radial heat loss by conduction	[W]

Q_s	stem heat storage	[W]
Q_v	rate of vertical heat loss by conduction	[W]
R^2	coefficient of determination	[-]
R_x	resistance of the storage compartment	[kg h MPa^{-1}]
s	projected leaf area	[m^2]
T	absolute temperature	[K]
T_1, T_2	thermodynamic temperature	[K]
t_1, t_2	time	[s]
T_a	air temperature	[°C]
T_c	cuvette temperature	[°C]
T_d	dew point temperature	[°C]
T_l	leaf temperature	[°C]
T_v	temperature in volume V	[°C]
u	flow rate of air through chamber	[l min^{-1}]
u	voltage	[V]
u_c	flow rate in a closed system chamber	[l min^{-1}]
V	volume of a system (molar) @ (T_v, P_v)	[m^3]
V_m	molar gas volume	[l mol^{-1}]
$V_{m,0}$	molar gas volume at STP	[l mol^{-1}]
w	mixing ratio of water vapour	[mmol mol^{-1}]
W	water storage in plant tissues	[kg]
w_a	water vapour outside leaf	[mmol mol^{-1}]
w_i	water vapour concentration inside leaf	[mmol mol^{-1}]
ΔT	temperature increase of the xylary sap	[°C]

Greek symbols

Γ	compensation point of photosynthesis	[µmol m^{-2} s^{-1}]
Ψ_{air}	atmospheric water potential	[MPa]
Ψ	total water potential	[MPa]
Ψ_l	leaf water potential	[MPa]
Ψ_s	soil water potential	[MPa]
σ	standard deviation	[]

LIST OF FIGURES

LIST OF TABLES

CHAPTER 1 INTRODUCTION

1.1 Motivation and Background

Shading is a cultural practice that has been used mainly in greenhouse crops to reduce the radiation heat load, increase light-use efficiency (Bailey, 1981), and reduce pest and disease pressures (Glenn *et al*, 1999; McBride, 2000). But quantitative information on its effects on tree crops like citrus trees is sparse. Waggoner *et al*. (1959) found that 'cheese-cloth' tents reduced the amount of direct radiation below the nets. Non-reflective (white, black, or coloured) nets and reflective sprays have also been used to reduce canopy temperature and relieve water stress (Stanhill *et al*., 1976).

The fact that the leaf surface temperature of citrus trees often exceeds the air temperature during the day-time has been reported by many researchers (Davies and Albrigo, 1994; Spiegel-Roy and Goldschmidt, 1996; Jifon and Syvertsen, 2000). But the reasons for the elevated leaf temperatures have rarely been explained clearly.

The low transpiration rates triggered by the cyclic opening and closure of the stomata through the day in navel orange trees lead to the reduced evaporative cooling of the canopy under the conditions of high radiation loading characteristic of the semi-arid tropics. Thus high leaf surface temperatures (as much as 10 °C above the air temperature) occur (Dzikiti *et al*., 2006; Steppe *et al*., 2006). It is known that when leaf surface temperature for most plants exceeds 35 °C, the photosynthetic rate is severely inhibited due to reduced enzyme activity (Spiegel-Roy and Goldschmidt, 1996). Reduction in the photosynthetic rate inevitably leads to lower productivity levels. Thus the potential of canopy shading is explored in this study as a means of reducing the radiation loading on the canopies of two cultivars of orange trees commonly grown in citrus orchards in northern Zimbabwe. The effects of different shading intensities on gas exchange and tree water relations of potted navel orange trees are investigated. Effects of the shading on the productivity of the orange trees are inferred from the CO_2 and H_2O exchange measurements of the cumulative water use efficiency (WUE) of the navel orange trees using the infrared gas analyser.

The hypothesis to be tested in this study is that reducing the radiation load on the canopies of navel orange trees in the semi-arid tropics potentially enhances their productivity through increased water use efficiency.

1.2 Specific objectives

This study sought to:

(1) quantify the extent of citrus leaf temperature suppression under various shading levels;
(2) investigate the effects of canopy shading on gas exchange (CO_2 and H_2O) and on the water relations of citrus trees and
(3) compare the water use efficiency of two citrus cultivars under different levels of shading.

1.3 Justification

Water is increasingly becoming a scarce resource the world over. At the same time, populations are increasing. This has put a large strain on available resources. In Zimbabwe, citriculture has the potential to become a major foreign currency earner for the country. There are agro-ecological regions in the country where the staple maize does not thrive because of inadequate rainfall and insufficient growing heat units. There are also other areas which are thickly forested and unsuitable for growing maize. It is here that perhaps citrus trees can be grown, shielded by the shade from larger trees in the canopy. The results of this experiment can be applied to a forestry plantation whereby citrus trees can be grown underneath the tall trees (e.g. pine or gum). For intensive, highly commercial applications, the results from this study can be used to grow citrus trees using suitable shade nets from the recommendations at the end of this thesis. All this may go a long way towards improving the foreign currency earnings of the country and at the same time serve the local market with fresh, delicious oranges which will provide the much needed vitamins to maintain a healthy and vibrant population.

1.4 Thesis outline

This thesis consists of six chapters. **Chapter 1** introduces the thesis and gives reasons why this research was carried out. **Chapter 2** is the literature review chapter whose main purpose is to give the theoretical framework of the research carried out in the thesis. This includes previous related research carried out involving dynamic chamber techniques for CO_2 and H_2O flux measurements with particular reference to citrus, photosynthetic water use efficiency, citriculture, sap flow measurement, infrared gas analysis and modelling. In addition, the application of various sensors and instruments used in the experiments carried out is explained briefly as well as alternative micrometeorological techniques for measuring CO_2 and H_2O fluxes. **Chapter 3** follows up on **Chapter 2** by giving a detailed description of the particular materials introduced in **Chapter 2** used in the experiments carried out. It also explains the methods used to calibrate, test and set up various equipment used in the research. Furthermore details of how data and metadata was manipulated to come up with meaningful results and error limits are presented here. A description of the modelling aspect of the experiments is also given. **Chapter 3** gives the required information necessary to understand **Chapter 4** - the results chapter. **Chapter 4**, the longest and most elaborate chapter in the thesis, lays out the results of the described experiments and methods in **Chapter 3** in an almost chronological manner to the way the methods were described in **Chapter 3**. Discussions are included to aid understanding and for interpreting graphs and other visual aids. **Chapter 4** also discusses the results and other aspects of the experiments carried out with the aim of interpreting the results and meeting the objectives explained in **Chapter 1**. It also here that we find out if reducing canopy temperatures by using shade nets can give us a solution to the stated problem. Finally the thesis is summarized in **Chapter 5** where conclusions and recommendations are made. Suggestions for improving the experimental techniques for measuring fluxes, sap flow and other parameters are made here. **References** then follow after which there are **Appendices** for details which may be relevant to a particular section of the thesis but was not included in the main thesis. An example is data logger programs.

CHAPTER 2 LITERATURE REVIEW

2.1 Introduction

The term citrus includes different types of fruits and products. Oranges are the major fruits in the citrus fruit group, accounting for about 70 % of the world's citrus output.

2.2 Citrus production in Zimbabwe

Citrus has been one of Zimbabwe's major successes. In 2003, FAO reported that the sector accounted for about 55 % of total horticultural exports by volume and 10 % by value. About 6000 hectares are under citrus production in Zimbabwe (Zimbabwe International Travel Expo 2007 website, 2007).

In Zimbabwe, citrus production is mainly in areas in the Limpopo Valley, Save Valley and the Mazoe Valley. Beitbridge, in the Limpopo Valley, is the most important area in Zimbabwe for citrus production (Sithole, 2005). Farmers there concentrate on the Valencia and grapefruit varieties. The area is drought-prone and citrus growers rely on irrigation from a recently built large dam. According to FAO (2003) the area is responsible for almost 70 per cent of Zimbabwe's production. Another Lowveld area around Chiredzi (Save Valley) is developing into an important production zone having lemons in addition to the other varieties grown in the Limpopo Valley. The Mazoe Valley, in which Mazoe Citrus Estates is situated, also includes farming areas in the Glendale, Bindura, and Shamva districts. Being at a relatively higher altitude, temperatures are cooler and this has enabled different varieties of citrus to be grown there. Navels, lemons and some soft citrus varieties make up the production. The Chegutu and Marondera regions grow similar varieties to the Mazoe Valley. Mvurwi is the main soft citrus growing area of Zimbabwe. Production expanded rapidly in the late 1990s but has dropped dramatically as a result of land reforms in Zimbabwe (FAO, 2003).

2.3 The Citrus Crop

Citrus species are small to medium-size shrubs or trees that are cultivated throughout the tropics and subtropics. They are native to parts of India, China, northern Australia, and New Caledonia. Citrus is adaptable to many subtropical and tropical environments and soils and has traditionally been cultivated in home gardens. Citrus is primarily valued for the fruit, which is either eaten alone (sweet orange, tangerine, grapefruit, etc.) as fresh fruit, processed into juice, or added to dishes and beverages (lemon, lime, etc.). All species have traditional medicinal value. Citrus has many other uses including animal fodder and craft and fuel wood.

2.4 Climatic limits to citriculture

The evergreen *Citrus* species and cultivars - oranges, mandarins, grapefruits, pummeloes, lemons, limes and citrons – grow and produce fruit under varied climatic conditions, ranging from equatorial, hot-humid climates through warm subtropical and even cooler maritime climates. The sensitivity of the tree and fruit to frost, varying somewhat between species and rootstocks, is a major factor limiting the regions and localities where *Citrus* can be successfully grown. A sufficiently long, warm summer is also required to enable the fruit to grow and reach maturity. This constraint becomes important at

the cooler margins of the Citrus growing area (except for lemons, which can be consumed before full maturity). In the Mediterranean and similar climates with long dry summer periods, irrigation is required to maintain satisfactory tree growth and fruit development.

The main difficulties of citriculture in the tropics are the distortion of the productivity cycle and the reduced fruit quality. In tropical equatorial regions, with high temperatures and humidity prevailing through the whole year, trees often tend to flower sparsely, resulting in lower productivity. Where periods of drought occur, trees burst into bloom following the rains that terminate the drought; in many cases this results in several crops during the year, a situation that is difficult to handle by the export and processing industries. While the uninterrupted high temperatures of the tropics enhance fruit growth and maturation, several aspects of fruit quality may suffer. The internal quality of fresh orange and mandarin cultivars may become inferior because of low acid content. Low mean temperatures are required for the development of the highly pigmented rind of oranges and mandarins, and their fruit in the tropics generally does not attain the desired colour. These factors are of less significance in yellow and high-acid cultivars (e.g. limes), which are indeed widely grown in the tropics. In addition, under the warm and humid conditions of the tropics fruits often suffer from rind blemishes and pests disfiguring their appearance. These factors have limited the expansion of commercial citriculture in the tropics. During the last few decades, however, due to improvements in cultural conditions and to the investment that has been made, the growing and marketing of citrus in many tropical areas has been considerably expanded. In the belt of subtropical latitudes (roughly 20 º to 40 º latitude north and south of the equator), which has definite seasons, the rhythm of blossoming and growth is controlled by seasonal changes in temperature. Humidity is generally lower and considerable daily changes in temperature may occur. Local frosts and occasional severe freezes are also encountered. There is a cessation of growth in winter and the trees start to grow and blossom uniformly in the spring (Spiegel-Roy and Goldschmidt, 1996), with a subsequent concentrated crop ripening (except for lemons). In semi-tropical Florida, Brazil and the citrus-growing regions of Argentina and East Asia, a rainy season occurs during summer; a dry season, if it occurs, is of shorter duration in the fall, spring or both.

Citrus cultivars with anthocyanin-coloured rind and juice are successfully grown mainly in areas with low midwinter temperatures, as in Italy. Early-ripening cultivars attain the natural orange colour during cool autumn weather. Coloured grapefruit, the colour being mostly due to lycopenes, can be grown in a variety of climates. While anthocyanins develop in blood oranges during low winter temperatures, lycopene production in grapefruit is achieved mainly with prolonged fairly high temperatures. Thus, pigmented grapefruit attains an excellent colour in Texas and Florida.

2.5 Growth and development

Citrus trees belong to the ‘evergreens’, which do not shed their leaves during autumn. The evergreen habitat has important consequences for leaf longevity and physiological activity, which must be reflected in leaf design and structure. In the absence of autumn abscission the longevity of leaves may extend to a whole year and beyond. The year-round presence of leaves enables uninterrupted, day-by-

day photosynthetic activity, and thus a continuous supply of photosynthates. However, in subtropical climate zones winter temperatures might be quite low so that photosynthetic gains during winter are lowered. The evergreen habit may have significant implications with regard to the role of nutrient reserves, particularly during springtime. Whereas deciduous trees are totally dependent for early spring growth upon their carbohydrate reserves, evergreens like citrus may at least partly rely on the supply of photosynthate from the previous season's foliage. The evergreen character also has far-reaching consequences for the annual cycle of flowering and fruiting.

2.6 Leaf activity

Citrus belongs to C_3 plants, with photosynthetic rates lower than those of C_4 plants. Even among C_3 group citrus are in the low activity range (together with other tropical and subtropical trees), being considerably lower than annual crop plants and lower still compared with deciduous fruit plants such as apple and grape (Kriedemann, 1971). Assimilation rates of 4 to 8 µmol CO_2 m^{-2} s^{-1} seem realistic under optimal field conditions; higher rates are frequently obtained in greenhouse experiments. Low assimilation rates of citrus are accompanied by low rates of transpiration and extreme sensitivity to moisture deficit (Kriedemann and Barrs, 1981). Morning activity rates are generally somewhat higher than afternoon rates (Fischler, 1985). Photosynthetic activity of citrus saturates at relatively low intensities of 600 to 700 µmol m^{-2} s^{-1} PAR (Syvertsen, 1984; Vu and Yelenosky, 1988), which is about 30 % of full solar radiation.

However, in the orchard, these PAR levels are attained only for a few hours and only in external layers of the canopy. In shaded portions of the canopy of certain cultivars, (e.g. Marsh grapefruit) light intensities may be less than 1 % of full solar radiation (Monselise, 1951). The spectral composition of the light filtered through several leaf layers is also different from that of original sunlight. This variability in exposure of the leaves to radiation makes it difficult to provide reliable, whole-tree irradiation estimates. The daily course of transpiration does not seem to be closely linked to solar radiation but rather to leaf temperature and leaf water potential. Cyclic oscillations at individual plant level occur in photosynthesis and transpiration. Such oscillations have been recorded initially under controlled growth conditions by Kriedemann (1968) and then under field conditions by Levy and Kaufmann (1976) but their physiological significance is still not yet fully understood although major progress has been made in the last few years to explain them. These oscillations present another serious problem of attempts to integrate the photosynthetic activity over time, at the single leaf as well as at the whole-tree level. Such oscillations were recorded in the experiments reported in this thesis and an attempt will be made to explain them in the last chapter.

Although citrus trees thrive in hot, dry environments, leaf photosynthesis has a relatively low temperature optimum (Kriedemann, 1968). Temperatures of 25 to 30 °C are optimal, temperatures of 35 °C and above definitely reduce photosynthetic activity. Extremely high light intensities, as those occurring in subtropical desert areas, cause leaf temperatures to rise considerably beyond the ambient temperature, due to insufficient evaporative cooling (Syvertsen and Lloyd, 1994). This rise in leaf

temperature may also be involved in high-irradiation damage to the photosynthetic apparatus, which has recently been observed in citrus leaves.

Moisture stress is frequently encountered in natural habitats as well as in commercial citrus groves. Soil water deficits result in stomatal closure followed by severe inhibition of photosynthesis, presumably involving impairment of the ribulose bisphosphate carboxylase oxygenase (RuBisCO) system (Vu and Yelenosky, 1988, 1989). Increases in the leaf-to-air vapour pressure deficit (VPD), as observed under low relative humidities, are closely correlated with decreases in stomatal aperture and reduction of photosynthesis (Khairi and Hall, 1976; Kriedemann and Barrs, 1981). The sensitivity of the stomatal apparatus to water deficits may present an evolutionary adaptation towards water conservation (Syvertsen and Lloyd, 1994). Midday depression of transpiration and photosynthesis has been observed during hot summer days in the orchard (Oppenheimer and Mendel, 1934, Sinclair and Allen, 1982**).** The midday stomatal closure might be associated with an upsurge in VPD but perhaps also with transient leaf water deficits, resulting from difficulties in supplying sufficient soil water to satisfy the high evaporative demands. Under prolonged, severe water stress stomata open in the morning for a short while and then close for the rest of the day (Mendel, 1951).

Integration of the photosynthetic activity of a whole tree is a complex assignment. A first step in this direction has been the assessment of the photosynthetic area of trees by Turrell (1961). In his pioneering study Turrell determined the total leaf area and crown surface area for Valencia orange trees of different ages. In trees of 6 years and older the crown surface represented about 32 % of the total leaf area, indicating considerable light interception. When transformed into the current leaf area index (LAI), Turrell's data suggest LAI of 8-15 for Valencia orange. Values of 4.5-11.8 were obtained for other cultivars by Janh (1979) and Cohen (1984). These values are much higher than those reported for deciduous fruit trees (Jackson, 1980). Integration of whole-tree photosynthetic activity may be obtained by modern computer simulation modelling. The construction of such models takes into account light-saturated photosynthetic rates and seasonal canopy light interception as well as solar radiation and temperature inputs (De Jong and Grossman, 1994). Early models of citrus' photosynthesis have been discussed by Syvertsen and Lloyd (1994).

The export of photosynthate from source leaves of citrus is extremely slow as compared with herbaceous species, and so is the phloem translocation rate. This has been repeatedly shown by $^{14}CO_2$ labelling techniques (Kriedemann, 1969; Wallerstein *et al*., 1978). In addition to their assimilatory role, citrus leaves function as storage organs. The principal storage carbohydrate of citrus is starch but considerable amounts of soluble sugar are also present. Large amounts of starch reserves are found in all tree organs; leaf starch content may reach 12 % dry weight (Goldschmidt and Golomb, 1982). Whereas leaves of naturals show a clear diurnal cycle with all starch removed during the night, citrus leaves retain most of their starch and only slight diurnal fluctuations are evident (Goldschmidt *et al*., 1991). An extensive discussion of citrus' source-sink relations and carbohydrate economy may be found in Goldschmidt and Koch (1996).

2.7 The root system

The root system is the hidden part of the plant. Its importance as an anchor in the ground and as a source of water, mineral nutrients and hormones is well recognized. In woody plants, roots also serve as major carbohydrate storage organs (Loescher *et al.*, 1990). Differences between root systems assume special significance in stock grafted fruit trees, including citrus.

Roots in general and tree root systems in particular are less accessible to observation and experimentation than aerial, above ground organs. Many questions regarding root development and physiology remain, therefore, unanswered. It is particularly difficult to follow the behaviour of roots in their natural, soil environment. Plexiglas-walled root observation chambers filled with a reconstituted soil profile were used by Bevington and Castle (1985) for detailed observation of citrus root development. The use of minirhizotrons (Eissenstat and Duncan, 1992) facilitates further, advanced study of citrus root systems. Citrus plants are tap rooted, like most other dicots. The taproot is easily recognised at the seedling stage but its identity is often lost in the course of nursery practices and transfer of trees to the orchard.

Young, actively growing roots are immediately identified by their white colour. As roots grow older they acquire a yellow-light-brownish appearance. It has been believed for a long time that only white, actively growing rootlets are involved in uptake of water and mineral nutrients. This view has been disputed, however, and recent evidence suggests that brown roots also participate in uptake processes. Thin, dark-brown fibrous roots are usually dead. The citrus root cap has a typical, pointed shape. The occurrence of root hairs in citrus has been debated for a long time (Castle, 1980) but has eventually been convincingly demonstrated by Castle and Krezdorn (1979). The abundance of root hairs and their physiological activity nonetheless needs further clarification. Root growth takes place uninterruptedly, as long as soil temperature, moisture and aeration are adequate, but its intensity varies considerably. Citrus root growth commences in spring, when soil temperatures rise above the biological zero of 13 °C (Spiegel-Roy and Goldschmidt, 1996). Root growth resumes earlier in sandy soils that warm up quickly than in heavy, clay soils. Root growth is rather limited at temperatures below 18 °C.

Citrus growth is extremely sensitive to soil moisture deficits. Following the withholding of irrigation, root growth stops as soon as the soil matric potential drops to -0.05 MPa. Upon rewatering, recovery of root growth takes place. However, in previously dry zones of the soil profile there is a two-day lag before the emergence of new rootlets can be observed (Bevington and Castle, 1985). Thus, periodical orchard irrigation regimes produce corresponding root growth cycles.

Fruiting also has marked effects on root development. In trees with a heavy crop load, (e.g. during the ‘on’ year of alternate-bearing cultivars) root growth is completely checked, presumably due to depletion of carbohydrates (Jones *et al*., 1975; Smith, 1976; Goldschmidt and Golomb, 1982). Root growth of other plant species is also closely dependent upon carbohydrate availability (Farrar and Williams, 1994).

The alternating cycle of root and shoot growth periods suggests the existence of competition for nutrients between roots and shoots. Shoots seem to have the priority; this is also indicated in pruning

experiments which show that shoot regrowth occurs at the expense of root growth (Syvertsen, 1994). However, the antagonistic root-top relationship might also have a hormonal background. According to classical concepts, root growth is inhibited by the basipetal stream of auxin produced by growing shoot meristems (Monselise, 1947).

2.8 Eco-physiological perspective

The genus *Citrus* is believed to have originated in tropical and subtropical parts of South East Asia and spread from there to other continents. Different ideas have been proposed, however, with regard to climatic adaptation of citrus**.** Kriedemann and Barrs (1981) hypothesized that ancestors of present day cultivars evolved as understorey trees in tropical rainforests. This hypothesis is in accordance with the view that citrus is essentially a mesophyte, as indicated by its luxurious foliage and relatively shallow root system. On the other hand the mature leathery leaves with their thick cuticle and epicuticular wax reveal considerable xeromorphic adaptation, which is particularly striking in sun leaves (Kriedemann and Barrs, 1981). Moreover, citrus transpiration rates are low and the trees can survive rather extended periods of drought yet upon exposure to direct, high irradiance leaf temperatures may rise by 8-10 °C above air temperature, due to insufficient evaporative cooling (Syvertsen and Lloyd, 1994). This again indicates that citrus leaves are better adjusted to shaded environments, as also suggested by their high chlorophyll content (Syvertsen and Lloyd, 1994).

The apparently contradictory mesophytic and xerophytic features of citrus may, perhaps, be accounted for by some modification of the 'tropical rain forest origin' hypothesis, as recently proposed by Goldschmidt and Koch (1996). In semitropical as well as in most tropical climate zones there are periods of drought. Whereas major vegetative and reproductive growth activity takes place during periods of abundant moisture, plants are subsequently exposed to shorter or longer periods of drought and must, therefore, have the ability to cope with water stress situations. The mature, firm textured leaves (but, not the younger, juicy leaves, which are extremely drought sensitive) seem indeed to be well adapted, both structurally and physiologically, for such harsh conditions. The fruit too, although juicy on the inside, is efficiently protected against water loss by the thick, wax coated peel as well as by the unique structural features of the juice sacs. The need of citrus to adjust to periods of drought has resulted in a high priority for water conservation, as revealed by the numerous structural and physiological traits mentioned above.

2.9 Citrus irrigation and water use

Irrigation is the most costly practice in citrus growing and in arid and semi-arid climates with long dry periods. It is also increasingly employed in humid and sub-humid climates to maintain yields that are often reduced because of dry, rainless periods. Water use involves loss through transpiration from the crop and evaporation from the soil. The sum of the two components of water loss is termed evapotranspiration (ET). ET will be a function of the stage of plant growth, the crop and the evaporative demand of the atmosphere, depending on soil water availability. If the crop is subject to stress, ET will decline. *Citrus* water use efficiency (WUE), representing the amount of CO_2 fixed per

amount of water transpired, is rather low compared with that of many crop plants. As early as 1646, Ferrarius noted that citrus trees require abundant moisture but cannot endure stagnant water. Citrus roots are only slightly less sensitive to deficient aeration than avocado roots. They seem to be highly sensitive to hydrogen sulphide, which arises in flooded soils due to the activities of sulphur-fixing bacteria. (ref)

Citrus is considered a typical mesophyte, the leaves have many xeromorphic characteristics. The adaxial epidermis is covered by a thick waxy cuticle. The rigid leaf shows wilting only at low leaf water potentials. Osmotic potential rarely rises over -10 bars, even in a relatively turgid leaf. Under favourable conditions, high transpiration rates are observed, while transpiration is limited under unfavourable edaphic and atmospheric moisture conditions. Under high evaporation demand, stomata generally close. Stomata are much more abundant on the lower leaf surface than on the adaxial surface (800 mm^{-2} versus 40 mm^{-2}). The high stomatal density predisposes citrus toward potentially high transpiration, but the network of first and second order leaf veins is relatively sparse. Leaf life is usually between 9 and 24 months. The largest leaf drop occurs immediately after blossoming.(ref)

Girton (1927) found the minimum temperature for root development to be 12 °C, the optimum to be 26 °C, and maximum to be 37 °C. The decreased water absorption at low root temperatures is due mainly to a decrease in permeability of root membranes and an increase in the viscosity of water. Feeder roots are sparse in *Poncirus*, and rather abundant in Rough lemon.

Castle (1980) noted that the shallow suberized root system was generally equipped with only vestigial root hairs. Root hydraulic conductivity in citrus is relatively low. Hydraulic conductivity increases with higher root temperature (Syvertsen, 1981).

2.10 Principles of Shading

Covering crops with screen materials is a practice used to attain a number of agricultural objectives. These can be divided into several categories: shading from supra-optimal solar radiation, improving the thermal climate (e.g. for reducing nocturnal heat loss, Bailey, 1981), exclusion of insects (with insect-proof screens), birds and fruit bats and changing the solar spectrum for induction of light mediated processes (e.g. use of coloured screens). The most common shade screens are made of black plastic and rated according to the reduction in solar radiation that they produce. Thermal screens are made of highly reflective low emissivity materials designed to prevent losses of thermal radiation that they produce (Tanny and Cohen, 2003). Thermal screens are made of highly reflective low emissivity materials designed to prevent losses of thermal radiation. They are used mostly in greenhouses to reduce heating costs, and have been shown to reduce the incidence of radiative frost in field crops (Teitel *et al*., 1996). Coloured screens filter out different colours in the visible spectrum, causing changes in flowering and branching patterns produce (Tanny and Cohen, 2003). A recent development related to coloured screens is the use of ultraviolet (UV) absorbing screens, which reduce the populations of pests whose vision is limited to the UV portion of the spectrum (Antigonus *et al*., 1998). Perhaps the most important type is the insect proof screen, the use of which is expanding rapidly because of the increasing demand for produce grown with less insecticides and fewer insect

vectored studies. Studies showing that citrus productivity may be reduced in environments with high radiation, temperature and water vapour pressure deficits (Syvertsen and Lloyd, 1994; Bustan, 1996) led Cohen *et al*. (1997, 2001) to investigate the use of reflective nets in citrus orchards. These applications have spurred research to characterise the radiative properties of reflective nets (Kurata, 1991; Teitel and Segal, 1995; Cohen and Fuchs, 1999).

Environmental stress such as temperature and water deficits during critical periods of fruit development and maturation are known to influence fruit yield (Goldschmidt, 1999), peel colour, °Brix, and acid content, probably by reducing photosynthesis (Reuther, 1973; Syvertsen and Albrigo, 1980). Maximum net CO_2 assimilation of most citrus cultivars saturates at relatively low irradiance (600-700 µmol m^{-2} s^{-1}), which is about 30-35 % of full solar radiation (1500-2200 µmol m^{-2} s^{-1}) on a typical growing season day (Syvertsen, 1984). The excess radiant energy predisposes plants to photoinhibition, heat stress and stomatal closure, resulting in a reduction in net photosynthesis (P_n), the ultimate source of fruit soluble solids. Sustained high temperatures (35-40 °C) during early reproductive development also promote physiological abscission of young fruitlets. One proposal is that fruitlet abscission is caused by sustained negative carbon balance due to a temperature induced reduction in net CO_2 assimilation (Davies and Albrigo, 1994).

Evidence from a variety of sources indicates that citrus productivity is limited by carbohydrate supply (reviewed by Syvertsen and Lloyd, 1994). Excessive radiation loads can contribute to this carbohydrate limitation through heat stress effects on evaporative demand, impaired enzyme activity, and reduced net photosynthesis (Sinclair and Allen, 1982).

2.10.1 Reasons for shading

Shading is a preharvest cultural practice that has been used in some countries in greenhouse and orchard systems to reduce radiation heat load, increase light-use efficiency (Bailey, 1981), and reduce pest and disease pressures (Glenn *et al.*, 1999; McBride, 2000). Waggoner *et al*. (1959) found that 'cheese-cloth' tents reduced the amount of direct radiation below the nets. Non-reflective (white, black, or coloured) nets and reflective sprays have also been used to reduce canopy temperature and relieve water stress (Stanhill *et al*., 1976). Jifon and Syvertsen (2000) established that moderate shading could reduce leaf temperature and evaporative demand, resulting in increased net photosynthesis.

2.11 Dynamic chamber techniques

The following sections in quotation marks were adapted from Long and Hällgren (1993):

2.11.1 "The potential value of CO_2 exchange measurements

The growth of plants and crop stands, in terms of dry weight or carbon gain, has traditionally been measured by sampling, drying, weighing and chemical analysis of the dried material. Direct measurement of carbon dioxide (CO_2) uptake provides a complementary approach. Whilst harvesting methods are appropriate in assessing long-term changes, they are unsuitable when interest centres

either on short-term carbon gain, i.e. intervals of days, hours or minutes, or on contributions made by individual organs, e.g. the flag leaves of cereals. Measurement of CO_2 uptake provides an alternative and direct method of measuring carbon exchange, with important advantages: it is instantaneous and non-destructive. Furthermore it allows: measurement of the total carbon gain by the plant or stand; separation of the uptake by the different photosynthetic organs of a plant; and separation of photosynthetic gain from respiratory losses. In studying photosynthesis *in vivo*, measurements of O_2 evolution, and of fluorescence and absorption spectroscopy, now provide valuable methods for interpreting limitations and efficiencies. However, only measurement of CO_2 uptake can provide an unambiguous and direct measure of the net rate of photosynthetic carbon assimilation.(ref)

2.11.2 Measures, symbols and units

Many measures, terms and units have been used in the study of plant gas exchange. Those used in this thesis have largely been adopted from those described by von Caemmerer and Farquhar (1981). This system allows the direct comparison of fluxes, conductances and derived terms such as quantum efficiency using SI units.

The CO_2 concentration in air may be described by the mole fraction (*c*). This equals both the partial volume ($cm^{-3}\ m^{-3}$) and the ratio of the partial pressure of CO_2 to the total pressure of the body of air ($Pa\ MPa^{-1}$). Many instruments for CO_2 measurement indicate content as %, vpm (volumes per million), or ppm (parts per million); this is directly proportional to the mole fraction, where $1vpm=1cm^3\ m^{-3}=1ppm=1\mu mol\ mol^{-1}$. The assimilation rate (*A*) is expressed as the amount of CO_2 assimilated per unit leaf area and time ($\mu mol\ m^{-2}\ s^{-1}$). Amount rather than mass is used since this simplifies the comparison of the molecular fluxes of different gases and simplifies calculation of quantum efficiency. Mass flux is simply obtained by multiplying *A* by the molecular weight of CO_2, i.e. $44\ g\ mol^{-1}$.

The conductance (*g*) of the diffusion pathway is the ratio of flux to the CO_2 gradient. As the CO_2 concentration gradient (described as a mole fraction) is dimensionless, the dimensions will be those of *A*. Conductance is thus the hypothetical flux when the concentration gradient is unity.

To avoid the use of exponents, sub-multiples of the SI base units may be used, but only in the numerator. Thus, $\mu mol\ m^{-2}\ s^{-1}$ would be correct for *A*, but $mol\ dm^{-2}\ h^{-1}$ should not be used. Sub-multiples in the denominator add unnecessary complexity to the calculation of derived terms and complicate comparisons (Incoll *et al.*, 1977)

2.11.3 The approach to measuring leaf gas exchange

The majority of CO_2 exchange studies have involved the use of a leaf, plant, or stand of plants in a transparent chamber. The rate of CO_2 assimilation by the material enclosed is determined by measuring the change in the CO_2 concentration of the air flowing across the chamber.

2.11.3.1 Closed systems

In a closed system, air is pumped from the chamber enclosing the leaf or plant into an IRGA which continuously records the CO_2 concentration of the system. The air is then recycled back to the chamber. No air leaves the system or enters it from outside. If the leaf enclosed in the chamber is photosynthesising, the CO_2 concentration in the system will decline, and continue to decline until the CO_2 compensation point of photosynthesis (Γ) is reached. In practice, the CO_2 concentration is allowed to drop typically by about 30 µmol mol^{-1} from the ambient level. The rate of CO_2 assimilation is equal to the change in the amount of CO_2 in the system per unit time. Temperature (T) and pressure (p) are common and can introduce significant errors which must be corrected for (ref):

$$A = \frac{\left[c_1\left(p_1 / T_1\right) - c_2\left(p_2 / T_2\right)\right]V \cdot T_v}{\left(t_2 - t_1\right)s \cdot p_v} \qquad [2.1]$$

Where c_1, p_1 and T_1 are the mole fractions of CO_2 (µmol mol^{-1}), pressure (kPa), and temperature (K), respectively, of the system at time t_1 (s); $c2$, p_2 and T_2 are the corresponding values for time t_2. V is the volume (mol) of the system determined at temperature (T_v) and pressure (p_v). s is the projected surface area of the leaves (m^2).

If humidity is not controlled, transpiration will result in an increase in water vapour concentration and a dilution of the mole fraction of all other gases, including CO_2. Closed systems are the simplest configurations, being least demanding of the IRGA and requiring no measurement of flow rate. Such systems have important disadvantages: Recirculation of the air will result in a continuous rise in humidity. A wet humidity trap cannot be used since this will produce a variable volume of liquid water which would represent a sink for CO_2 and complicate the determination of V. Alternatively, a portion of the recirculated air may be passed through a drier as in the LI-6200 photosynthesis meter (LI-COR Inc., Lincoln, Nebraska, USA). However, this necessitates measurement of flow rate and removes one of the key advantages of a closed system. Errors resulting from CO_2 adsorption/desorption to and permeation through tubing and chamber walls will be amplified by continuous recirculation. A theoretical objection to closed systems is that since the CO_2 concentration is changing, A cannot reach steady-state and the measured value might not be a true reflection of the rate which would be obtained at a constant CO_2 concentration. Oscillations in CO_2 such as those produced by stomatal cycling at low humidity or those produced through feedback effects in carbon metabolism, may occur at a lower frequency than the period required for a measurement; thus cyclic variations in A, which would be apparent in a system capable of continuously monitoring A at constant c_a, would appear as random noise in measurements made in a closed system. The simplicity of closed systems makes these the most easily adapted for field use.

2.11.3.2 Semi-closed or null balance systems

Semi-closed systems, also known as null balance or compensating systems, are a variation on the closed system in which c_a is maintained at a constant value. The IRGA is used as a null-balance instrument which controls a flow of CO_2 into the system at a rate equivalent to the rate of uptake by the leaf. In practice, when CO_2 is removed by the photosynthesising leaf a decrease in c_a sensed by the IRGA switches on a supply of CO_2 to the system. This supply is then maintained at a rate just sufficient to keep c_a constant:

$$A = \frac{u_c}{s} \qquad [2.2]$$

To determine A in a semi-closed system it is necessary that the IRGA is calibrated in absolute mode and that the rate of addition of CO_2 is known with great accuracy, since error in the estimation of A will be directly proportional to and primarily dependent upon the measurement of u_c. The humidity within the system should either be maintained at a constant level or monitored so that the CO_2 concentration may be corrected to that of dry air. Assimilation rate will otherwise be overestimated, since the mole fraction of CO_2 within the system will decline not only as a result of photosynthesis, but also as a result of transpiration. In a semi-closed system, transpiration will increase humidity and thus dilute the concentrations of the other gases in enclosed air, including CO_2. A further requirement of the IRGA (less important in closed systems) is the absence of zero drift, i.e. long-term stability, since any drift will produce a systematic error in the estimate of A. Addition of CO_2 to semi-closed systems may be achieved with electronic flow controllers which allow injection of CO_2 into the system at a constant rate.

The advantage of semi-closed systems over closed systems is that c_a is maintained at a constant level so that A is determined at steady-state. Errors arising from permeation or leakage of CO_2 will be a constant rather than an accumulating error, as in closed systems. A further advantage is that A, and (if humidity control and measurement are included) E, may be studied at a range of values of c_a and w_a, simply by changing the set-point values in the system. The same measurements with an open system would require a complex air-conditioning system. Two practical disadvantages of semi-closed systems should be noted. Firstly, only one chamber can be monitored by one IRGA; thus such systems can be expensive relative to the number of measurements that are made. Secondly, rapid transient changes in A, such as those arising from sudden changes in light level, cannot be resolved easily. If the recirculation of air is slower than the transient change, a damped oscillation in the system will be set up which is a function of the system and not the plant material. To monitor transient changes, the volume of the system would need to be minimised and the air rapidly circulated.

2.11.3.3 Open or differential system

In an open or differential system there is a net flow of air through the system with no addition of CO_2 to compensate for photosynthesis. The IRGA is used to measure the difference in CO_2 concentration

between the chamber entrance (c_e) and outlet (c_o). Where the air streams are dried prior to entering the IRGA, the assimilation rate, A, will approximate to:

$$A = \frac{u(c_e - c_o)}{s} \qquad [2.3]$$

If the air is not dried before entering the IRGA the effects of water vapour on the measurements must be considered. Increase in the water vapour content of the air as it passes over the leaf will affect calculation of *A* in the above equation in two ways:

(1) Increase in the water vapour mole fraction must decrease the mole fraction of all other gases. Thus, c_o will be less than c_e simply because of transpiration. If the change in humidity is determined then dilution of c may be accounted for in calculating *A*:

$$A = \frac{u(c_e - c_o)}{s} \times \frac{(1 - w_o)}{(1 - w_e)} \qquad [2.4]$$

where u is the flow rate

c_o is the CO_2 mixing ratio at the chamber inlet

c_e is the CO_2 mixing ratio at the chamber inlet

w_o is H_2O mixing ratio at the chamber inlet

w_e is H_2O mixing ratio at the chamber inlet

s is the total projectd leaf area inside the chamber

(2) Sensitivity of CO_2 IRGAs to water vapour may cause an underestimate of c_o. This may be accounted for if both the response to water vapour and the increase in water vapour (w_o-w_e) are known. Many CO_2 IRGAs incorporate optical filters which decrease the response to water vapour. However, the presence of water vapour will alter the spectral composition of infrared radiation in the cells and may alter the response to CO_2 in a complex manner dependent on concentrations, path-lengths, source spectra and detector sensitivity. Since these errors can be substantial and not easily predicted it is probably simplest to avoid the uncertainties by routinely drying the IRGA inlet air streams. This may be achieved by passing the air through columns of calcium chloride and magnesium perchlorate in series (Day, 1985). Silica gel should not be used for this purpose as it can exchange CO_2. In the LI-6262 (LI-COR), CO_2 and water vapour are measured simultaneously within the same optical path allowing direct correction for water vapour interference via the instrument's microprocessor.

In an open system it is necessary that:

a) the IRGA is calibrated in differential mode; b) the changes in both humidity and CO_2 across the leaf are known; c) the flow rate of air (*u*) through the leaf chamber is constant and accurately known; and d) the leaf surface area is determined accurately.

The main disadvantages of such a system are the initial expense, in particular, the requirement for an air-conditioning system and for an IRGA which can accurately sense small differences in CO_2 mole fraction between two air streams, i.e. of the order of ≤ 1 µmol mol^{-1}. However, there are advantages to such a system:

1. By use of a switching device, *A* can be simultaneously determined for a number of chambers.
2. The CO_2, O_2 and water vapour concentrations around the leaf can easily be manipulated.
3. Transpiration and photosynthetic CO_2 assimilation can be measured simultaneously for several chambers.
4. Transient changes in gas exchange with step changes in the microclimate of the leaf may be monitored easily.**"**

2.12 Steady-state water flow

2.12.1 Electrical analogy of water movement through the SPAC

Van den Honert (1948) considered the pathway of water movement through the soil-plant-atmosphere continuum (SPAC) as a catenary process, where each part of the SPAC (each catena element) is viewed as a hydraulic resistance (analogous to an electrical resistance) across which water (analogous to electrical current) flows (Figure 2.1).

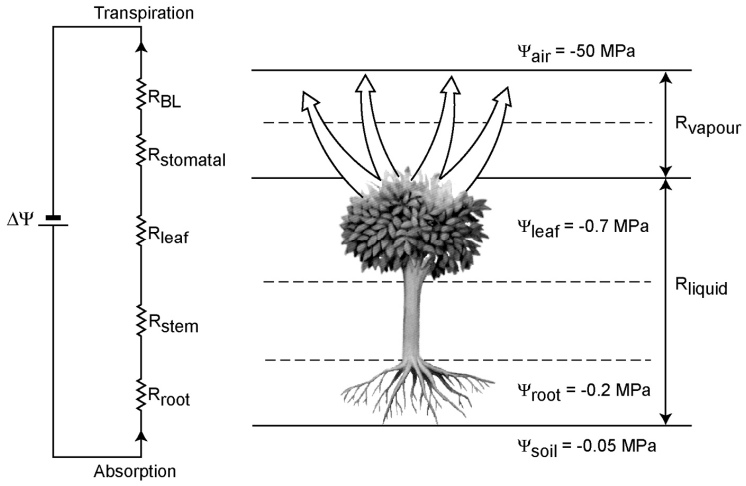

Figure 2.1 *On the right a schematic representation of the pathway of water movement through the soil-plant-atmosphere continuum (SPAC), and on the left its Ohm's law analogy. The water flow is driven by the differences in water potential between the soil (Ψ_{soil}) and the atmosphere (Ψ_{air}). The total resistance (R) against water flow is seen as the resultant of the root, stem, leaf, stomatal and boundary layer (BL) resistances in series. As the water potential difference (here 49.3 MPa) is maximal between the leaves and the air, the resistances in the vapour phase are more important than in the liquid phase (from Steppe, 2004).*

2.13 Dynamic water flow

2.13.1 Basic aspects of water transport

Plant and tree water transport in the soil-plant-atmosphere continuum (SPAC) cannot be seen any more as steady-state flow in simple rigid tubes. The assumption that the water uptake by the root system exactly equals the water losses from the leaves is not true in reality (Steppe, 2004). It has been shown that leaf transpiration can start several minutes to hours earlier than water flow in the

stem (e.g. Schulze *et al*., 1985). Thus, the beginning of water uptake by the roots can significantly lag behind the onset of transpiration at crown level. This is a consequence of water consumption from internal water storage reservoirs in the tree. Besides functioning as a pathway for water transport, tree stems also act as important water storage compartments (Meinzer *et al*., 2001).

Generally, transpiration exceeds water uptake from the soil during the early morning hours. This causes plants and trees to deplete water from their internal water storage reservoirs which are closely located to the sites where water is finally lost to the atmosphere. Thus, while the soil is the ultimate (and often the largest) source of water for transpiration, it may not be the most significant one when small time scales are considered (Holbrook and Sinclair, 1992). During the late afternoon, the reverse usually happens and the internal water storage pools are refilled whenever water uptake exceeds transpiration. Furthermore, the fact that stored water is depleted daily during the morning and subsequently replenished during the evening is also demonstrated by the marked diurnal variations in stem radius (Tatarinov and Cermak, 1999).

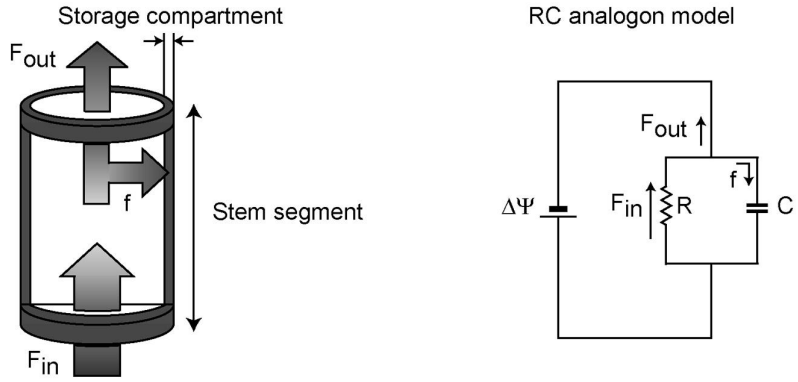

Figure 2.2 *Schematic view of the dynamic water flow through a stem segment that can store water (left) and its electrical RC analogue (right). The flow into the stem segment (F_{in}) equals the flow out of the segment (F_{out}) plus the flow into the storage compartment (f); the latter is represented by the capacitance C of the RC analogon model. During flow, the water encounters a resistance R .(from Steppe, 2004))*

2.14 Water use efficiency

2.14.1 Definition of water use efficiency

Water use efficiency (WUE) does not have a single precise definition. Its definition depends upon the particular context in which it is being discussed, including whether the water is in relation to the plant (i.e. inside the plant or its environment), the time scale over which efficiency is measured (e.g. instantaneous exchange of water vapour for carbon dioxide gas versus biomass accumulation or yield) and the precise measure of efficiency in relation to carbon gain (i.e. carbon dioxide flux, biomass accumulation or economic yield). In most of the current plant physiology literature, WUE is discussed either in terms of an instantaneous measurement of the efficiency of carbon gain for water loss; or as an integral of such an efficiency over time, commonly expressed as a ratio of water use to biomass accumulation, or harvestable yield.

2.14.2 Carbon metabolism and WUE

Water use efficiency can be defined as the ratio of CO_2 assimilation into the photosynthetic biochemistry (A) to water lost, via transpiration, through the stomata (E). A and E are regulated by stomatal conductance (g_s) to water and CO_2 and the respective concentration differences in water vapour (w_i-w_a) and CO_2 (c_i-c_a) between the inside (w_i and c_i, respectively) and outside of the leaf (w_a and c_a, respectively). Assuming w_i/w_a is independent of c_i/c_a, the so-called 'intrinsic' water use efficiency (W_T) is a negative function of c_i/c_a. Under any particular set of conditions, the driving force for CO_2 uptake will be enhanced by lowering c_i, while the driving force for water loss will remain relatively unchanged, leading to an increase in water use efficiency.

A plant can achieve a lower c_i/c_a ratio (with a concomitant increase in WUE) by decreasing stomatal aperture (lowering c_i by limiting CO_2 diffusion into the leaf interior); increasing photosynthetic capacity for CO_2 (lowering c_i by increasing carboxylation) or more likely, a combination of the two. Indeed, it is commonly observed that stomatal movements can conserve proportionality between c_i and c_a (Wong *et al*., 1978) with continued debate over if and how photosynthetic capacity, carbon dioxide concentrations and transpiration are sensed and integrated to produce an optimal stomatal aperture (e.g. Cowan, 1982; Farquhar and Sharkey, 1982; Farquhar and Wong, 1984; Jarvis and Davies, 1998).

2.14.3 Stomata and WUE

Regulation of the stomatal aperture is central to the water use efficiency of plants. Radiation, temperature, humidity and carbon dioxide concentrations will all act in some way either directly or indirectly on the stomatal aperture, together with internal circulation rhythms, leaf water status and xylem borne signals (e.g. cytokinins, abscisic acid, etc.). At any point in time, all of these signals must in some way be integrated to deliver a particular aperture under a particular set of environmental conditions. While work at the cellular and molecular level is beginning to illustrate how such integration may occur (e.g. Webb and Hetherington, 1997) uncertainty on how (or if) stomatal guard cells actually sense some of these environmental signals (particularly CO_2) has remained a source of active debate (e.g. Raschke, 1976; Jarvis and Davies, 1998) particularly in relation to the indirect role of mesophyll photosynthesis in controlling stomatal conductance (Farquhar and Wong, 1984).

Irrespective of these uncertainties it seems intuitive (and clearly advantageous) that stomatal guard cells continually integrate environmental signals from both the aerial environment and the soil, to generate a stomatal aperture, which optimises water loss and carbon dioxide gain under a given set of environmental conditions. Optimisation theory of stomatal aperture (Cowan, 1982; Farquhar and Sharkey, 1982) predicts that stomatal aperture varies during the day to ensure minimum water loss for maximum carbon gain. As such, while any increase in stomatal conductance generates a proportionally greater increase in transpiration than assimilation, optimisation theory predicts that such variation will keep the ratio of such changes in transpiration and assimilation rate constant, thus preserving intrinsic WUE (Jones, 1992). Cowan (1982) provides a detailed discussion of optimisation theory, illustrated by considerations of optimisation in relation to diurnal fluctuations in leaf

microenvironment and soil water supply, over time periods of relevance to the overall WUE of a plant throughout its development.

While the role of stomata in governing the driving force for CO_2 influx is well appreciated, stomata do have a limited ability to change the driving force for water loss via transpirational leaf cooling. An enhanced ability to achieve leaf cooling (in the absence of any changes in stomatal function), will reduce the internal partial pressure of water vapour and the concomitant driving force for water loss via evaporation. While only a minor trait conferring a theoretical degree of water use efficiency, novel thermal imaging technology can now detect such subtle differences in leaf temperature in both laboratory and field environments (Jones *et al*., 2003).

It is important to recognise that changes in stomatal conductance (and resultant changes in the efficiency of water use) may not necessarily scale to the crop and ecosystem level, due to a series of crop level factors (i.e. canopy boundary layer conductance and temperature due to latent heat of vaporisation from the crop surface) which reduce and 'decouple' the stomatal influence on transpiration (Jones, 1993). These factors are also central to understanding the discrepancies often observed between predicted and realised increases in water use efficiency which may be achieved as global atmospheric CO_2 concentrations rise (Polley, 2002).

2.14.4 Leaf growth and WUE

While changes in leaf size may also change CO_2 and H_2O fluxes into and out of the leaf, due to modification to the boundary layer, differences in leaf thickness will also have a significant effect on water use efficiency, with thinner leaves (with a lower ratio of internal volume to leaf surface area) predicted to exhibit lower water use efficiencies than comparable thicker leaves (Stanhill, 1986). It has also been suggested that rapid leaf development in annuals contribute to the efficiency of water use. By establishing a high specific leaf area quickly, evaporation of water from the soil is minimised and 'stored' close to the plant throughout the rooting zone, such that it can be drawn upon later in development when water may become limiting (López-Castañeda *et al*., 1996). This trait has recently been exploited with some success to deliver more water use efficient and high yielding wheat lines (Asseng *et al*., 2003). As well as the potential direct effects on soil water evaporation, Blum (1996) also suggests that such an adaptation will also minimise the potential for surface roots to come into contact with drying soil, and reduce the likelihood of initiating root-borne signals inhibitory to stomatal conductance. Conversely however, rapid leaf area development may actually prevent soil interception of precipitation, enhancing the rate at which soil water is depleted (Blum, 1996). Clearly this will depend upon the rainfall patterns in a particular environment.

Increasing the photosynthetic capacity of the mesophyll will enhance water use efficiency. However, increased photosynthetic capacity is often associated with a decrease in leaf size (Bhagsari and Brown, 1986), reducing whole plant transpiration and light interception, such that WUE on a plant biomass basis, over time, may actually decrease. The decline in leaf area is likely to occur if any increase in photosynthetic capacity results from an increase in the concentration of enzymes associated with the photosynthetic biochemistry. Under such circumstances, enhanced photosynthetic capacity and limited

nitrogen resources are optimised, such that specific leaf area declines (i.e. there is an increase in the dry matter content of leaves on a leaf area basis).

When soil water availability is limited, leaf expansion rates are commonly observed to decline (Bacon, 1999) in line with transpiration. The innate relationship between transpiration and yield would suggest that this leads to an overall decrease in biomass production (and yield productivity of commercial crops). In a majority of cases this is certainly the case. However, under some circumstances, yield and WUE can be sustained or even enhanced even though there is a decline in biomass accumulation at the whole plant level.

2.14.5 Roots, hydraulic conductivity and WUE

Deep and expansive root systems are an apparent strategy to ensure maximal water use efficiency in terms of water extraction from the soil, particularly when water availability in soils may decline. An ability to continue to develop deep and advantageous roots when soil conditions become increasingly limiting to root growth will enhance the ability of plants to extract available water efficiently. It is a commonly observed phenomenon that as soil water availability declines; the ratio of roots to shoots typically increases. There are very few data that suggest that root growth can actually be increased by soil drying. Those that do (e.g. Sharp and Davies, 1979), attribute such effects to a stress of particular magnitude which results in increased availability of assimilates to roots, as shoot growth is limited by water deficit in the absence of any effect on carbon gain. More recently, however, Mingo (2003) has reported that under particular circumstances, root growth can be simulated when roots are rehydrated after a drying episode, relative to roots in moist soil.

Water use efficiency in terms of ability to sustain water extraction from the soil, becomes increasingly difficult as the soil dries. Soil drying places a number of different constraints on the growth and functioning of roots and most of these are poorly understood due to the highly heterogeneous nature of the rooting environment, the delicate nature of the relationship between roots and soil structure and the difficulty of investigating root growth and functioning without disrupting this relationship. One of the common responses to soil drying is that roots show enhanced geotropism (Sharp and Davies, 1985). An increased rooting depth can significantly increase water uptake by root systems even when relatively few roots are involved. The adaptive significance of sustaining root growth (even if at a reduced rate) is only clear, however, if plants are competing in natural communities for different soil water resources. There would appear to be nothing to be gained by plants in a monoculture investing increased carbohydrate into deeper rooting when all plants in the stand are competing for the same reserves of soil water (Bacon *et al*., 2003). As soil water potentials fall, in substrates with low mechanical impedance (i.e. roots can penetrate the substrate easily), roots have been observed to thin, an adaptation presumably to commit limited carbohydrate supply to extension growth and allow plants to explore deeper water reserves (Sharp *et al*., 1988). However, in most soils, decreasing water potentials are commonly associated with increased mechanical impedance, such that roots have been shown to swell as soil dries, particularly behind the root apex (Spollen *et al*., 2000). The prevalence of this phenomenon may allow roots to continue to penetrate the soil as its mechanical impedance

increases on drying which may be related to a capacity to generate high turgors in root tips (Richards and Greacen, 1986; Atwell and Newsome, 1990). Roots of many plants in compacted soils are restricted to cracks in the soil structure. As a result, roots will often grow down these fissures causing substantial localised drying, even when the water content of the bulk soil is still substantial.

Overall transpirational flux through a plant is determined by the characteristics of a plant's hydraulic architecture. Any change in these characteristics could lead to an alteration in the response of open stomata to transpiration rate and an effect on water use efficiency. This may be particularly important when considering water use efficiency over a prolonged period of time during development. Narrower xylem vessels in roots will result in an overall increase in the hydraulic resistance to water flow throughout the plant (Richards *et al*., 2002). Consequently, efficiencies in water use may be gained by restricting water uptake early in the development of the plant to ensure sufficient soil water is available during the reproductive stage. This trait has been confirmed as advantageous in breeding programs for xylem diameter in wheat (Richards and Passioura, 1989) in which introduction of decreased xylem diameter as a selectable trait increased yields by about 7 per cent. Sperry and co-workers have recently developed a hydraulic model of water transport through the soil-plant-atmosphere continuum in relation to the component driving forces (and the encountered resistances) to predict transpirational rates, on the basis that plants have evolved hydraulic stomatal optimisation mechanisms to ensure that water loss does not exceed uptake by the roots (Sperry *et al*., 2002). However, the growing evidence of the root-sourced signals emanating from the root eliciting control of transpiration, does question such a purely hydraulic model. It is becoming increasingly clear that root-sourced signals appear to play a key role in regulating stomatal aperture in response to soil water availability, such that these signals may provide the means by which water supply would appear to regulate water loss (Bacon, 2004).

When soil water availability falls below a certain level, root water potentials and turgors can reach very low values and stimulate the synthesis of several plant growth regulators including abscisic acid (ABA) (Wright, 1977). It is now well-established that the production and export from roots of ABA can be related to soil water status and may act as a suitable candidate messenger to ensure the demand for water from the plant is closely controlled by water supply from the roots. The exact roles of hydraulic and chemical regulation of transpiration water loss will continue to attract serious debate and be the subject of future research, with potentially significant impact on understanding (and exploitation of) the physiological basis to water use efficiency.

2.14.6 Water use efficiency and photosynthesis

Although the expression 'water use efficiency' may be misleading, as plants lose water rather than use it as a raw material for the production of biomass (Stanhill, 1986; Monteith, 1993), it shall be used in this thesis because of its wide acceptance, and will be defined as the ratio of some measure of carbon assimilation or growth to some measure of the correspondent water loss. We shall also consider it in different spatial and time scales, such as at the level of the leaf or whole plant, and over short-time measurements (instantaneous WUE) or the whole growing season (long-term WUE). At the leaf level,

instantaneous water use efficiency (WUE_i) can be estimated by gas exchange measurements and calculated as the ratio of carbon assimilation to transpiration (A/E, μmol CO_2 $mmol^{-1}$ H_2O).

2.14.7 The relationship between CO_2 uptake and transpiration

Because carbon dioxide and water vapour share the same stomatal diffusion pathway, and the diffusion gradient that drives water loss is much larger (around 50 times) than that for CO_2 uptake, an increase in leaf stomatal conductance (g_s) that enhances CO_2 diffusion (and hence photosynthetic rate, *A*), inevitably leads to a large increase in transpiration. On the other hand, there is evidence that C_3 species' stomatal conductance is normally such that photosynthesis tends to be co-limited by CO_2 carboxylation and by ribulose-biphosphate regeneration. In other words, the actual rate of net CO_2 assimilation that is dictated by CO_2 availability (and therefore by stomatal conductance), corresponds normally to the intercellular CO_2 partial pressure (p_i) where the balance between the two biochemical limitations to photosynthesis occur. This p_i is called the 'operating point' for photosynthesis. If g_s, and hence p_i, increase above the operating point, leaf photosynthetic rate would only marginally increase and WUE will tend to decrease. If, on the other hand, CO_2 supply is strongly limited by stomata closure (e.g. as a result of soil drying), there may be the need for the down-regulation of photosynthesis to avoid photo-inhibitory damage of the chloroplast, and WUE may also decrease.

In summary, it seems that under certain limits, stomata are able to balance the need for the entry of CO_2 to the intercellular spaces – to allow photosynthesis to occur – with the need to avoid dehydration by excessive water loss; in other words, stomata will open to the extent required to provide sufficient CO_2 to meet the requirements for photosynthesis. In fact, there is strong evidence indicating that the ratio A/g_s is conservative for a broad range of conditions, a feature that appears to have an important ecological significance (Schulze *et al*., 1994). This has led to the hypothesis that an optimisation of water use has accompanied plant evolution (Cowan and Farquhar, 1997), so that the partial pressure of CO_2 in the intercellular spaces (p_i) and the instantaneous WUE would remain constant. Cowan and co-authors argued that, within the constraints set by maximal and minimal stomatal conductances for a particular leaf type, stomatal response to humidity and temperature would result in maximal daily CO_2 assimilation for a specific daily water use. Numerous observations showed that $\delta A/\delta E$ remained constant with variations in air humidity and leaf temperature or even irradiance (Farquhar *et al*., 1980, Hall and Schulze, 1980), except when changes are too fast to produce a decrease in *A* with stomata still open (Wong *et al*., 1979, 1985). The hypothesis of the influence of the mesophyll photosynthesis on stomatal opening, via some unidentified chemical or electrical signal, was supported by the different behaviour of stomata in detached epidermis and in intact leaves (Lee and Bowling, 1995). This hypothesis had been the basis for several models that explain the responses of g_s, p_i, and *A* of well-watered plants to a range of environmental factors (Ball *et al*., 1987, Leuning *et al*., 1995). One possibility earlier raised for the mesophyll control of stomata was via the intercellular CO_2 effect on stomatal conductance (Raschke, 1976). This may be an important mechanism in the response of C_4 plants to light but does not seem significant in C_3 species (Wong *et al*., 1979).

p_i tends to be maintained constant in leaves kept under well-watered conditions. When the water supply is declining, stomata respond to leaf water potential, and both respond to and control the supply and loss of water by the leaves (Leuning *et al*., 2003). Under these circumstances, intercellular CO_2 could control stomatal opening in response either to the supply of CO_2 to the chloroplast (a function of the diffusion from the air to the site of carboxylation), or to the demand of CO_2 by photosynthesis, governed by chloroplast biochemistry, irradiance or sink strength (Mott, 1988; Assman, 1999). It is usually observed that the decrease in g_s in response to mild water stress leads to a linear decline in transpiration (under constant VPD) and of p_i, because the demand for CO_2 by the chloroplasts stays the same. In this case, because the gradient p_i-p_a increases, photosynthesis either does not decrease or decreases relatively less than g_s, and therefore WUE increases (Lambers *et al*., 1998). In other words, intrinsic WUE commonly increases in response to mild water deficits, because drought-induced stomatal closure restricts water loss more than CO_2 uptake; this is even more evident for C_4 plants, because their CO_2 uptake is less sensitive to the initial decline in g_s than C_3 plants (Long, 1999; Ghannoum *et al*., 2002). In long-term water deficits, WUE may be positively or negatively correlated with relative growth rates of plants (Chaves *et al*., 2004).

Chapter 3 MATERIALS AND METHODS

3.1 Introduction

This study was carried out from October 2006 to February 2007. The first two months were used to set up the experiment and to become acquainted with the elaborate functions of the equipment, especially the Infrared Gas Analyzer (IRGA).

3.2 Experimental site description

Measurements were carried out on a level, open-air laboratory on the roof of the Physics Department of the University of Zimbabwe (17º46.964S', 031º03.090'E, elevation 1450 m.a.s.l) located in the north-eastern part of Zimbabwe. The site is 10 m above ground level. The concrete surface of the roof is overlain with gravel crushed out of granite rock. For protection of sensitive instruments from the rain, a transparent plastic shelter was used with all sides open to allow free circulation of air. Measurements showed that the transmittance of the plastic to solar radiation (global) was 73 (±1) %. The plastic was approximately 200 µm thick and was supported by a frame measuring 7 m × 4 m × 2 m (length × width × height).

3.3 Plant material

Six 5-year-old actively growing citrus trees [*Citrus sinensis* (L.) Osbeck] were used for the experimental measurements. Of the 6 trees, 4 belonged to the *Baianinha* selection and two belonged to the *Navelina* selection. All 6 trees were grafted on a troyer citrange rootstock (*Citrus sinensis* × *Poncirus trifoliata* L. Raf).

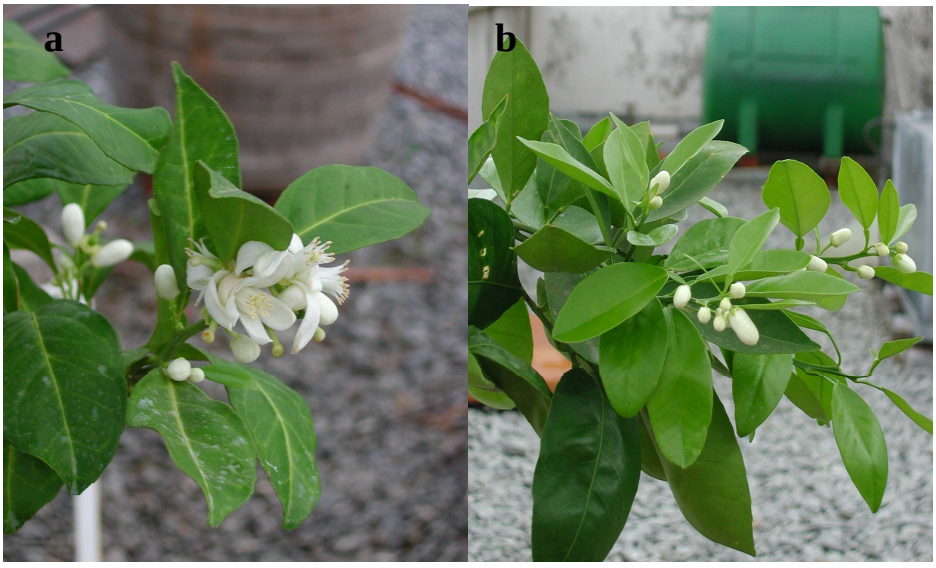

Figure 3.1 *The two citrus cultivars (a) Navelina and (b) Baianinha used in the experiment*

The trees were transplanted in asbestos pots 0.7 m diameter and 0.5 m high filled with dark-red clayey loam soil (Hussein, 1982). The trees were 90-100 cm tall at the time of transplanting (August 2006). The diameter of the trees at soil level ranged from 12 mm to 18 mm.

The soil water content was maintained close to field capacity (45 % v/v) by watering for 20 minutes at the end of each day using a drip irrigation system. The trees were also fertilized and sprayed with fungicides and insecticides as needed throughout the experimental period.

Figure 3.2 *The young navel orange trees a few days after they were transplanted to the pots on the roof of the Physics Department (September 2006).*

3.4 Physical setup

The experimental setup could be split up into 5 units:-

1. the cuvette –IRGA unit,
2. the plant physiological/soil compartment unit,
3. the external environment sampling unit,
4. the data acquisition unit and
5. the power supply/backup unit.

A simplified schematic diagram of the major components of the experimental setup is shown in Figure 3.3.

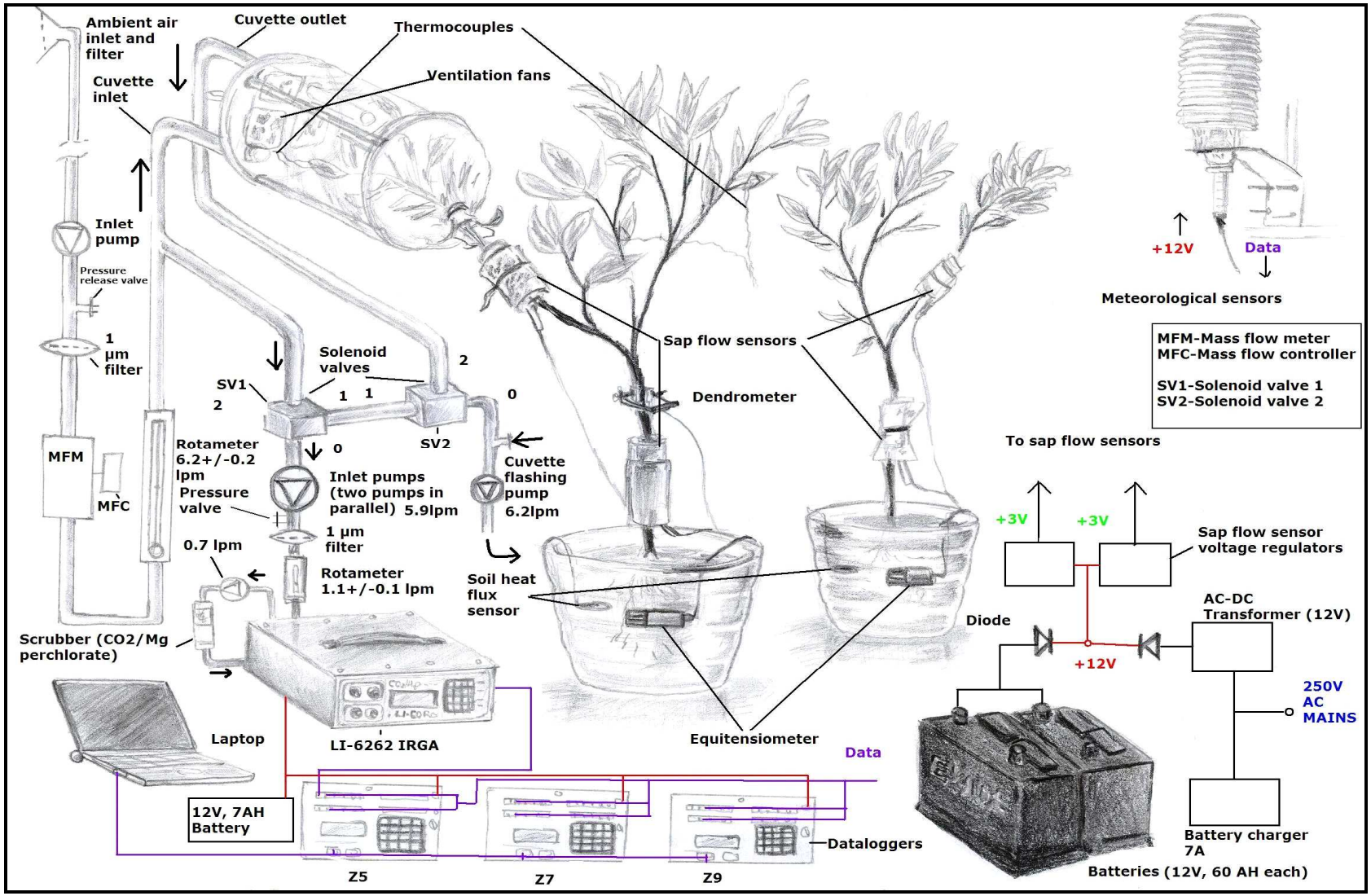

Figure 3.3 *A simplified schematic of the major components of the experimental setup.*

Table 3.1 *List of physical and physiological parameters measured and sensors used in the experiment*

Parameter	Time resolution or averaging time	Technique or sensor	Model, manufacturer	Detection limit/precision
CO_2 mixing ratio	0.1s	Infrared closed-path absorption	IRGA LI-COR LI-6262 (LI-COR Inc., Lincoln, Nebraska, USA)	± 1 %
H_2O mixing ratio	0.1s	Infrared closed-path absorption	IRGA LI-COR LI-6262 (LI-COR Inc., Lincoln, Nebraska, USA)	± 1 %
Air temperature (inside and outside shelter)	1 min	Pt 1000 (IEC 751 1/3 Class B)	Model HMP45AC, Vaisala, Finland	± 0.2 ºC
Relative humidity (inside and outside shelter)	1 min	Vaisala HUMICAP® 180 Capacitive sensor	Model HMP45AC, Vaisala, Finland	± 5 %
Temperatures: Cuvette Leaf Fruit skin	1 min	Seebeck thermoelectric effect	K-type thermocouples; METATEMP Industrial Temperature measurement, Steenbergen, Netherlands	± 0.1 ºC
Global radiation flux (external)	1 min	Pyranometer sensor	CM11; Kipp and Zonen, Netherlands	< ± 3 %
Global radiation flux (inside shelter)	1 min	Pyranometer sensor	LI-200SZ Pyranometer sensor; LI-COR, Lincoln, Nebraska, USA)	< ± 3 %
Photosynthetically-active Photon Flux Density (PPFD)	1 min	PAR quantum sensor	LI-190SZ Quantum sensor; LI-COR, Lincoln, Nebraska, USA)	± 5 %
Wind speed	1 min	Cup anemometer	Type A100L2; Vector Instruments, Wales, UK.	± 0.05 m s^{-1}
Wind direction	1 min	Wind vane	Wind sentry, UK	± 5 %
Net Radiation	1 min	60-junction thermopile	REBS Q*7 net radiometer; Radiation and Energy Balance Systems, Seattle, Washington, USA	< ± 6 %
Soil matric potential	1 min	Soil moisture sensor (Equitensiometer)	Type EQ2; Delta-T Devices Ltd, Cambridge, UK)	± 5 %
Sap flow- branch and stem	1 min	Sap flow gauge	Dynagage SGA5 and SGA9; Dynamax, Texas, USA)	±10 %
Soil heat flux	1 min	Heat flux plates	Hukseflux	±5 %
IRGA Pressure	1 min	Piezoelectric pressure transducer	Model PT101FB, Vaisala, Finland	±2 %
Rainfall intensity	1 min	Tipping bucket rain gauge	Model ARG100; Campbell scientific Ltd, Leicestershire, UK.	±4 % (for ≤ 25mm/hr) ±8 % (for ≥ 133mm/hr)
Stem diameter	1 min	Linear variable differential transducer (LVDT) (Dendrometer)	DEX-20; Dex Inc., USA	±0.001 mm

3.4.1 Cuvette-IRGA unit

A cuvette was set up on the branch of a young citrus tree at any given time as shown in Figure 3.4. It was made of two rigid Teflon plates which were joined together by Teflon-coated stainless steel rods of dimensions 12 mm × 224 mm. Stabilized Teflon film was used to create the cuvette airtight enclosure which prevented leakage of gases from the chamber. The branch chamber was cylindrical with dimensions 25.5 cm × 20 cm (length × diameter). The individual rods could be joined to increase the length of the chamber, and hence the volume if so desired. The bottom end of the chamber had openings for supporting the ventilation fans and for connecting air tubes and any other accessories.

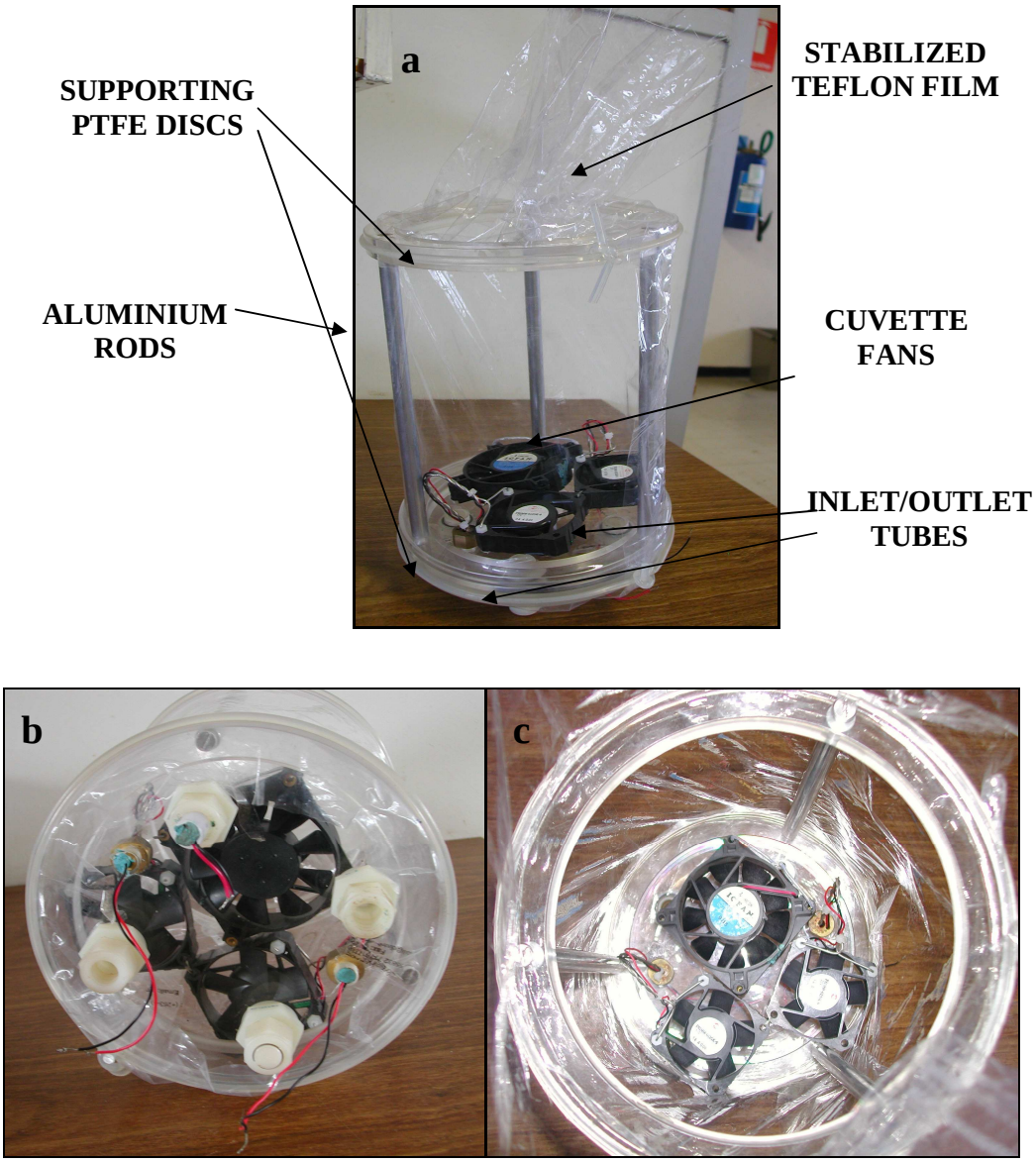

Figure 3.4 *The cuvette: (a) showing the three ventilation fans and the aluminium rods, (b) a view of the inlet and outlet connectors for the sampling tubes and the thermocouples (c) a closer look at the inside of the cuvette.*

Three ventilation fans; two small (type F62MM-012G K-9; MICRONEL LTD; Switzerland) and 1 large (SHICOH ICFAN Model 0820-12; SHICOH GIKEN CO. LTD, Japan) were connected to the

rigid Teflon plate on the cuvette. In addition two PTFA Teflon tubes were also connected, one for the air inlet and the other for the air outlet. The inlet tube was connected in such a way that it was just behind one of the ventilation fans to enhance suction of inlet air (Ennis *et al*., 1990) while the outlet tube was made to extend right up to the middle of the chamber so that the air that it collected could be as representative of the chamber conditions as possible. Three constantan-chromel thermocouples were introduced into the chamber through a hole in one of the ventilation fan supports. The hole was then sealed with putty to prevent air leakages and contamination. Metal clamps were use to join the Teflon plate to another hollow Teflon disc to create an air-tight seal.

Figure 3.5 *Picture showing how the cuvette was suspended above the branch.*

The metal clamps were also use to suspend the cuvette in the air over the branch so that the branch could be inserted into the chamber without damaging any part of the young branch's delicate structure. An elastic sealer was used to seal the chamber and keep it airtight when the branch was inserted.

3.4.2 Infrared gas analysis system

A closed path LI-COR LI-6262 (LI-COR Inc, Lincoln, Nebraska, USA) infrared gas analyzer operating in absolute mode was used to alternately measure ambient and cuvette values of CO_2 and H_2O mixing ratios.

Solenoid valves controlled by the first CR23X data logger (Z5) were used to switch the airflow between sampling the ambient and the cuvette air. Equal time intervals were used, i.e. 4 minutes sampling ambient air and 4 minutes sampling the cuvette. During the times when ambient air was being sampled, a pump flushed the cuvette with ambient air. The sampling unit consisted of a 3 m long

inlet sampling tube with a 47 µm Gelman filter at the inlet. A pump (Antriebstechnik GEFEG GmbH & Co. KG Hannover, Germany) operating on 12 V DC and capable of displacing 10 standard litres per minute (l min^{-1}) sucked in ambient air and passed it through a rotameter (Sho-Rate™ Brooks Instrument GmbH; Germany) which was used to regulate the flow rate and keep it nearly constant at 6.2 l min^{-1}. Between the pump and the rotameter, a pressure release valve was put in place to dissipate any excess pressure created by reducing the flow rate at the rotameter. This helped to increase pump life by decreasing the amount of work that it had to do to overcome the excess pressure. From the rotameter, the air passed through a thermal mass flow meter (MFM) (Model HFM 200; Teledyne Hastings Instruments, Hampton, Virginia, USA) which, in conjunction with a flow controller was used to monitor the inlet flow rate and to ensure that it remained reasonably constant. From the MFM, the inlet sample was split into two with a T-connector. One tube connected to the cuvette sample inlet while the other one was connected to solenoid valve 1 (**SV1**) (Fluid Automation Systems S.A.; Versoix, Switzerland). When the cuvette was being sampled, **SV1** ensured that the air entered through the cuvette only by closing the valve from the sample in side while allowing the air from solenoid valve 2 (**SV2**) (Fluid Automation Systems S.A.; Versoix, Switzerland) which was the air from the cuvette, to pass through it. While this was happening, the AC-powered flushing pump (KNFLab LABOPORT Vacuum Pump; KNF Neuberger GmbH, Freiburg, Germany) was venting air from the ambient through a T-tube.

On the other hand, when valve inlet 0 was open, air from the ambient entered straight through and to the outlet (2). In this position, inlet 0 for **SV2** was also open, allowing the flushing pump to flush the cuvette while ambient air was being sampled. Just after **SV1**, there were two dc 12v Teflon pumps (KNF Neuberger GmbH, Freiburg, Germany) each pumping 2.8 lmin^{-1} connected in parallel to give an effective suction rate of 5.6 l min^{-1}. These pumps were connected to the cuvette sample out tube and sucked the air from the cuvette. Their flow rate was slightly less than that of the inlet pump to ensure that there was always a slight positive pressure inside the cuvette while it was being sampled. This minimizes the contamination of the cuvette by additional external air through sucking while it is being sampled (Ennis *et al*., 1990). The other end of the two pumps was then first connected to a pressure-releasing valve before being connected to another manually controlled valve for reducing the flow rate. This valve was used to maintain the flow rate to the IRGA sample inlet at (1.2 ± 0.1) l min^{-1}. The same flow rate was used for calibration to ensure that the calibration and the measurement results were consistent and to cancel out pressure variations. A rotameter (Cole-Parmer Instrument Company Ltd; London, UK) with a full scale deflection of 5 l min^{-1} was placed just after the valve to monitor the flow rate and keep it constant. A 1 µm PTFE filter (Gelman Acro® 50; Pall GmbH, Germany) was placed after the rotameter just before the air entered the IRGA sample inlet to filter the air before it entered the IRGA. This was replaced once every month.

Since the IRGA was operating in absolute mode, airflow created by movement of the chopping shutter disc is sufficient to purge the reference cell of CO_2, but is not sufficient to remove all of the water vapour in the reference cell (LI-COR LI-6262 IRGA user manual). Therefore it was necessary to

purge the reference cell with CO_2 and H_2O free air. To do this, a scrubber containing equal measures of magnesium perchlorate and soda lime, separated by fibreglass wool was used. A small pump with a flow rate of 0.7 l min^{-1} was used to draw the air from the chopper (FROM CHOPPER) and scrub it in the scrubber before it went into the REFERENCE IN port at the IRGA. LI-COR's proprietary auxiliary reference pump LI-6262-04 pumps approximately 0.2 to 0.5 l min^{-1}. LI-COR claims that this is enough to purge the reference cell (LI-COR, 1996); therefore the 0.7 l min^{-1} used in this experiment was adequate for purging the reference cell. To ensure that magnesium perchlorate was not forced into the reference cell, the paper disk filters in the soda lime/desiccant tube were replaced whenever the contents of the tube where changed to avoid having torn filters. Additionally, a 1 µm PTFE filter (Pall Gelman) was placed between the soda lime/desiccant tube and the IRGA REFERENCE IN.

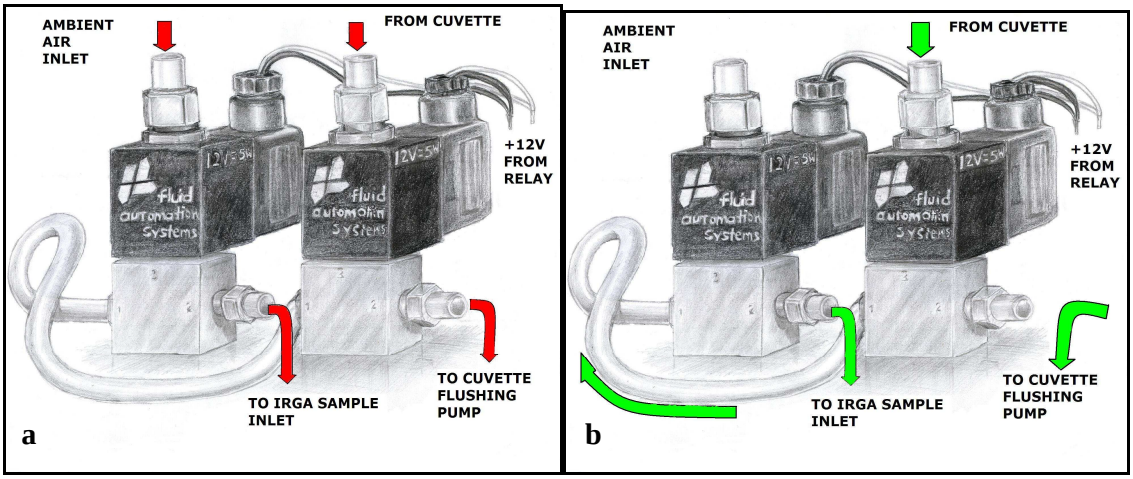

Figure 3.6 *Schematic diagrams of the switching valve mechanism. (a)shows the air flow through the valves when the system is sampling ambient air while the diagram (b) shows the airflow when the cuvette is being sampled*

Raw signals of CO_2 and H_2O were taken as single-ended voltages (in mV). The display of the IRGA was set to display signals in mV. Raw data was sampled at 10 Hz and the outputs were fed to the first CR23X data logger (Z5). Outputs collected from the IRGA were LI-COR temperature [ºC], CO_2 mixing ratio [mV] and H_2O mixing ratio [mV]. Pressure in the LI-COR sample cell was also monitored using an auxiliary pressure transducer (Pressure Transmitter Type PTB101B; Vaisala, Finland). All raw data collected was sampled at 0.2 Hz and averaged after every one minute. To ensure that errors incurred during valve switching and the time lag of airflow due to the long tubes were not included, the first minute of each 4 minute sampling interval for the H_2O and CO_2 raw data was not included in the flux calculations. Instead interpolation was done using ORIGINPro™ statistical software to fill the ensuing data gaps.

Condensation can be a major problem in setups where there are long tubes especially when water vapour flows through the tubes. In this experiment, water vapour condensation tended to occur mainly in the early morning when temperatures on the cuvette walls were still low. It also occurred in the regions of high pressure in the tubes (i.e. just before pressure regulating valves). Condensed water

vapour can create under-estimates of CO_2 mixing ratios (McDermitt *et al.*, c. 1990). Underestimation of mixing ratios due to water vapour was, however, expected to be minimal because the LI-6262 IRGA can, and was set to make water vapour and temperature corrections to CO_2 measurements of all sampled air. The real danger lay in having water condensing on the optical bench inside the analyzer. This had the potential to inflict damage on the IRGA which would require a lot of expensive repairs. Therefore, to avoid such a potential disaster, 22 mm diameter insulating jackets (Polymen® Schutzschlauch TYP 22/4 B2; Germany) were fitted on all external sampling and transmission tubes. Insulating jackets were also added on to the tubes from all pumps inside the sampling enclosure and on all tubes with valves and high pressure regions. The sample inlet also had a jacket fitted to it. Water vapour accumulation inside the cuvette due to transpiration was eliminated by maintaining a high flow rate through the cuvette (6.2 l min^{-1}) which resulted in a mean residence time of 88 s (cuvette volume was 7.948×10^{-3} m^3).

3.4.2.1 Calibration of the analyzer

The LI-COR IRGA is sensitive to temperature and pressure fluctuations. When it is moved from one place to another, the calibration values can shift easily Therefore calibrations were done *in situ,* i.e. all calibrations were done on the open-air lab on the roof where the experiments were carried out. Over a period of time, depending on the operating conditions, calibration values drift. As a result of this, it was essential to calibrate the IRGA regularly and to adjust the zero and span from time to time. All calibrations were done according to the recommendations of the manufacturer outlined in the IRGA user manual.

3.4.2.1.0 Water vapour calibration

Water vapour calibrations were done using the LI-COR LI-610 dew-point generator (LI-COR). Calibration points were at the dew-point temperatures of 0 ºC, 10 ºC, 20 ºC, 30 ºC and 40 ºC. The dew-point generator was set at 0 ºC initially and a flow rate of 1.2 ± 0.1 l min^{-1} was maintained at the IRGA sample inlet. A 1.0 µm Gelman filter was connected to the sample inlet tube. The dew-point generator was left to run while data from the IRGA was sampled every 5s and averaged every 10s. This was done to ensure that the resolution was as high as possible. When the reading for H_2O on the IRGA stabilized, which usually took just over an hour, the dew-point generator was set to the next dew-point temperature and further measurements were taken. Afterwards, the soda lime/desiccant was changed as well as the Gelman filter in preparation for the CO_2 calibration. The data points used to draw the calibration curve were derived from the average of the last stable readings (usually taking 10) of H_2O mixing ratio (mV) at each dew-point temperature. The signal was converted from mV to mmol mol^{-1} by using the exponential equation 3.1.

$$w(T_d) = 6136.5e^{\frac{17.502T_d}{240.97+T_d}} \quad [3.1]$$

where $w(T_d)$ is the mixing ratio of water vapour [mmol mol^{-1}] at any given dew-point temperature T_d [ºC].

The water vapour mixing ratios computed above where then plotted against the voltage signals and the calibration curve of LICOR mV reading against mixing ratio i.e. $w=w(u)$ was obtained.

3.4.2.1.1 Carbon dioxide calibration

For CO_2 calibration, two gas tanks with NIST traceable CO_2 at concentrations of 334.8 and 335.6 ppm were used. Additionally, NIST traceable high purity (99.99 %) nitrogen gas (AFROX, South Africa) was used to find the CO_2 zero. Nitrogen is used to find the CO_2 zero in such calibrations because it is inert. All gas tanks were fitted with regulators when they were used.

Using the regulator fitted on the N_2 gas tank, the flow of gas was adjusted until it gave a reading of (1.2 ± 1) l min^{-1} on the rotameter connected to the IRGA sample inlet. A Gelman 1 µm filter was also connected to the sample inlet path. The gas was left to flow through the IRGA for an hour, by which time the reading on the IRGA had stabilized. At the same time the data was being logged into the data logger as in the H_2O calibration. Next, the 334.8 ppm CO_2 gas tank was connected to the IRGA sample inlet and using the same procedure as the N_2 gas, data was logged. Finally, the 335.6 ppm gas was used to get the final calibration point. The three data points for the CO_2 calibration were obtained by averaging the last 10 stable readings of CO_2 (mV) from the data logger outputs for each gas.

A calibration line was then plotted of CO_2 concentration [ppm] against CO_2 [mV] from the gas tanks i.e. $c=c(u)$ from which any CO_2 signal from the IRGA could be converted to ppm or, preferably, µmol mol^{-1}. It was assumed that the relationship between the LI-COR IRGA signal and the gas concentration was linear in the CO_2 range prevailing throughout the experiment. It must be remarked that the CO_2 calibration was essentially a two point calibration through zero (N_2) and 335 ppm concentrations since the two none zero CO_2 concentrations were within the error limits of each other. A wider CO_2 calibration range could not be obtained due to several constraints one of which was the fact that the calibration gases are not available in Zimbabwe and importing one from South Africa would have been too expensive given the numerous procedures that one has to go through to transport a large gas cylinder. The error margins for the CO_2 calibration were thus unknown and had to be estimated. The results were however consistent with theory.

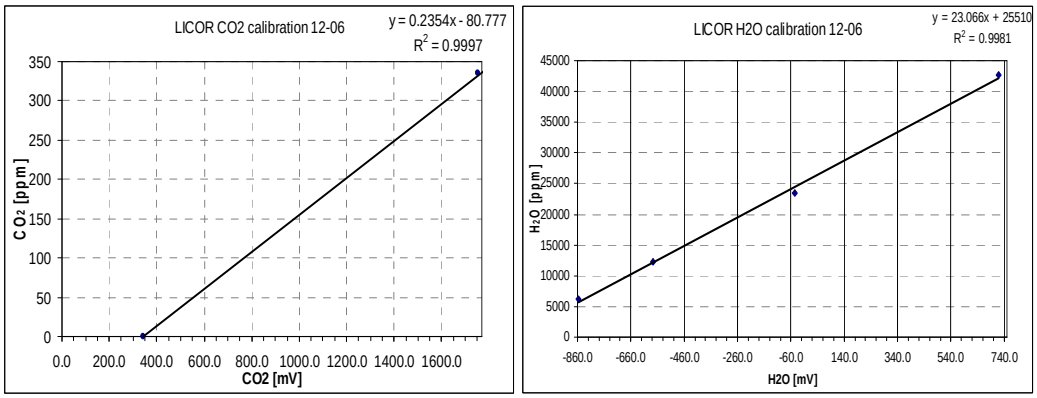

Figure 3.7 *Typical calibration lines for CO_2 and H_2O measurements from the IRGA. This particular calibration was done on 1 December 2006.*

3.5 Plant physiological and soil measurements

The physiological responses of the young trees to the changes in the microclimate were deduced from several processes such as carbon dioxide assimilation, transpiration rate, sap flow rate at stem and branch level and the diameter fluctuation at stem level. Each process was analyzed by specific components and/or sensors installed in the atmospheric and soil compartment of the potted plant (Figure. 3.1, Figure 3.3).

3.5.1 Transpiration and sap flow measurements

Transpiration, defined as the water vapour exchange between the leaves and the surrounding air, is the first process which is influenced when one of the atmospheric factors in the cuvette changes. The transport of water and dissolved substances (sap flow) occurs within the xylem vessels of the trees driven by the water potential gradients between the leaves and other organs of the tree. Thus in the short term, the sap flow rate is not equal to the transpiration rate.

3.5.1.1 Stem heat balance (SHB) theory

Most of this section of the thesis was extracted from the Dynagage sap flow sensor manual (van Bavel, 1999). The basic equations, the thermodynamics, and the calculation of the sap flow are all the same for both the SGA5 and SGA9 sap flow sensors – the ones used throughout this experiment.

3.5.1.1.0 Stem and heat balance basics

The SHB method requires a steady state and a constant energy input from the heater strip inside the gauge body. Therefore the stem section must be insulated from changes in the environment.

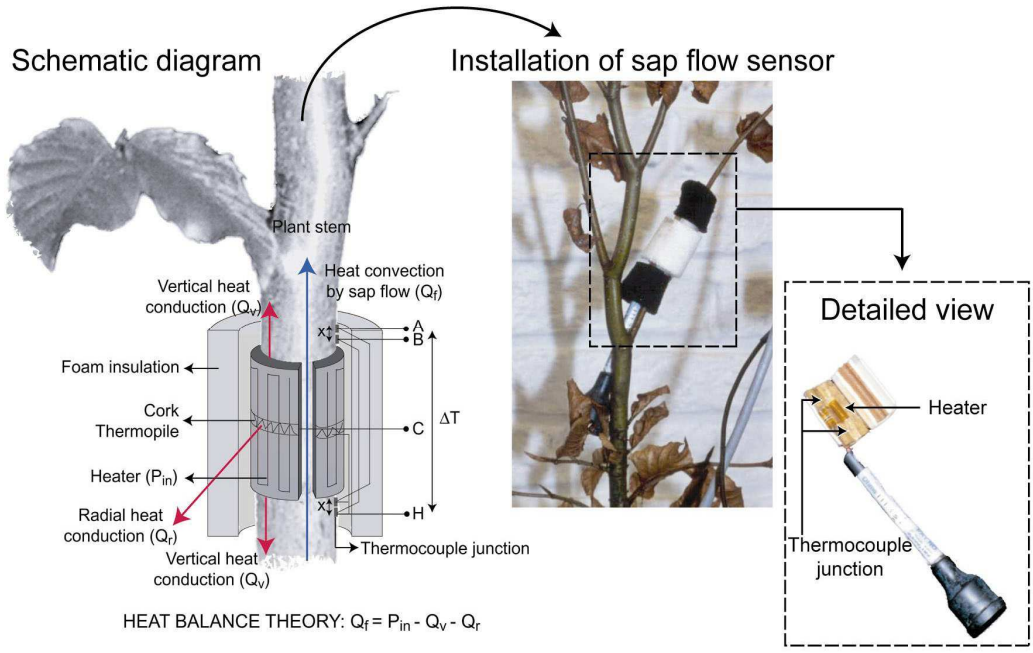

Figure 3.8 *Schematic diagram of the working principle of a Dynagage sap flow sensor (left). The heat balance of the stem section heated by the sensor is shown: P_{in} is heat applied to the stem, Q_v is the rate of vertical heat loss by conduction, Q_r is radial heat loss by conduction and Qf is the heat uptake by the sap stream. The wiring of the thermocouples in the sensor is also shown. For the determination of sap flow, the temperature differences ΔT_a, ΔT_b and ΔT_c are obtained from measurements of the voltages across AH, BH and CH, respectively. Installation of a sap flow sensor on a branch is shown on the right, along with a detailed view of the inside of the sensor (Steppe and Lemeur; 2003b, reproduced with permission).*

Figure 3.8 shows a stem section and the possible components of heat flux, assuming no heat storage. The heater surrounds the stem under test and is powered by a DC (Direct Current) supply with a fixed amount of heat; Q_h. Q_h is the equivalent to the power input to the stem from the heater, P_{in}. Q_r is the radial heat conducted through the gauge to the ambient. Q_v, the vertical or axial heat conduction through the stem has two components, Q_u (upward axial heat conduction through the stem) and Q_d (downward axial heat conduction through the stem). By measuring P_{in}, Q_u, Q_d and Q_r, the remainder, Q_f can be calculated. Q_f is the heat convection carried by the sap. After dividing by the specific heat of water and the sap temperature increase, the heat flux is converted directly to mass flow rate.

3.5.1.1.1 Energy balance equations

The energy balance is expressed as:

$$P_{in} = Q_r + Q_v + Q_f \qquad [3.2]$$

$$P_{in} = \frac{V^2}{R} \quad \text{from Ohm's Law} \qquad [3.3]$$

Fourier's Law describes the vertical conduction components:

$$Q_v = Q_u + Q_d \qquad [3.4]$$

where
$$Qu = K_{st} A \frac{dT_u}{dX} \quad [3.5]$$

$$Qd = K_{st} A \frac{dT_d}{dX} \quad [3.6]$$

where K_{st} is the thermal conductivity of the stem [W m^{-1} K^{-1}];

A is the stem cross-sectional area [m^2];

$\frac{dT_d}{dX}$ and $\frac{dT_u}{dX}$ are temperature gradients with T_u as the temperature of the upward axial sap flow and T_d the temperature of the downward axial sap flow.

dX is the spacing between thermocouple junctions [m].

One pair of thermocouples is above the heater and one pair is below the heater as shown on the schematic in Figure 3.8.

There are two differently wired thermocouples both measuring the rise in sap temperature. Channel *AH* measures the difference in temperature *A*-H_a (mV). Channel *BH* measures the difference in temperature *B*-H_B (mV). By subtraction of these two signals:

$$BH - AH = (B - H_b) - (A - H_a) = (B - A) + (H_a - H_b) \quad [3.7]$$

The result yields the two components of axial heat conduction out of the stem section, Q_u and Q_d. Since the distances, *dX*, separating the upper TC pair and lower TC pair are fixed by design for each particular gauge to the same value; the components of Q_v are combined with a common denominator:

$$Q_v = \frac{K_{st} A(BH - AH)}{dX \times 0.040\ mV/^oC} \quad [3.8]$$

The factor 0.040 mV/ºC converts the thermocouple differential signals to ºC. K_{st} values are given for varying stem conductivity:

0.42 W/m K –Woody stem;

0.54 W/m K – Herbaceous stem and

0.28 W/m K – Hollow stem.

3.5.1.1.2 Sap thermodynamics

After solving Equation 3.2 for Q_f, the flow rate per unit time is calculated from the equation for sap flow as described by Sakuratani (1981) and Baker-Van Bavel (1987). This equation takes the residual of the energy balance in Watts, and converts it to a flow rate by dividing by the temperature increase of the sap and the heat capacity of water. Water is 99 % of the sap content and it is safe to assume the heat capacity, C_p, is constant in all stems. It is understood that a Watt, being 1 J s^{-1}, will be converted to a flow rate (g s^{-1}) when divided by 4.186 J g^{-1} ºC^{-1} and divided by the temperature increase in °C.

$$F = \frac{(P_{in} - Q_v - Q_r)}{C_p dT} \quad [3.9]$$

where F is the sap flow rate [g s^{-1}].

In Equation 3.2 the radial heat loss is computed by:

$$Q_r = K_{sh} CH \qquad [3.10]$$

K_{sh} is the thermal conductance constant for a particular gauge installation explained in more detail in the next section.

C_p is the specific heat of water (4.186 J g^{-1} $^oC^{-1}$), and

dT is the temperature increase of the sap.

The temperature increase of the sap dT, is measured in mV by averaging the AH and BH signals, and then converted to ^oC by dividing by the thermocouple temperature conversion constant as follows:

$$dT = \frac{(AH + BH)/2\,(mV)}{0.040\,mV/^oC} \qquad [3.11]$$

3.5.1.1.3 Apparent K_{sh} calculation

The thermodynamics equation of a heated fluid in an insulated cylindrical section at a constant temperature is included below to indicate the source of the K_{sh} computation and the effects of the cylinder's thermal conduction.

$$Q_r = 2\pi K_{co} L \frac{(T_i - T_o)}{\ln\left(\frac{r_i}{r_o}\right)} \qquad [3.12]$$

where K_{co} is the thermal conductivity of the cork substrate surrounding the heater. This is where the thermopile junctions, typically 8 to 12 in Dynagage construction, alternately measure the temperature adjacent to the heater and on the outside of the cork.

L is the length of the cylinder.

T_i and T_o are the inner and outer temperatures of the insulating cylinder.

r_i is the inner radius, and

r_o is the outer radius. For an installation of a fixed diameter, the

K_{sh} represents all of the parameters and constants in the above equation, and relates the radial heat flux to the thermopile output CH by a constant factor as follows:

$$Q_r = K_{sh}(C - H_C) \qquad [3.13]$$

Since the signal (C-H_C), or simply CH, input to the data logger is directly proportional to the temperature difference between inner and outer layers of the cork substrate and therefore the heat transfer radially. The sheath conductance is calculated when the user establishes a no-flow condition.

The calculation for K_{sh} is determined by solving Equation 3.2 when setting Q_f =0 as follows:

$$P_{in} = Q_r + Q_v \qquad [3.14]$$

and

$$Q_r = K_{sh}(CH) = P_{in} - Q_v \qquad [3.15]$$

So after computing P_{in} and Q_v,

$$K_{sh} = \frac{P_{in} - Q_v}{CH} \qquad [3.16]$$

Apparent K_{sh} (the calculated value) is computed at all times for observation. Values of the first overnight K_{sh} were checked at a predawn average, and the average was entered in the logger sap flow computation program as the K_{sh} zero set point, or the K_{sh} setting in use. The other parameters required for solving the equation above were also entered into a sap flow calculation spreadsheet. The heater impedance, the stem area, the TC gap, and the thermal constant K_{st}, were required to compute P_{in} and Q_v, before a proper K_{sh} could be determined. A default value of 0.2 was used as the K_{sh} zero set. After determining the first K_{sh} value, two further adjustments were done to the predawn K_{sh} values on the two following days as the sensor conformed to a snug fit and adjusted to the shape of the stem.

The minimum K_{sh} occurs at the point when CH is at its peak value one to two hours before dawn. When the radial loss is at a maximum it is because the convection heat flux is at a minimum. Since crops and other plants grow, the K_{sh} will creep up as time goes on, noting the effect on the ratio of inner to outer diameter in the third equation. The K_{sh} was routinely checked to ensure that it had not drifted, and if it had, it was recomputed and reset to obtain the best results.

3.5.1.1.4 Low flow rates

There are two data filters advised for general logger programs to check the quality of the data, and reject flow computation at periods when the sensor signals are either below the minimum threshold or above the maximum flow capacity of the sensor. The flow rate filter takes care of the initial conditions where dT approaches zero, or less than zero, and it can also flag the user when negative Q_f is computed, in the instance of a K_{sh} setting not being made at its minimum value. It was performed on a spreadsheet after downloading the data.

When the vertical and radial heat fluxes are subtracted from the power input, Q_f is the remaining power carried by the sap. In the case of a zero flow rate on a very small stem, the temperature increase dT approaches zero. For these cases the flow may be grossly exaggerated with a minor residual Q_f. A true zero flow rate with accompanying dT of zero is rarely noticed on large plants, trees, or crop plants in a natural, growing condition. It takes only 3-4 grams per hour water flow to cause a positive dT on a 16 mm diameter plant. (van Bavel, 1999).

To make proper use of the accumulator at low flow rates the algorithm tests first to see:

$$\text{IF } 0 \leq Q_f < 20\ \%\ P_{in}\text{, AND IF } dT < dT_{MIN}$$
$$\text{(i.e. } dT_{MIN} = 0.75\ ^{o}\text{C in a normal program default)} \quad \text{THEN } F = 0 \qquad [3.17]$$

However:

dT_{MIN} = 1.0 ºC to 1.2 ºC for plants that use water at night.

In the study of small stems, dT may be negative during the evening and may be at near zero for an entire evening. Negative and distorted flow rates are screened out using the first filter procedure.
The second phase of this filter is:

$$\text{IF } Q_f < 0$$
$$\text{THEN } F = -0.036\ \text{gh}^{-1} \qquad [3.18]$$

Forcing a -0.036 g h^{-1} into the flow rate output provides a convenient flag value to be noted by the user. A flag is then set for condition 1 when it is necessary to inspect the data for re-evaluation of the K_{sh} setting. The K_{sh} may not be set perfectly, and it is possible that a negative residual Q_f is computed, especially after sundown when a loss of heat storage gets interpreted as a negative Q_f for a few hours. By using the second phase of the low filter, the disruption of the accumulator is avoided. Minor negative excursions in Q_f are possible in circumstances of released heat storage in the stem and the gauge jacket. During the evening hours when the heat storage is negative, caused by the ambient and gauge dropping in temperature, a negative Q_f is commonly noted for a few hours after sunset. However these effects are normally short in duration and will not affect the overall performance of the Dynagage.

3.5.1.1.5 High sap flow rates

The temperature increase of the sap is a concern when flow rates are very large. There is a hyperbolic dependence of the flow rate on the temperature difference dT. Since the minimum temperature corresponds to the maximum flow rate, the practical limitation of high flow rate is computed from an analysis of the instrument sensitivity and the estimate of the practical limits on thermal noise. The maximum gauge flow rate can be determined by a signal analysis that compares the maximum output error due to the expected limits of input error for various situations, and then checking the maximum error against accuracy goals. This procedure is explained in this section with a specific example.
The assumption of thermal sensing error in the sensors is that dT can be measured with about 0.1 ºC accuracy, and the accuracy of the data logger is assumed to be no less than ± 1 µV (representing a 0.025 ºC error). For error analysis the ±dT of 0.1ºC is superimposed on dT, and then the potential error

can be expressed as a percentage of the total flow rate. If the potential error is over 30 %, the flow data is judged to be unacceptable. When the flow rate is exceptionally high, the Q_v component becomes very low, the radial flux approaches zero, and almost all of the heat is absorbed by the sap. These conditions are characterized by Q_f greater than 80 % of P_{in}. During the conditions of Q_f nearing P_{in}, the major determining variable left is the temperature increase, *dT*. As the flow increases, *dT* asymptotically approaches zero, as the trend in the afternoon indicates. As *dT* becomes smaller with increasing flow rates, thermal noise from radiation or other effects can cause a major exaggeration in flow. The use of a high flow-rate filter prevents a distortion of the accumulated flow over those rates that are reasonable:

$$F_{max} = AV_{max}$$

If $F > F_{max}$,

Then $F=F_{max}$, SET OVERFLOW FLAG IF AVAILABLE [3.19]

At *dT* values under about 0.24 º C, the maximum flow rate, and therefore an overflow condition is reached. The temperature stability of the Dynagage and the interconnections can be assumed to be no better than ± 0.1º C. Therefore the flow rate errors at dT = 0.24ºC, ± 0.1ºC, could indeed be significant if it were not prevented by the high flow rate filter. A flag may be set in software, depending on the sap flow system to indicate a possible error condition.

To prevent thermal noise from becoming a large percentage of the measured signal, the power to the heater was kept at a constant value by using a heater voltage of 3V. This voltage not only reduced thermal noise, but it was low enough to prevent the early morning sap temperature from rising beyond the safe limit of 6-7 º C.

3.5.1.2 Gauge installation and maintenance

Gauge installation on the young citrus trees was performed according to the recommendations of the manufacturer outlined in the installation manual by van Bavel (1999). A brief overview of the installation process is outlined below:

3.5.1.2.0 Preparing stems and branches

First, the stems and branches were measured to ensure that the diameter was within the range of the specified gauge. A micrometer screw gauge (Mitutoyo, Japan) was used for this purpose without a problem since the trees were young and had diameters within the measurable range of the micrometer screw gauge.

Noting the installed height in the mechanical specifications, the girth was measured at the midpoint for the gauge position; the diameter was recorded from which the sectional area (in cm^2) was calculated for entering into the setup constant settings. The procedure was repeated two more times to obtain an average reading for the sectional area. This was done both for the stem and the branch for all four trees

on which sap flow gauges would be installed. The sections of the stems or branches were carefully selected such that they were free from petioles, leaves, large scars, or other irregularities.

Accumulations of naturally occurring dead bark (see Figure 3.9) was removed by very light sanding with medium-fine sand paper. Sanding was kept to a minimum to prevent penetration through the live, green, cambium layer. It was not required at all for the branches because they had very thin layers of bark which looked almost herbaceous.

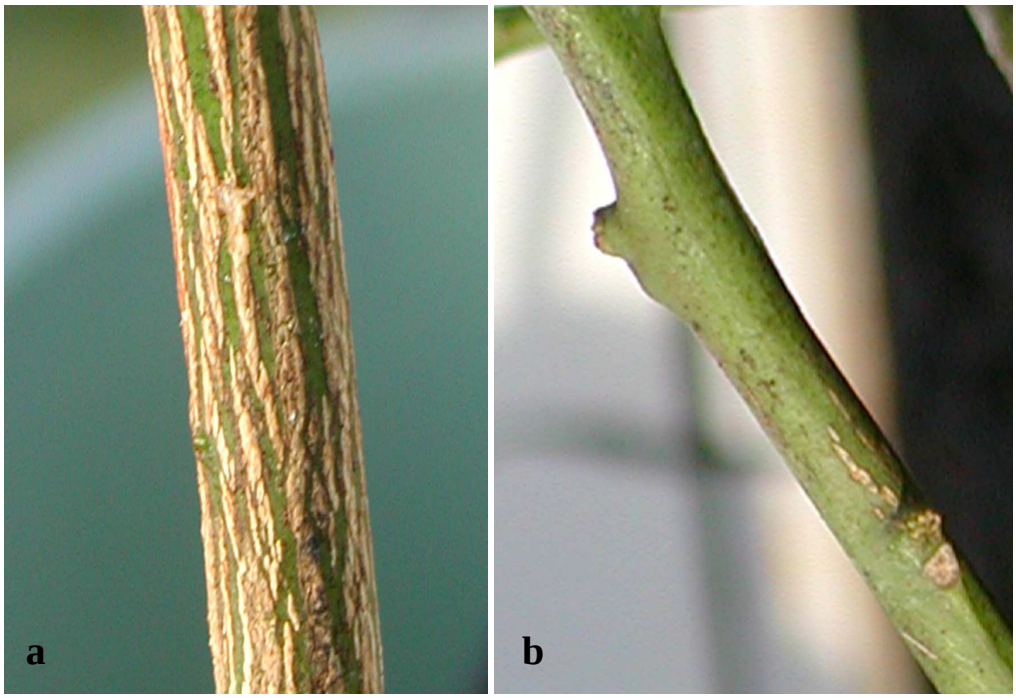

Figure 3.9 *Illustration of the consistence of the trunk stem and the branch stem of one of the young citrus trees. Note the absence of bark on the branch stem (right).*

Care was taken to ensure that the stem installation was not close to the ground to prevent excessive temperature gradients. Installations were also carried out above the rootstock graft to prevent errors that are likely to occur from taking measurements on the scar tissue of the graft. The appropriate sap flow gauges were installed on the stem or branch after using the manufacture's diameter to gauge suitability criterion. The diameters and corresponding sensors used are outlined in Table 3.2.

Table 3.2 *List of parameters for the sap flow gauges*

TREE	STEM DIAMETER (±0.005 mm)	BRANCH DIAMETER(mm) (±0.005 mm)	STEM GAUGE/RESISTANCE (±0.005 mm)	BRANCH GAUGE/RESISTANCE (±0.005 mm)
Tree1	6.492	4.837	SGA5/173.0Ω	SGA5/171.3 Ω
Tree2	10.092	4.495	SGA9/121.1 Ω	SGA5/162.2 Ω
Tree3	10.092	4.495	SGA9/121.1 Ω	SGA5/162.2 Ω
Tree4	6.492	4.837	SGA5/173.0Ω	SGA5/171.3 Ω
Tree5	-	-	-	-
Tree6	-	-	-	-

A completed setup on Tree2 is shown in Figure 3.10.

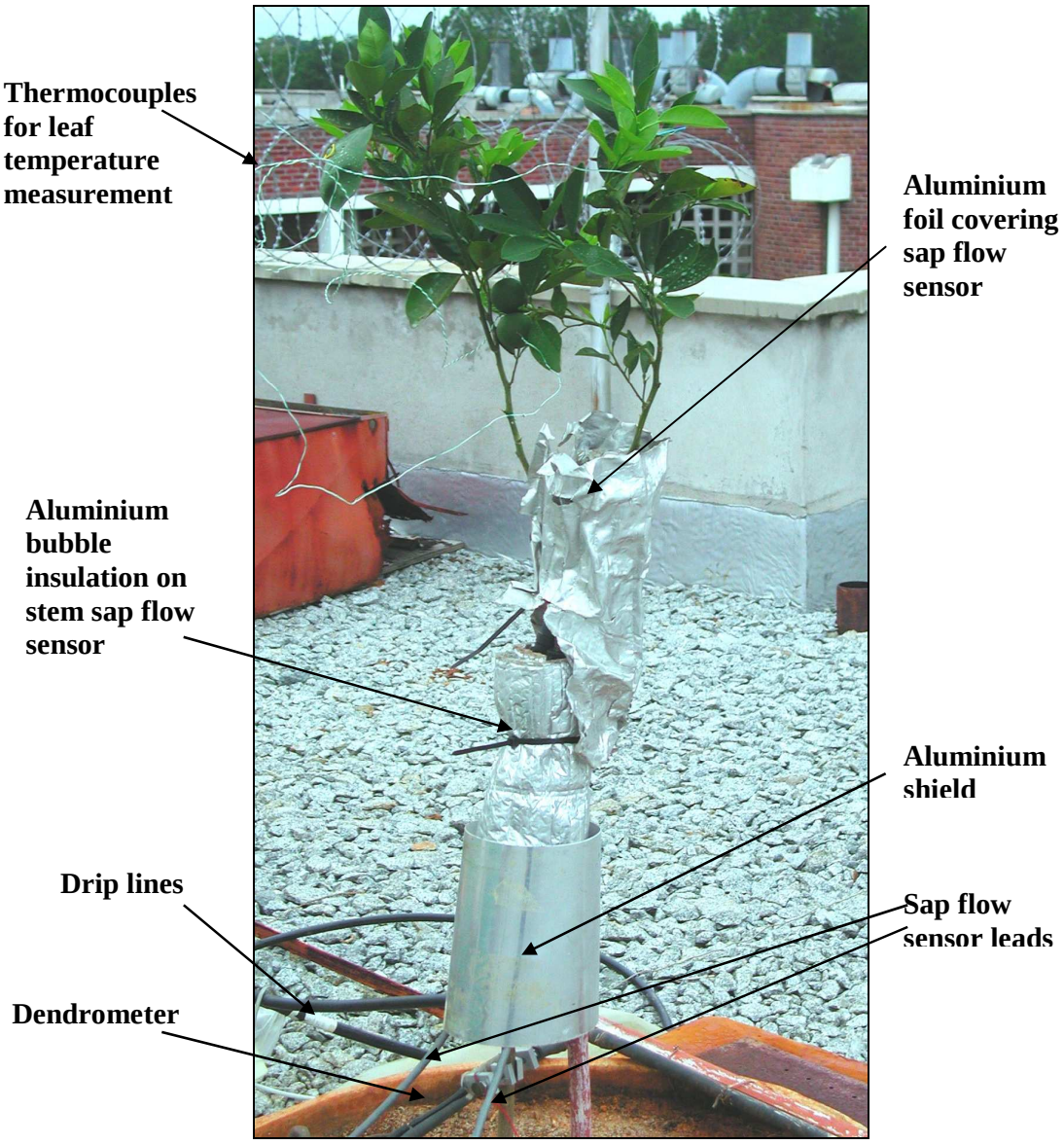

Figure 3.10 *Sap flow sensors on Tree2 showing the radiation shields and aluminium foil*

The shield kept out water and prevented radiation from affecting readings. Additionally, an aluminium foil was put in place as a form of shading to prevent sunlight from affecting the sensitive energy balance readings on the exposed trunk or stem below the gauge. Accurate sap readings on branches and vines were aided by triple wrapping the segment below the gauge as well as above with foil, since the sun could strike the branch at various times of day.

3.5.1.3 Stem diameter measurements

The stem diameter was measured for each tree at the time that the branch cuvette was connected to the tree. This was done using a carefully calibrated DEX-20 (DEX Inc., USA) dendrometer. In brief, calibration was carried out by determining the voltages resulting from a range of displacements of the dendrometer strain gauge. It was installed as illustrated in Figure 3.10. The stem diameter measurements were useful for determining growth of the young trees under different imposed radiation levels.

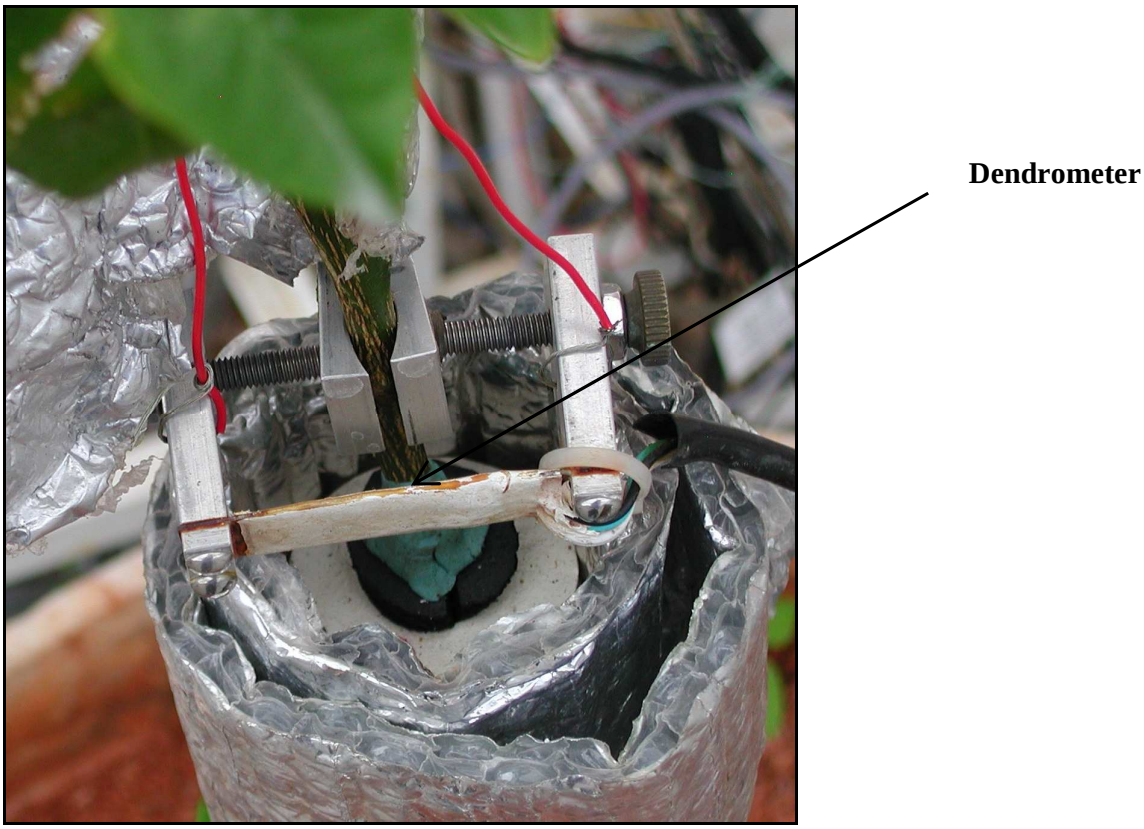

Figure 3.11 *The dendrometer, a linear variable displacement transducer (LVDT) installed on a stem*

3.5.1.4 Leaf and cuvette temperature measurements

Leaf temperature was one of the most important parameters required in the efforts to fulfil the objectives of the thesis. Measurements of leaf temperatures were made using calibrated thermocouples on 4 sample leaves –two inside the cuvette and two on the branches outside the cuvette. Monitoring of the difference between the cuvette temperature and the ambient temperature was done to ensure that there were no large differences between cuvette leaf temperature and external leaf temperature. Large, temperature differences, typically those above 5 °C meant that the cuvette measurements were not as representative of the whole tree as possible. It must be stated, however, that the cuvette microclimate could never be fully representative of the ambient conditions but efforts have to be made to ensure that the plant does not feel that it is in an enclosure by mimicking the external environmental conditions as far as possible. This was achieved by maintaining high ventilation rates inside the cuvette as explained

earlier in this Chapter. Additionally, another thermocouple was used to monitor the cuvette temperature.

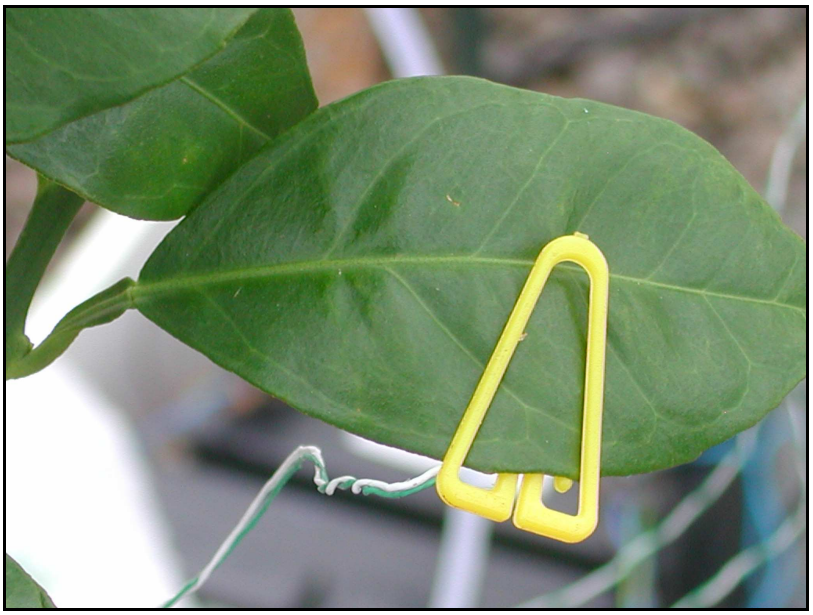

Figure 3.12 *Leaf temperature measurement on a leaf, Tree4. Plastic paper clips like the one shown above were used to fasten the thermocouple to the bottom of the leaf. This arrangement also ensured that direct solar radiation, which would have induced errors, did not fall on the thermocouples*

3.6 Soil measurements

3.6.1 Soil water potential

Soil matrix potential was measured in 4 potted plants using Equitensiometers (Model EQ2; Delta-T Devices, Cambridge, UK). These measurements were useful, particularly in determining soil moisture status and also as one of the input variables for the modelling of sap flow.

3.7 Auxiliary measurements

3.7.1 Pressure

IRGA pressure was measured using a piezoelectric pressure transducer (Model PT101FB; Vaisala, Finland). It was important to continuously monitor the IRGA pressure so that corrections could be made to the IRGA data if the pressure changed significantly.

3.8 External environment measurements

3.8.1 Net radiation

Net radiation inside the shelter was measured at 1.8 m using a thermopile net radiometer (REBS Q*7.1; REBS, Seattle, Washington, USA). The sensor was placed near the cuvette to obtained data which could be as representative of the cuvette microclimate as possible. It was important to deduce how shade nets affected the net radiation under them.

3.8.2 Incoming solar radiation

Global solar radiation was measured with two sensors: a CM11 (Kipp & Zonen; Delft, The Netherlands) Pyranometer installed outside the shelter and a LI-COR Pyranometer (#PY3 7993) (LI-COR Radiation Sensors, Nebraska, USA) installed inside the shelter.

3.8.3 Temperature, relative humidity and wind speed

Temperature and relative humidity were measured using HMP45AC (Campbell Scientific Inc., Leicestershire, UK) temperature-relative humidity sensors. Two sensors were used: One monitored the conditions outside the shelter while the other was used to monitor the conditions near the cuvette and below the shade net (when one was in use).

Wind speed was measured with a wind vane (Wind Sentry) while wind direction was measured with an AL cup anemometer, A100L2 (Vector Instruments; Rhyl, UK)

3.9 Power supply and backup unit

To ensure that there was minimal interruption of the data logging process, extra care was taken in designing the power supply system to deal with potential causes of interruptions such as power cuts which were very frequent throughout the measurement period. All the equipment used could be powered from a 12V DC supply.

Two batteries (EXIDE 12V lead-acid accumulators; 60Ah; Battery World, Harare, Zimbabwe) were connected to the 12V rail of the setup's power supply through a simple diode-OR circuit (see Figure 3.3) which ensured that at any given time, the experimental system was being powered from the electrical 12V power supply or the batteries or both.

Spurious noise was generated by the electric motors in the 12 V dc lines, particularly as the brushes of the motors began to wear out. To avoid the noise affecting the digital signal lines in the data loggers, the data loggers were powered from a separate DC source. Two 6 V, 7AH batteries (Yuasa Enersys NP7-6 6V 7.0 Ah sealed rechargeable lead-acid battery; Enersys Inc., Taiwan) were connected in series and the 12 V output was then connected to all the 3 data loggers. The batteries were also connected to the LI-COR IRGA DC input, which acted as the battery charger when there was AC available. When there was power loss, the batteries powered the LI-COR in addition to the data loggers. The 7AH batteries were capable of powering the LI-COR and the data loggers continuously for a period of 5 hours, which was usually the maximum time for any electrical power outage event. The two 60 Ah batteries were capable of powering the rest of the equipment for about 3.5 days. The 60 Ah batteries were continuously charged using a 12 V battery charger (Batteriemaster, Einhel; Germany).

3.10 Data acquisition unit

A data acquisition system (Figure 3.3 and Figure 3.13) comprised of a Windows®-based computer and three Campbell Scientific CR23X data loggers, each with 1 MB of flash memory for data storage. Figure 3.13 summarizes the data logger setup.

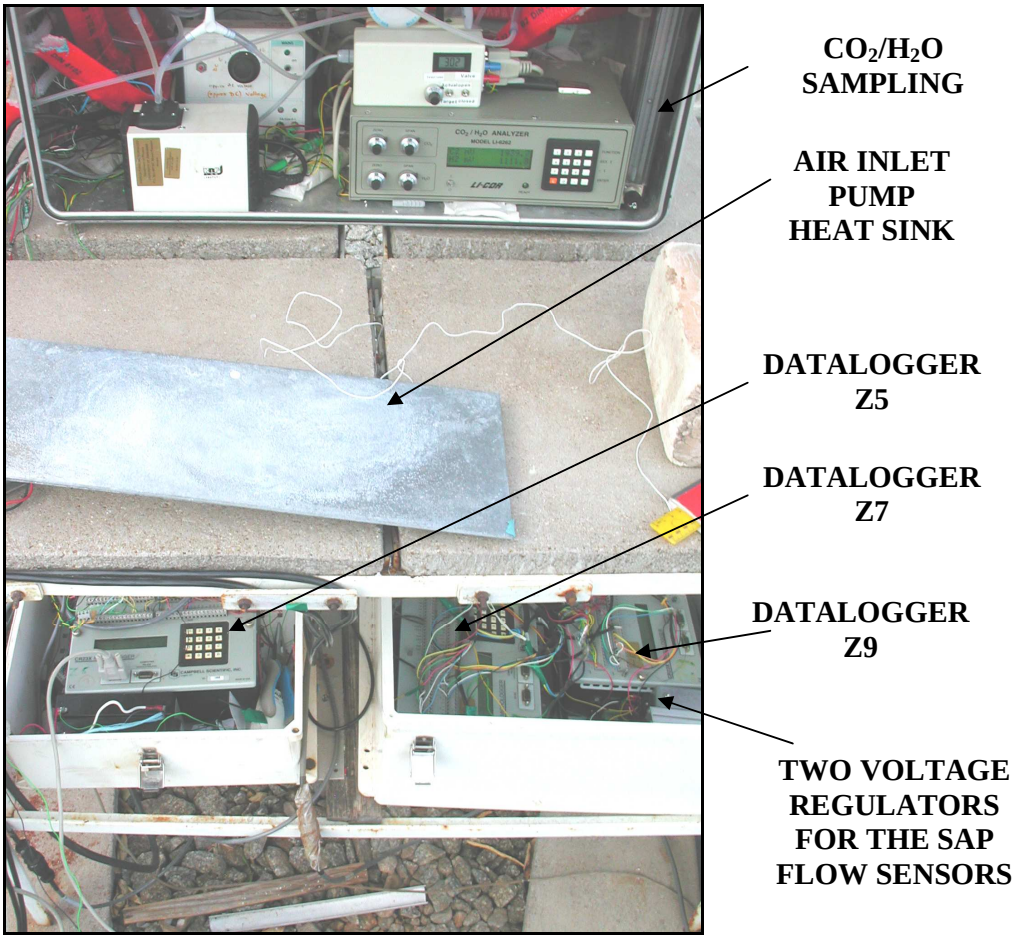

Figure 3.13 *The IRGA and the three data loggers*

Data loggers Z5, Z7 and Z9 sampled raw signals at 5 second intervals and averaged them at 1 minute intervals. Z5 had 3 output (P92) instructions and any attempt to keep the sampling interval at 1 second resulted in a Table Overflow Error. It was therefore necessary to increase the sampling interval and 5 seconds was the next most suitable interval.

Two programs were used for data acquisition: PC400 and PC208W (Campbell Scientific, Edmonton, USA). PC400 was the program that was used for downloading data throughout the measurement period particularly because of its versatility, ease of use and extended features such as Shortcut. Its subsidiary program Edlog was used for modifying and compiling the data logger input programs whenever necessary. On the other hand, PC208W was useful for calibration and test purposes because of its useful real-time graph function. This function enabled the variations in parameters under study to be followed in detail. Thus in a calibration or test situation, it was easy to tell when a signal became stable.

3.11 Data analysis

3.11.1 Gaseous Flux calculations

From the data collected from the IRGA and other related variables, we wish to calculate fluxes of CO_2 and H_2O to or from the branch inside the cuvette.

Using a mass balance technique adapted from Ennis *et al*. (1990) and Hari *et al*. (1999), fluxes of carbon dioxide and water vapour from the branch in the cuvette were calculated as

$$F_j = \frac{\lfloor q_{in} m_{in,j} - (q_{out} + q_l) m_{out,j} \rfloor}{A V_{m,0} (\frac{p}{p_0}) \left(\frac{273.15 + T}{273.15} \right)} \qquad ,j = CO_2, H_2O \qquad [3.20]$$

where F_j is the CO_2 or H_2O flux into or out of the branch

q_{in} is the flow rate at the cuvette inlet [l min^{-1}]

q_{out} is the flow rate at the cuvette outlet [l min^{-1}]

q_l is the leakage flow rate due to the difference between cuvette inlet and outlet flow rates [l min^{-1}]

$m_{in,j}$ is the mixing ratio of CO_2 or H_2O at the cuvette inlet (ambient CO_2 mixing ratio) [µmol mol^{-1}]

$m_{out,j}$ is the mixing ratio of CO_2 or H_2O at the cuvette outlet [µmol mol^{-1}]

A is the projected leaf area of the branch [m^2]

$V_{m,0}$ is the molar gas volume (22.4 l mol^{-1}) at STP (0 ºC, 101.25 hPa) [l mol^{-1}]

T is the temperature inside the cuvette [ºC]

p is the IRGA pressure [hPa]

p_0 is the standard atmospheric pressure (101.25 hPa)

Leakage tests performed on the cuvette proved that losses were ≤ 1%. Therefore q_l was neglected when carrying out the flux calculations using Equation 3.20 and also for the error analysis shown in Equation 3.21.

The total uncertainties in the flux measurements, σ_{Fj}, were calculated using the Gaussian error propagation technique:

$$\sigma_{F_j} = F_j \times \sqrt{\left(\frac{\sigma_{q_{in}}}{q_{in}}\right)^2 + \left(\frac{\sigma_{q_{out}}}{q_{out}}\right)^2 + \left(\frac{\sigma_{m_{in,j}}}{m_{in,j}}\right)^2 + \left(\frac{\sigma_{m_{out,j}}}{m_{out,j}}\right)^2 + \left(\frac{\sigma_A}{A}\right)^2 + \left(\frac{\sigma_p}{p}\right)^2 + \left(\frac{\sigma_T}{T}\right)^2} \qquad [3.21]$$

where σ denotes the calculated or estimated standard deviation of the subscripted character in front of it. All other symbols have their usual meanings explained earlier.

All variables were assumed to be independent of each other.

Calculated total uncertainties for all the variables usually did not exceed 20 %. The biggest contributors to the total uncertainty were the leaf area and the flow rate which fluctuated when the pumps were running on batteries during power outage events. The measurements can therefore be considered to be reasonably reliable.

3.11.1.1 Sign convention

The sign convention used throughout this thesis for CO_2 and H_2O flux is positive out of the branch (emission) and negative into the branch (deposition).

3.11.2 Performance of the sampling system

To minimize errors in flux calculations as much as possible, it was necessary to analyse the sampling system, particularly the cuvette, for possible losses of trace gases and water vapour by various processes. The main pathways of loss in branch chamber systems are adsorption by the walls of the cuvette (plastic), absorption, chemisorption and diffusion.

3.11.2.1 Cuvette Tests

Several tests were carried out on the cuvette, with the main purpose of the tests being to identify artefacts and other sources of systematic errors arising from the cuvette itself. The data from these tests was then used to make corrections on the actual data so that errors could be minimized.

3.11.2.1.0 Blank test

In order to test for leakages in the cuvette, a series of tests were run in which the cuvette was sealed but with no plant sample placed in it. The tests showed that the cuvette retained neither CO_2 nor H_2O greater than the error margin of the IRGA. Additionally there were was no significant gain of CO_2 or H_2O. The results are shown in Chapter 4.

3.11.2.1.1 Potted plant test

An elephant ear plant (*Colocasia Esculentum*) was placed in the cuvette and its CO_2 and H_2O exchange was monitored by the IRGA for 9 hours. This was done to compare its behaviour with that of the citrus trees. The elephant ear (Figure 3.14, left) is known to be a well-behaved potted plant while citrus trees are known to behave differently from many other plants in terms of their CO_2 and H_2O assimilation and emission (e.g. the occurrence of stomatal cycling). The projected leaf area of the elephant ear was measured using graphing paper with unit area of 1 mm^2. The results were then converted to m^2. The fluxes obtained were normal and there was no evidence of stomatal cycling at any stage. The test was run on a clear, sunny day. The results for this test are shown in Chapter 4.

3.11.2.1.2 Mixing test

Just after the cuvette was constructed, tests were run to determine its ventilation rate. First one fan was connected and measurements of air velocity were made perpendicular to and parallel to the long axis

of the cuvette at various distances from the position of the fan. The instrument used was a heated bead anemometer (Testo GmBH, Germany). After discovering that the mixing was not so good with one fan, two more fans were added (Figure 3.4) and the tests then confirmed that the mixing was quite good. The average air velocity near the cuvette fans was 4.03 ms^{-1}, which was good enough to thoroughly mix the air in the cuvette. Chapter 4 shows the results of the mixing test.

3.12 Characterization of the shade net

The shade net was woven out of a black plastic mesh. Two nets were available for the experiments with double shading being achieved by using two layers of nets. The dimensions of each net were 10 m × 5 m (L × W). To determine the properties of the shade net with respect to the transmission of solar radiation, a series of experiments was run. Two cross-calibrated pyranometers (LI-COR Inc.) serial numbers PY30406 and PY32951 were first exposed to full solar radiation on the experimental site for several days. A single layer shade net was used to cover pyranometer PY30406 for several hours while PY32951 and a KIPP Pyranometer acted as controls (exposed to full solar radiation). Later, a double-layered shade net was applied on the PY30406. A comparison of the two shaded regimes against the unshaded regime was used to derive the solar radiation transmission coefficients for the shade nets. The net was 1 .0 ± 0.1 m away from the sensor. This was the same distance away from the branch and the radiation sensors that the shade net was kept at during flux measurements.

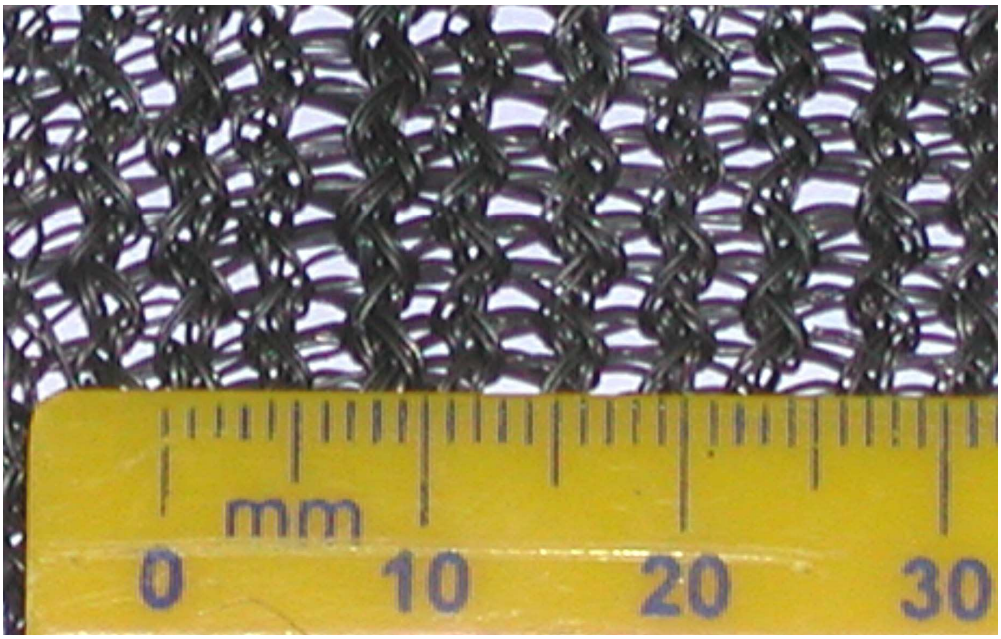

Figure 3.15 *A detailed view of the shade net used in the canopy radiation suppression measurements. The metre rule has been added to emphasize scale and to get an idea of the size of the meshes*

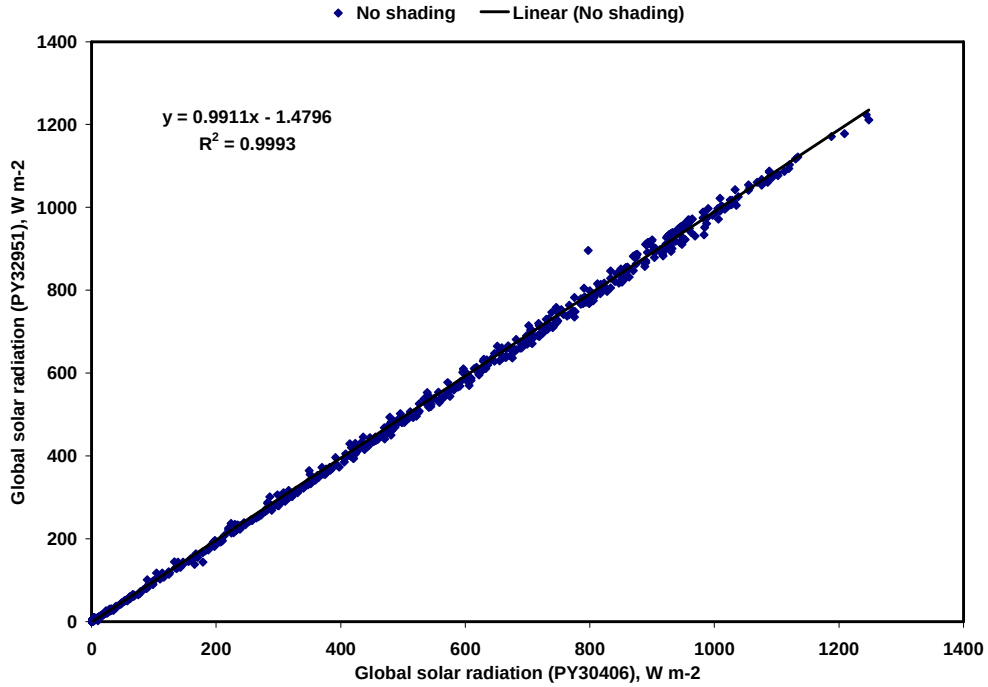

Figure 3.16 *Cross-calibration curve of the two LICOR pyranometers used for the shade net characterization. The calibration curve revealed that the error between the two instruments was less than 5 % and so there was no need to make adjustments to their original calibration constant.*

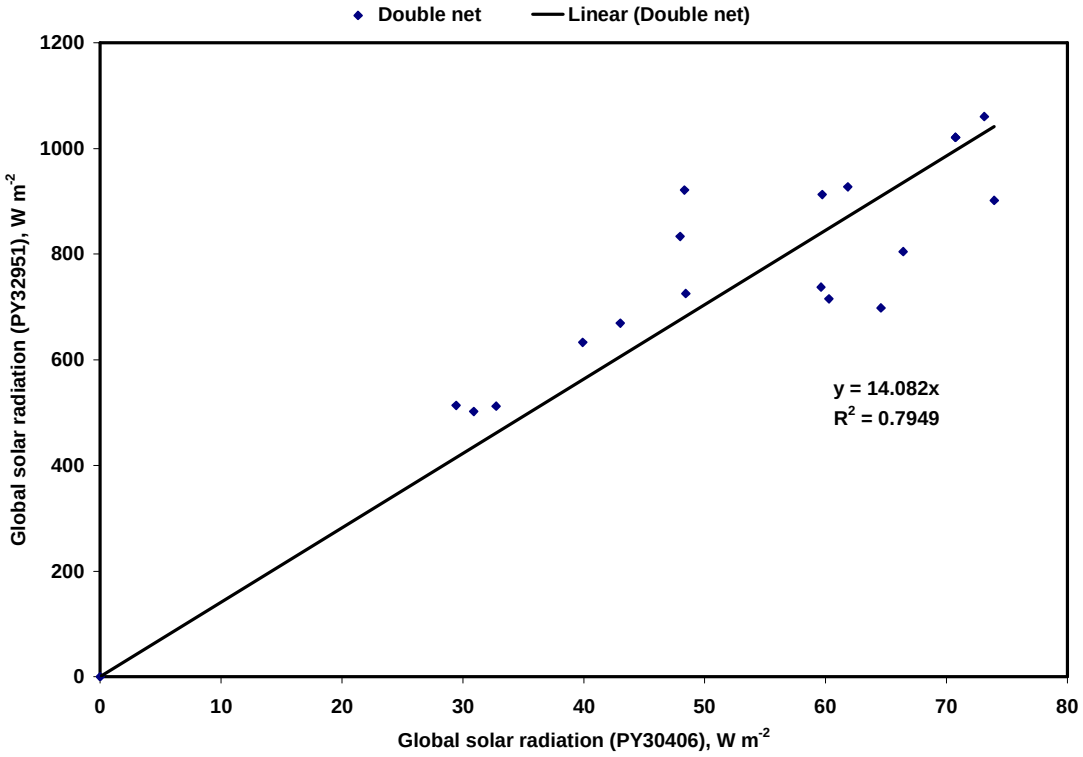

Figure 3.17 *Regression line of the Pyranometer cross-calibration with a double net on PY30406.*

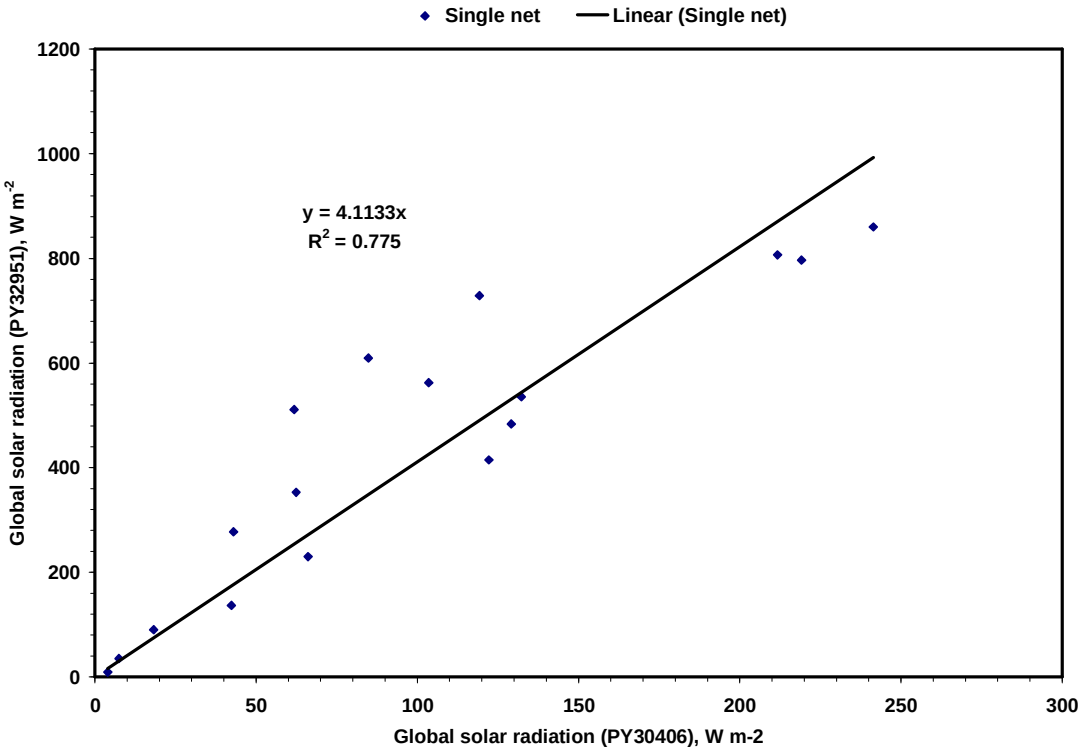

Figure 3.18 *Regression line of the Pyranometer cross-calibration with a single net on PY30406.*

Analysis of the data revealed that for a single layer net, the transmission coefficient is roughly 0.243 i.e. only 24.3 % of the incident solar radiation is transmitted through the net to reach the canopy. For a double layer shade net, the transmission coefficient was found to be approximately 0.071 i.e. 7.1 % of the incident solar radiation reaches the plants when the double layer net is in place.

3.12.1 Plant physiological calculations

The following plant physiological calculations were made from the data collected:

Stem sap flow

Branch sap flow

Stem diameter variation

CO_2 flux

H_2O flux

Leaf temperature

Photosynthetic water use efficiency which was calculated as:

$$WUE = \frac{\sum A_{CO_2}}{\sum E} \qquad [3.22]$$

where symbols have their usual meanings explained earlier in Section 3.10.1

3.12.2 Soil compartment calculations

Soil water potentials were measured in the soil for the pots containing Tree1, Tree3, Tree4 and Tree6 using soil matric potential sensors (EQ2 Equitensiometers, Delta-T Devices; Cambridge, UK). The equitensiometers were placed in the root zone at a depth of 30 cm below the surface of the soil so that the measurements could be as close to the conditions at the roots as possible.

3.12.3 External environmental/ micrometeorological calculations

Photosynthetically active photon flux density (PPFD)

Global solar radiation

Wind speed/direction/vector

Temperature/ Relative humidity

3.13 Experimental design

As explained earlier in this chapter, the experiment was run from 4 January to 19 February 2007. The main objective was to find the effect of leaf temperature on photosynthesis, transpiration, sap flow, and water use efficiency. In addition to this, the experiment also aimed to find out if there were any differences in water use efficiency and other water relations between the two varieties of trees used in the experiment. Tree4 and Tree3 belonged to the *Navelina* variety while the rest (i.e. Tree1, Tree2, Tree5 and Tree6) were from the *Baianinha* variety of navel orange trees. It may be useful to mention that in terms of physical appearance, the only difference between the *Baianinha* variety and the *Navelina* variety was the absence of thorns on the *Navelina* variety and also the leaves on the *Navelina* cultivar were on average smaller but thicker than the *Baianinha* leaves.

To study the effects of leaf temperature on photosynthesis and water use, a shade net was used to suppress canopy temperatures on selected trees from which measurements of flux, sap flow rate (branch and stem), stem diameter fluctuation, soil water potential, leaf and cuvette temperature, net radiation, PPFD, temperature and relative humidity were made.

Three solar radiation regimes were imposed on each tree under study. First the tree was left unshaded for a number of days (usually 3 days).

Starting with Tree4, the tree was left exposed to the full sun and measurements of the parameters mentioned above were taken throughout that period. After that a single layer shade net was used to cover the tree, taking care to leave enough space for air to flow freely within the shade net. Measurements were taken for three days and then a double layer shade net was used to cover the plant and measurements were also taken. After that the cuvette was moved to the next tree and then the series of measurements would be repeated. The cycle was Tree4, Tree3, Tree1 and then Tree2. Tree5 and Tree6 were left out because they were somewhat further away from the sampling unit and it would have been difficult to find long enough tubes to link the cuvette to those trees. Besides that, they were exactly the same variety as Tree1 and Tree2. Table 3.3 summarizes the sequence of measurements and the dates on which they were done during the measurement campaign.

Figure 3.19 *The cuvette on Tree2 (Baianinha variety) under a single layer shade net*

Only two sets of branch and stem sap flow sensors were available so these were also shifted together with the cuvette. The next tree in the sequence would have the other sap flow sensors installed on it while the one before it was being sampled.

Table 3.3 *Sequence of experiments for the canopy shading measurement campaign*

DATE OF EXPERIMENT	TREE #	SOLAR RADIATION REGIME
4 Jan 00:00 – 11 Jan 10:00	4	Single net (24 % S_{rad}*)
11 Jan 11:30 – 16 Jan 08:00	4	Double net (7 % S_{rad})
16 Jan 08:45 – 19 Jan 08:00	4	No shading (full S_{rad})
19 Jan 17:00 – 24 Jan 18:00	3	No shading (full S_{rad})
24 Jan 18:30 – 28 Jan 08:30	3	Single net (24 % S_{rad})
28 Jan 11:00 – 31 Jan 09:00	3	Double net (7 % S_{rad})
01 Feb 18:45 – 05 Feb 10:45	1	No shading (S_{rad})
05 Feb 11:15 – 07 Feb 10:00	1	Single net (24 % S_{rad})
07 Feb 11:15 – 10 Feb 12:00	1	Double net (7 % S_{rad})
10 Feb 13:30 – 13 Feb 08:00	2	No shading (full S_{rad})
13 Feb 09:45 – 16 Feb 07:00	2	Single net (24 % S_{rad})
16 Feb 07:35 – 19 Feb 19:00	2	Double net (7 % S_{rad})

*S_{rad} denotes the ambient global solar radiation flux

3.14 Modelling the effect of shading on plant-water relations

3.14.1 Leaf water potential

The amount of water present in a system is a useful measure of plant or soil water status for some purposes. More commonly, however, the water status in plant systems is measured in terms of water potential (Ψ), which is a measure of free energy available to do work.

3.14.2 The water balance model

The dynamics of the stem sap flow rate (F) as affected by changes in the transpiration rate (E) of the whole crown due to stomatal oscillations can be described using a simple water balance model (Philips *et al*., 2006; Steppe *et al*., 2006, Dzikiti *et al.*, 2007). The rate of change of the water stored in the tissues of the tree (W, kg) is related to the difference between water uptake (F, kg h^{-1}) and loss (E, kg h^{-1}) by

$$\frac{dW}{dt} = F - E \qquad [3.23]$$

In this equation it is assumed that there is a negligible capacitance in the roots such that the stem sap flow rate (F) equals the root water uptake. To estimate the total transpiration F, branch sap flow can be scaled up to the whole-crown level using the approach of Meinzer *et al*. (2003). In the Meinzer method (used in this study), the scaling factor is calculated as the ratio of the daily total sap flow at stem level to that at branch level. Multiplying the branch sap flow rate by this factor gave an estimate of the whole-crown sap flow rate. The whole-tree transpiration rate (F) was then estimated from the whole-crown sap flow rate by imposing a 20 minute time lead ahead of the whole-crown sap flow rate since the stomatal conductance led the branch sap flow by this amount. The time lag is probably a combination of the storage water use in the leaf-branch-stem system and the inertia of the sapflow system.

Given the fact that the stem sap flow (F) is driven by the water potential gradient between the soil and the leaves, a typical Ohm's law analogue can be used to describe the stem sap flow according to Jones (1992)

$$F = \frac{\Psi_s - \Psi_l}{R_x} \qquad [3.24]$$

where Ψ_s is the soil water potential measured in the root zone of the trees (MPa), Ψ_l the leaf water potential (MPa), and R_x is the hydraulic flow resistance of the whole tree (in MPa kg^{-1}) initially assumed to be a constant for the young orange trees. To describe the non-steady state nature of the flow due to the imbalances between water uptake and loss, the capacitance (C, kg MPa^{-1}) of the tree, which is a measure of its ability to store water, was defined according to Jones (1992) as the ratio of the change in the tissue water content to the change in the driving water potential difference.

$$C = \frac{dW}{d\psi} \qquad [3.25]$$

Model Maker Version 4 software package (Cherwell Scientific Ltd, Beaconsfield, UK) was used for the development, calibration and validation of the model.

3.14.2.1 Calibration of the model

The model calibration procedure involved systematically adjusting the values of the hydraulic parameters (R_x and C) and the soil water potential (Ψ_s) to minimize the squared differences between the measured and the modelled stem sap flow and the leaf water potential, weighted by the squares of the errors in the measurement of each quantity. This was achieved using various iterative optimization methods within the Model Maker 4 software package. The optimization method used depended on the type of data. Some data sets could only be optimized with the Marquardt iterative procedure while others only reached convergence when the Simplex method was used. Errors of 10 % for the stem sap flow measurements (Baker and van Bavel, 1987) and a larger error of 20 % for the leaf water potential measurements were used for the methods optimization. Data collected on 17 and 18 April 2007 was used for calibrating the model.

3.14.3 Experimental design

The main input components of the model were the leaf water potential measurements and the sap flow measurements (branch and stem). The experiment was run over four days: from 16 April to 19 April 2007. Leaf samples used for measuring leaf water potential were collected from the tree under experiment for that day using a puncher. The small, circular leaf samples were then wrapped up in plastic to reduce evaporation and then brought into the lab and were put into the previously calibrated C-52 sample chambers of the thermocouple psychrometer (Wescor Inc, Logan, UT, USA) connected to a microvoltmeter (HR-33T, Wescor, Inc., Logan, UT, USA).

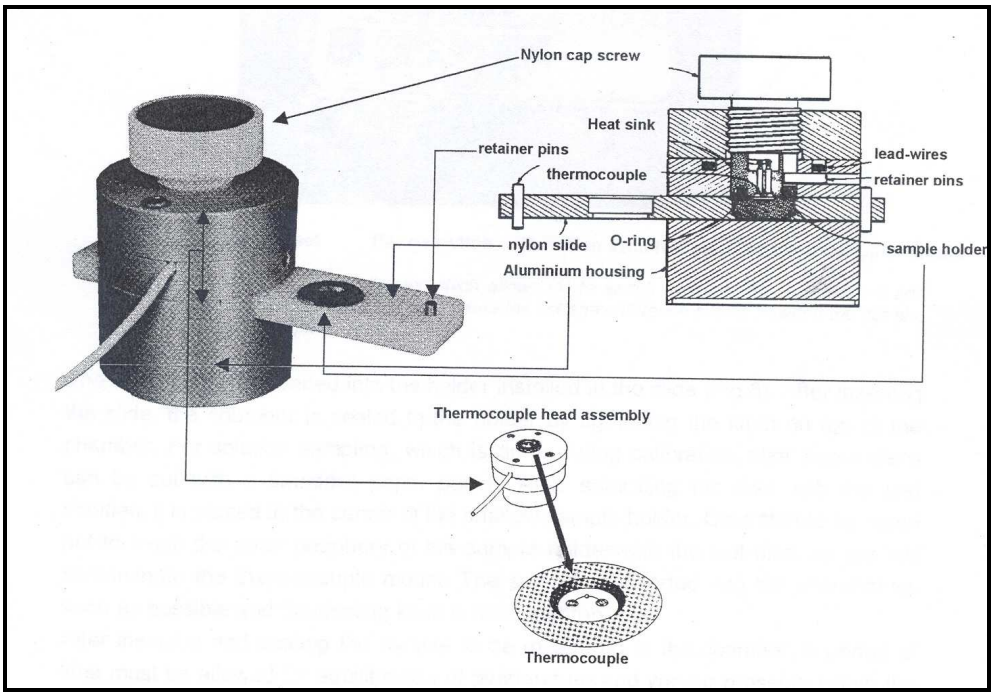

Figure 3.20 *A detailed diagram of the sample leaf chamber of thermocouple psychrometer (Wescor HR-33T user manual)*

The psychrometer had four sample chambers. Leaf samples were collected from the experimental trees on the roof every ten minutes from 8am local time (GMT +2 h) to 6 pm in the evening. The leaf water potential of the sample in each chamber (Figure 3.20) was measured after giving the leaf sample an equilibration time of 40 minutes. This meant that leaf water potential measurements were continuous running every 10 minutes throughout the day.

First, measurements were made on Tree2 without a shade net in place. Sap flow at stem and branch level was measured, together with temperature, relative humidity, PPFD, global radiation, soil water potential, and leaf temperature. The next day, a single layer shade net was added (77 % shade) and measurements were taken. On the third day, the experiment was shifted to Tree3 and the same procedure carried out on Tree2 was performed on Tree3. The collected data was analyzed and a model adapted from Dzikiti *et al.* (2007) was run in Model Maker v4 (Cherwell Scientific, UK). Additional measurements of sap flow (branch and stem), LWP and SWP were made and the model was subsequently calibrated from these additional measurements.

CHAPTER 4 RESULTS AND DISCUSSION

4.1 Introduction

Detailed results of the experimental manipulations and calibration procedures described in the previous chapter are given in this section. Specifically, whether changes in the canopy microclimate due to a reduction in radiation loading by shade nets potentially enhances CO_2 uptake and, hence, the productivity of citrus trees is explored. Although the results are presented for young potted orange trees, these results can be applied to mature field grown orange trees as demonstrated by Jifon and Syvertsen (2001). More detailed information is given in this study on the effects of canopy shading in orange trees on gas exchange and plant water relations based on continuous measurements of these variables using well calibrated eco-physiological devices.

Sample results of the calibration of the infrared gas analyser (IRGA) on several occasions during the experimental campaigns are presented first, followed by the performance tests carried out on the cuvette. A summary of the weather conditions throughout the experiment is then followed by a detailed presentation of the results of the flux measurements. After that results of cuvette and leaf temperature, sap flow dynamics and the effects of shading on photosynthesis, transpiration and water relations are presented. The last set of results covers the water balance model. Finally a table (Table 4.5) summarizing the results is presented to conclude the chapter.

4.2 Calibration of the IRGA sampling system

During the instrument performance evaluation period (September to December 2006) , it became clear that under the conditions at the experimental site, calibration values did not drift by more than 10 % per month with the drift being much less for CO_2 than for H_2O. Therefore it was only necessary to calibrate the LI-COR IRGA once every month. The reference cell scrubber was, however, changed every three days to counteract drifting of the span and zero. Table 4.1 shows typical calibration results for the calibration carried out on 29 September, 2 December 2006 and 31 January 2007 using the method described in section 3.4.2.1.

Table 4.1 *Summary of some of the calibration results for the infrared gas analyzer (IRGA) on several occasions during the experiments. The independent variable x in the equations in this table represents the voltage [mV] output from the IRGA while the dependent variables denote the analyser output of the appropriate physical variable*

Date	Variable	Calibration equation	R^2
29 Sept 06	CO_2	0.2371*x*-104.08	1.0000
	H_2O	19.198*x*-7096	1.0000
2 Dec 06	CO_2	0.2354*x*-80.777	0.9997
	H_2O	23.066*x*+25510	0.9981
31 Jan 07	CO_2	0.2315*x*-76.654	0.9998
	H_2O	42.235*x*-5753.6	0.9993

4.2.1 Carbon dioxide calibration

Calibration of CO_2 using three gases N_2 (CO_2 zero), CO_2 (334.8ppm & 335.6 ppm) were carried out. It was essentially a two-point calibration. The difference between the gradients of the two points, when taken separately, was less than 2 %.

4.2.2 Water vapour calibration

Water vapour calibration, done using the LI-COR LI-610 dew point generator at 5 dew point temperatures produced the expected linear trend after the dew-point temperatures had been converted to vapour pressures.

4.3 Cuvette performance tests

In order to reduce artefacts in the measurements of CO_2 and H_2O fluxes, some performance tests were carried out in the early stages of the experiment. The tests were to determine how significant chamber losses were in terms of the total measured quantities. Additionally, corrections could be made to the data once the chamber losses and other artefacts were known.

4.3.1 Cuvette blank test

A typical blank test, performed on 12 December 2006 showed that the losses and gains by the cuvette were less than ±1 µmol mol^{-1} for CO_2 mixing ratio (sometimes referred to as 'concentration') and slightly over ±1 mmol mol^{-1} for H_2O mixing ratio. Both of these ranges are close to the detection limit of the IRGA (0.1 µmol mol^{-1} for CO_2 and 1 % of the H_2O range). It was therefore concluded that losses in the cuvette due to adsorption by the walls and other processes were negligible.

4.3.2 Cuvette mixing test

The mixing test results shown in Figure 4.1 and Figure 4.2 showed that the modal airflow in the cuvette was higher than 2 m s^{-1} parallel to the axis of the cylinder. This meant that most of the leaves in the branch chamber interacted with air moving at 2 m s^{-1}. The air flow across the cuvette long axis was much less (< 1.08 m s^{-1}), being components of the wind speed blowing off the cuvette walls. The overall conclusion from this experiment was that the airflow was adequate to keep the cuvette well-ventilated and air well-mixed such that the sample extracted is representative.

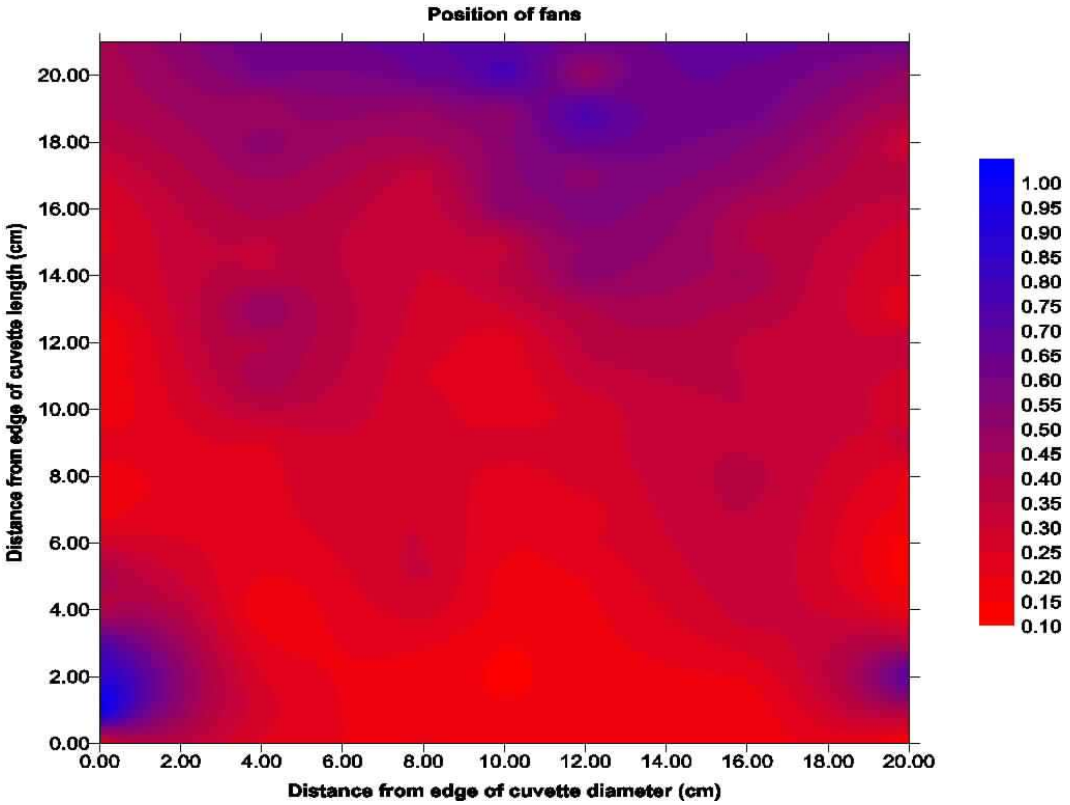

Figure 4.1 *Mixing test, with hot wire anemometer (Testo GmBH) parallel to the long axis of the cuvette. The legend shows values of wind speed in m* s^{-1}

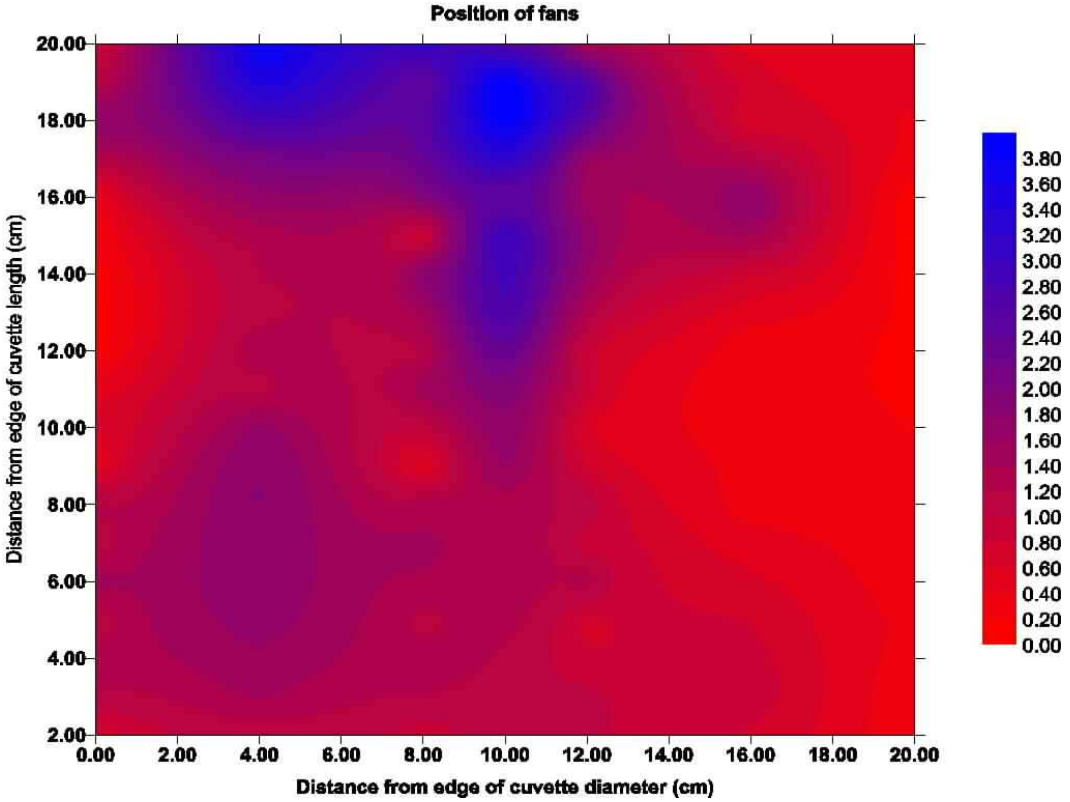

Figure 4.2 *Mixing test, with hot wire anemometer perpendicular to the axis of the cuvette. The legend shows values of wind speed in m* s^{-1}

4.3.3 Potted plant test

To verify whether the periodic oscillations in the CO_2 and H_2O flux were an artefact from the cuvette, a test to determine typical fluxes of CO_2 and H_2O for a regular plant (a plant whose photosynthetic response is known to be driven largely by solar radiation) was done using an 'elephant ear' (*Colocasia esculentum*). The results are shown in Figures 4.3 to 4.6.

The results, as shown in Figure 4.3 and Figure 4.4 showed that the *Colocasia esculentum* has a response that seems to be governed primarily by the amount of photosynthetically active photon flux density available at the time.

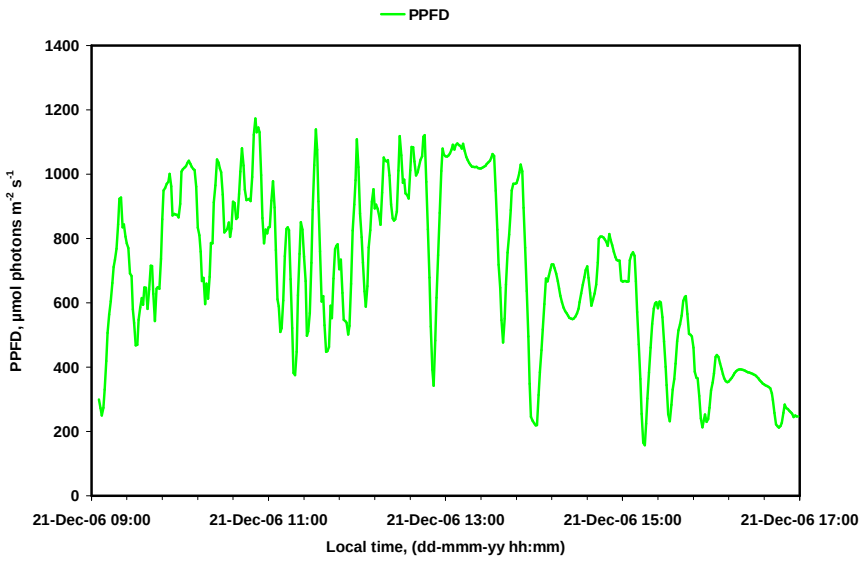

Figure 4.3 *Diurnal variation of photosynthetic photon flux density (PPFD) on an Elephant Ear flower measured on 21 December 2006*

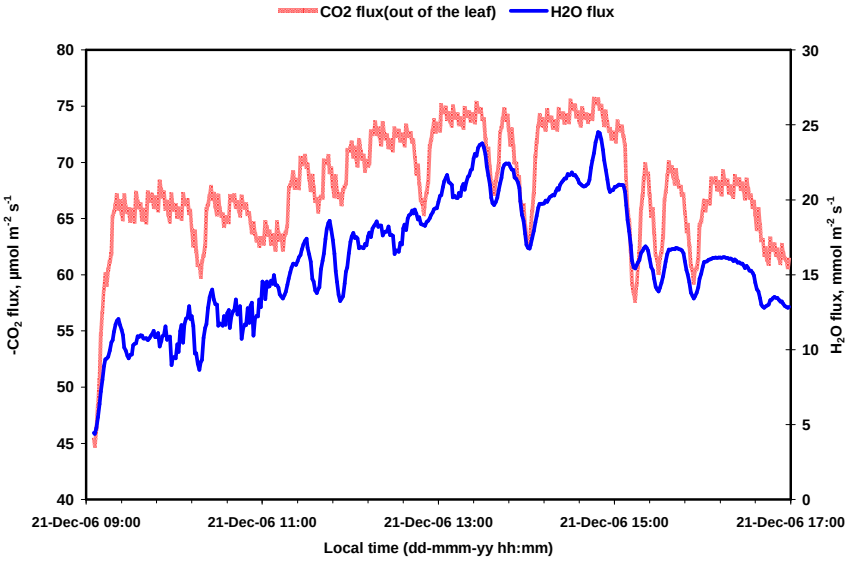

Figure 4.4 *Variation of CO_2 and H_2O flux on an elephant ear flower measured on 21 December 2006. dd-mmm-yy hh:mm denotes the time format used on the time axis.*

Figure 4.5 and Figure 4.6 show the photosynthetic response to variation in photon flux density and the WUE of the *Colocasia esculentum*. The typically low value of the photosynthetic WUE as well as the saturation of photosynthesis at about 400 µmol m^{-2} s^{-1} (Figure 4.5) are typical of C_3 plants. Data sampled at 1 minute intervals was used to plot these graphs. The CO_2 fluxes obtained were extremely high for a C_3 plant and this raised doubts about whether it's reallya C_3 plant or not. It was assumed that there were no errors in calculating the flux. Perhaps the plant was a hybrid between a C_3 and C_4 plant.

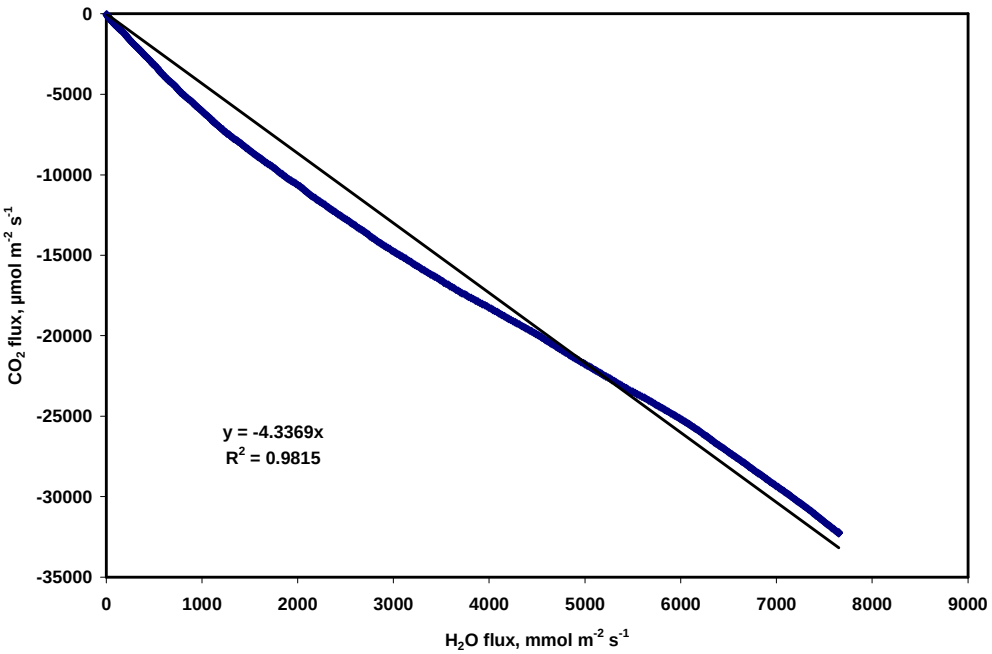

Figure 4.5 *Diurnal variation of water use efficiency of the Elephant Ear flower*

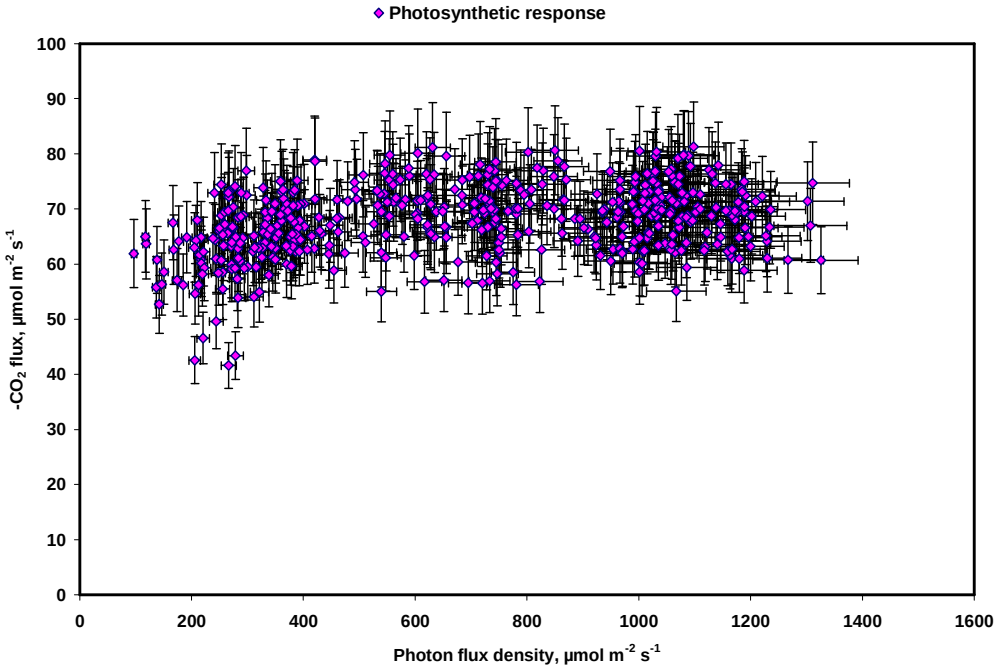

Figure 4.6 *The photosynthetic (A/Q) response of the Elephant Ear flower on 21 December 2006 from 9am to 6pm local time.*

4.4 Gaseous flux measurements

To make meaningful deductions of the effects of leaf temperature on photosynthesis, it was necessary to calculate diel variations of CO_2 and H_2O fluxes under different levels of solar radiation. In all cases percentiles were calculated so that the variation of measured or calculated quantities could be seen over various probability ranges. The probability ranges used were 0.01-0.99 (1 %-99 %) and 0.25-0.75 (25 %-75 %). Microsoft Excel was used for the calculations. The grey areas showing the probability ranges in the charts were created by plotting drop lines between the upper and lower probability ranges. The markers for those ranges were then removed to leave only the grey-coloured drop lines. The median was included in all cases. Figure 4.15 is the first example of this kind of plot.

4.4.1 Variation of environmental parameters during the flux measurements

In order to prove that fluctuations in environmental forcing was not the determining factor for the differences in fluxes between the different solar radiation regimes, relative humidity, ambient air temperature, the temperature and relative humidity under the shade net and PPFD above the cuvette were all measured and are plotted in the following Figures:

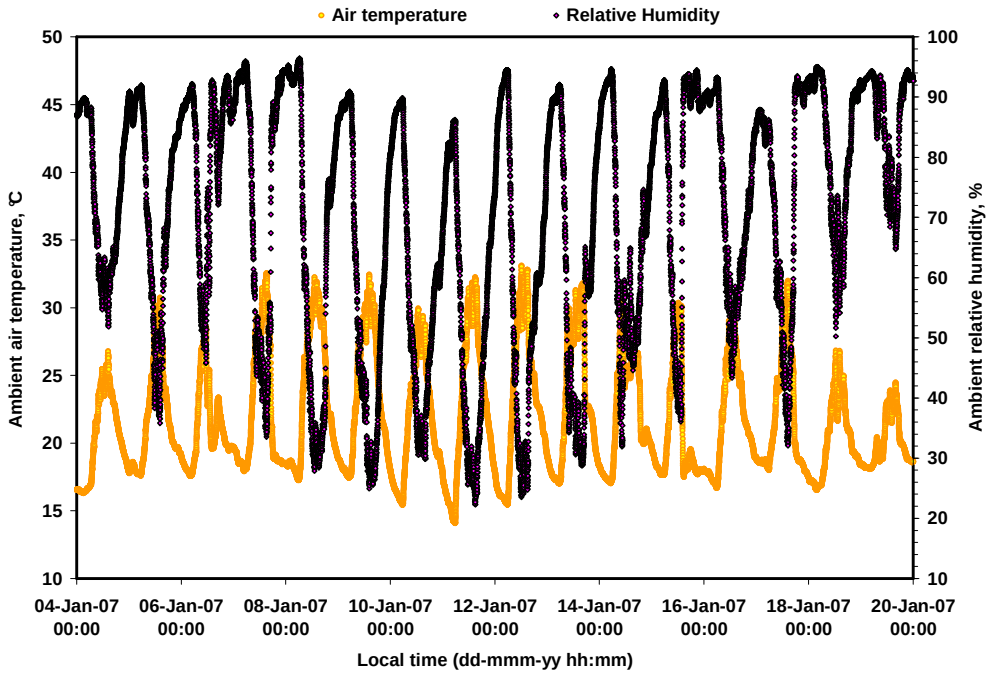

Figure 4.7 *Variation of temperature and relative humidity during Tree4 measurements (4 January to 20 January 2007).*

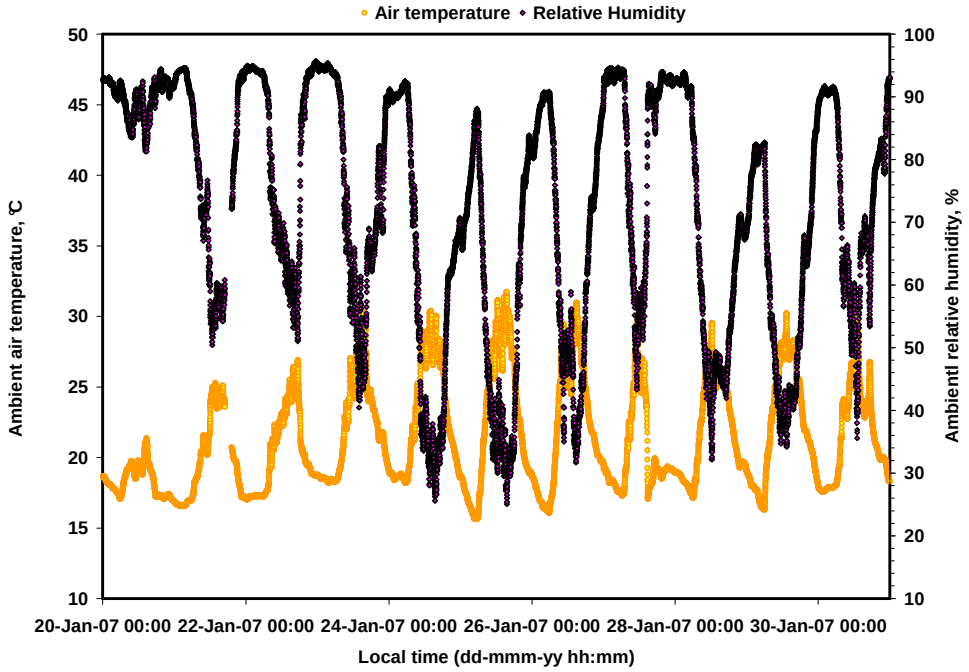

Figure 4.8 *Variation of temperature and relative humidity during Tree3 measurements (20 January to 30 January 2007).*

.

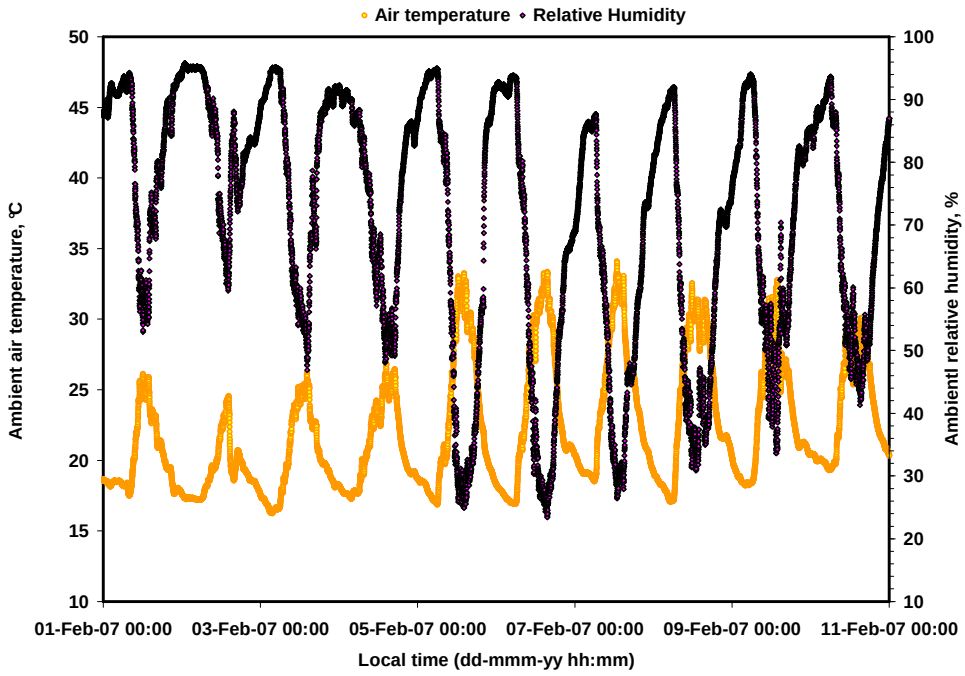

Figure 4.9 *Variation of temperature and relative humidity during Tree1 measurements (1 February to 11 February 2007).*

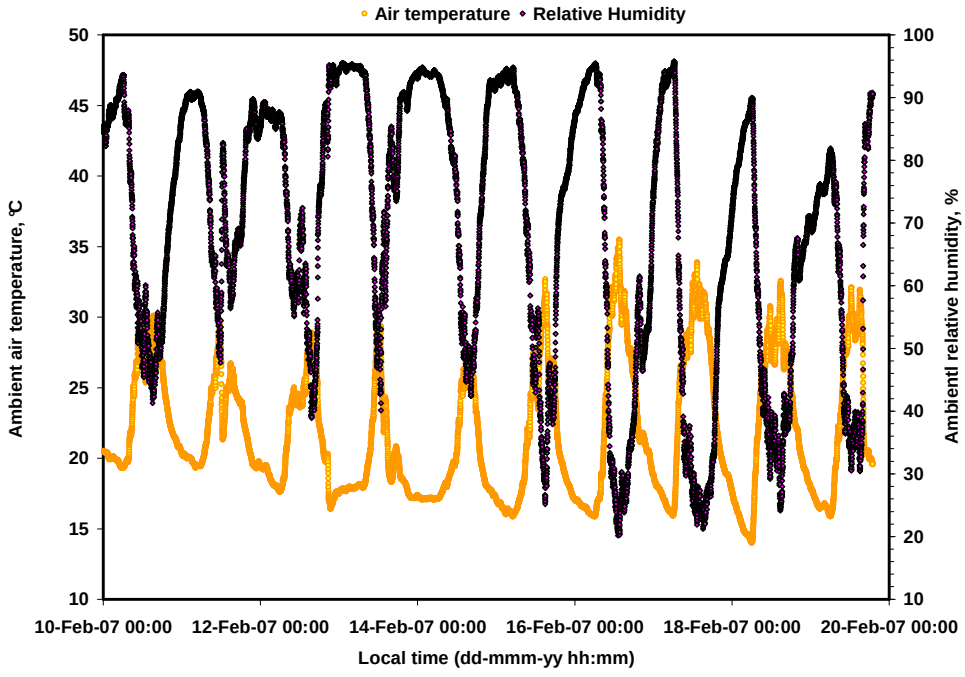

Figure 4.10 *Variation of temperature and relative humidity during Tree2 measurements (11 February to 19 February 2007).*

4.4.1.1 Effect of shade nets on the radiation microclimate of the young orange trees

The values of PPFD under a double shade net were much lower than those obtained without a shade net as can be seen from Figures 4.11 to 4.14. This was the major reason why, although the double layer shade net could lower leaf temperatures, it could not be used practically. The amount of radiation for photosynthesis would be too low.

In most cases, variation of the external parameters was minimal, and on the occasions that they varied considerably, they did not persist for the duration of the measurements for any of the solar radiation regimes. The CO_2 and H_2O fluxes, to a large extent, mirrored the variation in PPFD.

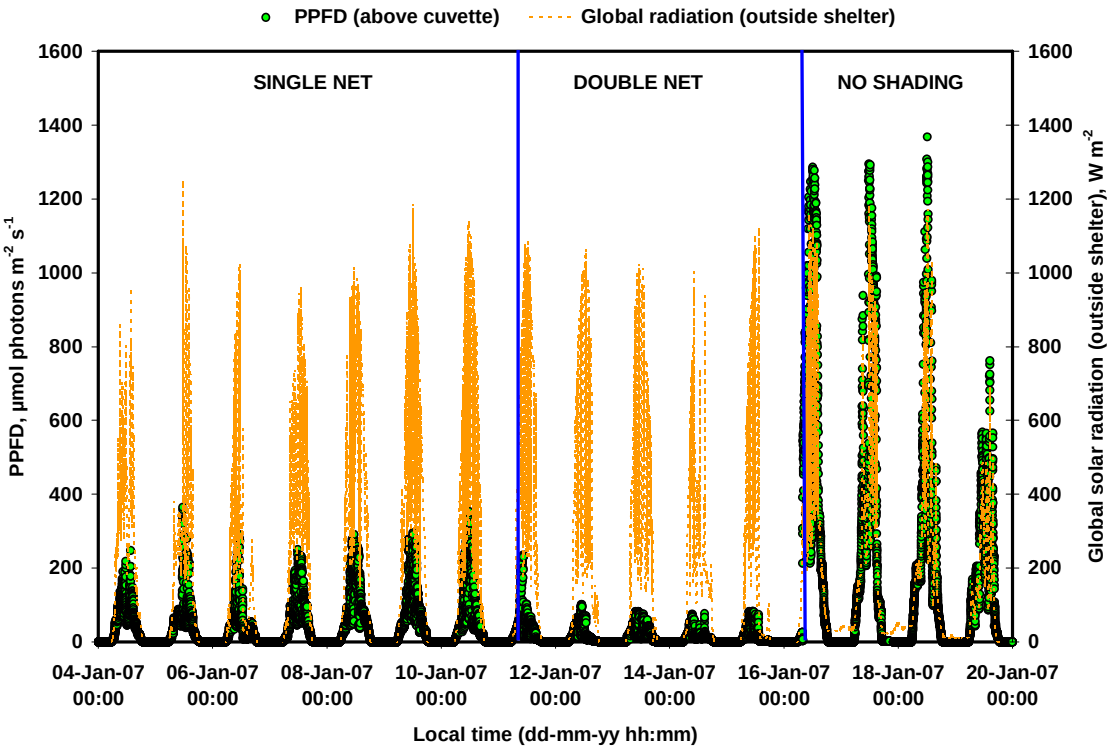

Figure 4.11 *Variation of PPFD and global solar radiation during Tree4 measurements*

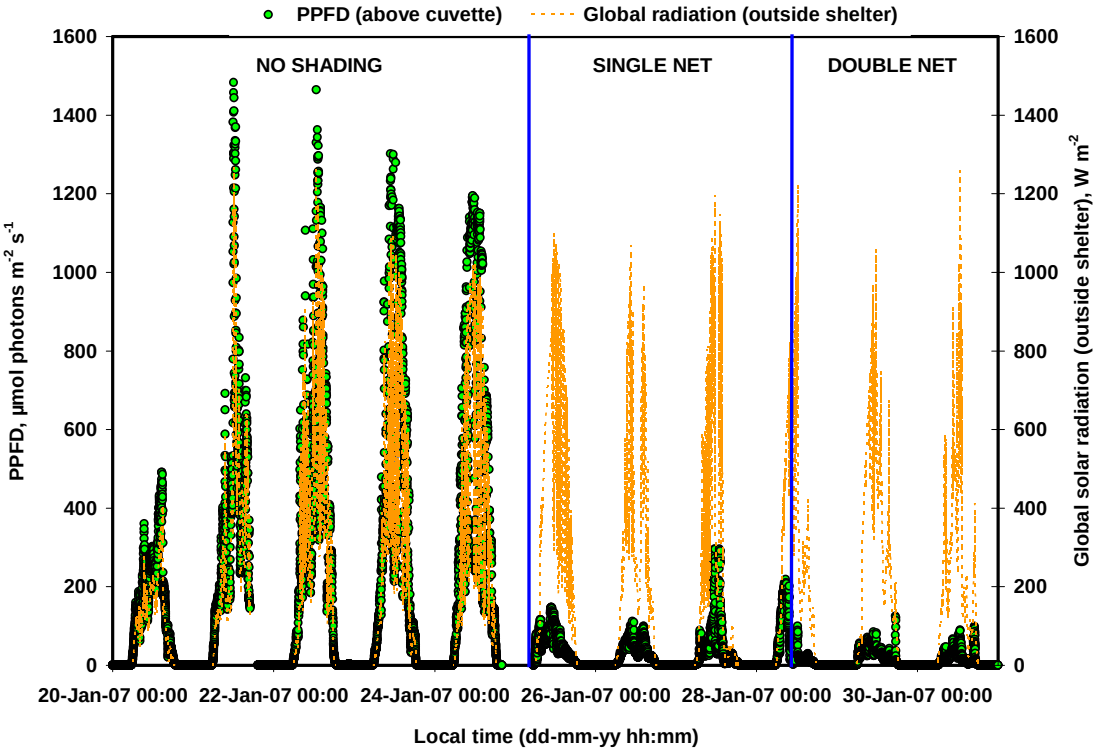

Figure 4.12 *Variation of PPFD and global solar radiation during Tree3 measurements*

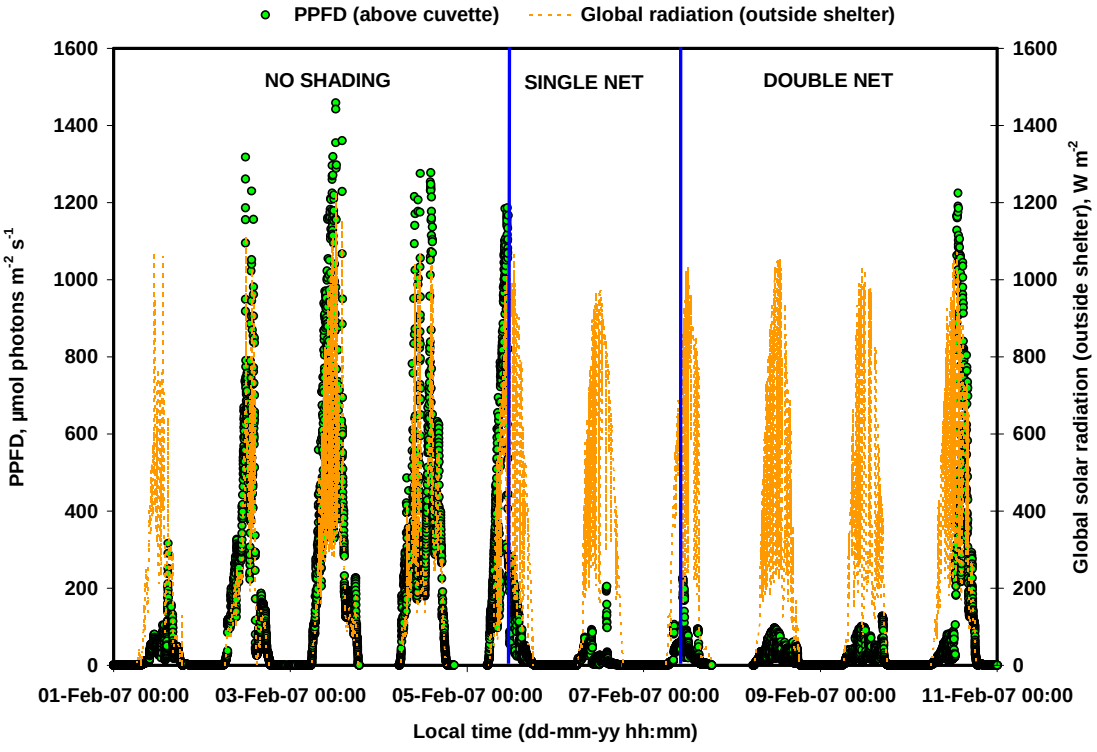

Figure 4.13 *Variation of PPFD and global solar radiation during Tree1 measurements*

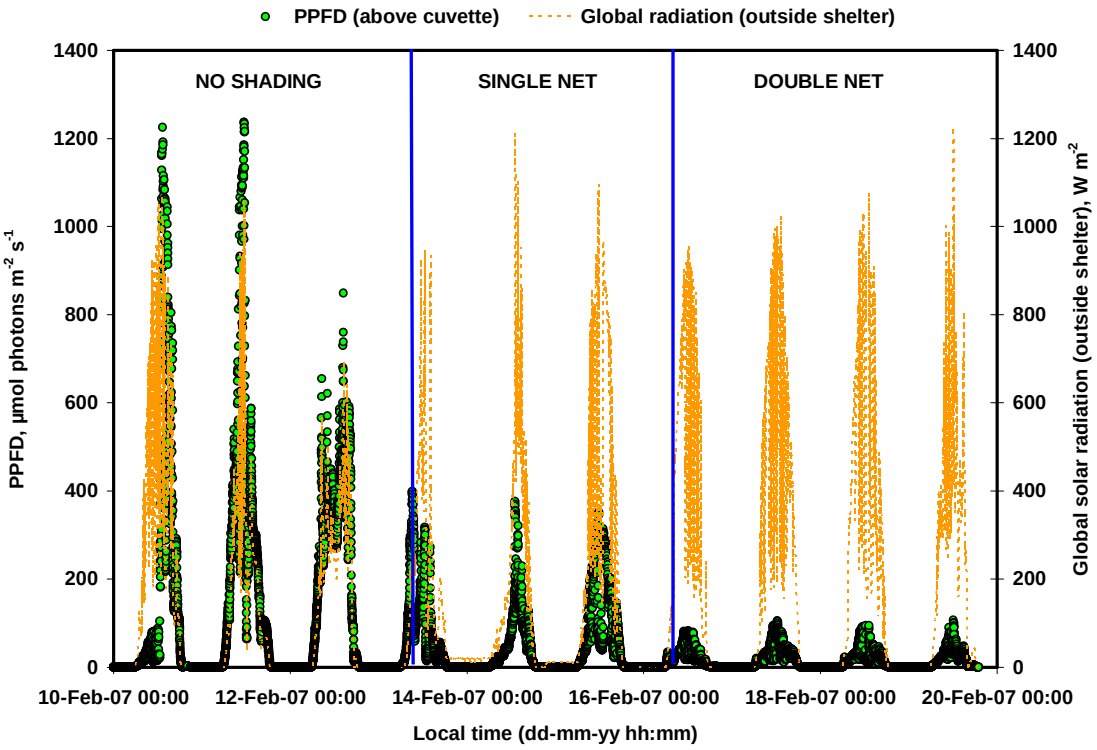

Figure 4.14 *Variation of photosynthetic photon flux density (PPFD) and global solar radiation during flux measurements on Tree2 from 10 February to 19 February 2007*

4.4.2 Median diel variation of ambient CO_2 and H_2O mixing ratios

The median diel variation of CO_2 mixing ratio was calculated in the 25 %-75 % range was calculated and the results are shown in Figure 4.15. The calculation was done using data from 4 January 2007 to 19 February 2007. The results showed that the median (taken from 1 min intervals) value of CO_2 at midday was about 370 ppm. Median CO_2 levels rose from 1700h local time until 0500h the next morning when it would start to drop rapidly. The sudden drop could be attributed to the breaking up of the nocturnal boundary layer which would have been low throughout the night, accumulating the CO_2 in the ecosystem (Meixner, personal communication). The results also showed that the average diel structure of atmospheric CO_2 is bimodal with a minimum between 1400 h and 1500 h and maxima at 0500 h and 2000 h (Figure 4.15).

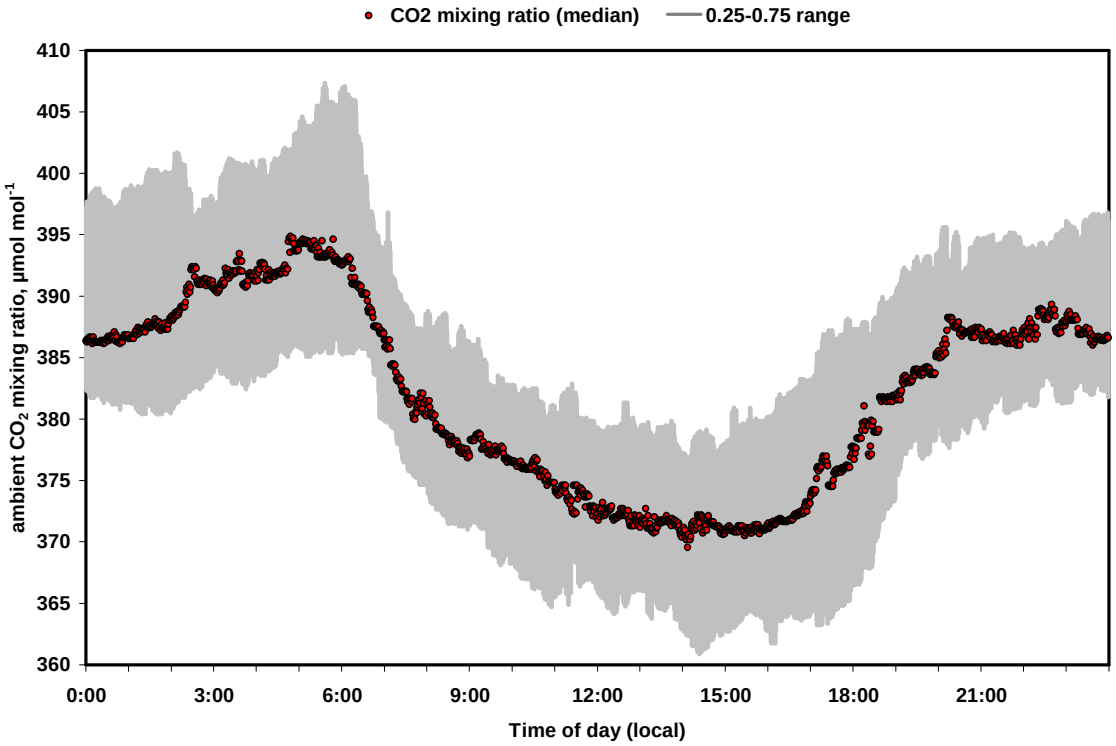

Figure 4.15 *Median diel variation of CO_2 mixing ratio from 4 January 2007 to 19 February 2007.*

Average daytime CO_2 mixing ratio in this study ranged between 370 and 382 ppm. Zollner *et al.* (2004) measured background CO_2 values of 355-362 ppm during the hot dry season (October-November) 1993 in North-western Zimbabwe. Considering the yearly rise of atmospheric CO_2 mixing ratios, the values obtained in this study seem realistic. They are further validated by the CO_2 mixing ratio observed regularly atop Mauna Loa (Hawaii) which currently stands at 380 ppm (Heartspring website (http://heartspring.net/global_warming_greenhouse.html), 2-June-2007).

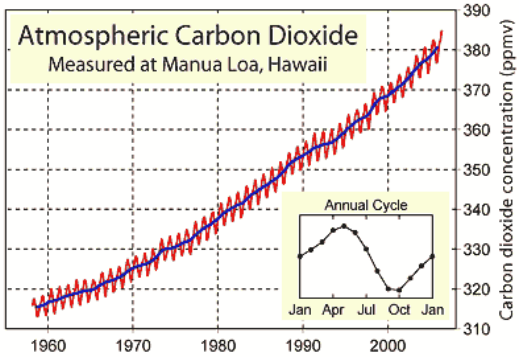

Figure 4.16 *The Keeling curve showing the variation of atmospheric background CO_2 levels .measured on Mauna Loa, Hawaii from 1958 to 2007.*

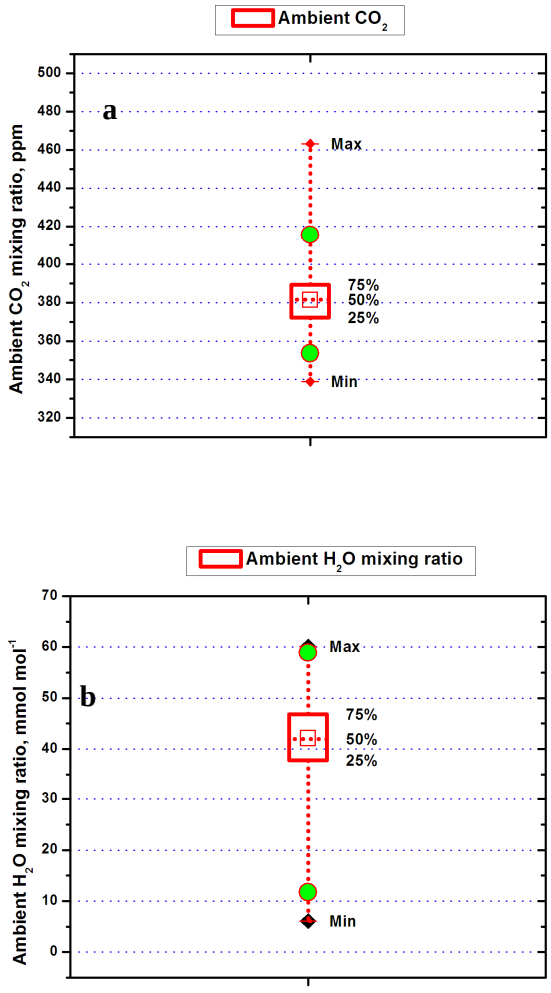

Figure 4.17 *Box and whisker plots showing the seasonal variation of ambient CO_2 (a) and H_2O (b) mixing ratios (4 January to 19 February 2007). The lower and the upper circles depict 1 % and 99 % respectively while the small box inside the box depicts the mean.*

4.4.3 Diel variations of mixing ratios

4.4.3.1 Carbon dioxide and water vapour

In order to understand the variation in the fluxes measured which are presented later in this Chapter, it was necessary to first get a view of the variation of the ambient mixing ratios of CO_2 and H_2O. Typical diel variations of CO_2 and H_2O for part of the measurement campaign are shown below (Figure 4.18(a) and (b) respectively). The variation of H_2O usually followed the same trend as the CO_2 except

a

when it rained in which case the H_2O mixing ratio would rise significantly.

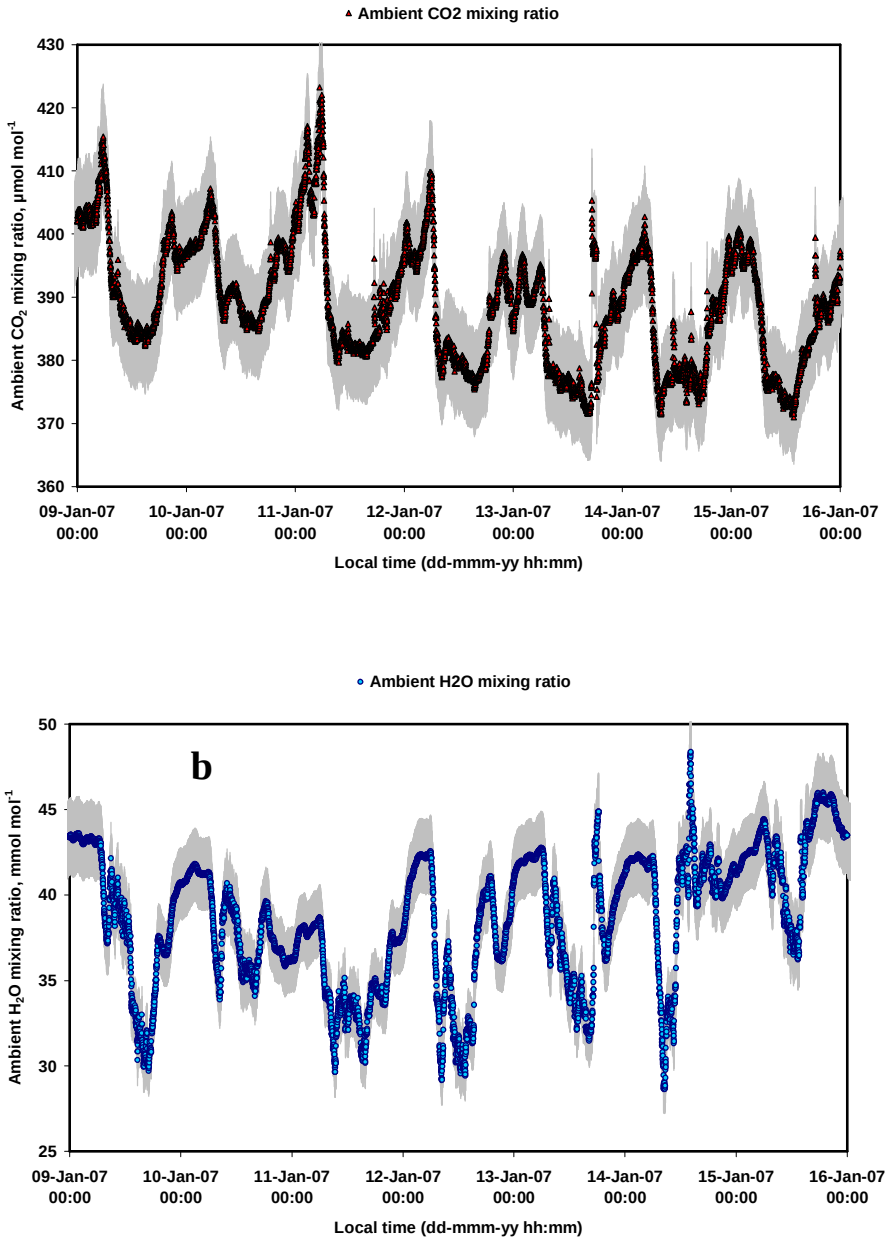

Figure 4.18 *Diel variation of (a) CO_2 and (b) H_2O mixing ratios between 9 January and 16 January 2007. The grey shading represents the error margin. Night time values of H_2O mixing ratio followed a similar trend except on rainy nights (e.g. 15 January).*

4.4.4 Carbon dioxide and water vapour fluxes

Long term variation of CO_2 and H_2O fluxes are presented in this section. These fluxes were important because they determined one of the objectives of the thesis: photosynthesis and transpiration which could be related to leaf temperature to find out the effect of leaf temperature on them. Box and whisker plots were made using a statistical and graphing software package (OriginPro™ 7.5, OriginLab Cooperation; MA, USA).

4.4.4.1 Long-term variation of CO_2 and H_2O flux

Variations of the two fluxes measured from the cuvette throughout the measurement campaign are shown in the box and whisker plots in Figure 4.19.

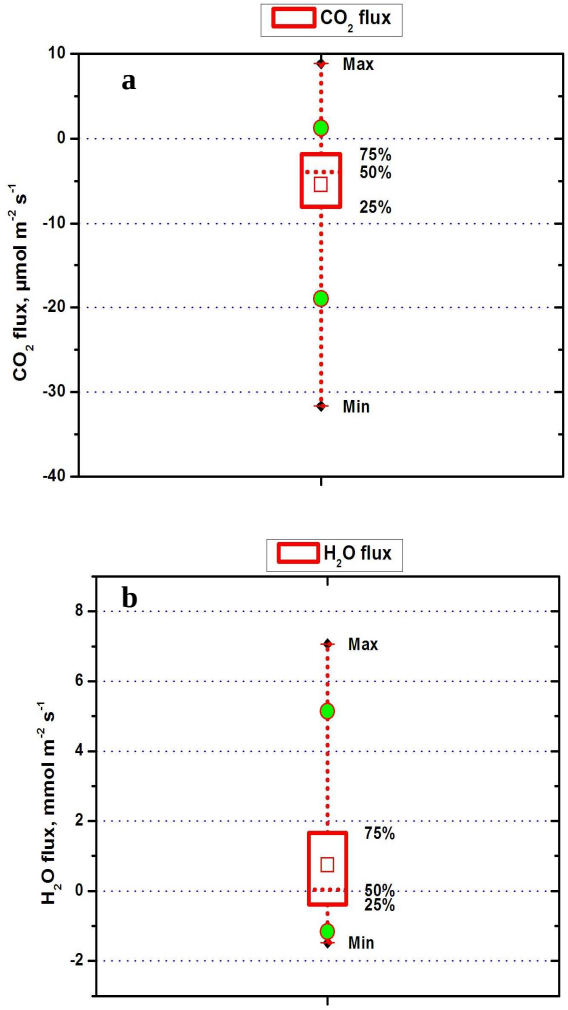

Figure 4.19 *Box and whisker plots showing range of CO_2 (a) and H_2O (b) flux inside the cuvette (4 January to 19 February 2007)*

Maximum respiration throughout the measurement period was only about 10 µmol m^{-2} s^{-1} which was recorded on Tree3 during a period in which the branch in the cuvette was blooming.

4.4.4.2 Variation of CO_2 and H_2O flux with leaf temperature

Diel variations of CO_2 and H_2O flux are presented for the duration of measurements made on each tree. This is done so that the relationship between leaf temperature and photosynthesis can be clearly seen given that solar radiation, hence temperature, were not controlled.

Leaf temperature plays a role in the rate of photosynthesis and transpiration as typified by the results presented in Figure 4.20 and 4.21. The results showed that leaf temperatures (which mirrored cuvette temperature) play an important role in determining CO_2 flux. When the leaf temperature was less than 35°C, CO_2 flux was high. CO_2 fluxes dropped by as much as 50 % when a double layer net was

introduced, even though leaf temperatures remained the same or were even lower on some days. This seems to suggest that PPFD is more important than leaf temperature in determining the rate of photosynthesis. When the shade net was completely removed, maximum CO_2 flux rose sharply on the first day to more than 100 % of its value under a double layer shade net. Interestingly this occurred even though maximum leaf temperatures had risen to as much as 40°C. The following day and subsequent days thereafter without shading resulted in a reduction in photosynthetic rates to vales which were about 50 % higher than those under a double shade net. The leaf temperature when no shade net was in place averaged 38 °C for Tree4.

H_2O fluxes followed an almost similar trend to the CO_2 flux. Leaf temperatures below 30°C resulted in high H_2O fluxes which peaked at about 4.5 mmol m^{-2} s^{-1} while those between 30 and 35°C yielded fluxes as high as 5.5 mmol m^{-2} s^{-1} when under a single layer shade net. The H_2O fluxes were somewhat reduced when the tree was under a double layer shade net. High temperatures above 38°C which were prevalent when there was no shading reduced H_2O fluxes (transpiration) by the same margin that it reduced CO_2 flux.

Figures 4.22 up to 4.25 show the long term and short term median diel cycle (MDC) of CO_2 and H_2O flux for all the trees used in the experiment. They illustrate the midday depression of both fluxes due, presumably, to high temperatures. This is proven by the MDCs of leaf temperature shown in Figure 4.29 and Figure 4.30. The occurrence of stomatal cycling is clearly visible in the figures illustrating the MDCs of both CO_2 and H_2O fluxes.

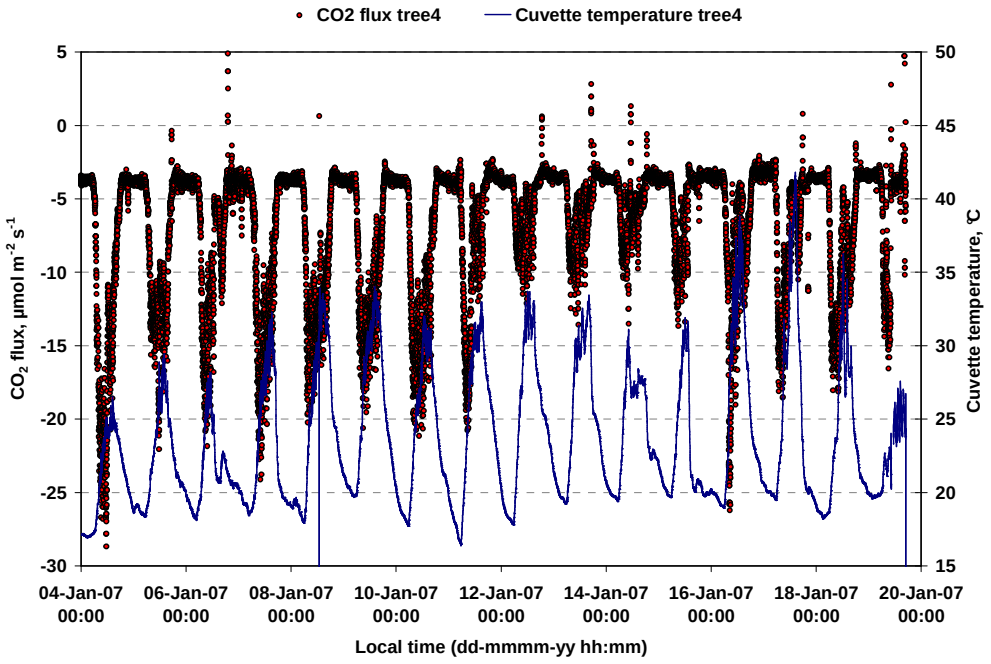

Figure 4.20 *Variation of CO_2 flux with time. The variation of cuvette temperature with time has been superimposed to show the effect of temperature on photosynthesis in young citrus trees.*

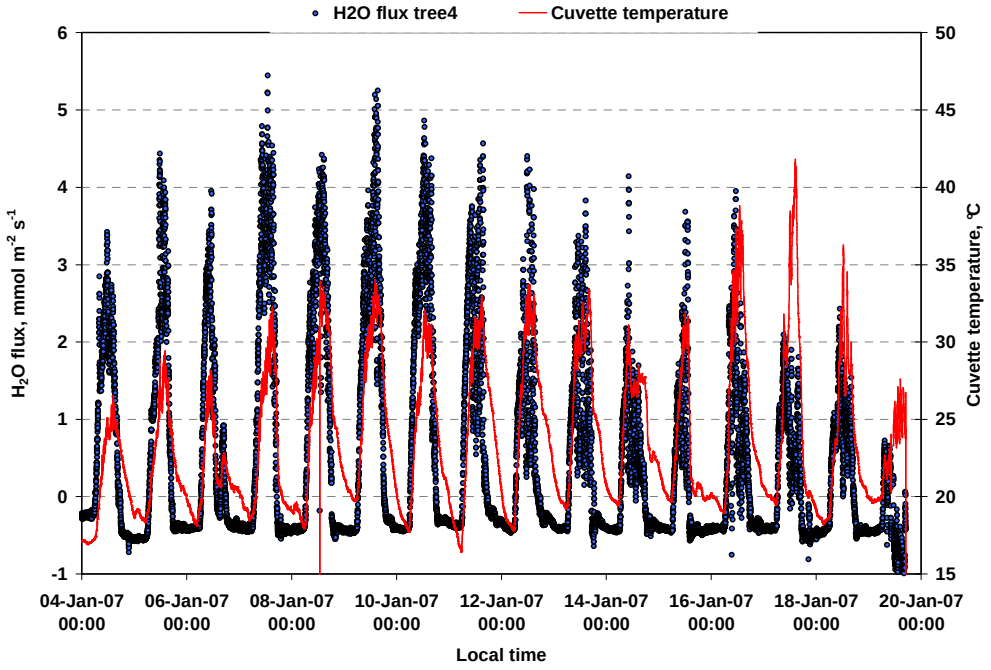

Figure 4.21 *Variation of H_2O flux and temperature with time.*

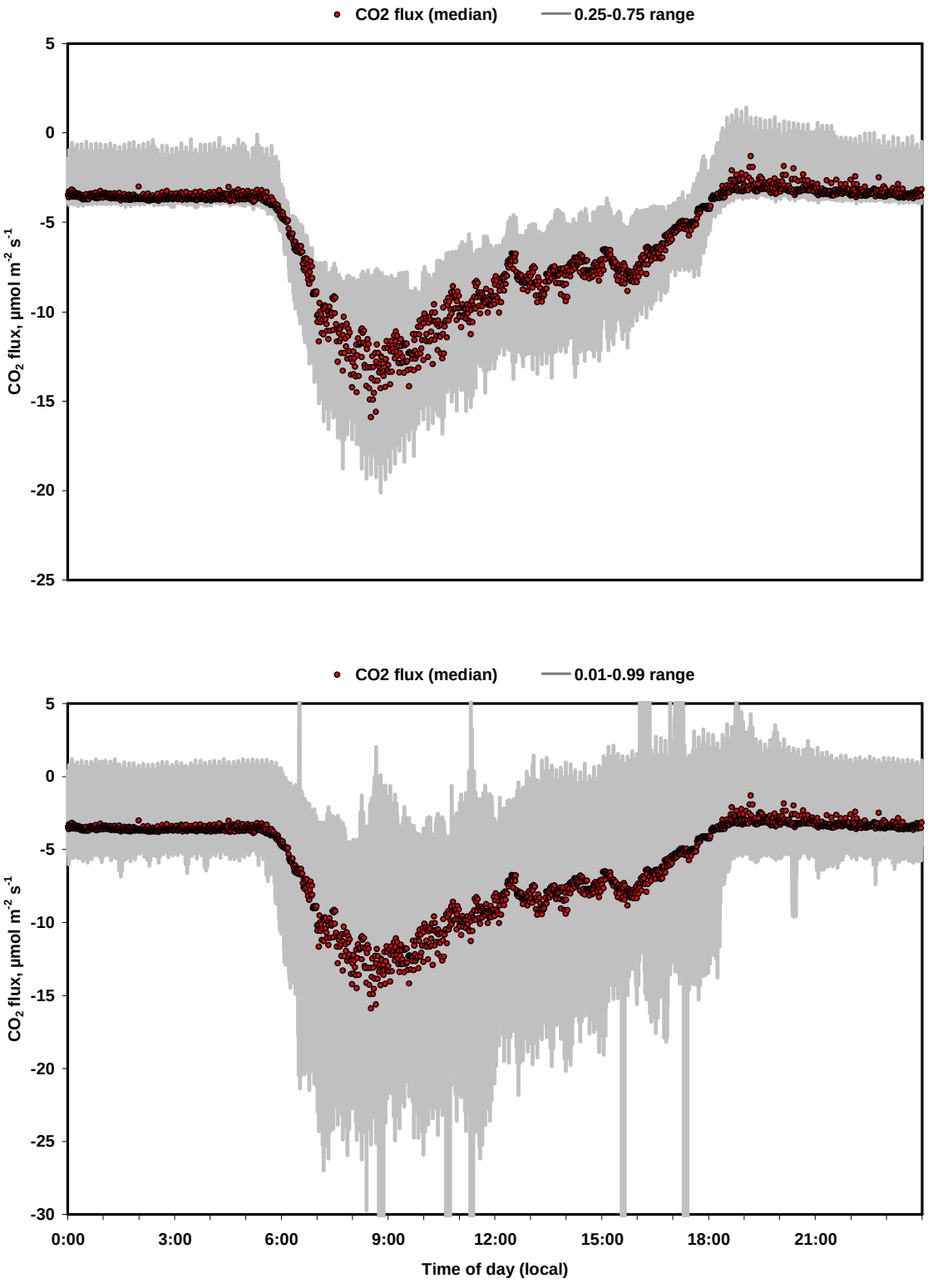

Figure 4.22 *Median diel cycle (MDC) of CO_2 flux, 4 January to 10 February 2007*

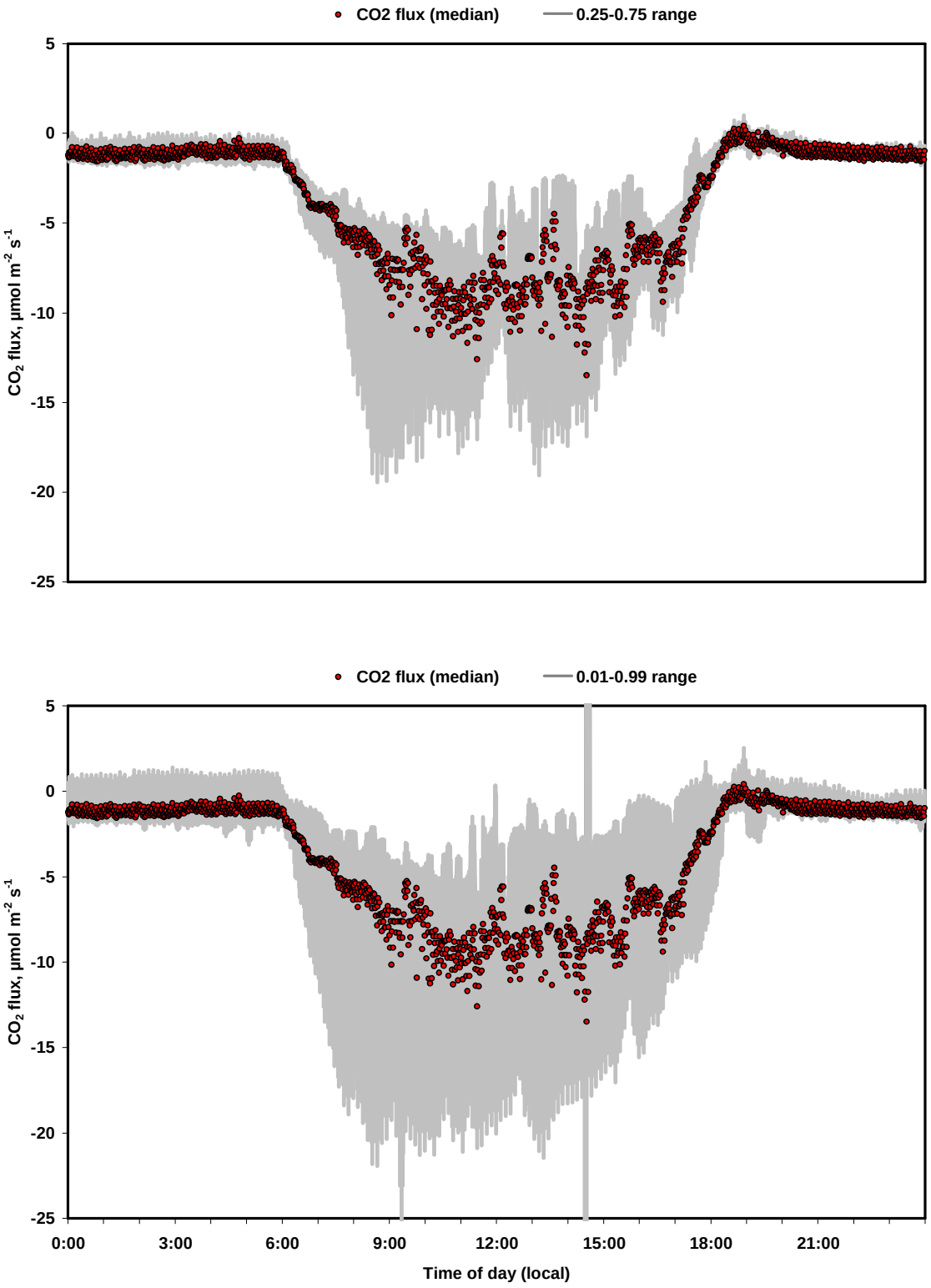

Figure 4.23 *MDC of CO_2 flux, 11 February to 19 February*

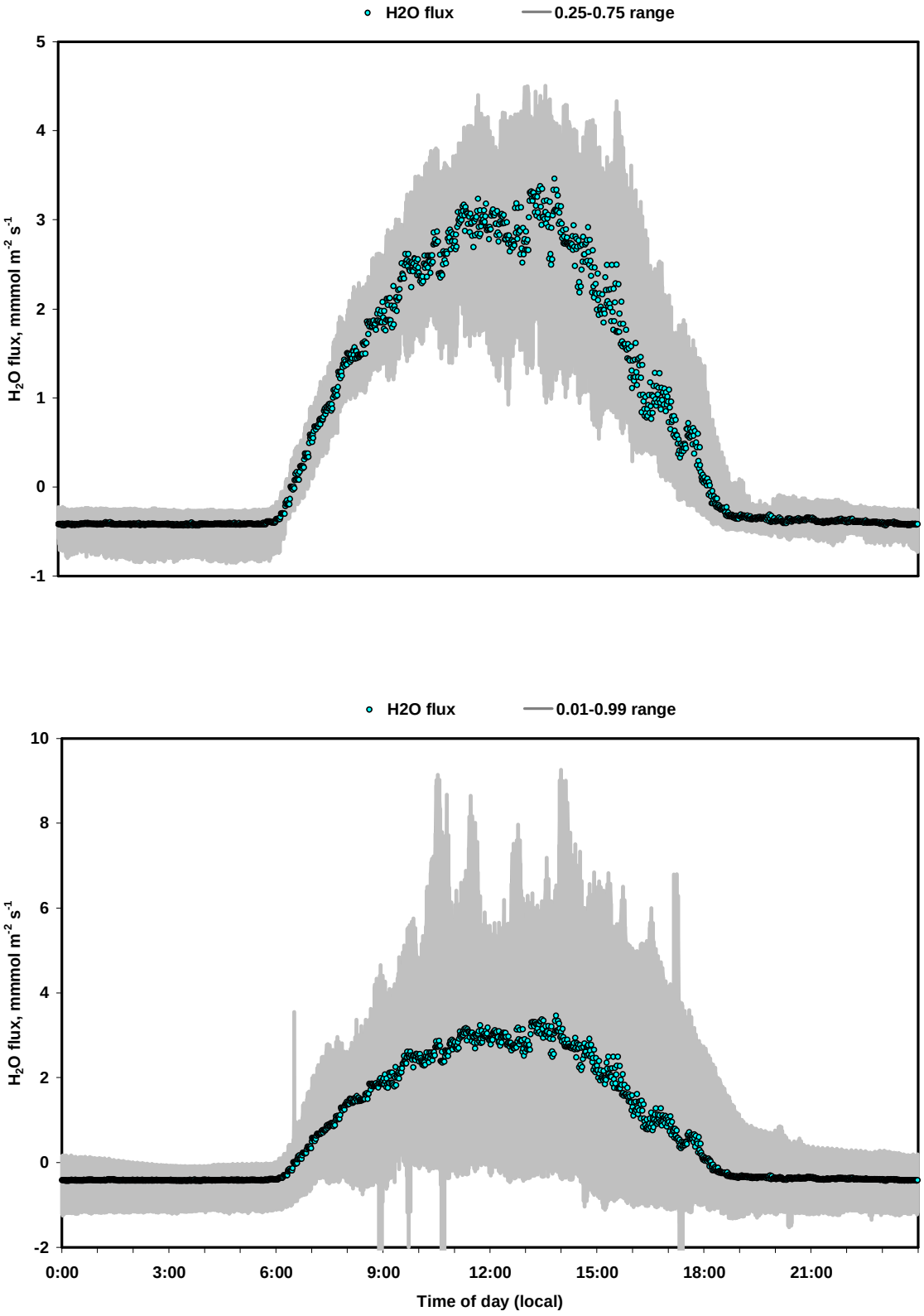

Figure 4.24 *Median diel cycle of H_2O flux, 4 January to 10 February 2007*

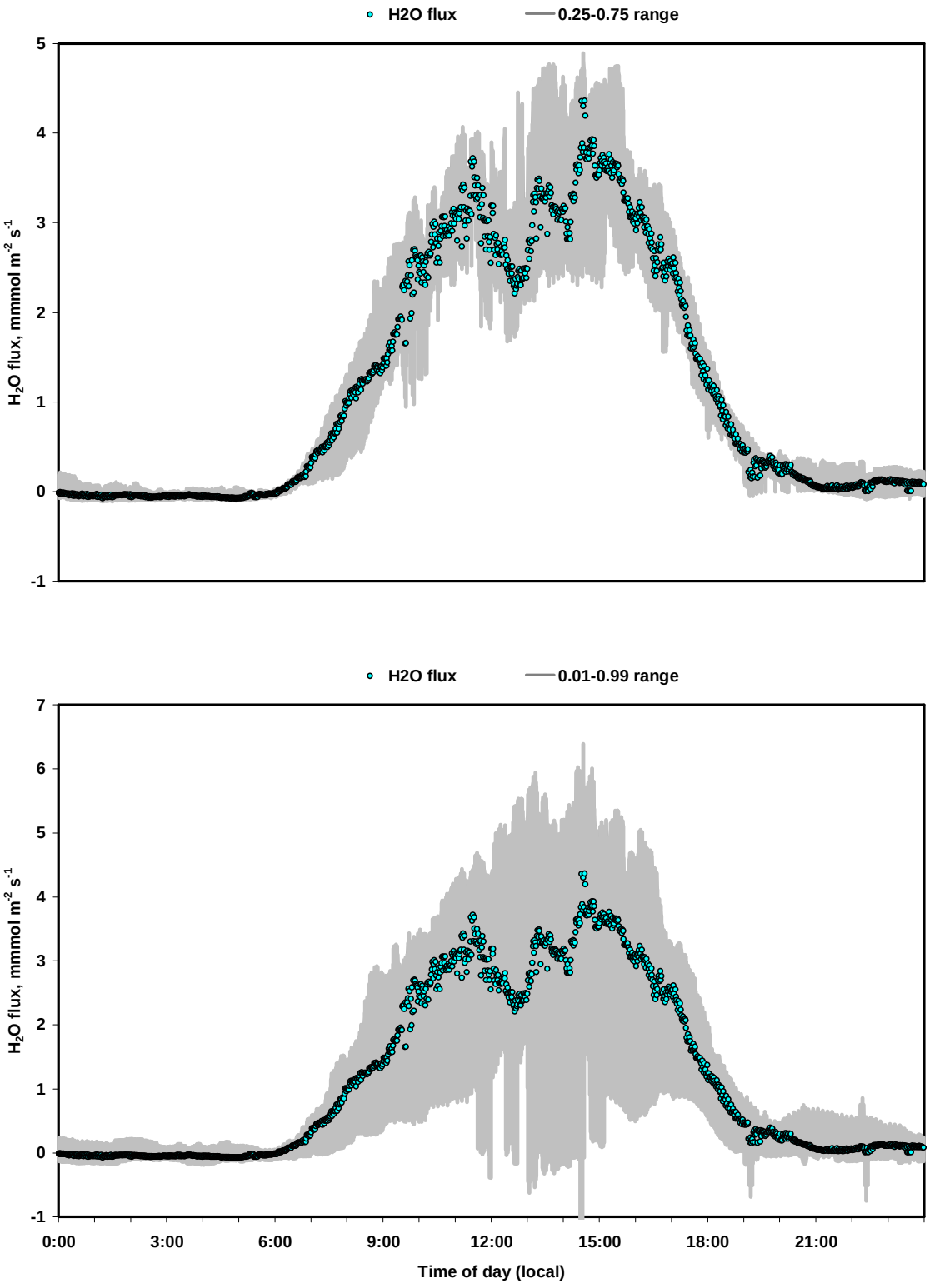

Figure 4.25 *Median diel cycle of H_2O flux from 11 February to 19 February 2007.*

4.5 Cuvette and leaf surface temperature dynamics.

Although the ventilation rate inside the cuvette was proven to be adequately high, differences still existed between cuvette leaf surface temperature and the temperatures of the leaves measured outside the cuvette. The maximum temperature differences occurred at midday and around 0600 h in the morning. These differences did not exceed 1.5 °C (Figure 4.26) and were therefore not expected to affect the results significantly.

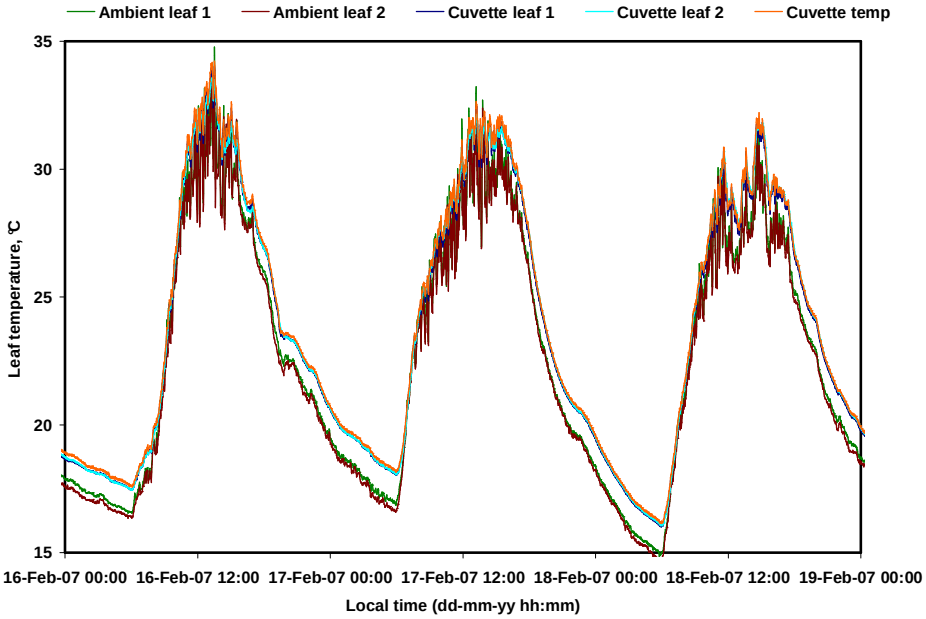

Figure 4.26 *Diel pattern of leaf temperature for a young navel orange tree (Tree2), 16 February to 19 February 2007 (double shade)*

Steppe et al. (2006) reported an anti-phase relationship between branch sap flow and leaf temperature on navel orange trees. The results obtained in this study shown in Figure 4.27 show that the branch sap flow and the leaf temperature have the same phase relationship and the time lag between them is negligible.

Similar relationships were found when comparing branch sap flow with CO_2 flux, H_2O flux and PPFD. The reason for the differences may lie in the fact that they were using at least 5 min averaging intervals for their data whereas 1 min averaging was used in this study.

It must be stated though that there is no easy way to quantify phase differences from such data.

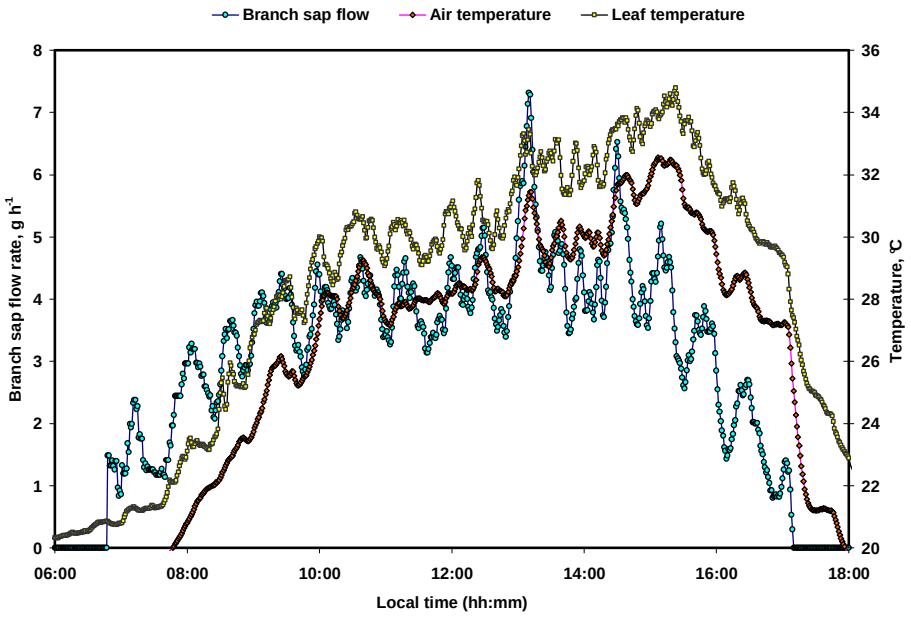

Figure 4.27 *Relationship between branch sap flow rate and leaf temperature on 7 January 2007. Air temperature has been added for comparison. The results showed that leaf temperature is in phase with sap flow rate, contrary to the findings of Steppe et al. (2006) who found an anti-phase relationship. The same phase relationship with leaf temperature as the one in this figure was found for CO_2 flux, H_2O flux and PPFD. Section 4.6 covers sap flow dynamics in more detail.*

4.5.1 Long-term variation of leaf /cuvette temperature.

Analysis of long term variation of leaf/cuvette temperature revealed that the maximum leaf temperature attained was about 42°C (Figure 4.28) while the lowest was about 16°C. The average temperature was about 24°C. The time interval of the analysis includes those times when the tree under experiment was shaded. Because the cuvette leaf temperature and the cuvette temperature were almost equal the term leaf temperature and cuvette leaf temperature will be used interchangeably.

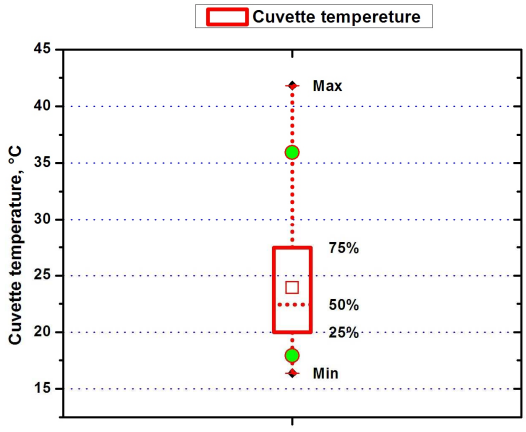

Figure 4.28 *Box-and-Whisker plot showing variation of cuvette temperature (4 January to 19 February 2007)*

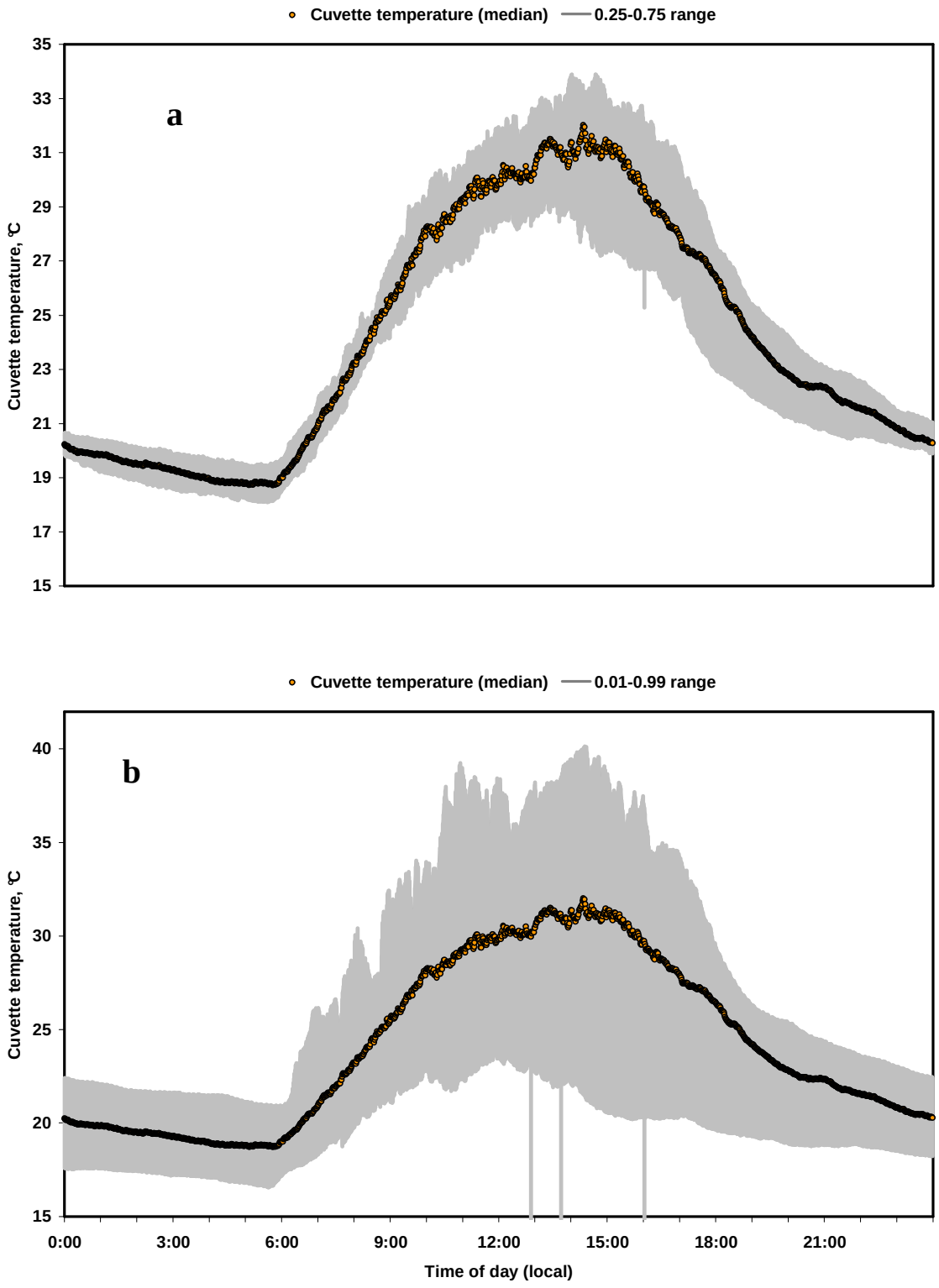

Figure 4.29 *MDC of cuvette temperature from 4 January to 10 February 2007. (a) and (b) show the variation within the 25 % - 75 % and 1 %-99 % probability ranges respectively.*

Leaf temperatures were, on average, highest around 1500h local time.

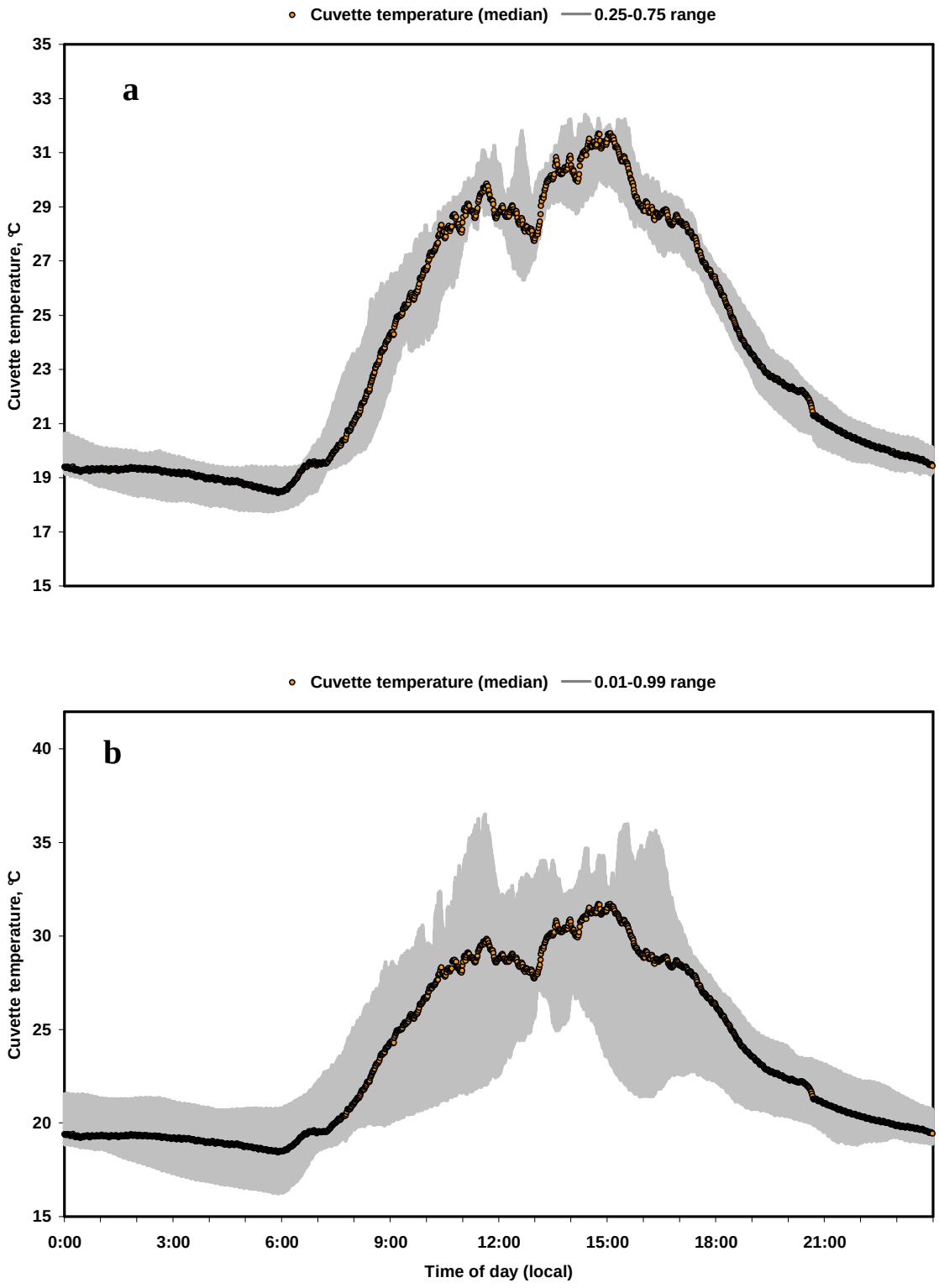

Figure 4.30 *Median diel cycle of cuvette temperature from 11 February to 18 February 2007. (a) and (b) show the variation within the 25 % - 75 % and 1 %-99 % probability ranges respectively.*

4.6 Sap flow dynamics

Sap flow measurements were an important component in trying to meet the objectives of the thesis. Stomatal oscillations were evident in all the measurements on both cultivars of the navel orange trees used in the experiment. These have previously been observed by Steppe *et al*., (2006b) and by Dzikiti *et al.,* (2007) for young navel orange trees at the same experimental site used in this study. They also observed similar oscillations on mature trees in the orchard at Mazoe Citrus Estate in North-eastern Zimbabwe. Steppe *et al.* (2006) postulated that xylem water potential is probably the signal transmitting agent for the oscillations.

From the graphs depicting the MDCs, one can pick out the major oscillations. This shows that the stomatal oscillations followed the same course over more than ten days. It may be argued that the oscillations are predefined, being independent of external environmental factors and only needing to be triggered by the start of the transpiration stream for them to continue until transpiration stops. Following up on that argument it can be said that only the amplitude of the oscillations depends on external environmental factors such as solar radiation and vapour pressure deficit. Thus one can envisage that if external environmental factors are controlled then the amplitude of the oscillations will be constant. Levy and Kauffman (1976) reported good oscillations on 4 year old citrus trees under controlled greenhouse conditions. The results for all four trees showed that maximum sap flow rate usually coincided with 1100 h local time. 1500 h was also associated with a high sap flow rate in most cases.

The hysteresis (Figure 4.33 and 4.36) between stem and branch sap flow has been attributed to high hydraulic capacitance and the formation of embolisms by several researchers (Steppe, 2004; Steppe *et al.*, 2006b; Dzikiti *et al.,* 2007).

Sap flow rates (stem and branch) in this study did not exceed 30 g h^{-1} for all trees. Steppe *et al.,* (2006) and Dzikiti *et al*. (2007) recorded stem and branch sap flows in excess of 120 g h^{-1} on 2 year old navel orange trees in the same pots used in this study. Given that the trees used in this study were 5 years old while the ones in the experiments by Steppe *et al.* and Dzikiti *et al.* were 2 years old one would expect the older trees to have higher sap flow rates. The reason for the difference is most likely to be the fact that the 5 year old trees used in this study had been in small plastic bags from the time they were budded onto their rootstocks until they were transplanted into pots in September 2006. It meant that the roots of the trees had not had the opportunity to expand and allow the tree to grow fully. As a result, the water transport mechanisms of the 5 year old trees were not as well developed as those of the 2 year old trees which were transplanted into pots while still very young. An expert at the citrus nursery where the trees were procured remarked that when young trees are not transplanted within two years of being grafted, they tend to become ‘pot-bound’ i.e. they stop growing like normal trees in the field even if nutrients are not limiting.

Comparison of the diel relationship between branch sap flow per unit leaf area and branch transpirational flux gave a coefficient of determination (R^2) of 0.92 (Figure 4.53). This result was an independent validation of sap flow measurements using the IRGA.

There was little difference between the results of the sap flow measurements. Tree4, however, had results which were on average 50 % lower than for the other trees. This was because its leaf area was correspondingly about 50 % less than that of the other trees on average.

An overview of the sap flow dynamics of two of the four trees under study is given from Figure 4.31 to Figure 4.46. It was unnecessary to show results for all four trees because of the similarity of the results.

4.6.1 Tree2

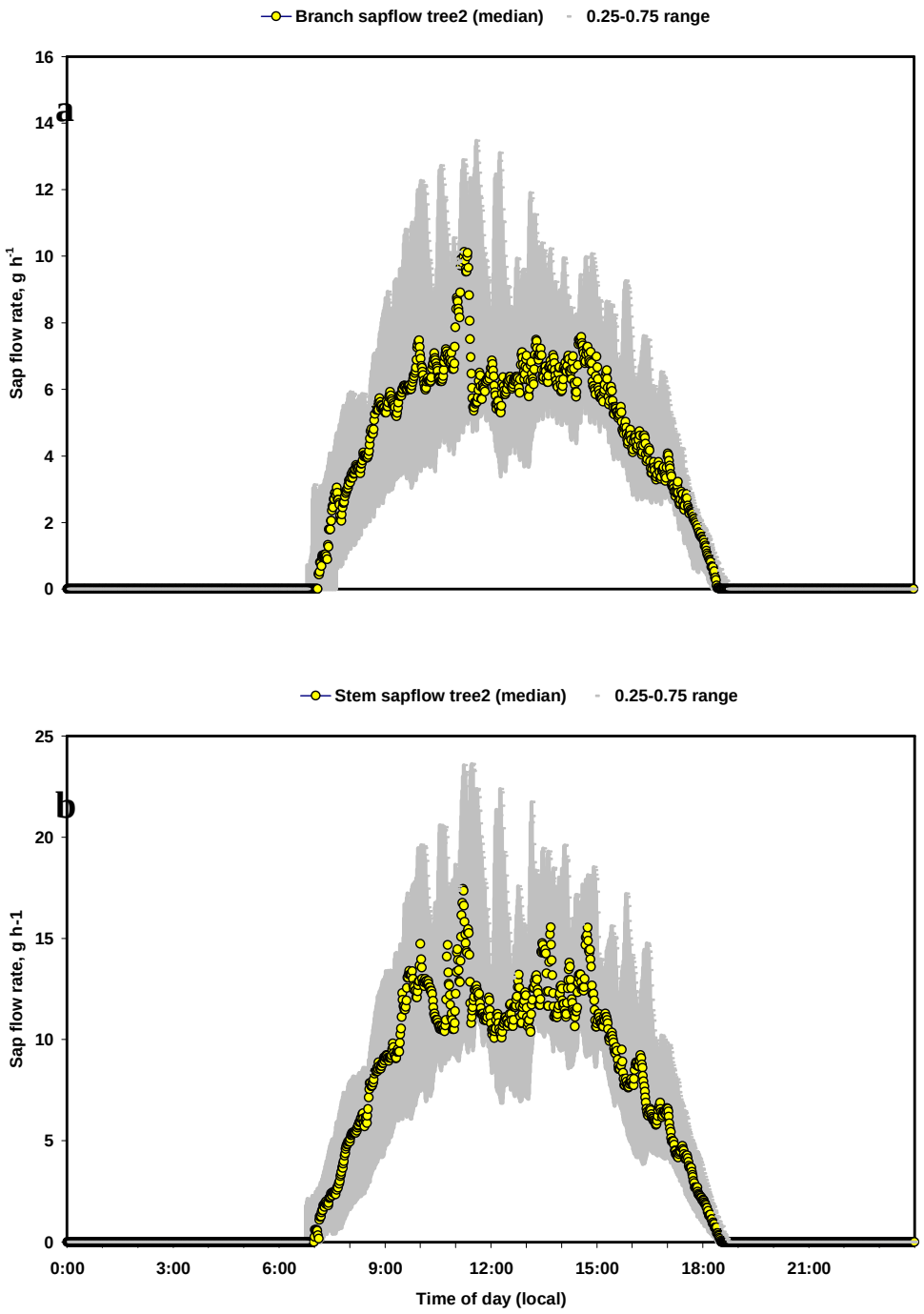

Figure 4.31 *Median diel cycle of branch and stem sap flow for tree2*

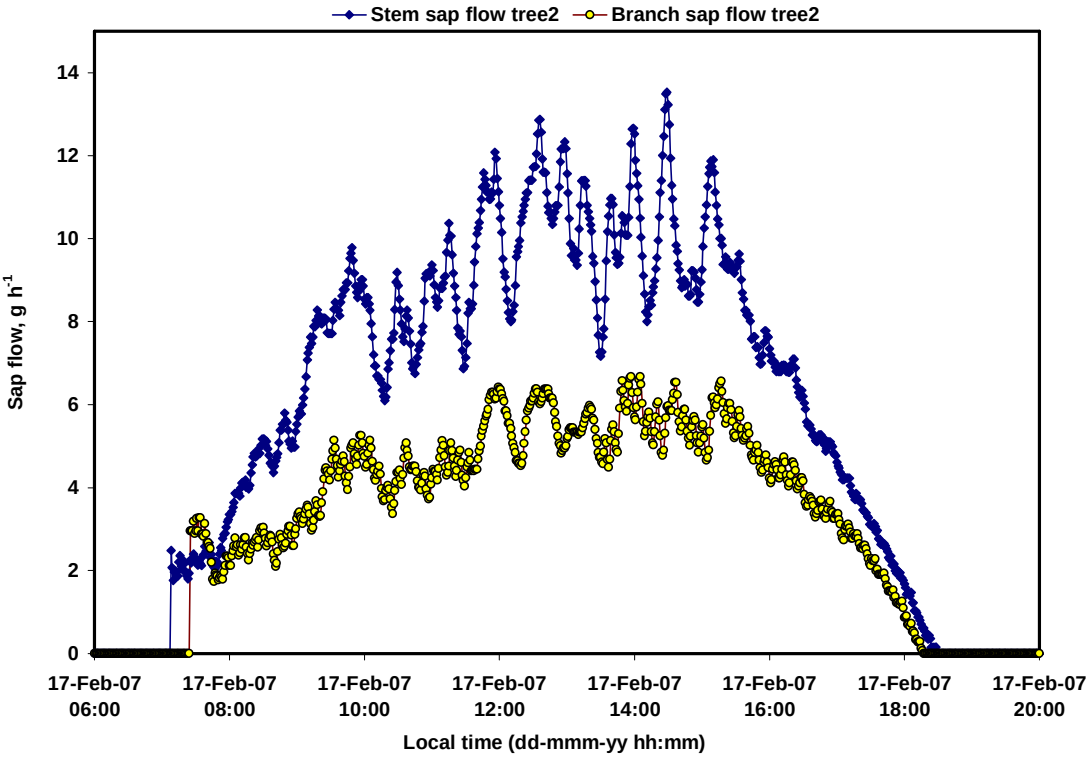

Figure 4.32 *Comparison of branch and stem sap flow on 17 February 2007 (double net in place).The stomatal oscillations were very clear on this day.*

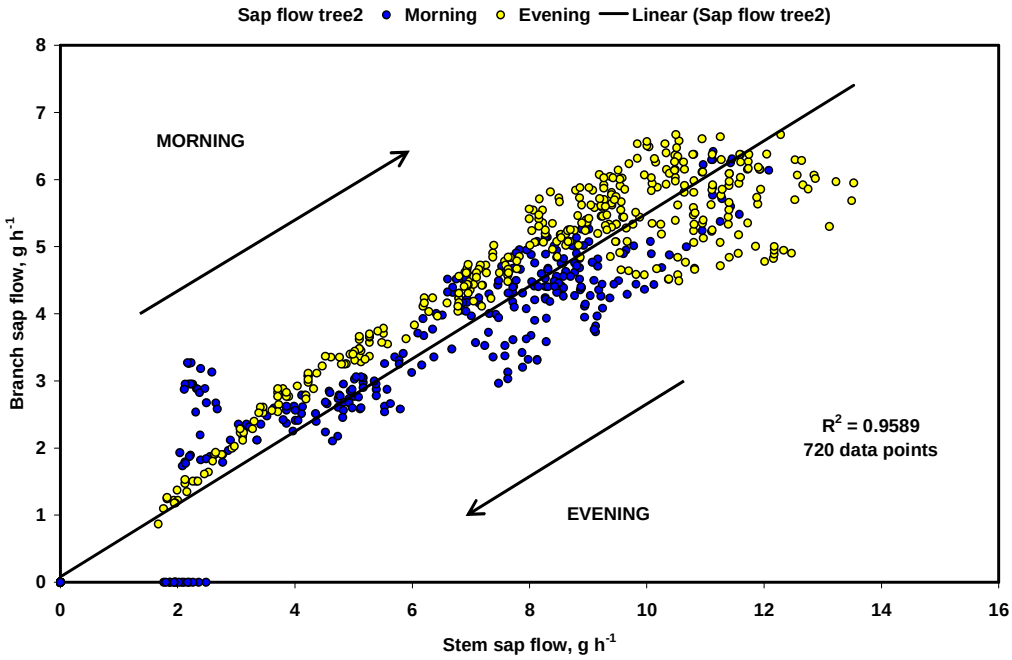

Figure 4.33 *Diel correlation between stem and branch sap flow of tree2 on 17 February 2007. A double layer shade net was in place.*

4.6.2 Tree4

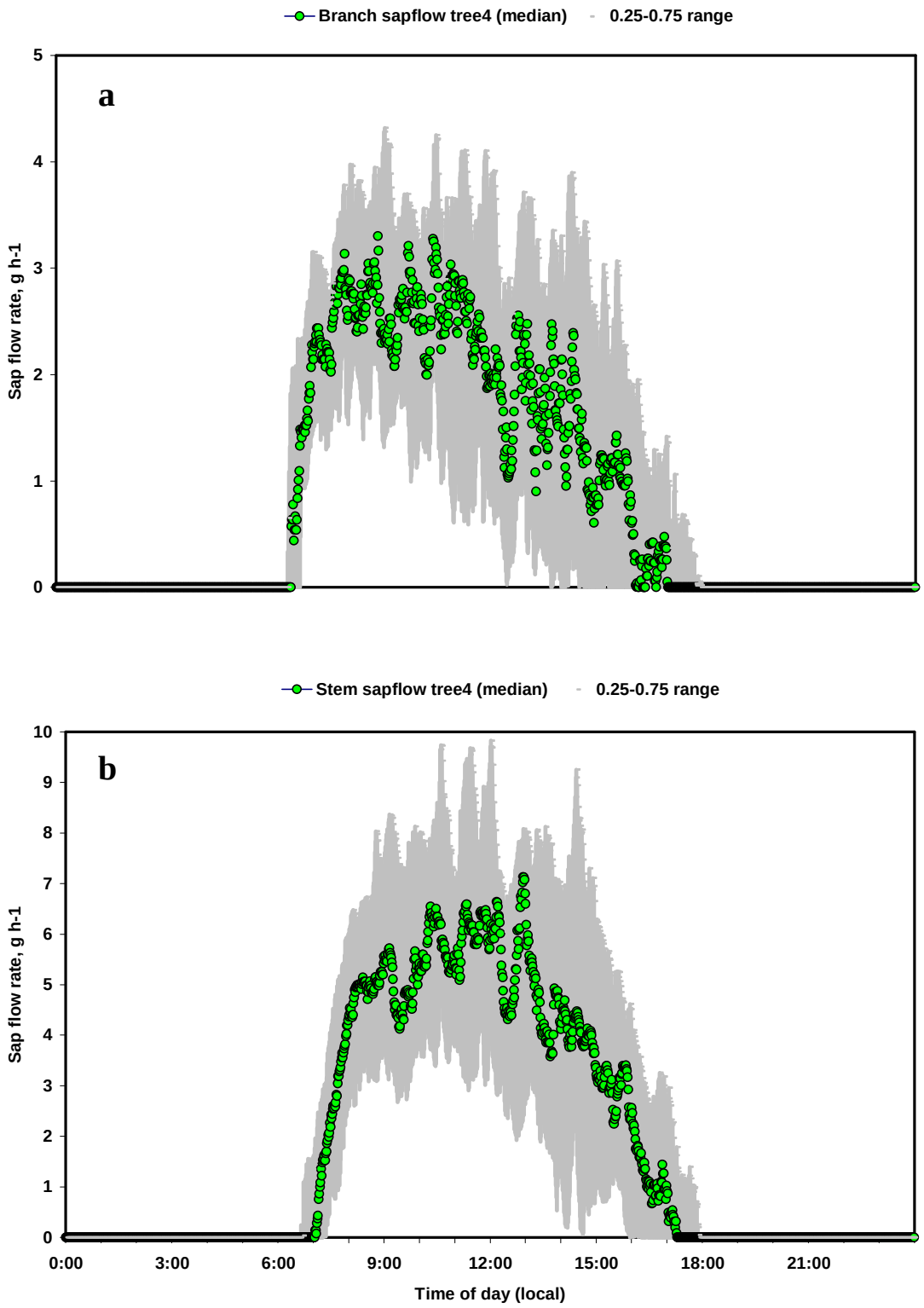

Figure 4.34 *Median diel variation of (a) branch and (b) stem sap flow forTree4*

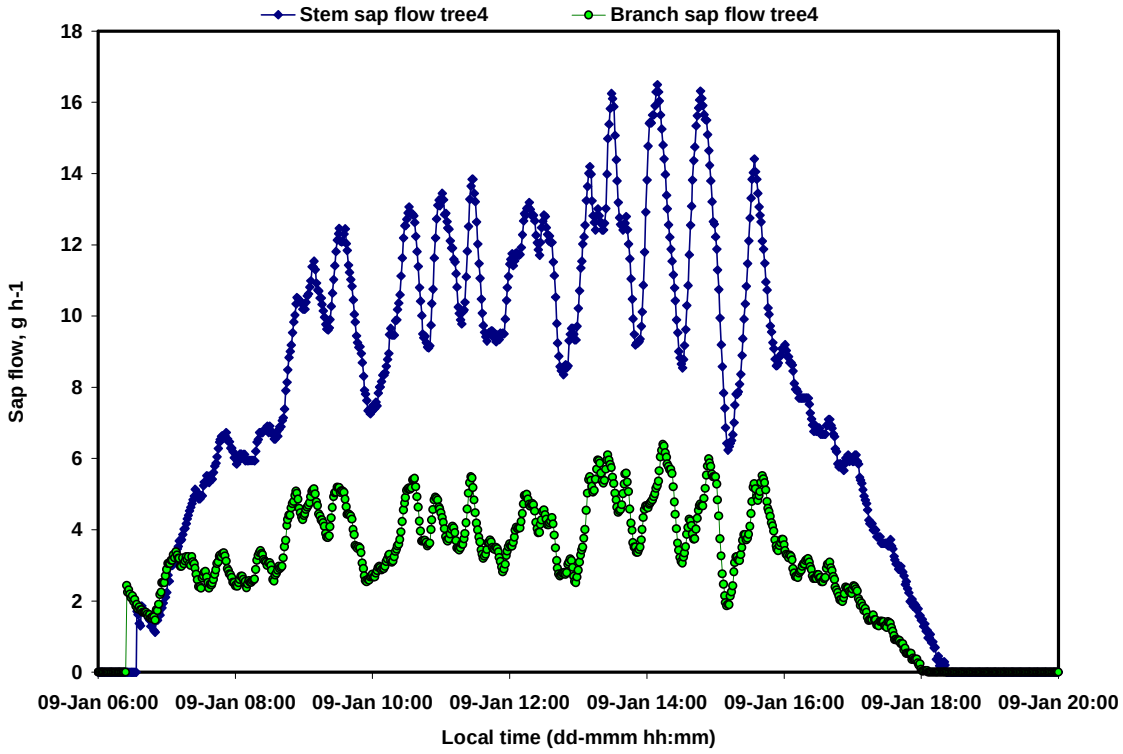

Figure 4.35 *Diurnal course of stem and branch sap flow for Tree4 on 9 January 2007*

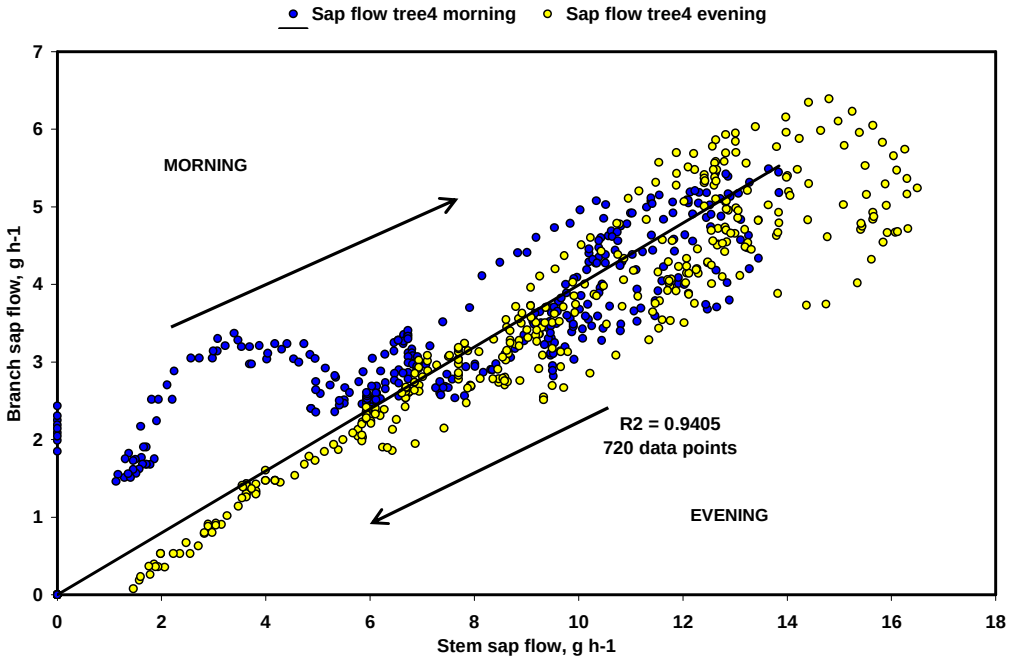

Figure 4.36 *Diel correlation between stem and branch sap flow for Tree4 on 9 January 2007.The hysteresis is much larger than that shown for Tree2 in Figure 4.33. The main reason for the difference is that this one was for measurements taken under a single layer net while the one in Figure 4.33 was for a double layer net in which the radiation regime is largely invariant*

4.6.3 Inter-varietal comparison of sap flow rates

There was very little difference between the sap flow dynamics of the pairs of citrus cultivars studied in this experiment. The results are shown in Figure 4.37-8.

4.6.3.1 *Navelina*

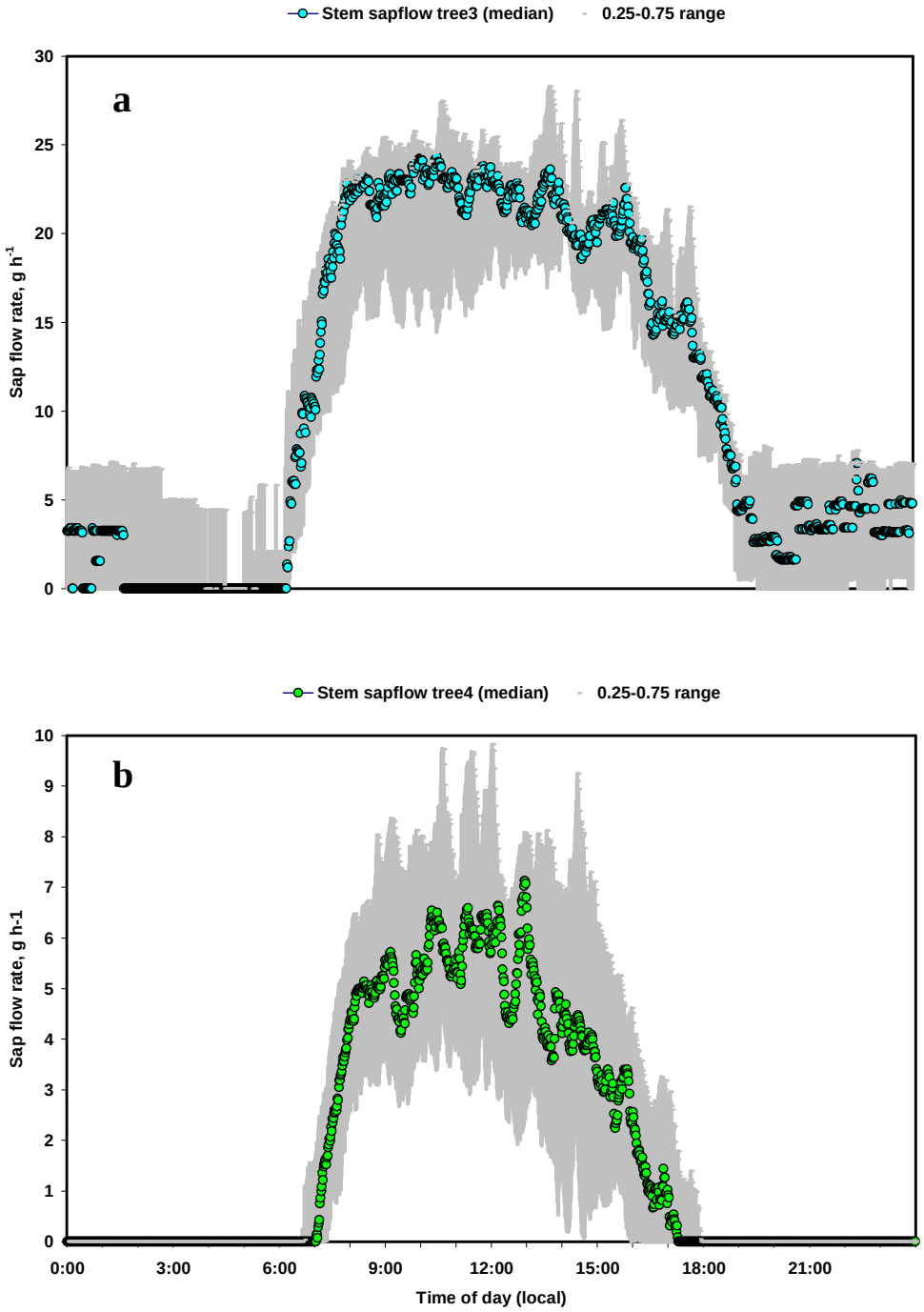

Figure 4.37 *Median diel cycle of stem sap flow rate: (a) Tree3-large night-time fluctuations were present for Tree3, possibly caused by temperature sensitivity; (b) Tree4 stem sap flow. The difference in maximum sap flow rate between Tree3 and Tree4 is noticeable. It was attributed to the difference in leaf area of the trees.*

4.6.3.2 *Baianinha*

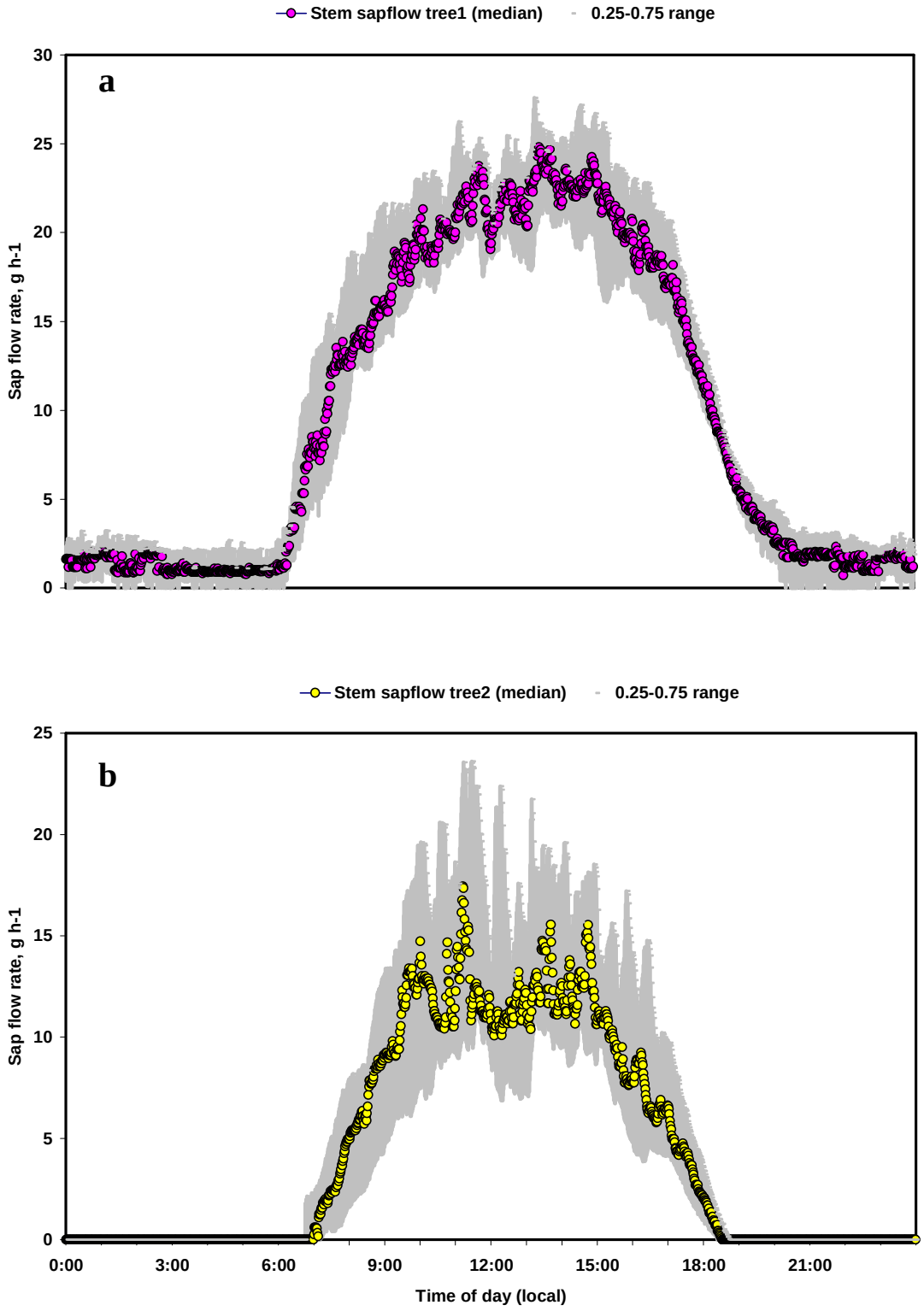

Figure 4.38 *Comparison of the MDC of sap flow rate for between (a) Tree1 and (b) Tree2*

4.6.4 Intra-varietal comparison

Variations of sap flow rates between the two varieties of navel orange trees are presented in this section. The results showed a general similarity between the sap flow rates of the two cultivars.

4.6.4.1 *Navelina* vs *Baianinha*

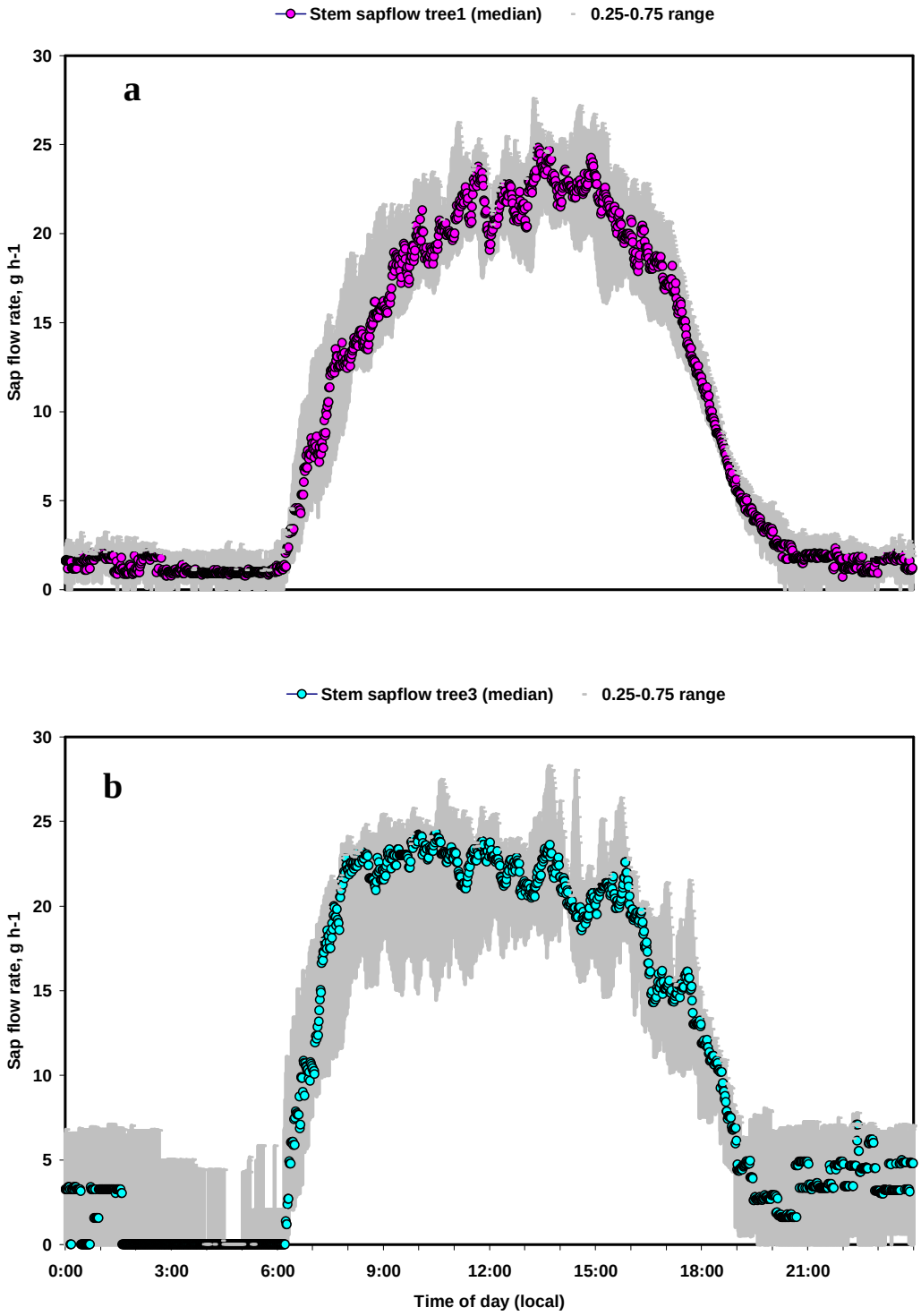

Figure 4.39 *Median diel cycle of stem sap flow rates*

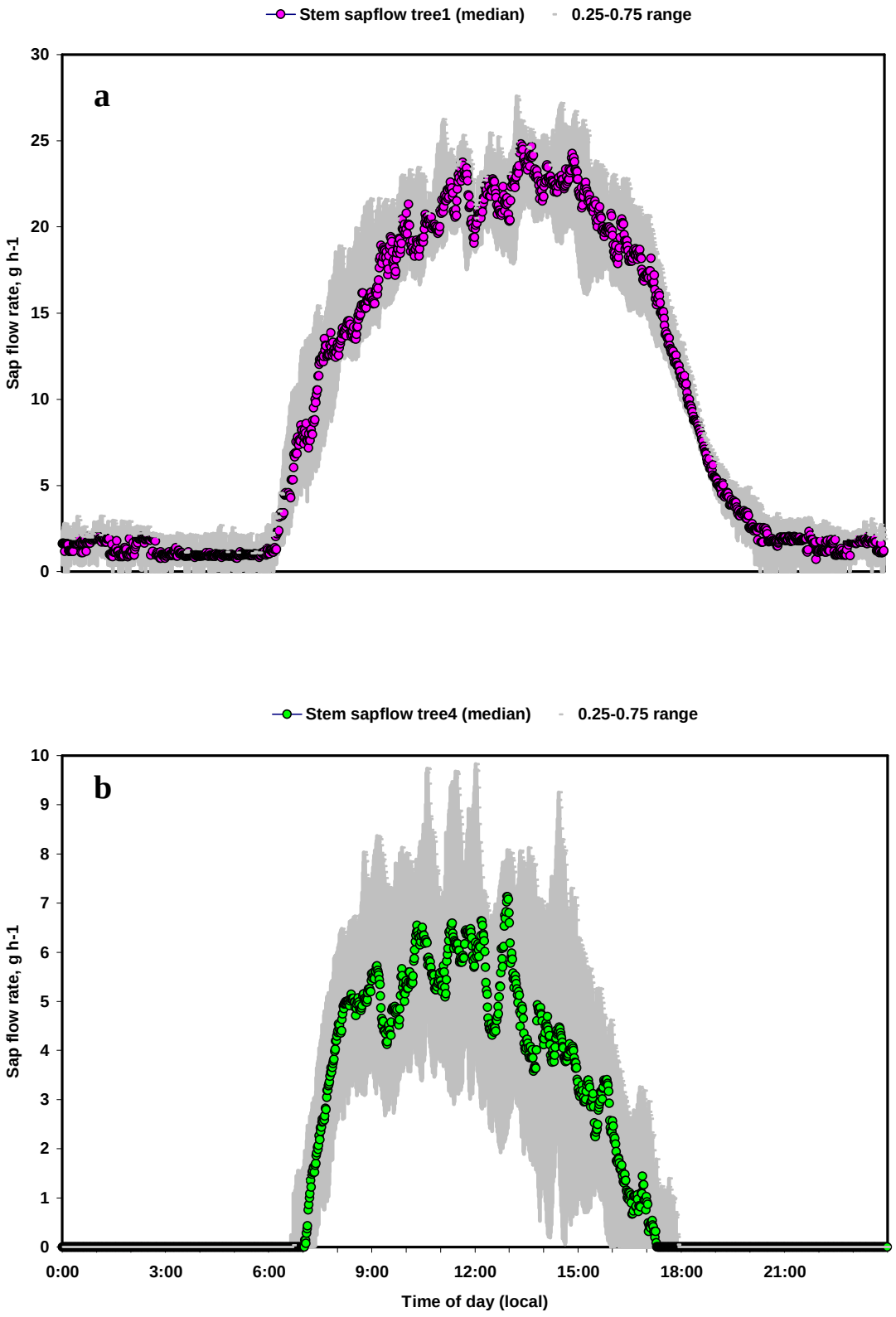

Figure 4.40 *Median diel cycle of sap flow rates*

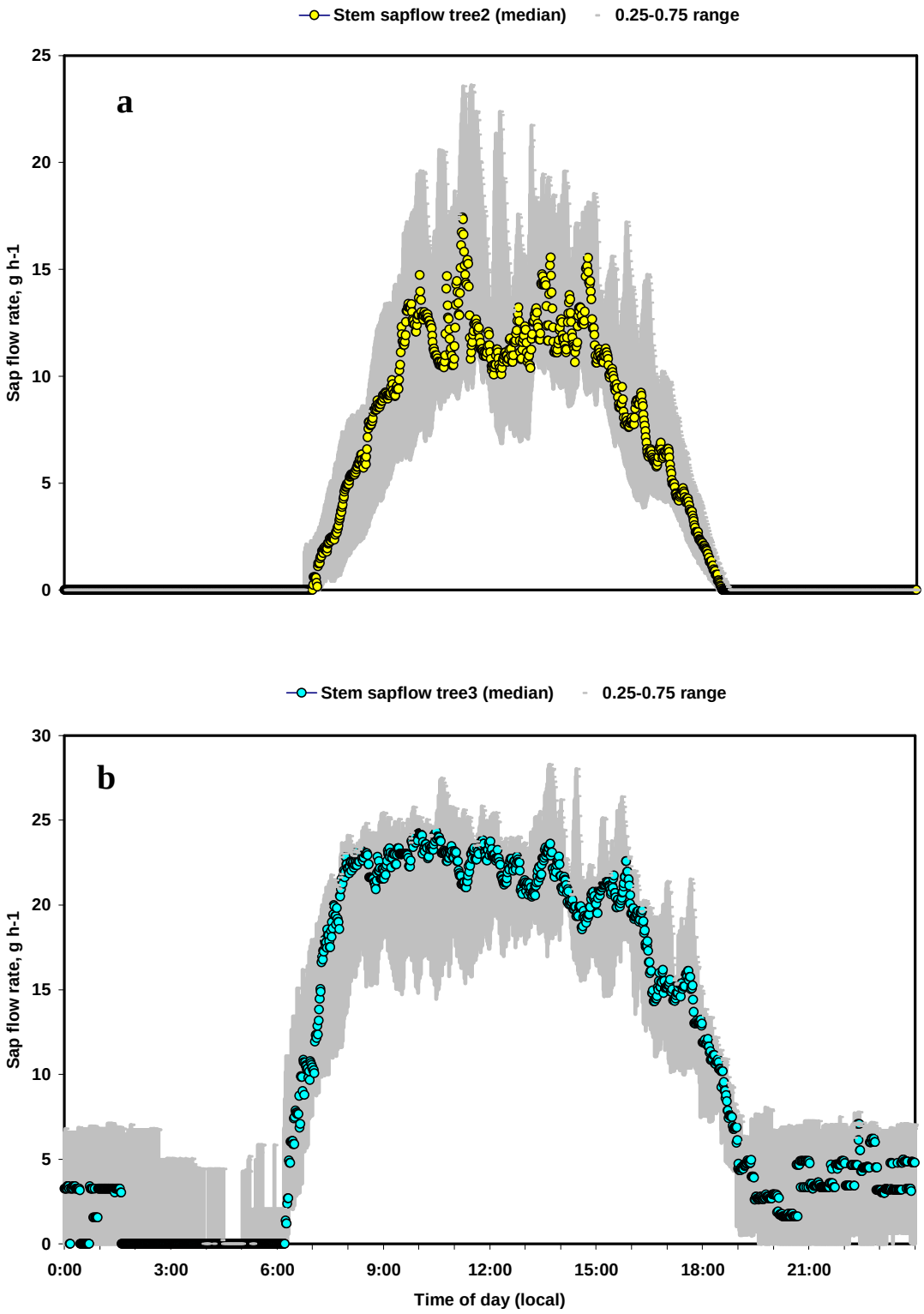

Figure 4.41 *Median diel cycle of stem sap flow rates*

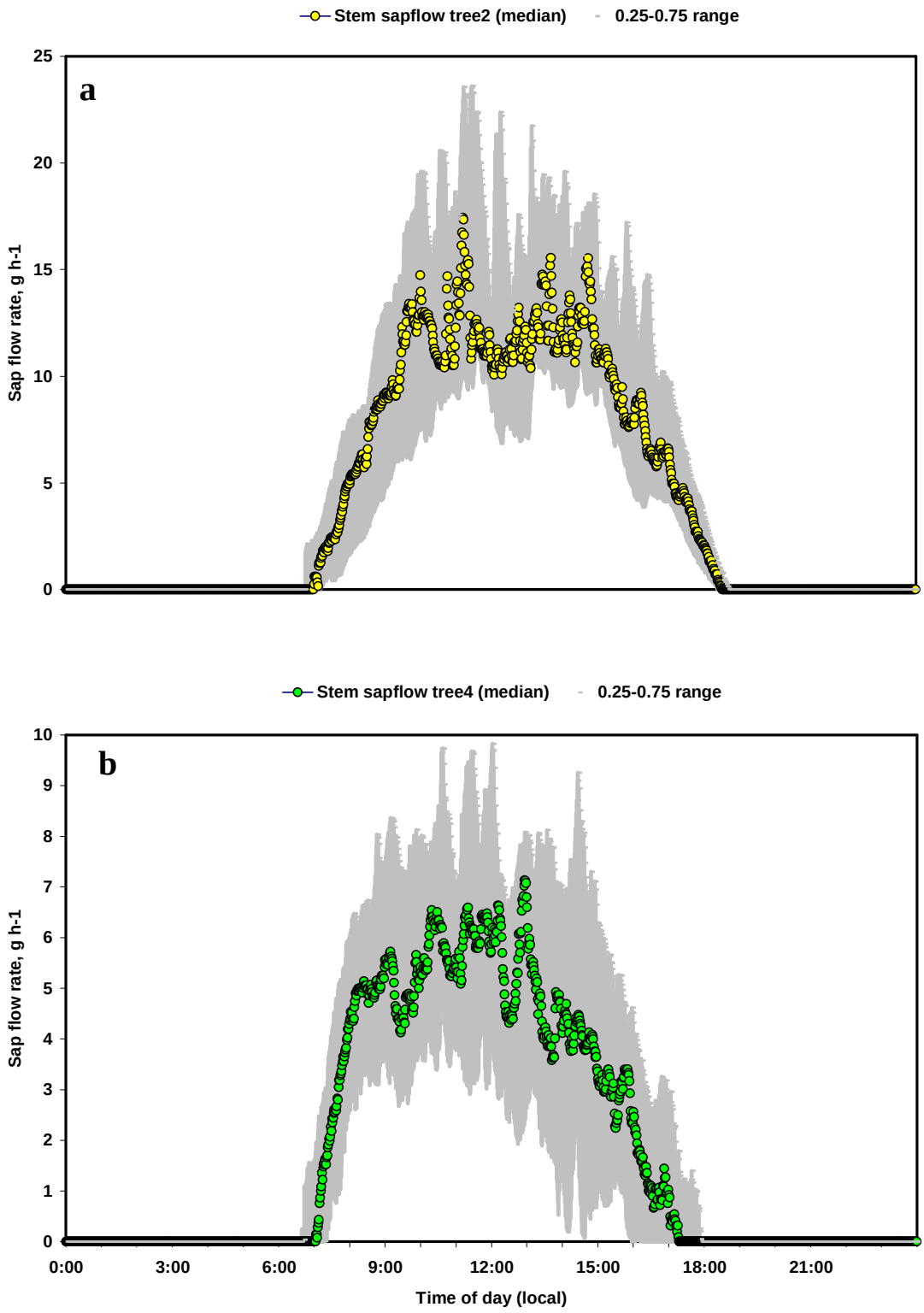

Figure 4.42 *Median diel cycle of sap flow rates. Sap flow ended much later for Tree2 (a) than Tree4(b) although it began at roughly the same time.*

4.6.5 Effect of shading on branch and stem sap flow rate

Figures 4.43 up to Figure 4.46 show that, in general, stem sap flow rates were lowest when there was no shade net in place, i.e. when temperatures and solar radiation were highest. This is the same trend that was followed by the transpirational fluxes shown earlier in this chapter. Transpiration rates for a single layer shade net and a double layer shade net were similar for Tree2 and Tree1. The reason for the low sap flow rates when the trees were fully exposed may be that the stomata tend to close when the radiation load is high, thus reducing sap flow.

The implication of this finding is that when temperatures are high i.e. when citrus trees are fully exposed to solar radiation, transportation of photosynthates is inhibited or at least slowed down

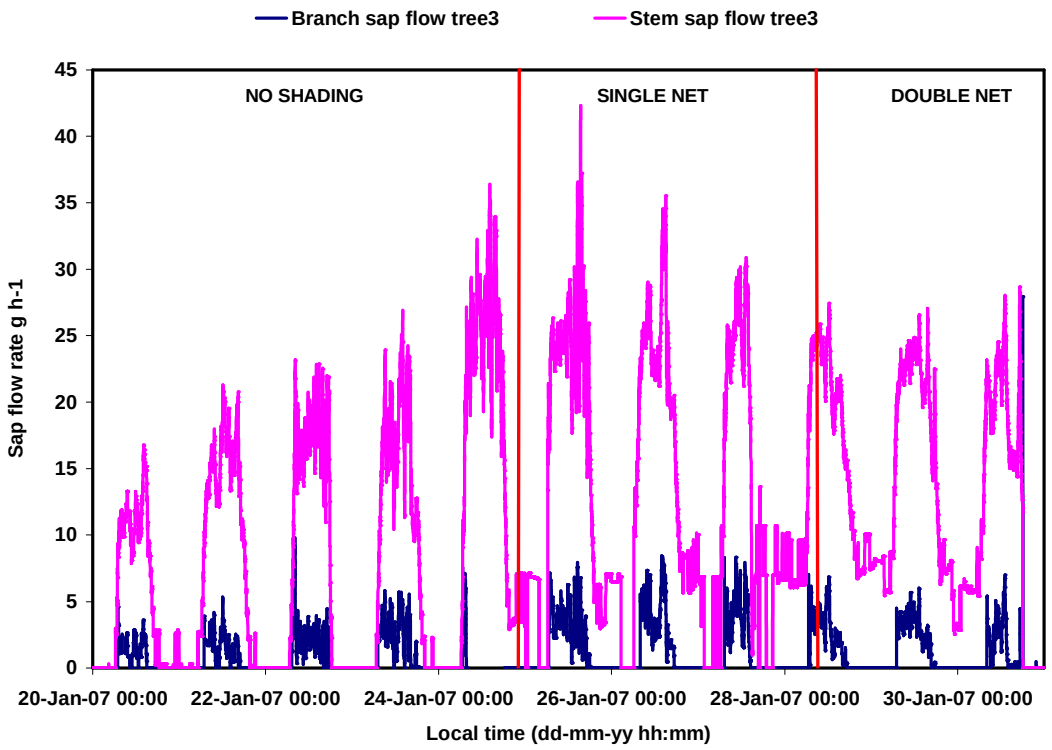

Figure 4.43 *Variation of sap flow rate on Tree3 from 20 to 30 January 2007 under different solar radiation regimes*

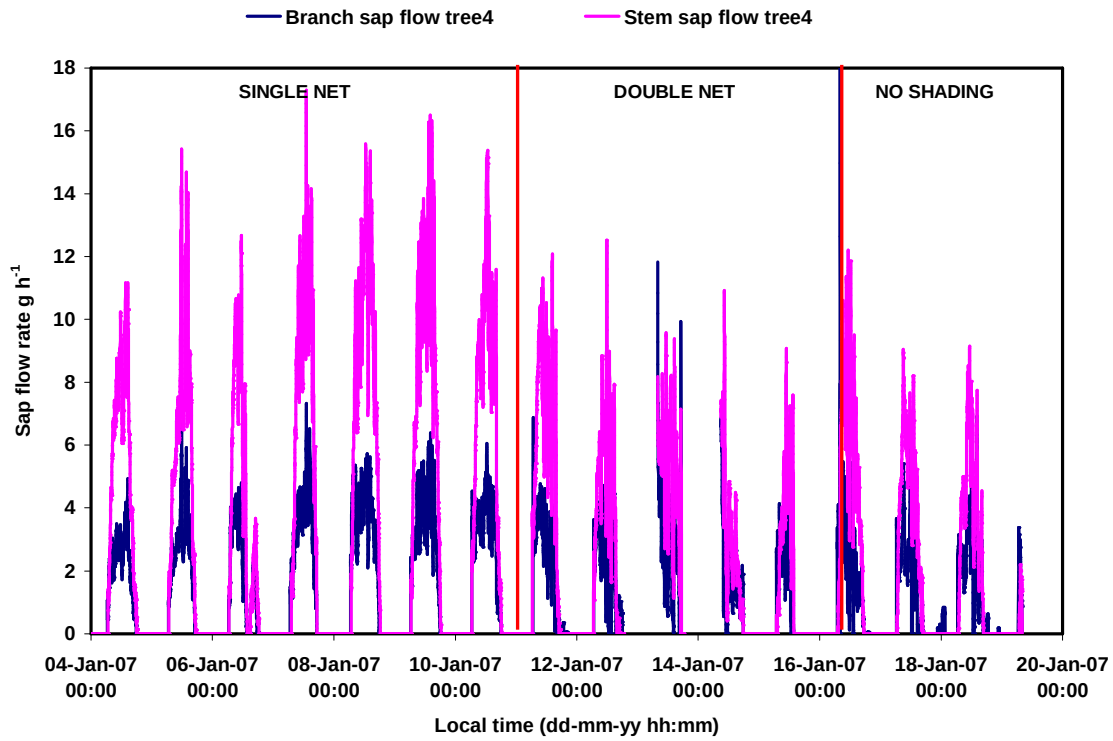

Figure 4.44 *Variation of sap flow rate on Tree4 from 4 to 20 January 2007 under different solar radiation regimes*

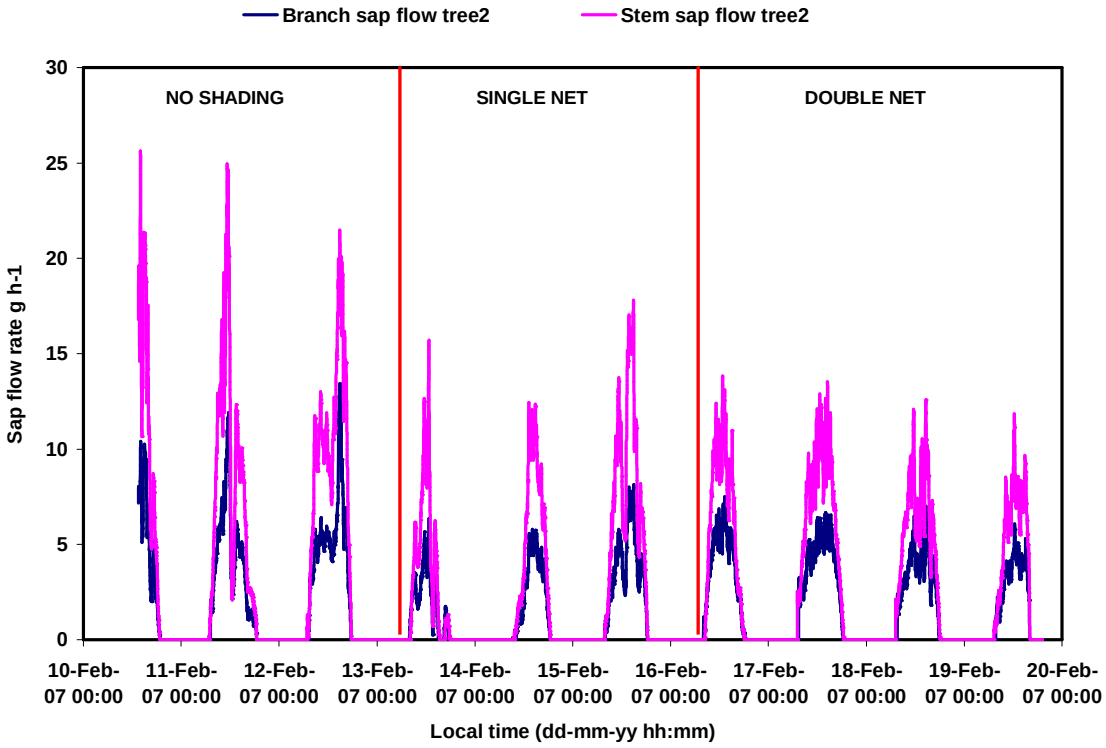

Figure 4.45 *Variation of sap flow rate on Tree2 from 10 to 20 February 2007 under different solar radiation regimes*

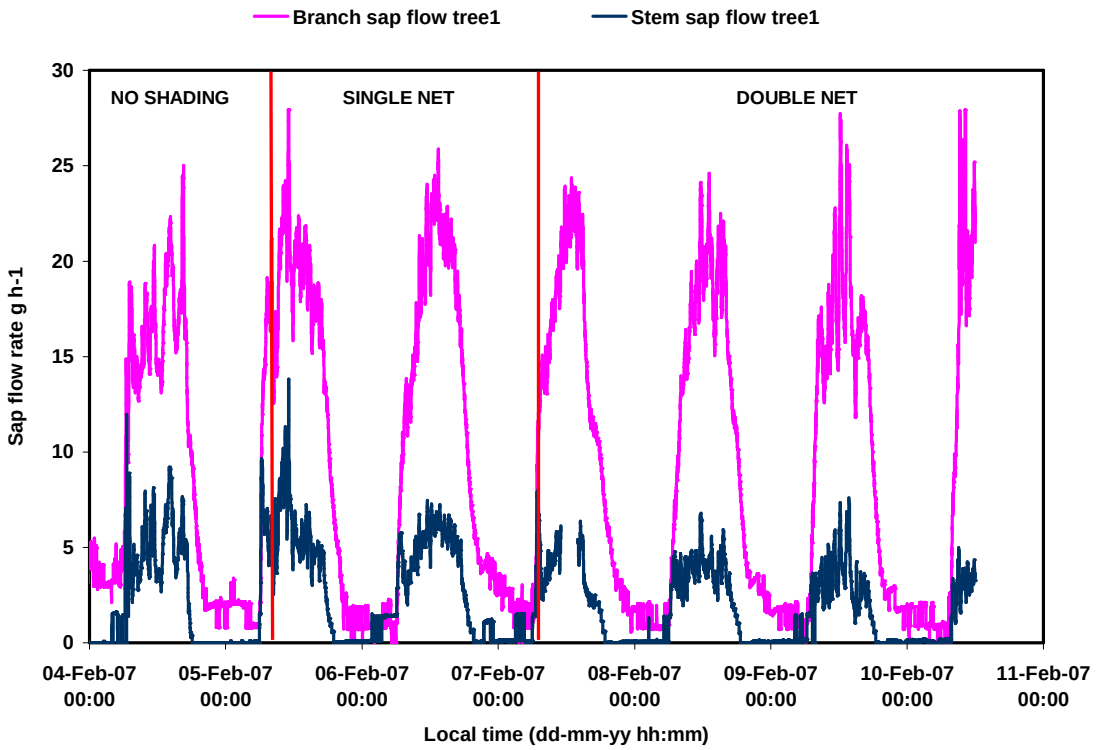

Figure 4.46 *Variation of sap flow rate on Tree1 from 4 to 11 February 2007 under different solar radiation regimes*

4.7 Effect of shading on photosynthesis, transpiration, leaf temperature and water relations

In this section we look at the effects of shading on the photosynthetic response, transpirational dynamics, leaf temperature, and water relations of the young citrus trees.

4.7.1 Effect of shading on photosynthesis

An analysis of the effect of shading on net photosynthesis is given from Figure 4.47 up to Figure 4.53. The results for Tree1 and Tree3 are not presented here but are shown in the summary at the end of this Chapter.

Maximum CO_2 uptake averaged 20 µmol m^{-2} s^{-1} while the maximum CO_2 loss averaged 1 µmol m^{-2} s^{-1} within the 75 % confidence limits. Spiegel-Roy and Goldschmidt (1996) report values of 4-12 µmol m^{-2} s^{-1} for citrus under optimal field conditions but state that much higher rates are frequently obtained in greenhouse experiments. Syvertsen *et al.* (2003) also found maximum citrus CO_2 assimilation rates of nearly 12 µmol m^{-2} s^{-1}. However, in all these cases the method of measurement was a portable single-leaf photosynthesis measurement system and measurements were not taken continuously but only around midday. Maximum CO_2 assimilation rates above 20 µmol m^{-2} s^{-1} e.g. 25-30 µmol m^{-2} s^{-1} for cherry as noted by Spiegel-Roy and Goldschmidt (1996) are frequently recorded in other trees. Documentation of citrus CO_2 assimilation measurements using a whole-branch are scarce.

The single layer shade net treatment gave the best overall results in terms of photosynthesis. Transpiration rates were also highest for a single shade treatment. Midday depression of photosynthesis was also reduced under both single and double shade nets. Similar results were found by Raveh *et al.* (2002) using 30 % and 60 % shade nets on 2-year old citrus trees. They found that a 30 % shade treatment increased leaf conductance by 44 % and photosynthesis by 29 % relative to an unshaded control. Syvertsen *et al.*, (2003). Jifon and Syvertsen (2001) also reported increases in CO_2 assimilation as a result of shading.

When comparing all four trees, the *Navelinas* had higher CO_2 assimilation and transpiration rates on average than the *Baianinhas*.

CO_2 fluxes showed that, despite the high leaf temperatures which were unsuitable for photosynthesis, the young citrus trees had the highest CO_2 flux when there was no shading. The poor performance of the trees under single and double shading may be explained by the very low transmittance to PPFD of the two shading regimes. It is possible that if a shade net which could transmit PPFD above the saturation values of 600-700 µmol m^{-2} s^{-1}, had been available, then the rates of photosynthesis would have been higher for the single-shaded regime. The photosynthetic rates of the *Navelina* cultivars were up to 20 % higher than that for the *Baianinha* cultivars.

Transpiration was highest under a single shade net for all four trees. The unshaded regime had the lowest transpiration rates, possibly due to a large number of stomata closing under stress from the high leaf temperatures. This is interesting because, it gives the impression that the photosynthetic rates could be even higher than they were in the unshaded treatment if more stomata were open. Transpiration and photosynthesis in the unshaded regime may have been, to a smaller extent, due to the contribution of shaded leaves and shaded sections of leaves within the branch.

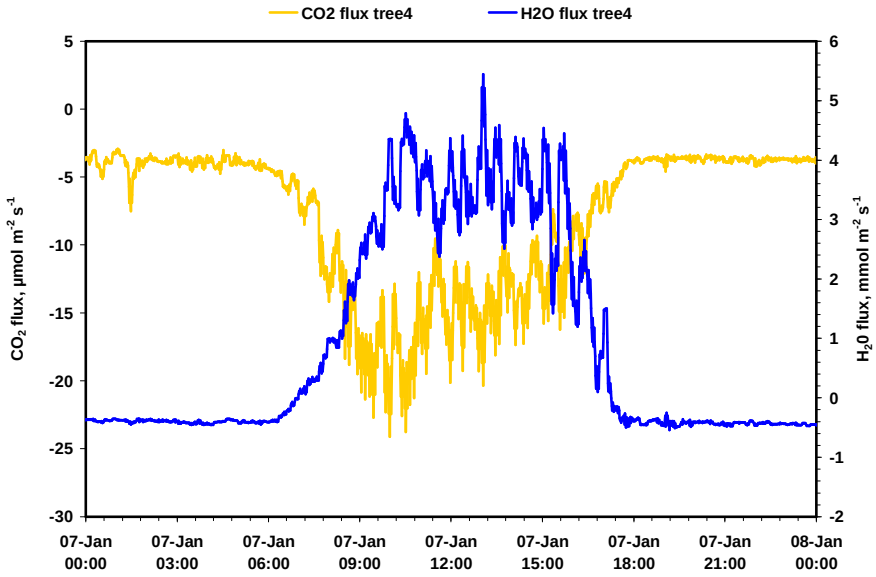

Figure 4.47 *Comparison of variation of CO_2 and H_2O flux on Tree4 on 8 January 2007.*

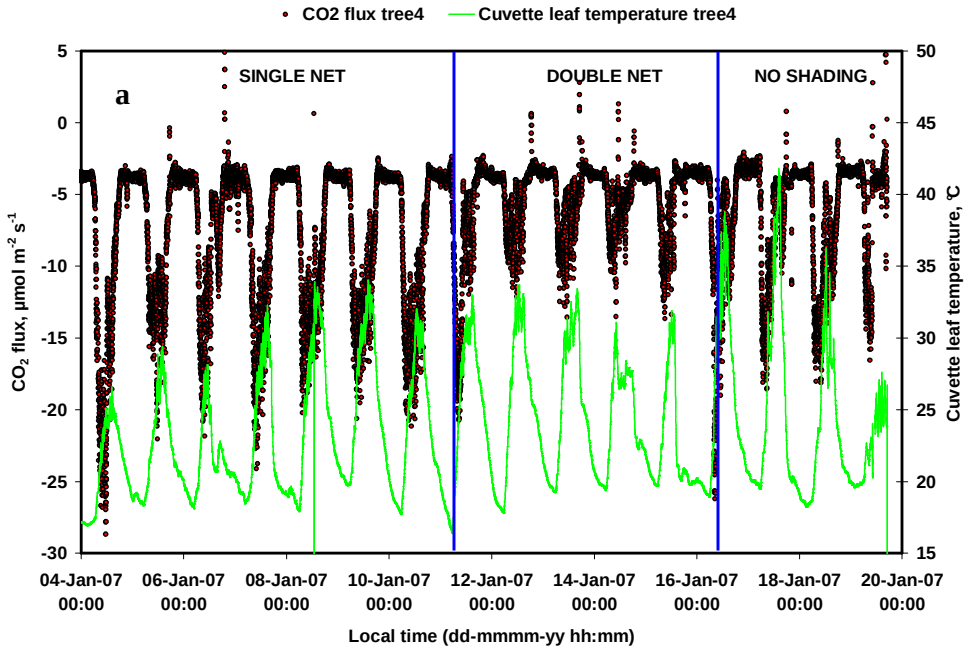
CO2 flux tree4
Cuvette leaf temperature tree4
a
SINGLE NET
DOUBLE NET
NO SHADING
CO2 flux, µmol m-2 s-1
Cuvette leaf temperature, ℃
5
0
-5
-10
-15
-20
-25
-30
50
45
40
35
30
25
20
15
04-Jan-07 00:00
06-Jan-07 00:00
08-Jan-07 00:00
10-Jan-07 00:00
12-Jan-07 00:00
14-Jan-07 00:00
16-Jan-07 00:00
18-Jan-07 00:00
20-Jan-07 00:00
Local time (dd-mmmm-yy hh:mm)

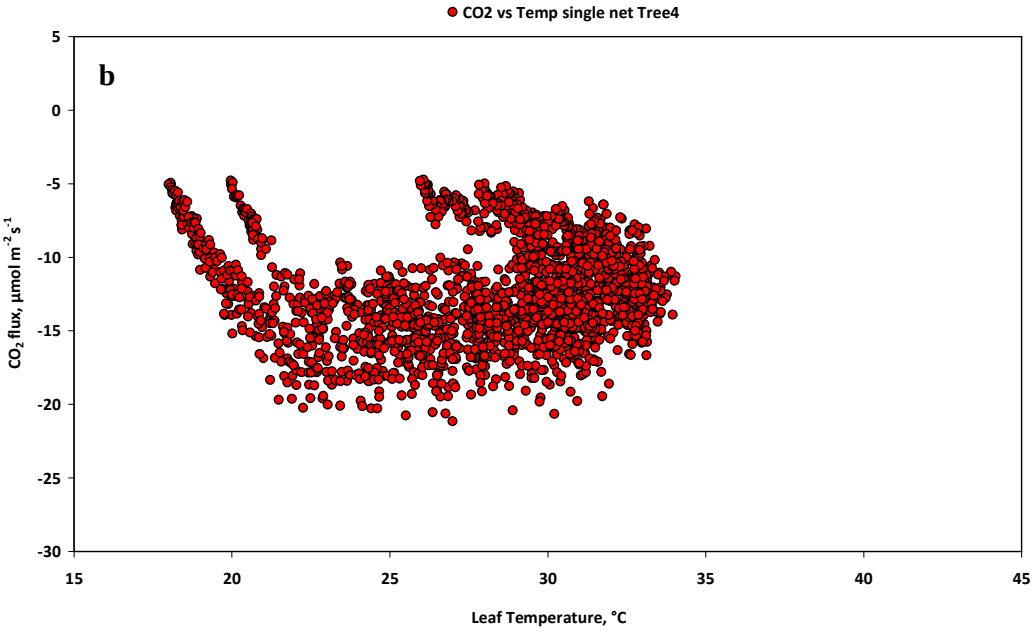
CO2 vs Temp single net Tree4
b
CO2 flux, µmol m-2 s-1
5
0
-5
-10
-15
-20
-25
-30
15
20
25
30
35
40
45
Leaf Temperature, °C

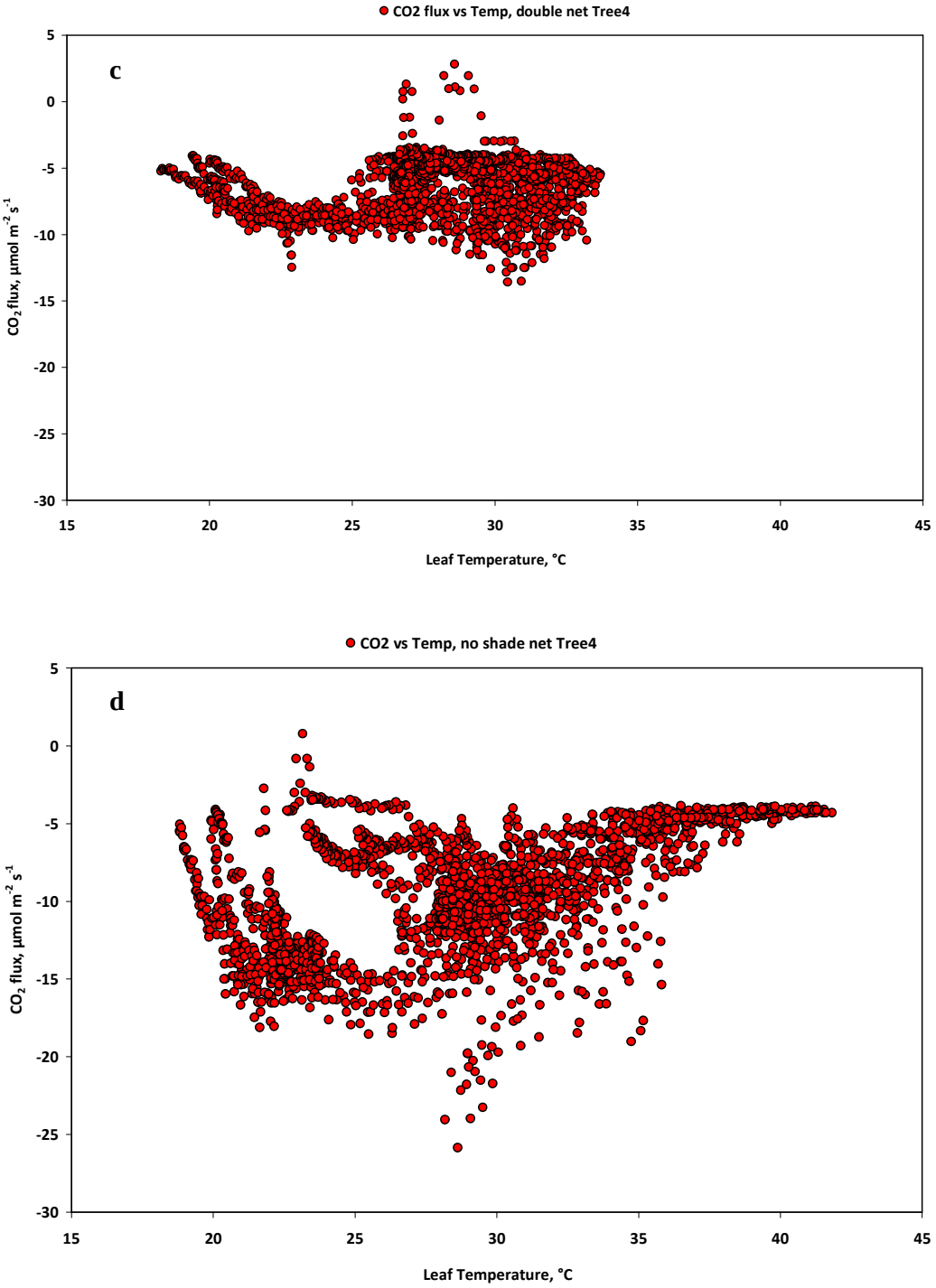

Figure 4.48(a-d) *Diel variation of CO_2 flux and cuvette leaf temperature under different solar radiation regimes from 4 January to 20 January on Tree4*

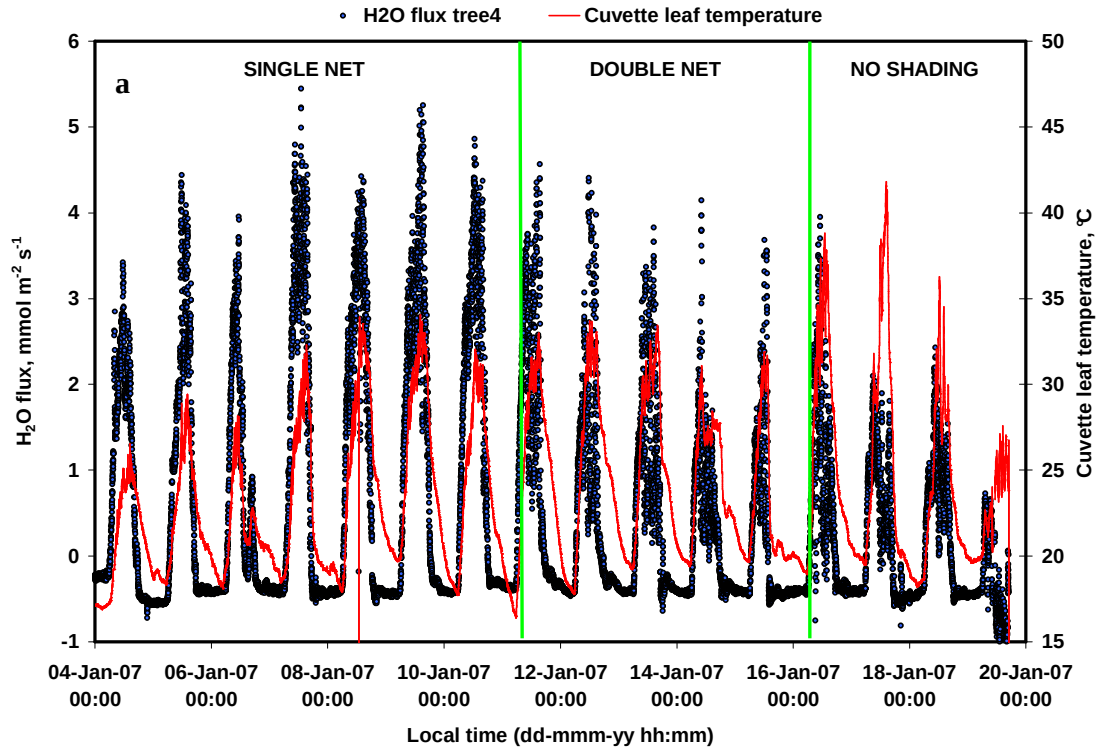
H2O flux tree4
Cuvette leaf temperature
a
SINGLE NET
DOUBLE NET
NO SHADING
H2O flux, mmol m-2 s-1
Cuvette leaf temperature, ℃
04-Jan-07 00:00
06-Jan-07 00:00
08-Jan-07 00:00
10-Jan-07 00:00
12-Jan-07 00:00
14-Jan-07 00:00
16-Jan-07 00:00
18-Jan-07 00:00
20-Jan-07 00:00
Local time (dd-mmm-yy hh:mm)

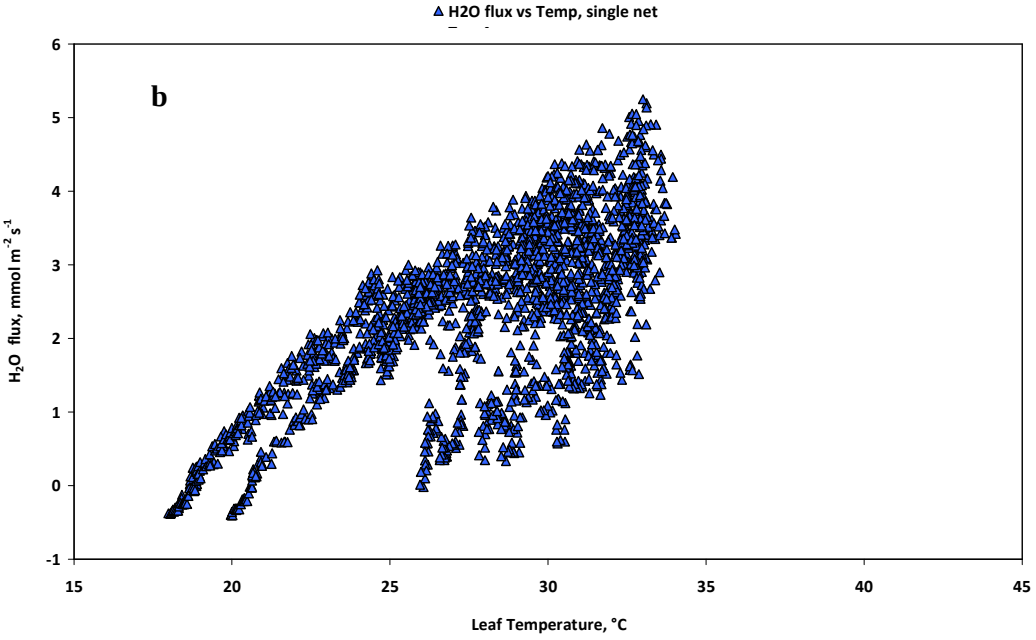
H2O flux vs Temp, single net
b
H2O flux, mmol m-2 s-1
Leaf Temperature, °C

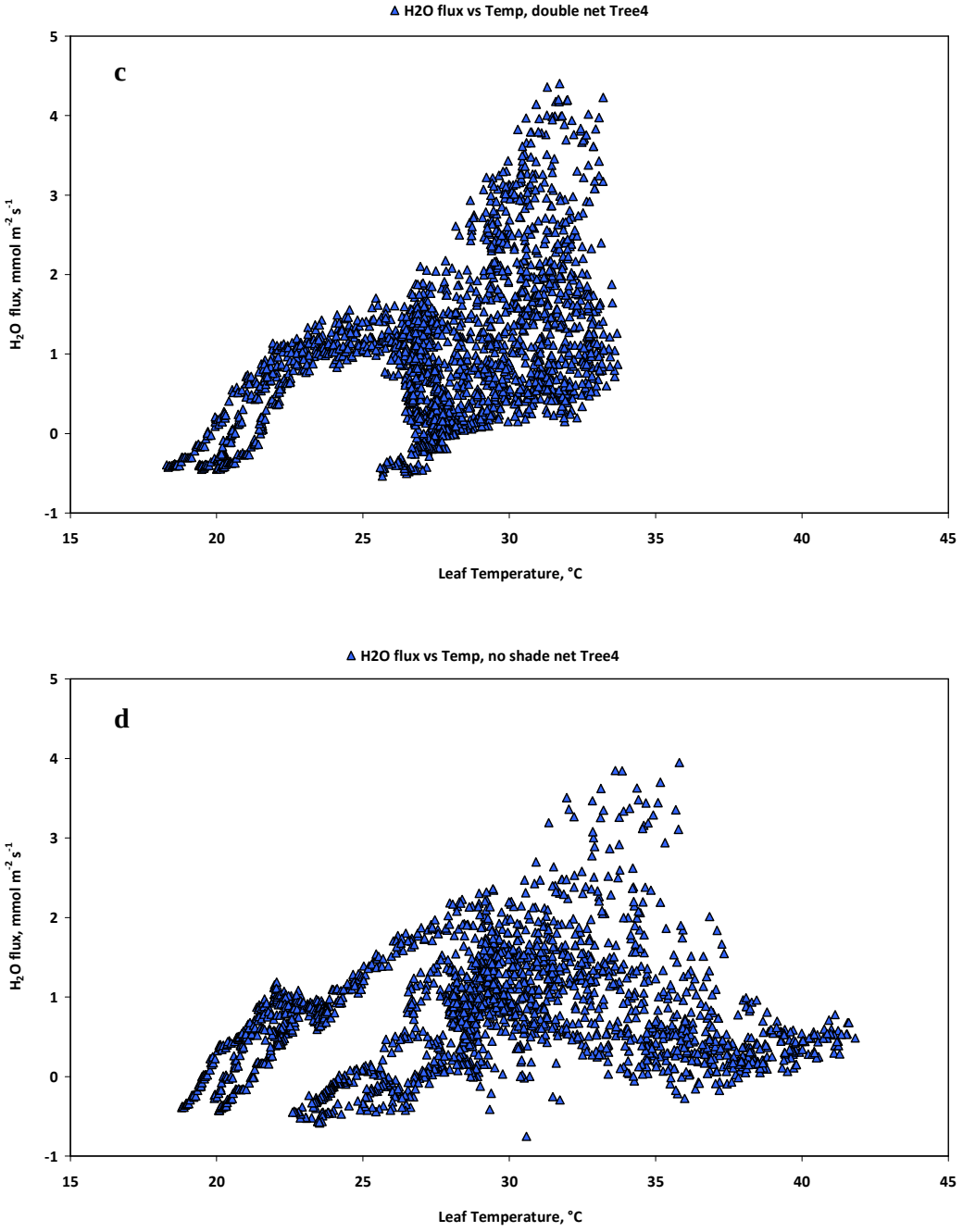

Figure 4.49(a-d) *Diel variation of H_2O flux (transpiration) and cuvette leaf temperature under different solar radiation regimes from 4 January to 20 January on tree4*

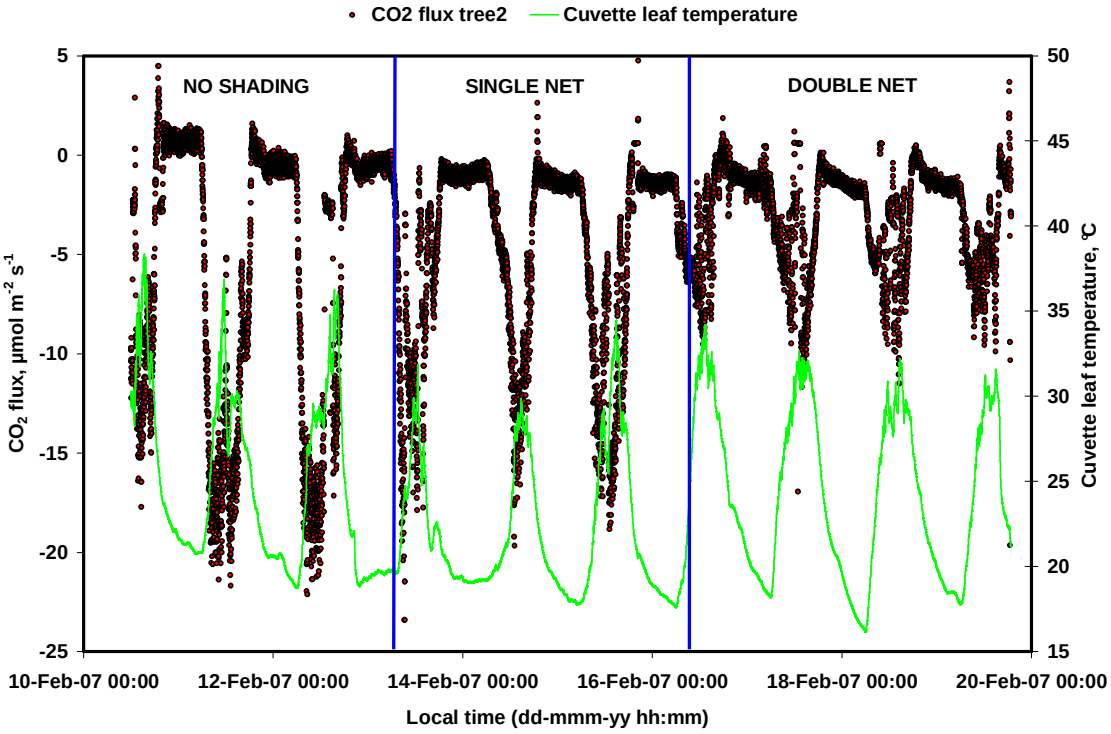

Figure 4.50 *Diel variation of CO_2 flux and cuvette temperature under different solar radiation regimes from 10 to 19 February 2007 on Tree2.*

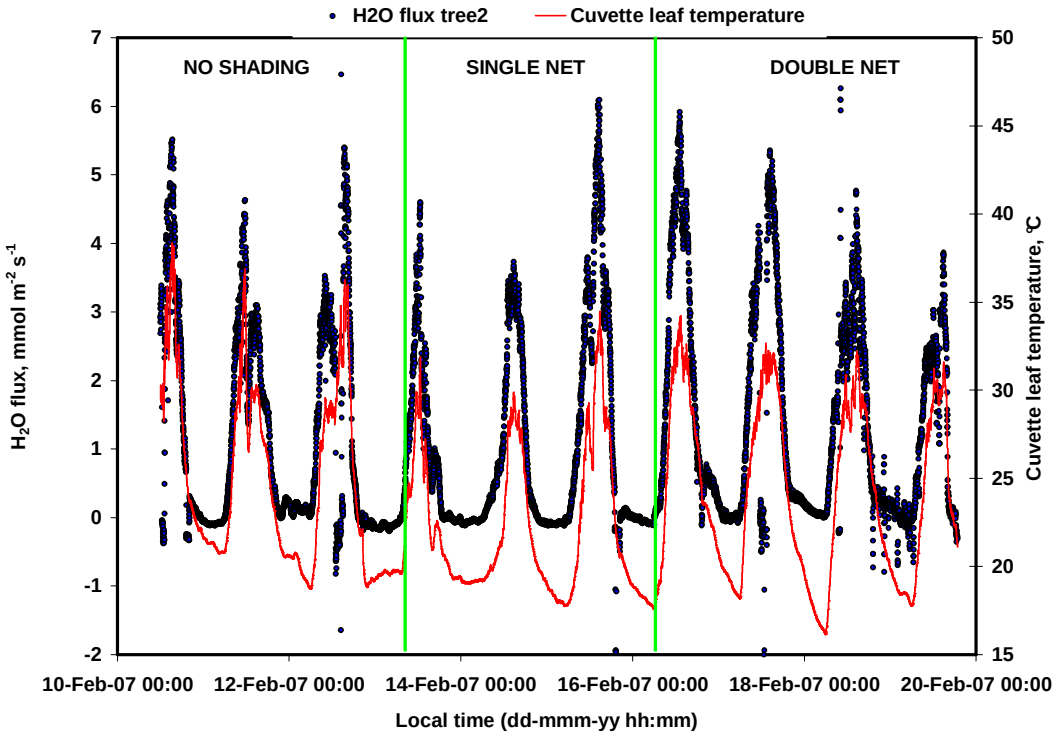

Figure 4.51 *Diel variation of H_2O flux (transpiration) and cuvette temperature under different solar radiation regimes from 10 to 19 February 2007 on Tree2.*

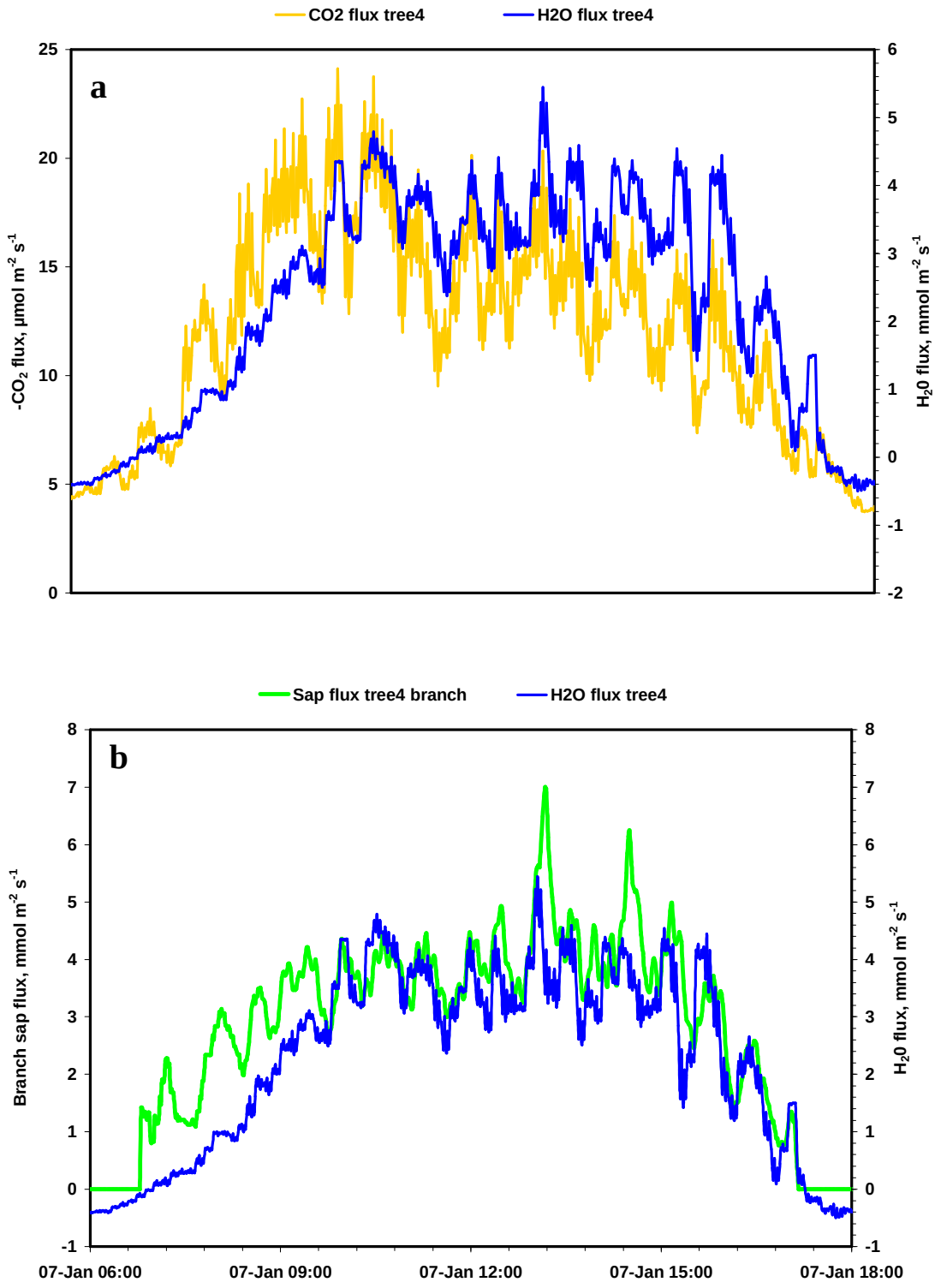

Figure 4.52 *Comparison between (a) -CO_2 and H_2O flux which showed good correlation (b)branch sap flux and H_2O flux for Tree4 on 7 January 2007. The results where a further validation of the sap flow measurements.The negative sapflow values were probably a results of distortions associated with the start and end of the transpiration stream. Such distortions were largely rectified by using a conditional filter for the sapflow data.*

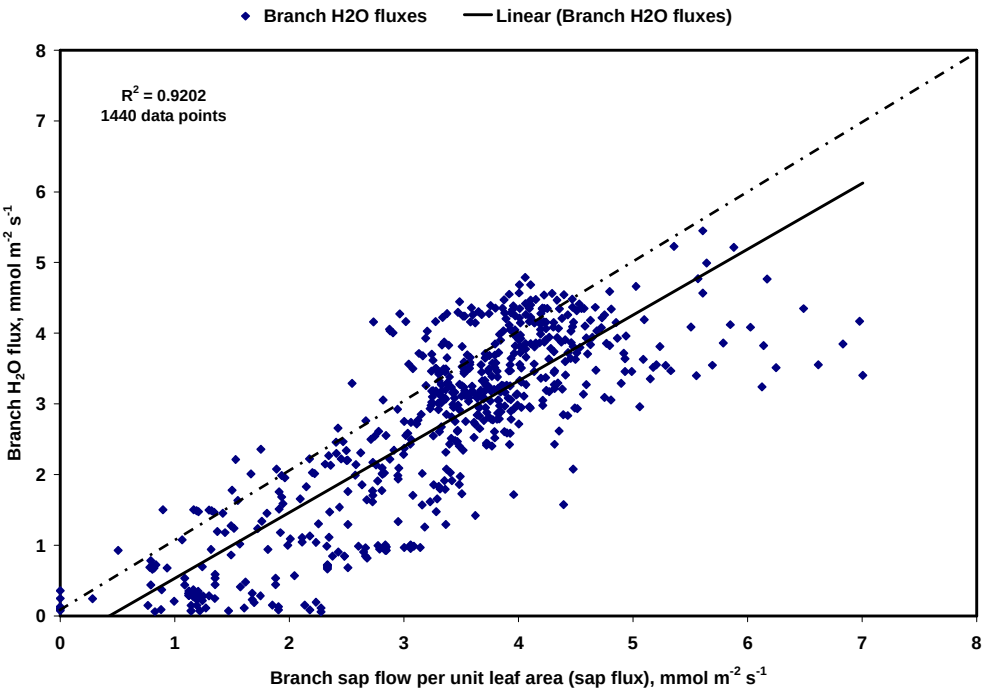

Figure 4.53 *Correlation between branch sap flux and branch H_2O flux (transpiration) on 7 January 2007 (Tree4). The dashed line represents the one-to-one correspondence. The hysteresis indicates that time lags exist between stem sap flow and evapotranspiration.*

4.7.2 Effect of shading on leaf-to-air temperature differences

It was important to know the effect of shading on the temperature differences between the leaves in the citrus tree canopy and the ambient air temperature. The measurements presented in Figures 4.54 to 4.58 are for leaves outside the cuvette. The measurements were made during the flux measurements on each tree under study. Results showed that when a single layer net was in place, the diurnal course of the temperature difference was negative (leaf was cooler than air), only becoming positive between 6pm and 6am. During the night, the leaf-to-air temperature difference maintained an almost steady value of 1°C for Tree4 and Tree2 while that for Tree3 and Tree1 was between 0°C and 0.5°C.

It would appear that the leaf-to–air temperature difference was controlled by environmental factors rather than by cultivar type. For instance Tree4 and Tree2 were respectively *Navelina* and *Baianinha* cultivars yet they had the same temperature difference characteristic. The same is true for Tree3 and Tree1.

Under all solar radiation regimes, midday values of leaf-to-air temperature difference were positive. Night-time values of leaf-to-air temperature differences were close to 0°C, showing that there was strong coupling between the leaf surface and the air at this time.

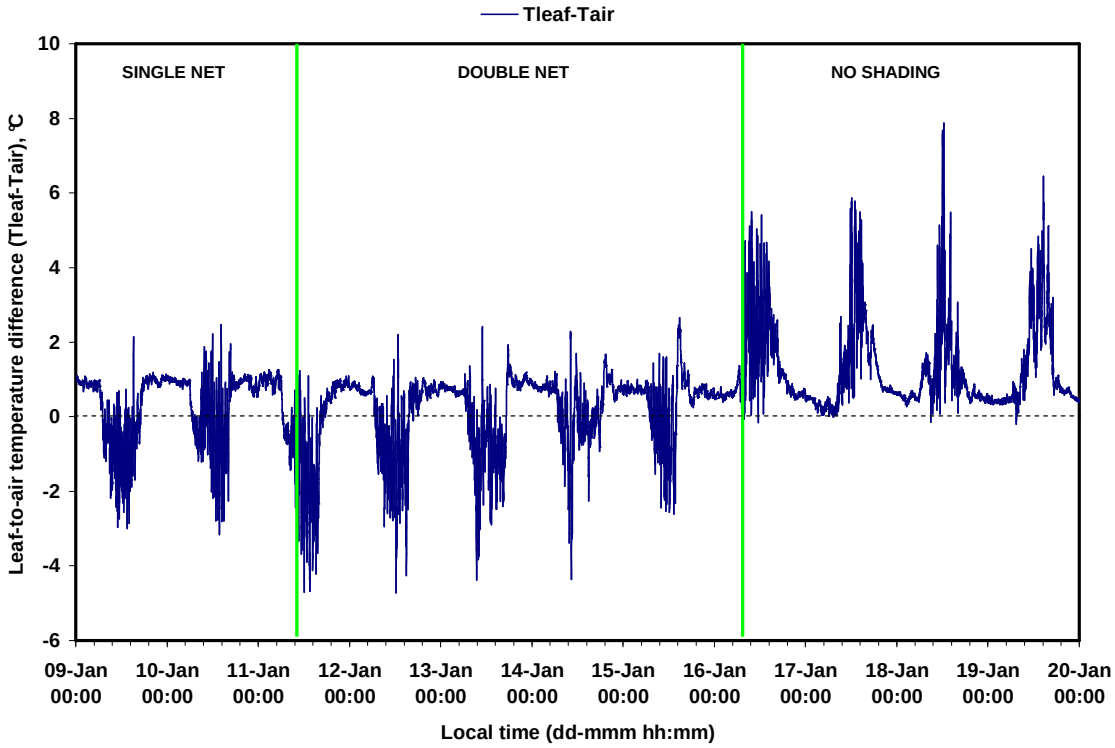

Figure 4.54 *Diel variation of the difference between a citrus leaf temperature (outside cuvette) and the ambient air temperature from 9 January to 19 January 2007 on tree4.*

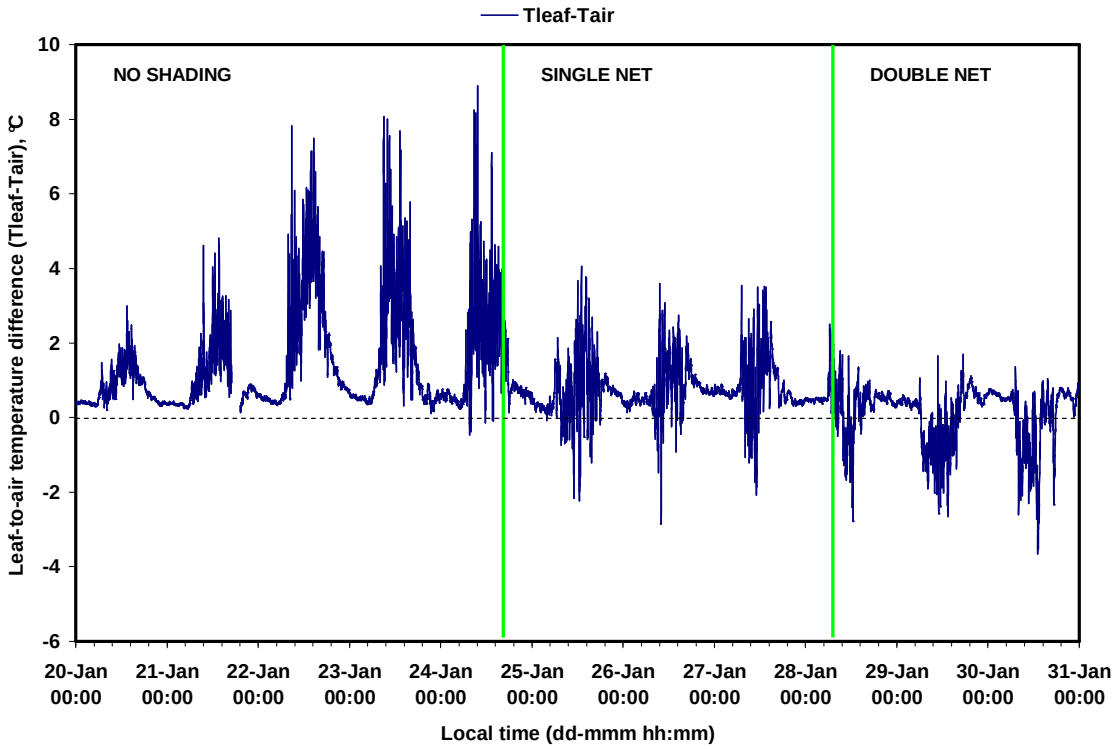

Figure 4.55 *Temperature difference between the ambient air and a leaf outside the cuvette; 20 to 30 January 2007 on Tree3.*

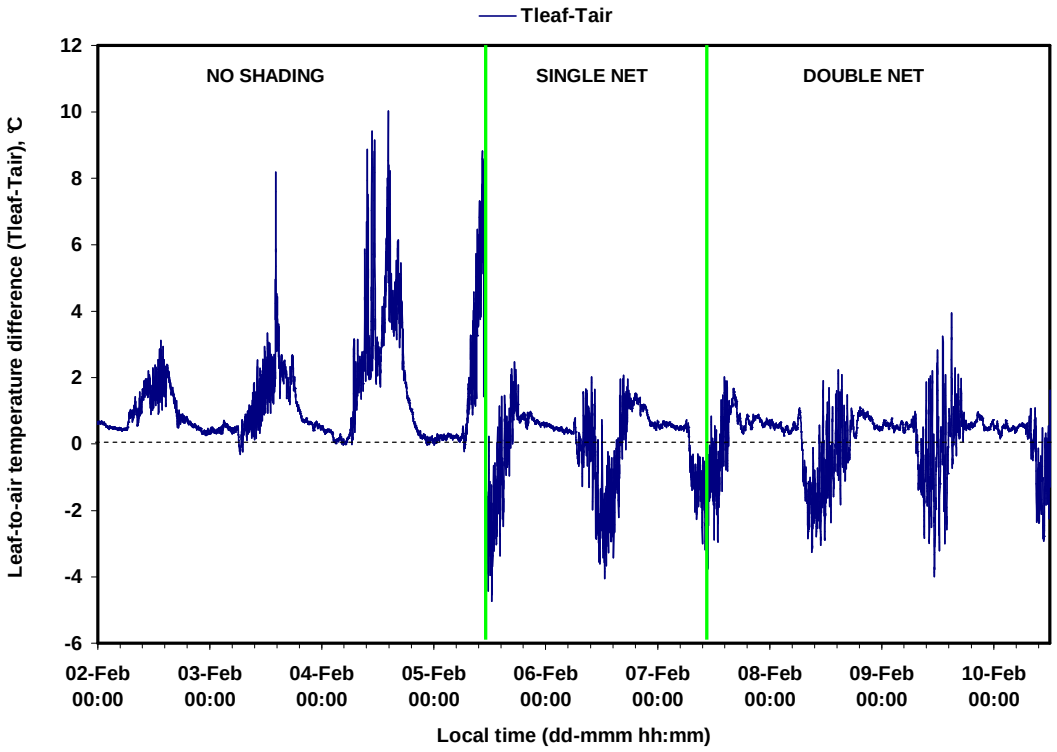

Figure 4.56 *Temperature difference between the ambient air and a leaf outside the cuvette; 2 to 10 February 2007 on Tree1.*

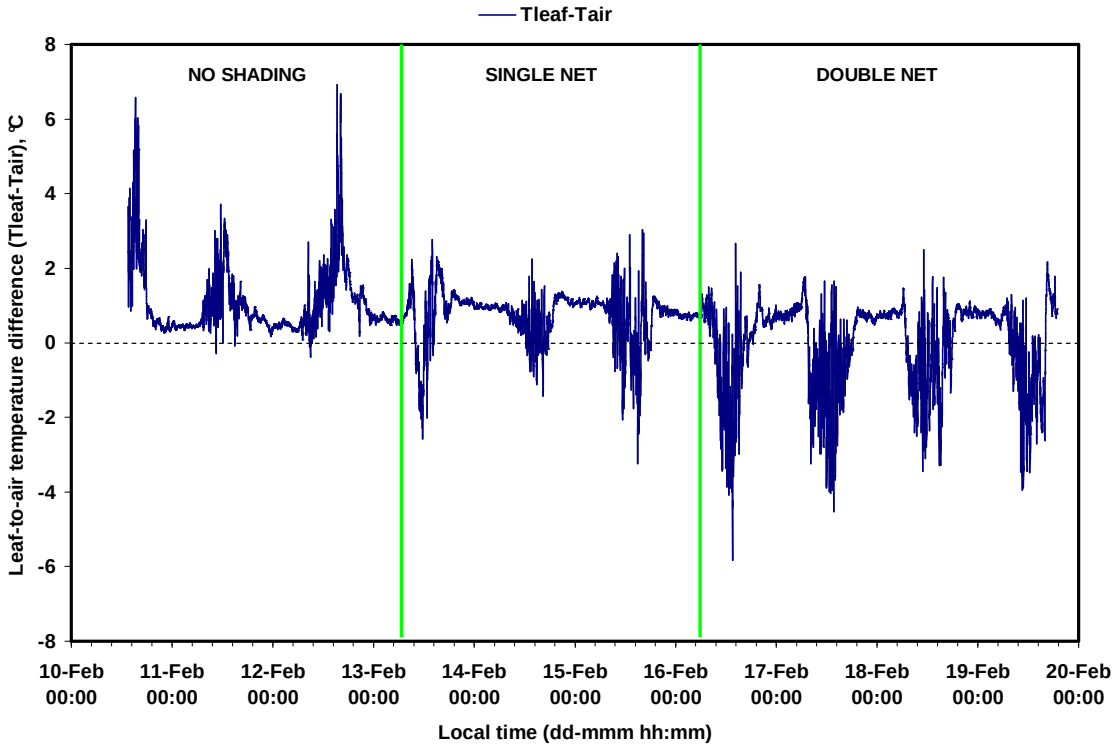

Figure 4.57 *Temperature difference between the ambient air and a leaf outside the cuvette; 10 to 20 February 2007 on Tree2.*

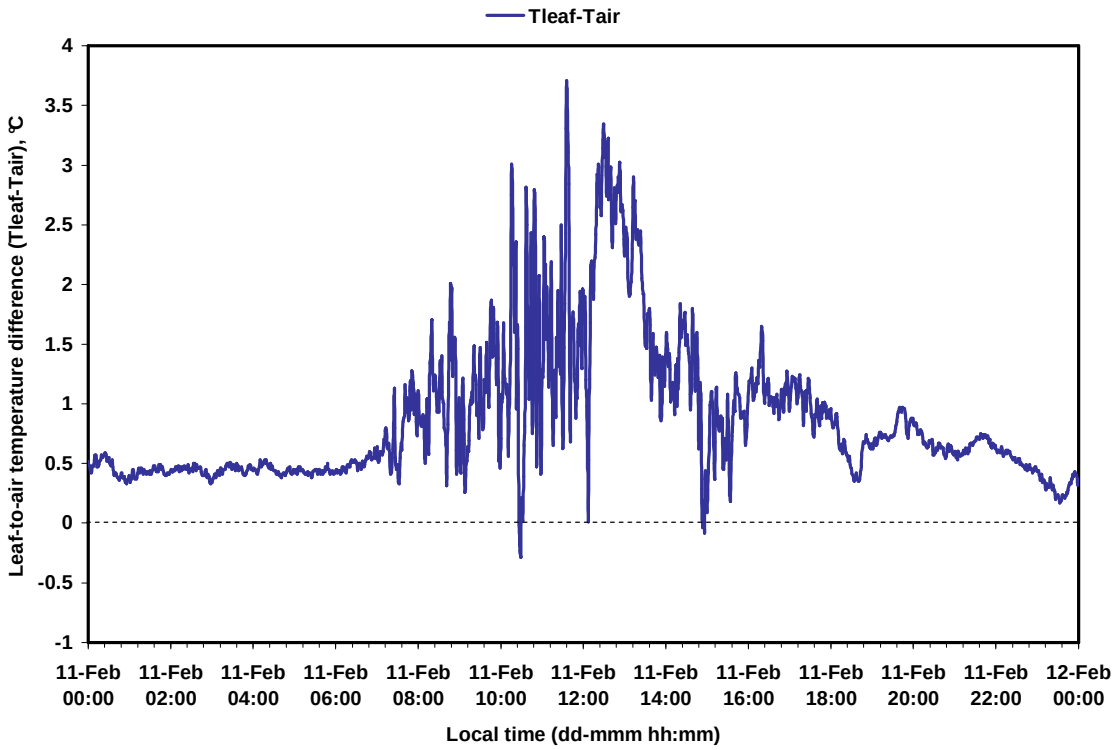

Figure 4.58 *Diel variation of the difference between leaf temperature and ambient air temperature for Tree2 on a partly cloudy cool day with no shading.*

4.7.3 Effect of shading on water storage

Water storage of the trees was found by taking the difference between the stem sap flow and the upscaled branch sap flow. Upscaling of the branch sap flow to tree level was achieved by multiplying the branch sap flow values by a scaling factor which was equal to the ratio of the total leaf area of the tree to the leaf area of the branch from which sap flow was measured. Results (Figure 4.59, 4.60) showed that water storage followed a diurnal course, being maximum (most negative) late in the evening (around 2000 hours) and minimum (most positive) early in the morning shortly after the start of the transpiration stream. There were some discrepancies between the water storage capacities of the two cultivars. The Navelinha (Tree4) had both positive and negative water storage values throughout a day while the Baianinha (Tree2) had only a few distinct mid-morning positive peaks and negative values for the rest of the time.

Water storage was highest for the double shaded regime and lowest with a single net. The most probable reason for this is that there was less transpiration under a double shade net resulting in water extracted from the soil being accumulated in the tree. On the other hand, the single shade net was associated with conditions more suitable for photosynthesis and transpiration. Therefore the higher evaporative demand under a single shade net resulted in most of the water extracted from the soil being lost due to transpiration because there was more stomatal opening. Large water storage deficits (prevalent on Tree4 Figure 4.59) have been reported to cause cavitation and embolisms by Steppe

(2004) . Dzikiti et al.(2007) speculated that cavitation and embolisms resulting from water storage deficits may be the cause of stomatal oscillations in citrus trees.

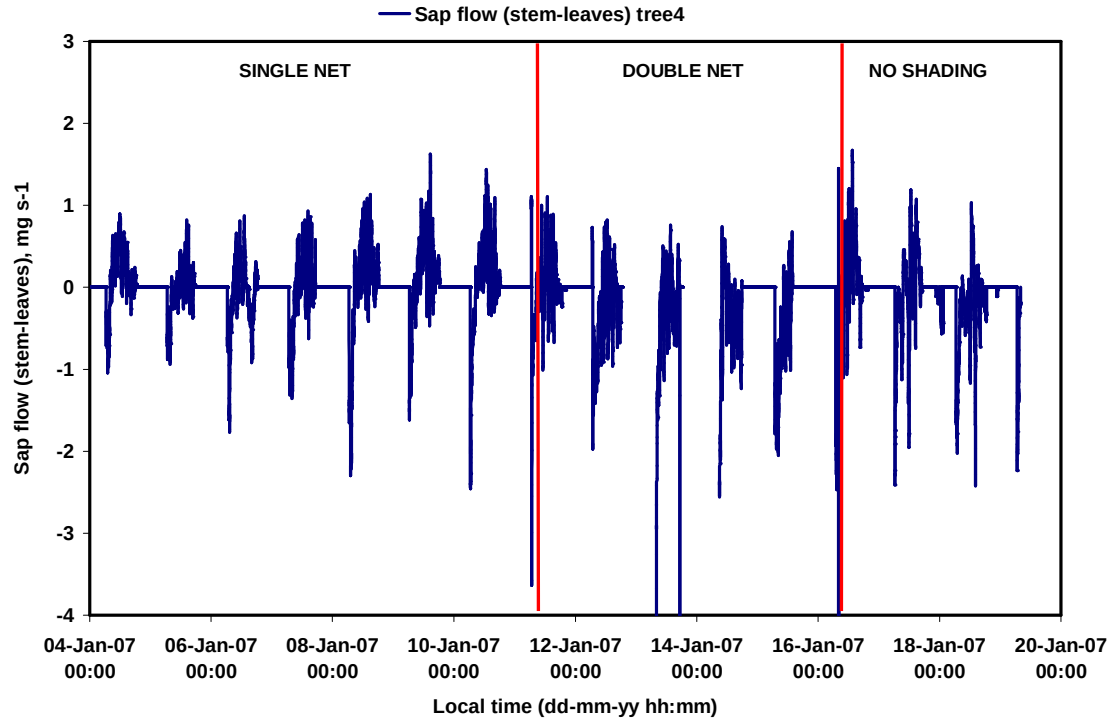

Figure 4.59 *Difference between stem sap flow and branch sap flow up-scaled to tree level on Tree4*

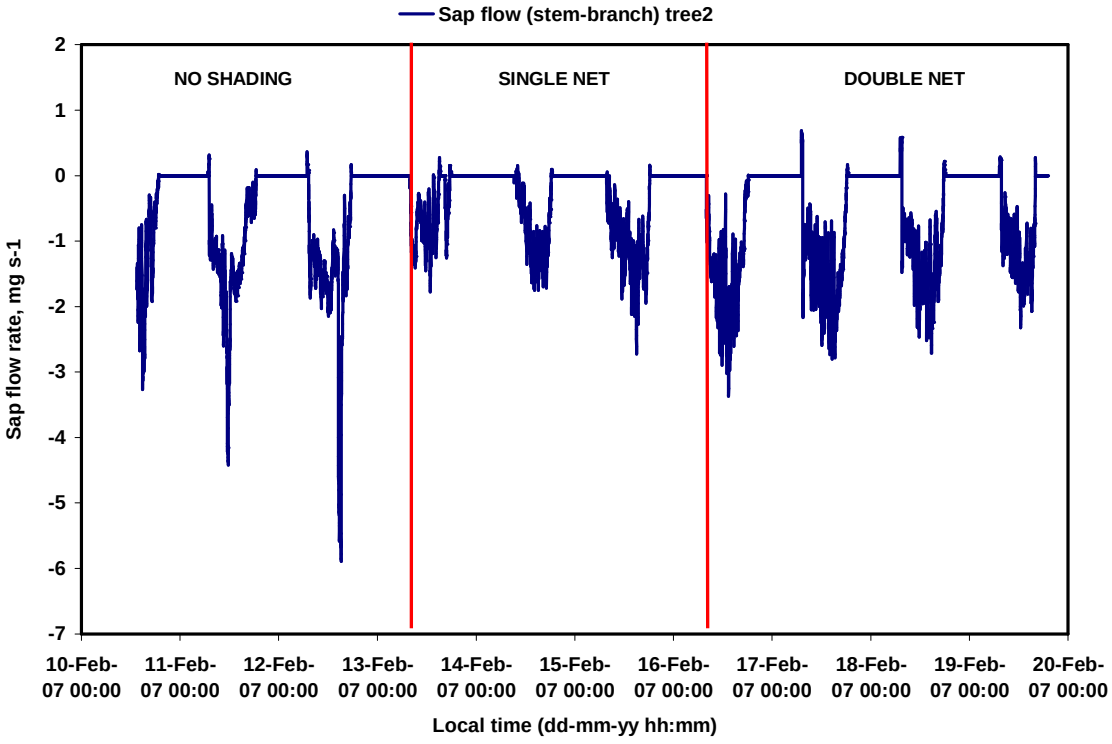

Figure 4.60 *Difference between stem sap flow and branch sap flow up-scaled to tree level on Tree2*

4.7.4 Effect of shading on stem diameter variations and a brief analysis of stem growth

Stem diameter variation, shown below, also showed that the citrus trees had storage cavities in which they stored water during the night and whenever stomata closed. The stem diameter variations had the same period as the stem sap flow but were 180° out of phase with the stem sap flow (Figure 4.61a). Experimental results showed that water storage was highest when a double shade net was in place. This is consistent with earlier results in this chapter and what is known from literature that sap flow rate is lowered when the rate of photosynthesis is inhibited (by low PPFD levels in this case).

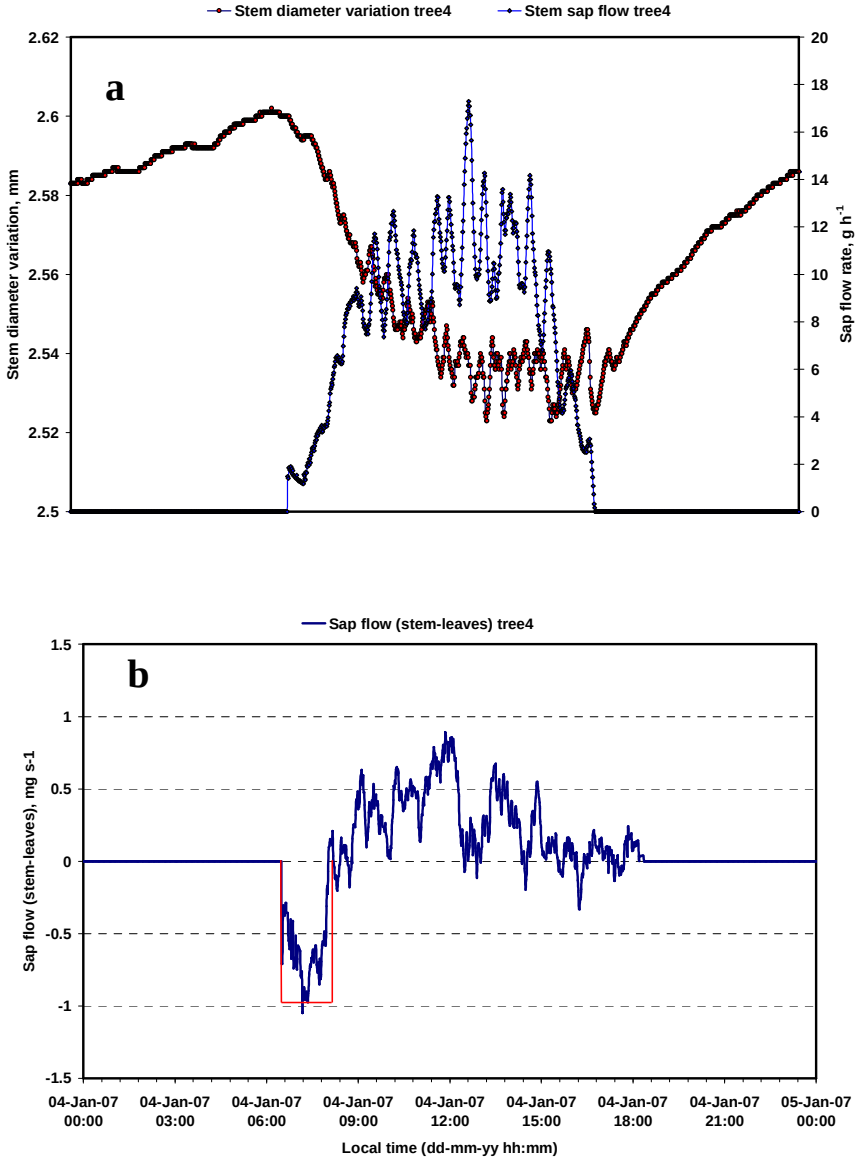

Figure 4.61 *Difference between stem sap flow and branch sap flow up-scaled to the whole crown. Time integration of the negative values of water storage rate over a day gives the amount of water stored per day. The area outlined in red has been taken as an estimate of the total negative water storage rates. The area contained in it was used to find the daily water storage for Tree4 under a single layer net.*

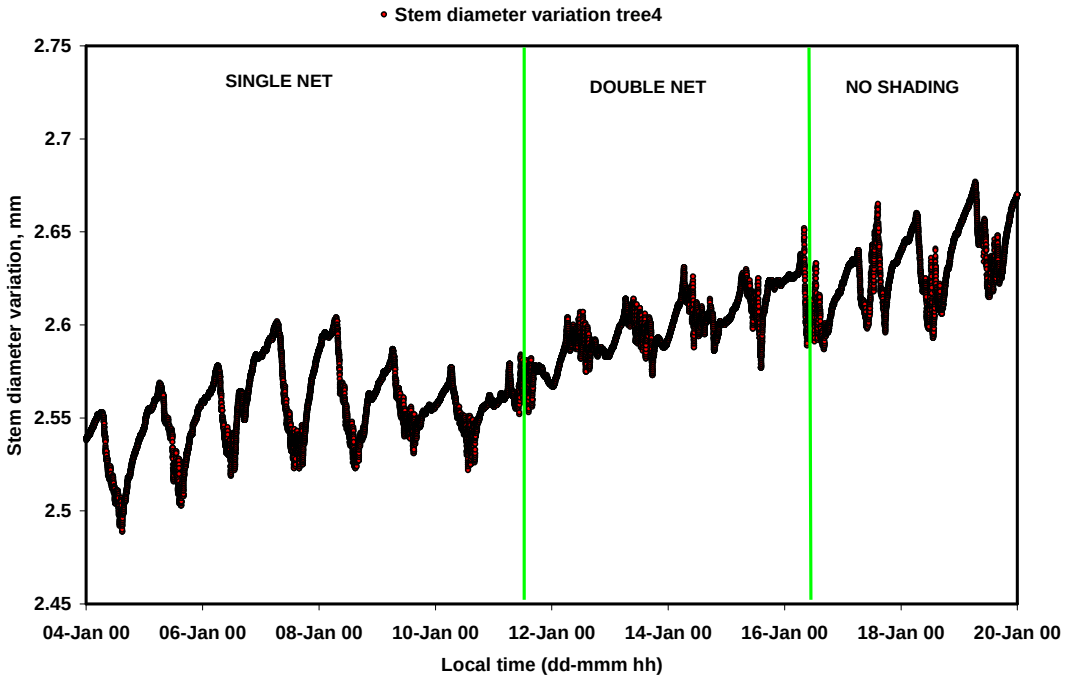

Figure 4.62 *Stem diameter variation during measurements on Tree4, 4 January to 20 January 2007.*

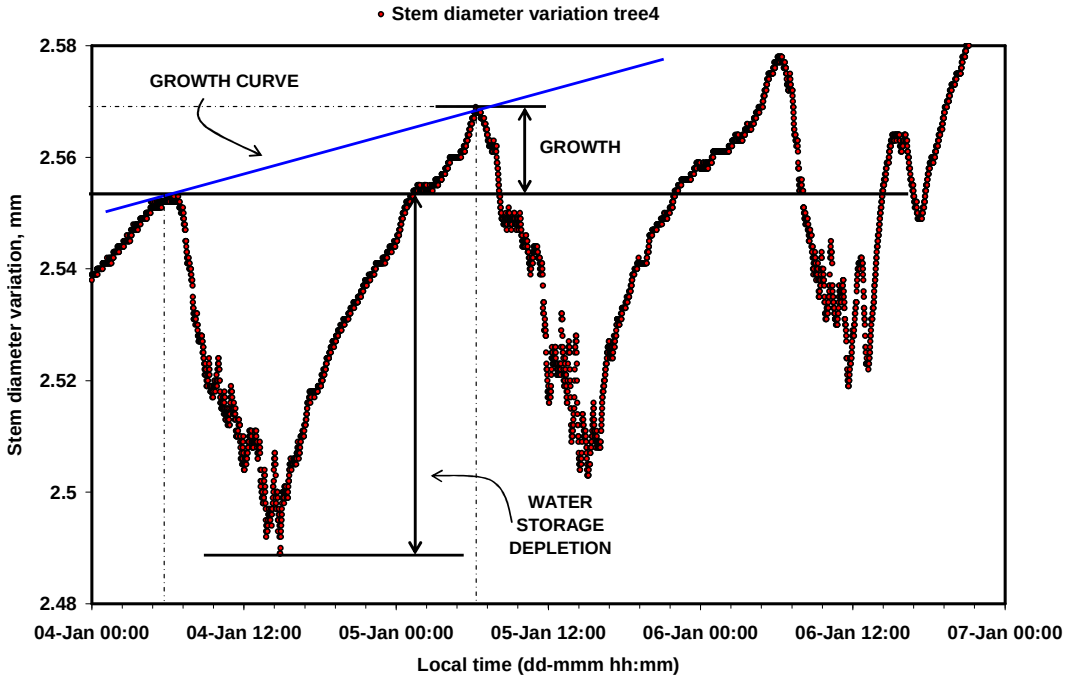

Figure 4.63 *A detailed view of the stem diameter variation on tree4 between 4 January and 7 January 2007. Diel stem growth was deduced by calculating the gradient of two successive peaks on the graph.*

From Figure 4.63, the growth rate of Tree4 stem between 4 and 7 January 2007 can be calculated as:

$$G_S = \frac{d(D_S)}{dt} \qquad [4.1]$$
$$= \frac{(2.568 - 2.555)mm}{5\,Jan\,630 - 4\,Jan\,630}$$
$$= \mathbf{13\ \mu m\ day^{-1}}$$

where G_S is the stem growth rate and D_S is the instantaneous stem diameter of the tree.

4.7.5 Effect of shading on photosynthetic water use efficiency

To quantify the effects of shading (hence temperature and solar radiation load) on citrus trees, measured fluxes of CO_2 and H_2O were used to calculate the photosynthetic WUE for each tree under each shading regime. The results are presented in Figures 4.64 to 4.69. Table 4.2 summarizes the results. The "cumulative approach" (Steduto *et al.*, 2007) was used to calculate water use efficiency.

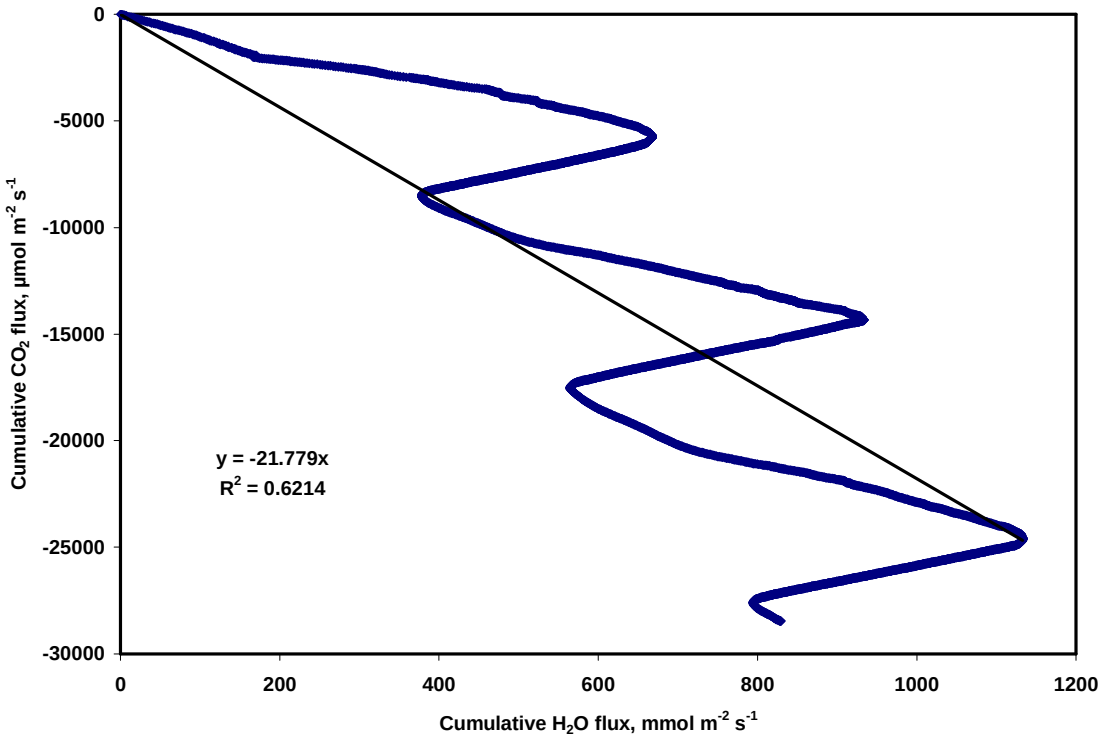

Figure 4.64 *Photosynthetic water use efficiency for Tree4 with no shade net installed*

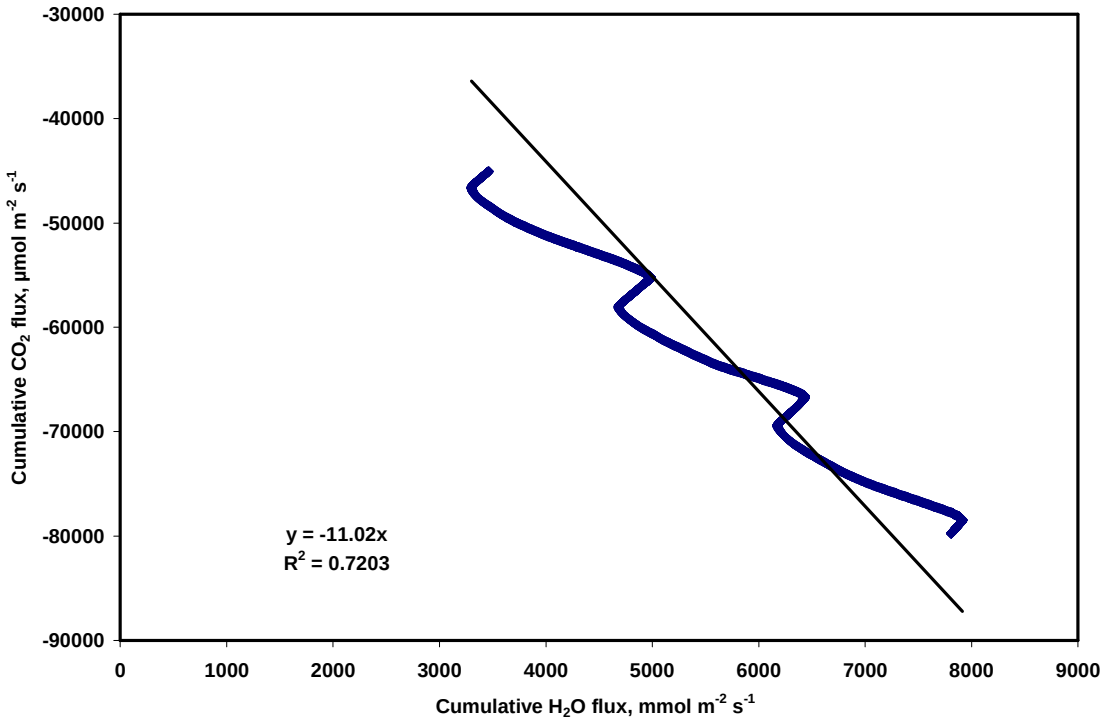

Figure 4.65 *Photosynthetic water use efficiency for Tree4 under a single layer net*

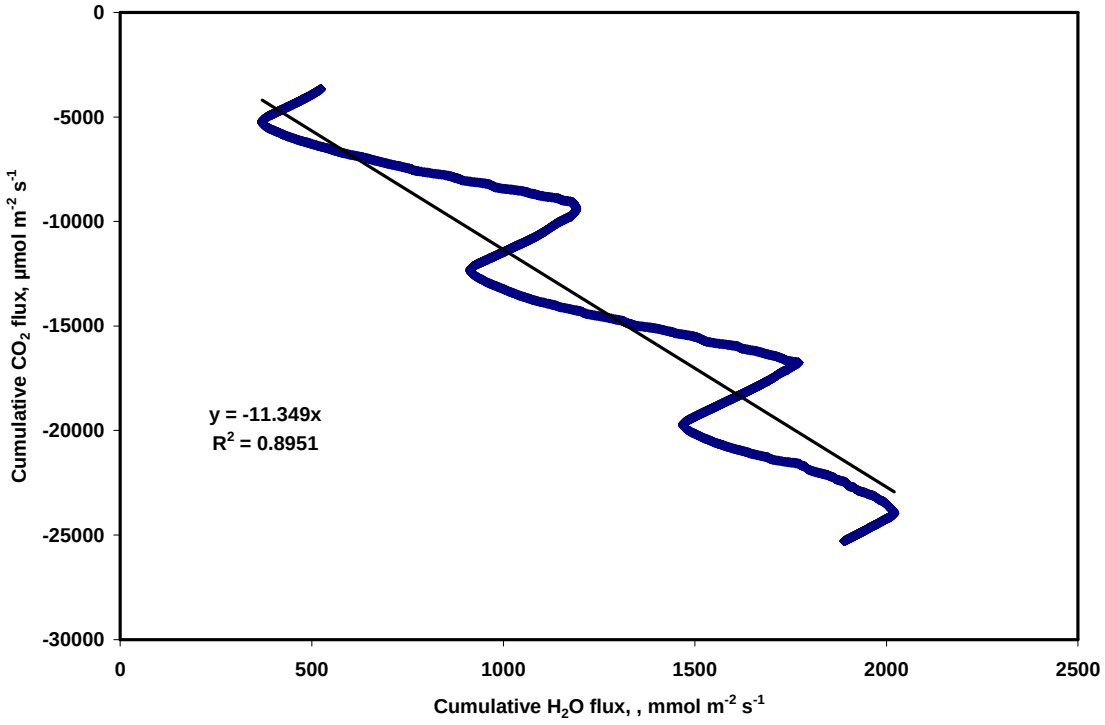

Figure 4.66 *Photosynthetic water use efficiency for Tree4 under a double layer net (12-15 January 2007)*

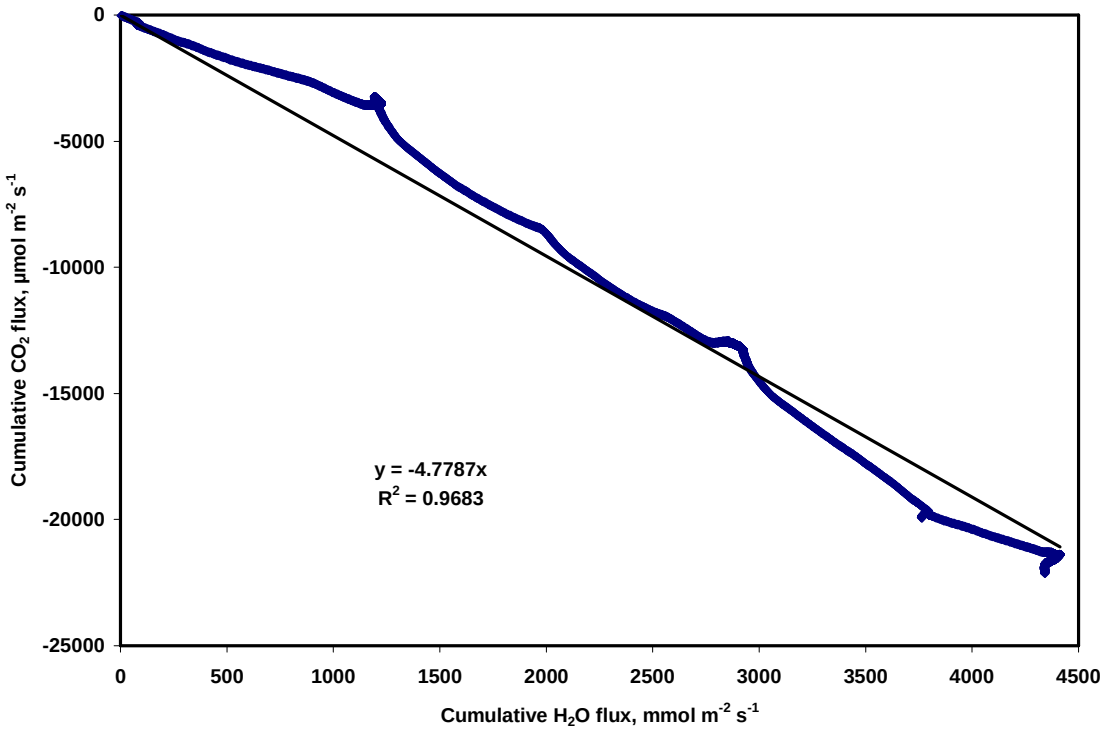

Figure 4.67 *Photosynthetic water use efficiency for Tree2 without a shade net*

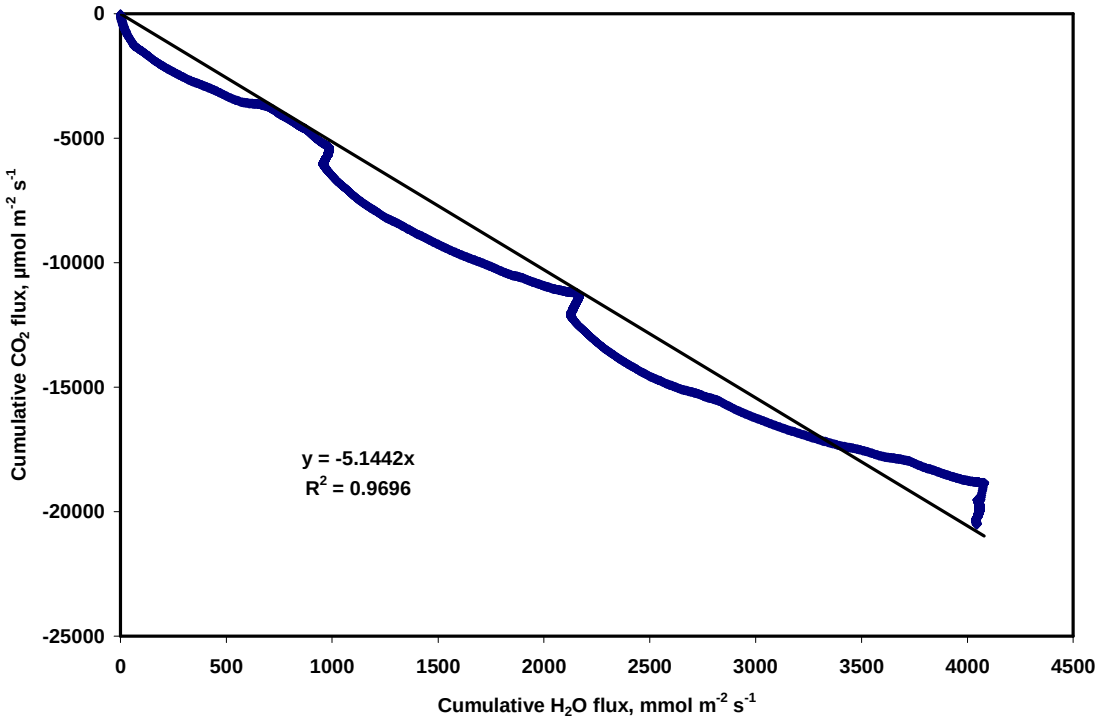

Figure 4.68 *Photosynthetic water use efficiency for Tree2 under a single layer net*

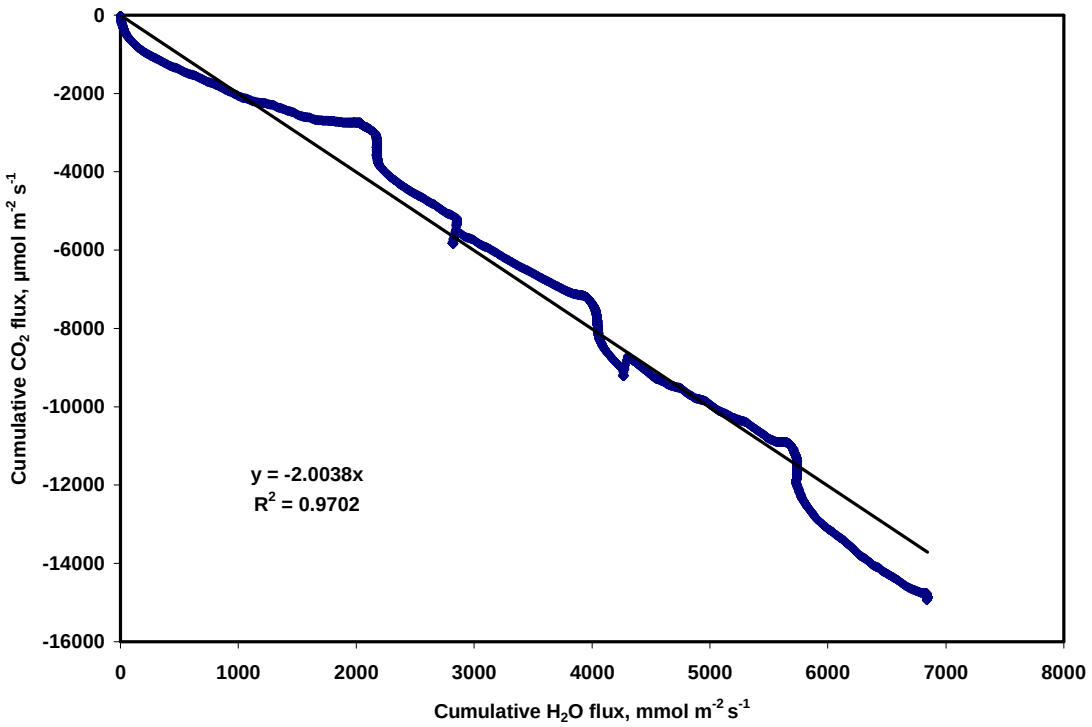

Figure 4.69 *Photosynthetic water use efficiency for Tree2 under a double layer net*

The results obtained show that WUEs are generally highest when there is no shading. This is not surprising given the fact that the shading material reduced PPFD incident on the leaves by at least 75 %, effectively preventing the leaves from capturing enough radiation to saturate photosynthesis. The single layer shade net had the next highest WUEs followed lastly by the double layer shade net. The WUE for Tree4 under a double layer net was anomalously high, suggesting that an outlier in some of data points could have resulted in the large deviation from the expected trend.

Table 4.2. *A summary of the photosynthetic WUEs of 4 navel orange trees used in the experiment. The values in brackets are the R^2 values for each measurement.*

TREE #	PHOTOSYNTHETIC WATER USE EFFICIENCY, [µmol CO_2 (mmol H_2O)$^{-1}$]		
	NO SHADING	SINGLE NET	DOUBLE NET
1	-4.697 (0.90)	-1.470 (0.92)	-1.343 (0.91)
2	-4.779 (0.97)	-5.144 (0.97)	-2.004 (0.97)
3	16.923 (-0.57)	-5.121 (0.90)	-3.042 (0.89)
4	-21.779 (0.62)	-11.020 (0.72)	-11.349 (0.90)
Elephant ear	-4.337 (0.98)	-	-

4.8 Model results

The model developed to simulate stem sap flow was implemented between 16 and 19 April on Tree2 (*Baianinha*) and Tree3 (*Navelina*). The climatic conditions prevailing throughout the 4 day measurements are presented:

Figures 4.70 and 4.71 show that the weather variables were roughly similar for all the 4 days that the experiments were run. Diurnal values of temperature and relative humidity inside and outside the shelter differed by as much as 20 % and this difference remained the same whether there was a shade net in place or not. It can be concluded that the shade net did not have any noticeable effect on ambient air temperature and relative humidity.

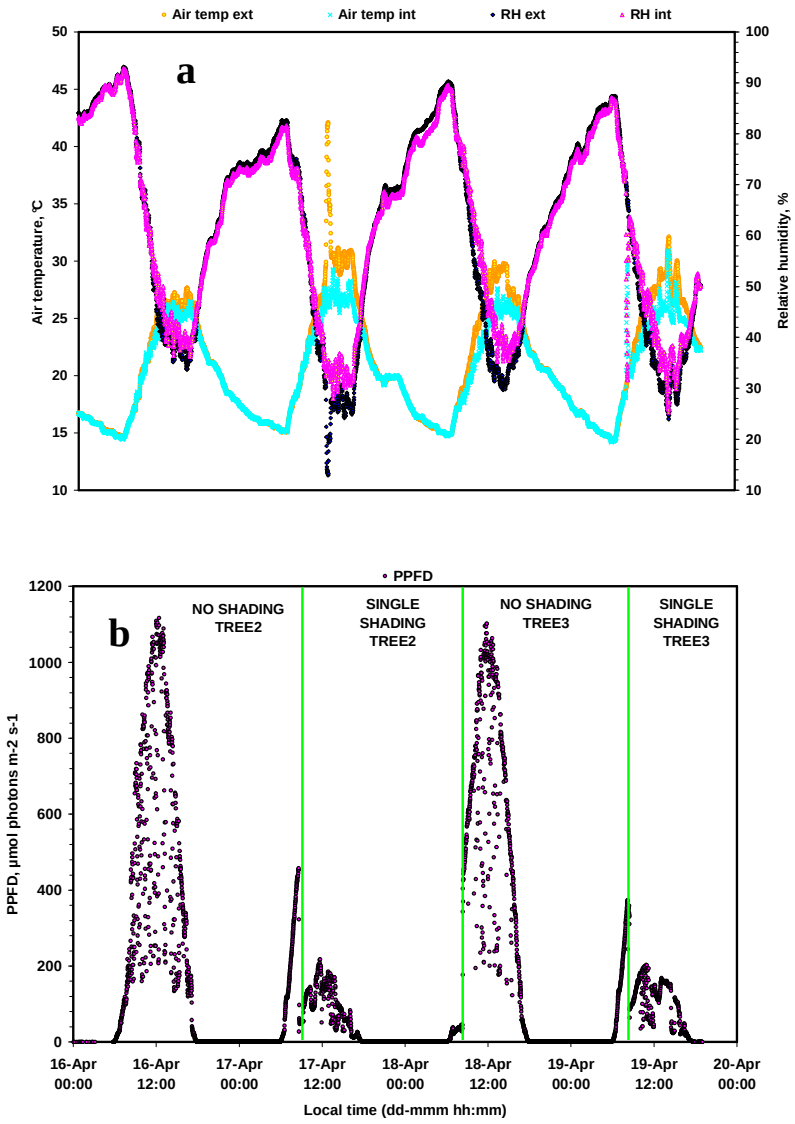

Figure 4.70 *Diel variation of (a) temperature and relative humidity next to the cuvette and outside the shelter (b)PPFD just above the cuvette throughout the model data collection period (16 to 19 April 2007). Note the large reduction in PPFD when a single net was introduced.*

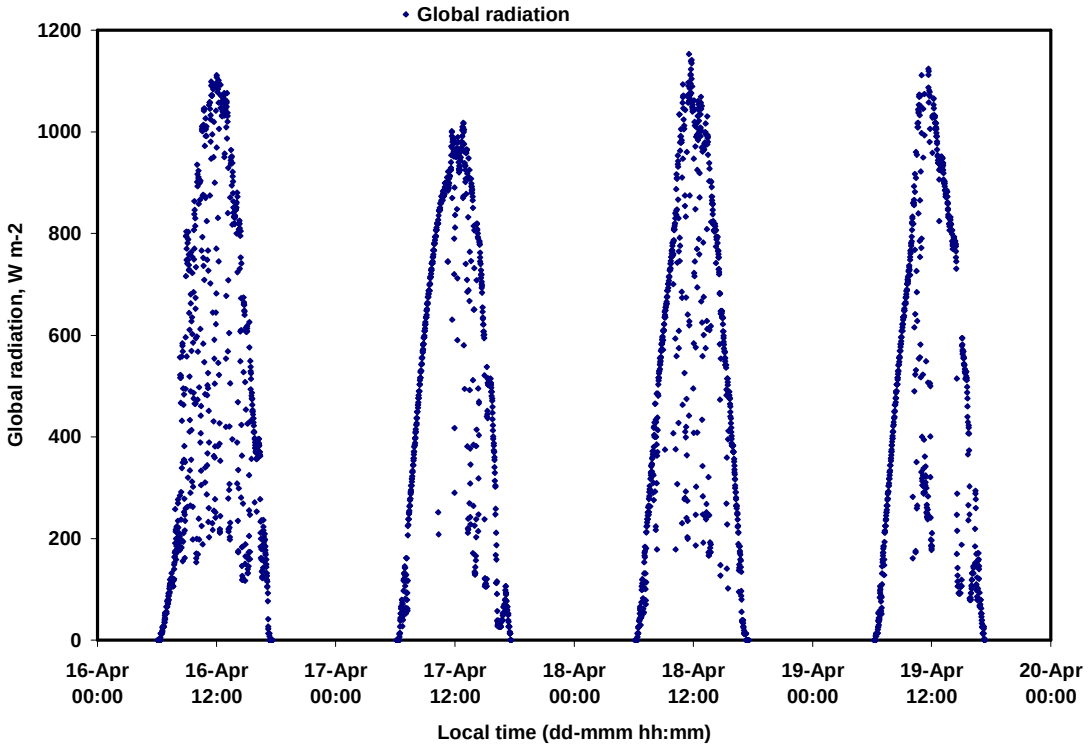

Figure 4.71 *Diel variation of global solar radiation throughout the model data collection period.*

4.8.1 Modelling leaf water potential

Measurements commenced at 0800h (0 min) local time and ended at 1800h (600 min) local time. Modelled leaf water potential (LWP) lagged behind measured LWP by 20 min (this might have been as a result of the a priori shifting of the stem sap flow by 20 min) on average but sometimes the difference was as much as 80 minutes. Modelled LWP was on average 33 % higher than measured LWP. Errors of 20 % were assumed for all measured LWPs and 10 % for the modelled LWPs. Therefore, within the bounds of experimental error, the model was able to predict the LWP.

For both *Baianinha* and *Navelina* cultivars, measured and modelled LWPs did not fluctuate much when there was a single layer shade net in place (Figure 4.72 and Figure 4.75).

In all cases, the model erroneously predicted that LWP had to be zero at the start and at the end of the integration interval. This error had a negative impact on the modelled LWP values near the boundaries of the control variable (time). Future refinement of the model must focus on this shortcoming. Although the model failed in this regard, its predictions of LWP away from the boundaries was accurate within the bounds of experimental error.

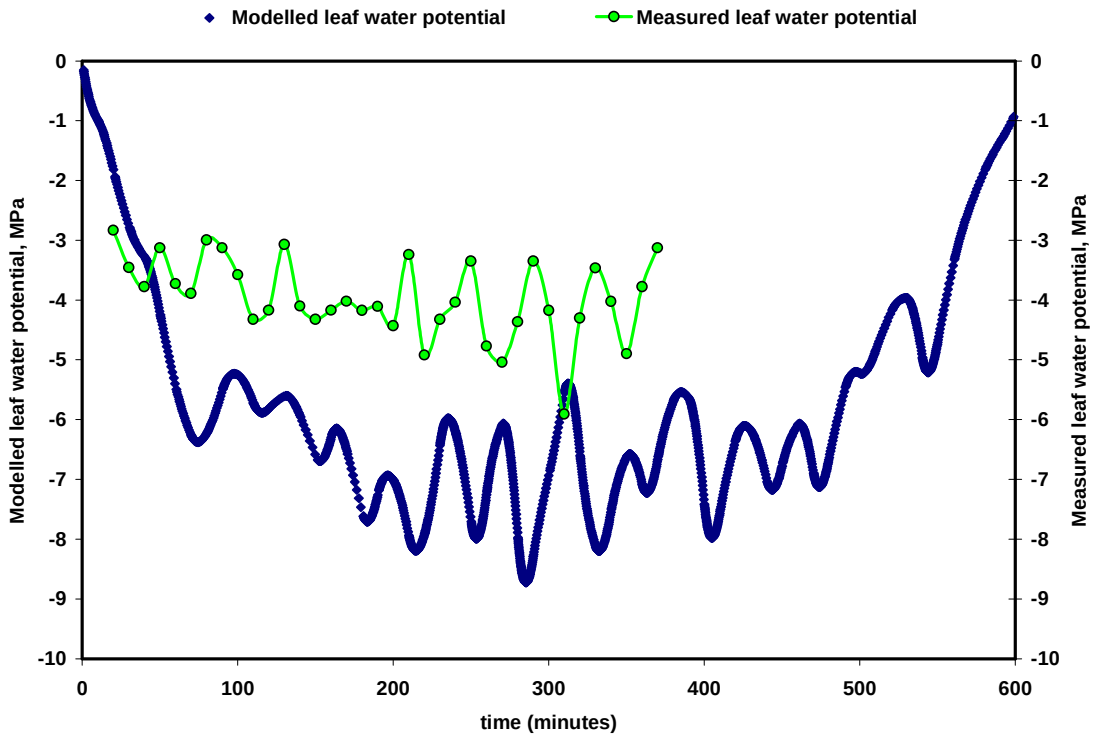

Figure 4.72 *Leaf water potential tree2 no shade, 16 April. Measurements ceased at 1330h LT due to electrical power loss.*

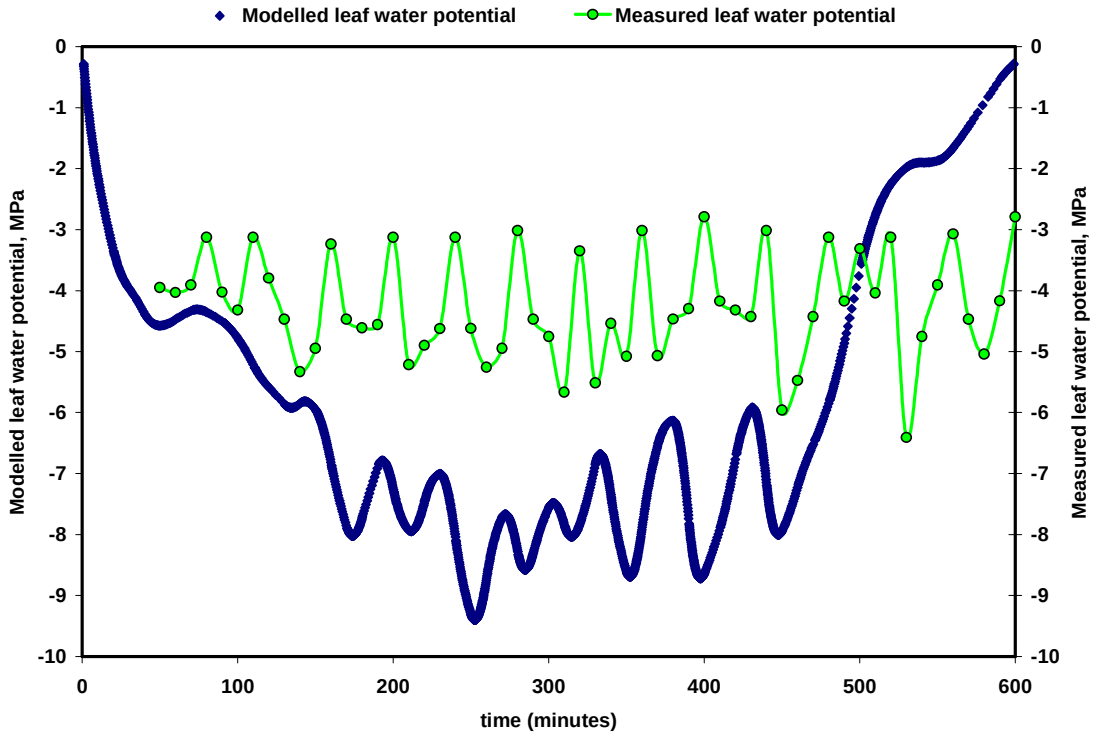

Figure 4.73 *Leaf water potential tree2 single net, 17 April*

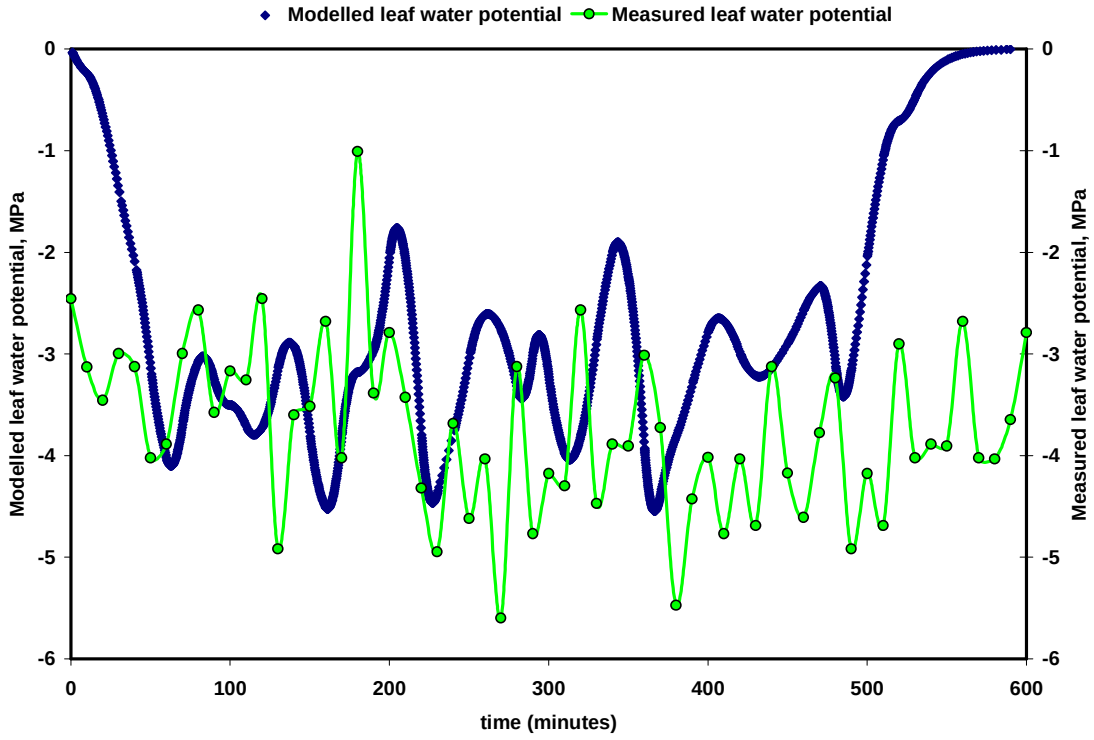

Figure 4.74 *Leaf water potential tree3 no shading, 18 April*

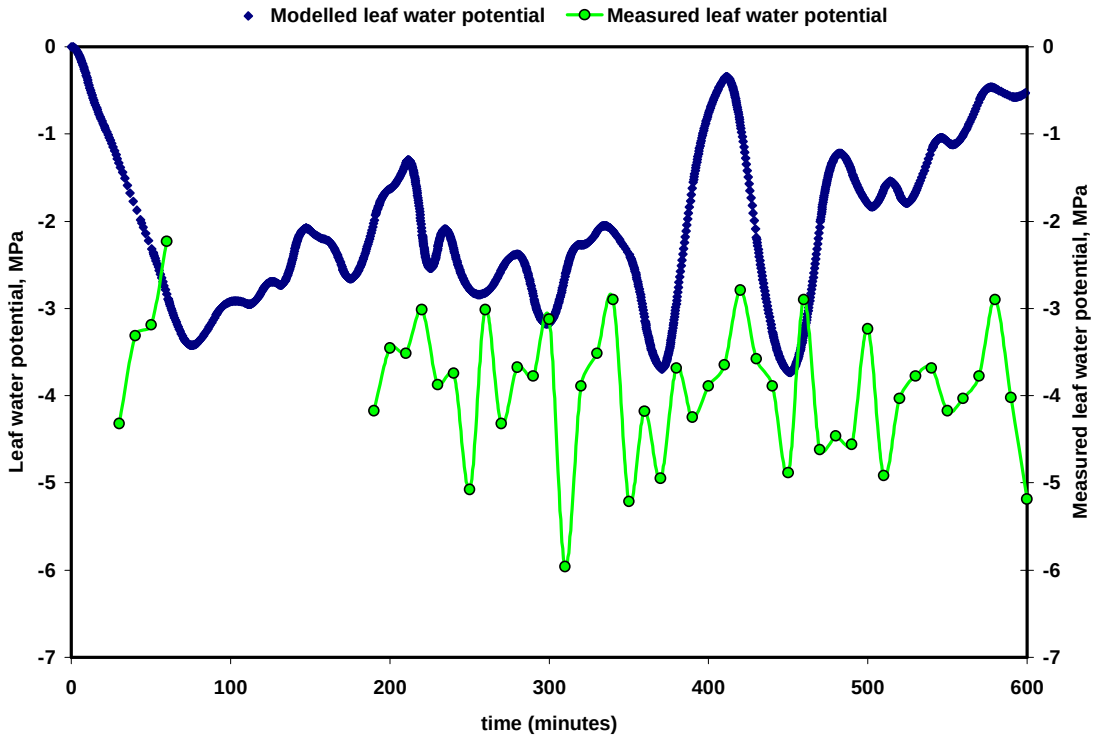

Figure 4.75 *Leaf water potential single net tree3, 19 April 2007.*

4.8.2 Modelling stem sap flow

Measured stem sap flow lagged behind modelled stem sap flow by 20 min on average. The model was better at predicting stem sap flow than LWP as evidenced by the results in Figures 4.76-4.79. The model was also able to give the expected results at the boundaries of the control variable (time). The model performed well for Tree2 but was not so accurate for Tree3. There was no obvious change in the model behaviour based on the whether there was shading or not for any case.

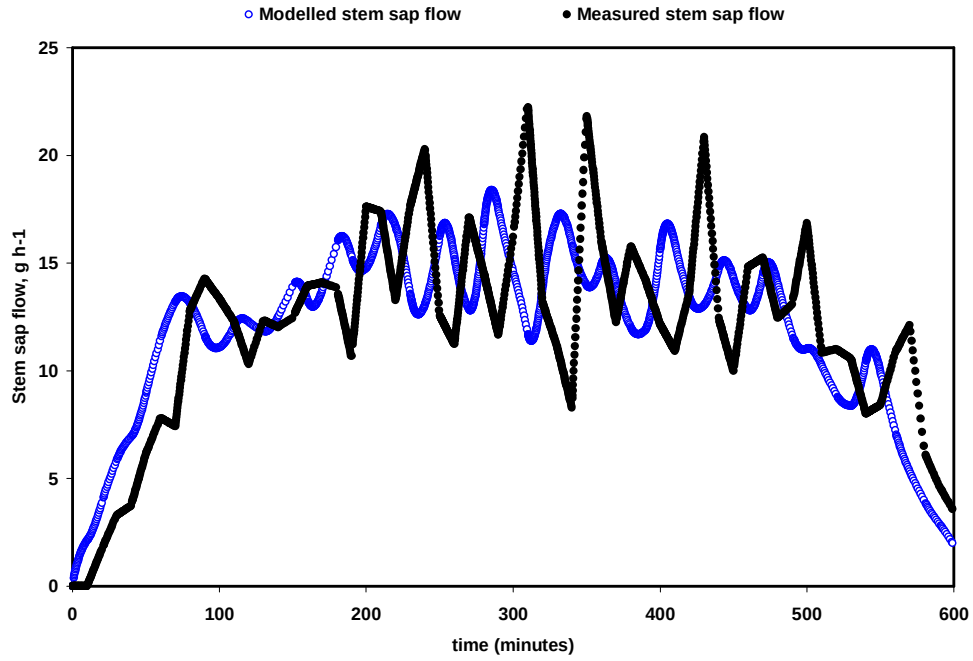

Figure 4.76 *Validation of stem sap flow measurements,Tree2 no shading 16 April 2007*

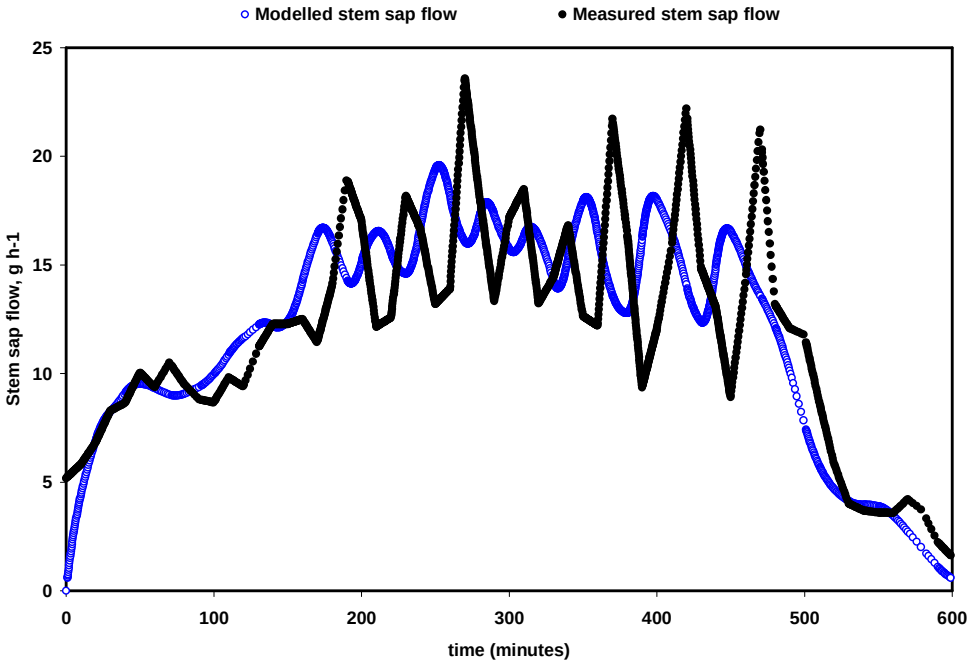

Figure 4.77 *Validation of stem sap flow measurements, Tree2 single net, 17 April*

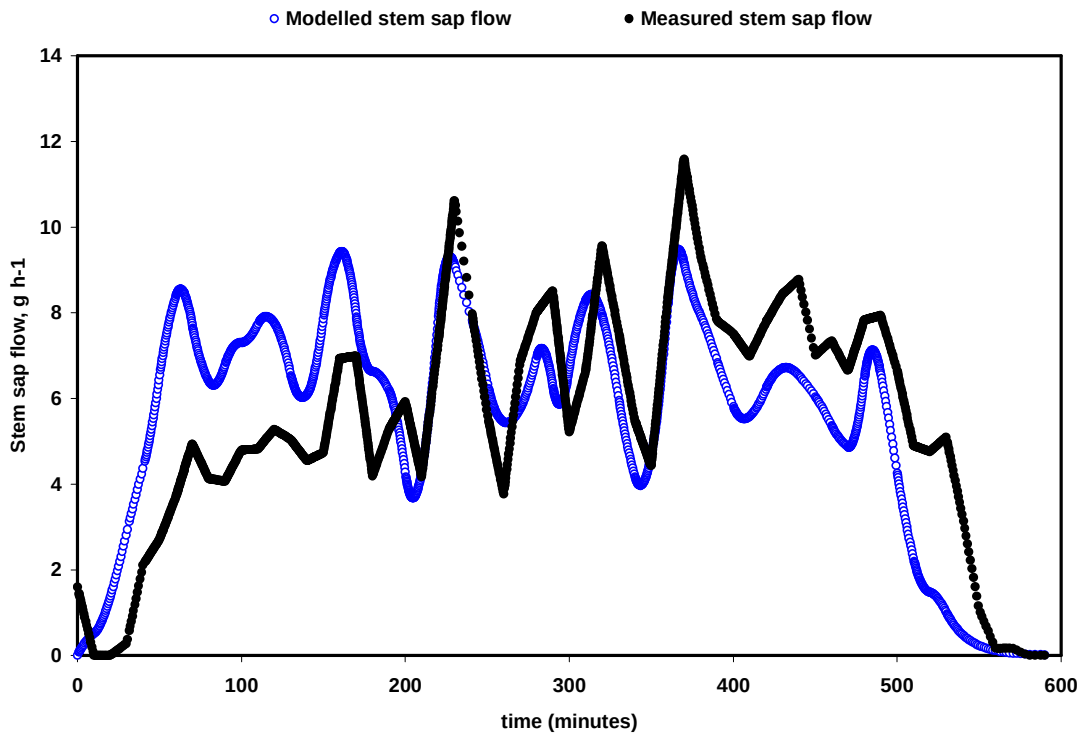

Figure 4.78 *Validation of stem sap flow measurements, Tree3 no shading, 18 April 2007*

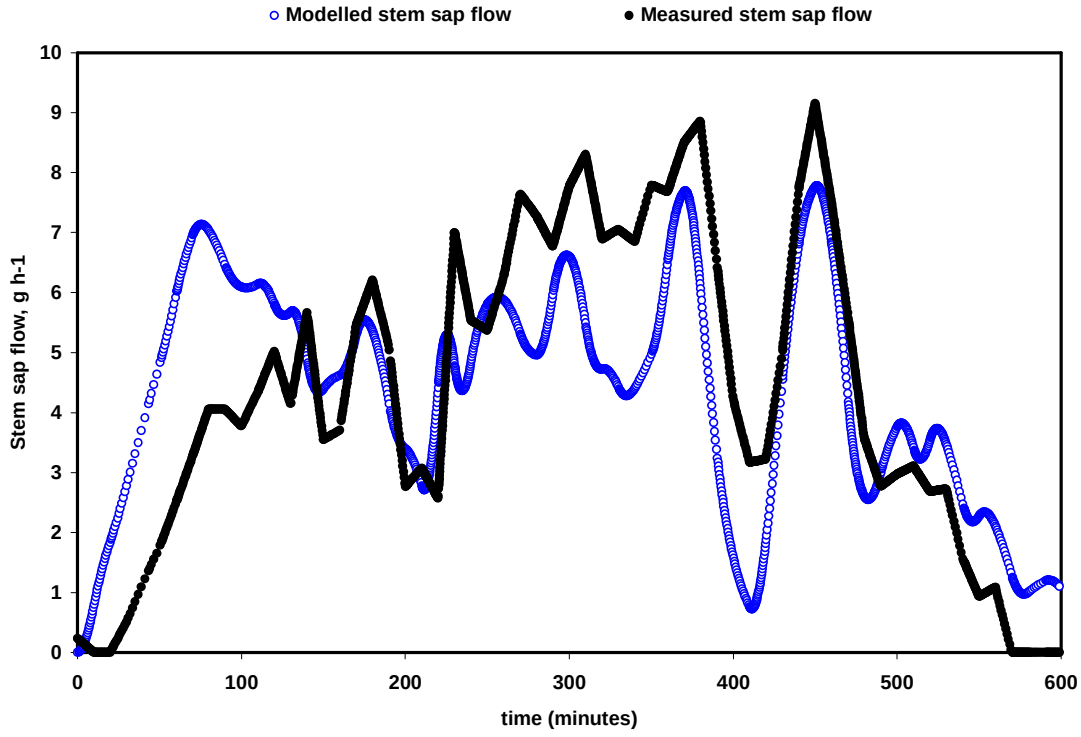

Figure 4.79 *Validation of stem sap flow measurements, Tree3 single net, 19 April 2007*

On the *Baianinha* (Tree2), the model predicted stem sap flow to within 20 % of the measured values. Stem sap flow had an error margin of 10 %. This meant that the values of modelled stem sap flow were outside the error bounds of the measured stem sap flow 50 % of the time. For the *Navelina* cultivar (Tree3) modelled stem sap flow deviated from measured stem sap flow by as much as 50 %. The deviations were largest early in the morning at the start of the transpiration stream.

4.8.3 Calibration of the water balance model

The calibration of the model (explained in section 3.14.3.1) yielded hydraulic parameters which were not consistent between the two different cultivars.

This was most likely due to the fact that not all data sets could be calibrated using the same optimization method due to the limitations of each method. As a result, more than one optimization method had to be used, in a trial and error method. Table 4.3 shows the hydraulic parameters and the optimization method for each tree.

A comparison was made between the hydraulic parameters found in this experiment and those obtained by Steppe (2004) and Dzikiti *et al.* (2007).

Tables 4.3 and 4.4 show a summary of the hydraulic parameters *C* (water storage capacitance) and R_x (resistance) as well as a comparison with other types of trees. The results obtained were not as expected. I expected more or less constant capacitance for each tree regardless of radiation load. The results showed random variation of the parameters. I can attribute this variation to the optimization procedure which did not perform well most of the time and generated numerous errors before parameters could be obtained. In particular, the measurements for Tree3 under a single shade net proved to be difficult to optimize with the Marquardt Realistic Error Estimates. A 'circular error' would be generated whenever any attempt was made to optimize. Optimization was successful with the Simplex method but the results, especially for resistance, were too different from the other results using the other optimization technique.

Table 4.3 *A summary of the hydraulic parameters determined from the model for each of the experimental trees.*

TREE #	SHADING REGIME	HYDRAULIC PARAMETERS		OPTIMIZATION METHOD
		C [MPa kg^{-1}]	$\mathbf{R_X}$ [MPa h kg^{-1}]	
2	No shading	5.64±0.03	8.9±0.1	Marquardt: Realistic Error Estimates
	Single net	18.3±0.2	4.97±0.04	Marquardt: Realistic Error Estimates
3	No shading	0.850±0.007	4.00±0.02	Marquardt: Realistic Error Estimates
	Single net	0.55±0.00	56.6±0.0	Simplex: Weighted Least Squares

Table 4.4 *Comparison of the hydraulic parameters of 3 young tree species: citrus (Navelina and Baianinha budded on Troyer citrange rootstock), beech and oak. Values in brackets are those measured by Dzikiti et al.(2007). Beech and Oak were measured by Steppe (2004)*

Parameter	Citrus				Beech	Oak
	Navelina		*Baianinha*			
	clear	single layer net	clear	single layer net	clear	clear
R_X [MPa h kg^{-1}]	4.00±0.02	56.5899±0	8.9±0.1 (48.3±3)	4.97±0.04	39.7±0.4	17.2±0.1
C [MPa kg^{-1}]	0.850±0.007	0.549457±0	5.64±0.03 (0.28±0.02)	18.3±0.2	0.0016±0.0003	0.0031±0.0007

4.8.4 Validation of the water balance model

Data from Tree2 and Tree3 was used to validate the water balance model without a shade net and with a shade net installed. Without a shade net, the validation gave a coefficient of determination which was 0.6858 (Figure 4.80) while that for a shaded tree was 0.5349 (Figure 4.81). The results show that the model performance was acceptable. It may be feasible to use it in the field to find rough estimates of the hydraulic parameters (capacitance and resistance).

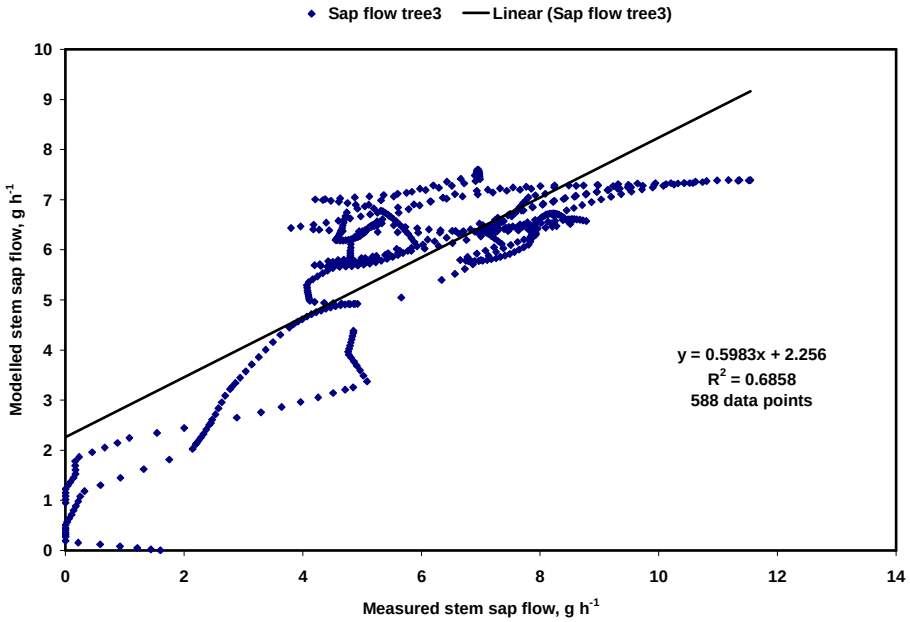

Figure 4.80 *Validation of sap flow measurements on tree3 using calibration parameters from tree2 no shade experiment run on 16 April 2007*

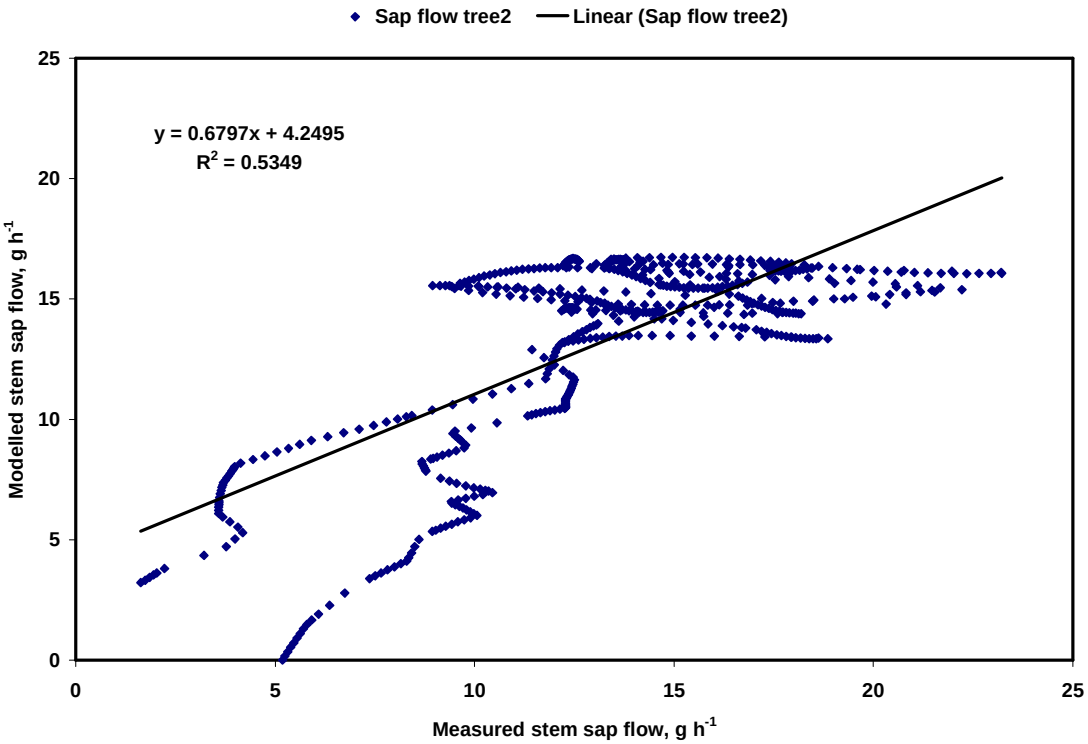

Figure 4.81 *Validation of sap flow measurements on Tree2 shaded data using calibration parameters from Tree2 no shade experiment run on the 16 April 2007*

CHAPTER 5 CONCLUSION AND RECOMMENDATIONS

5.1 Summary

A dynamic chamber technique was applied to study the CO_2 and H_2O gas exchanges from four young navel orange trees comprising two different cultivars in North-eastern Zimbabwe. It was shown that the most important correction for the flux measurement data was the elimination of the transients which occurred when the valve switched from ambient sampling to cuvette sampling. In terms of the effects of shading on photosynthesis, transpiration, water productivity and the other water relations, the following conclusions can be drawn:

Table 5.1 *A summary of the effects of shade treatments on the average mid-day (except for WUE) values of the parameters measured in the experiment.*

Parameter	***Baianinha***			***Navelina***		
	Unshaded	**Single net**	**Double net**	**Unshaded**	**Single net**	**Double net**
Leaf temperature [°C]	36	32	30	38	31	30
Leaf-to-air temperature difference [°C]	7.0	-2.5	-3.5	6.5	-2.0	-2.0
Net photosynthesis, [µmol m^{-2} s^{-1}]	16.0	16.0	8.5	18.0	20.0	9.5
Transpiration, [mmol m^{-2} s^{-1}]	3.0	5.5	4.0	3.0	5.0	4.0
Abs. photosynthetic WUE, [µmol CO_2 (mmol $H_2O)^{-1}$]	4.738	3.307	1.674	21.779	8.181	8.109
Sap flow rate, [g h^{-1}]	23	19.5	16.5	16.5	22	15.5
Water storage, [mg s^{-1}]	2	2	3	2	2	3

Leaf temperature and leaf temperature differences

-Leaf temperatures can be suppressed to levels which are optimum for photosynthesis by the use of suitable shade nets

-the unshaded treatments had the highest leaf temperatures which, during most of the day, were above 35 °C. During the day, leaf temperatures as high as 7 °C above air temperature were prevalent. This had the potential to reduce photosynthesis.

Single and double shade nets gave leaf temperatures which were in the suitable range for optimal photosynthesis. Additionally, daytime leaf temperatures were cooler than the air temperature by up to 3.5 °C.

Carbon dioxide flux

Carbon dioxide fluxes showed that, despite the high leaf temperatures which were unsuitable for photosynthesis, the young citrus trees had the highest CO_2 flux when there was no shading. The poor performance of the trees under single and double shading may be explained by the very low transmittance to PPFD of the single and double layer nets. It is possible that if a shade net which could transmit PPFD above the saturation values of 600-700 µmol m^{-2} s^{-1}, had been available, then the rates of photosynthesis would have been higher for the single-shaded regime. The photosynthetic rates of the *Navelina* cultivars were up to 20 % higher than that for the *Baianinha* cultivars.

Water vapour flux

Transpiration was highest under a single shade net for all four trees. The unshaded regime had the lowest transpiration rates, possibly due to a large number of stomata closing under stress from the high leaf temperatures. This is interesting because, it gives the impression that the photosynthetic rates could be even higher than they were in the unshaded treatment if more stomata were open. Transpiration and photosynthesis in the unshaded regime may have been largely due to the contribution of shaded leaves and shaded sections of leaves within the branch.

Photosynthetic water use efficiency

Water use efficiency mirrored CO_2 flux in that it was highest in the unshaded regime. Since it is a ratio of CO_2 to H_2O flux, this was expected given that CO_2 flux was high while H_2O flux was low.

WUE without shading for the *Navelina* was more than 4 times higher than that for the *Baianinha*. Single shaded trees produced the next highest values of WUE while the double shaded trees had the lowest water use efficiency.

These results for WUE also bring attention to the fact that the transmittance to solar radiation of the shade nets used was too low.

Sap flow rate

The results showed that sap flow rates were, in general, highest when the tree was in full solar radiation. Sap flow rates for the *Baianinha* cultivars fell by 10 % in moving from the unshaded to the single shade regime and by a further 10 % when changing from single shading to double shading.

The *Navelina* cultivar showed an almost similar trend when moving from the single shade to the double shade regime. The only anomaly was the low maximum sap flow rate for Tree4 in the unshaded regime. It was 8 g h^{-1} which was almost 3 times less than that for the other *Navelina* cultivar (Tree3) which had 23 g h^{-1}.

The high sap flow rates when the trees where unshaded are consistent with the high photosynthesis rates which were obtained for the same solar radiation regime.

Water storage

Instantaneous water storage was the same for single shade and unshaded regimes. It was 30 % higher for the double-shaded regime. This was expected since the evaporative demand was higher for the unshaded and single shaded regimes.

Model

The model performed reasonably well and it is envisaged that it could be used to find estimates of hydraulic parameters for citrus trees in the field. The important factor is that the leaf water potential measurements may need a better method of measurement than the one used in this experiment if better results are to be obtained.

5.2 Concluding statements, recommendations and outlook

For future experiments related to this one, it is recommended that at least 3 cylinders of CO_2 with different concentrations, say between 100 and 600 ppm are made available. A single 1000 ppm tank could also be used, provided that additional equipment to dilute the CO_2 is also procured. Having adequate calibration gases is critical in any photosynthesis experiment of this nature because errors at the calibration stage of an experiment affect all other results related to that stage and the error may be amplified many times. It is also recommended that future measurements be done in differential mode.

Recent advances in design have resulted in IRGAs that are more user-friendly and easier to maintain, such as the LI-COR 7000 series. Such instruments can dramatically improve the quality of measurements.

Shade nets can be used for reducing midday depression of CO_2 assimilation.. It is recommended that shade nets with photosynthetic photon flux (PPF) transmittances between 50 and 60 % be used so that PPFD is not reduced below the optimal levels of 600-700 $\mu mol\ m^{-2}\ s^{-1}$. They are recommended for intensive commercial production of navel oranges. Besides increasing net assimilation, shade nets have been shown to enhance fruit quality and external colour, characteristics which are important for commercial producers exporting to international markets.

Admittedly, shading an entire orchard with nets is not a practical thing to do both financially and technically for a subsistence farmer trying to eke out a living. The value of the results in this study lies in the fact that it was determined, by the use of the shade nets, which temperatures and solar radiation levels are suitable for citriculture. Therefore, from a Zimbabwean perspective, the results from this study can be used for selecting regions within the country which have, based on the suitable radiation and temperature regimes recommended in this study, the potential for large scale citriculture. The current trend in terms of citriculture in the country suggests that growers only consider the

traditionally accepted areas such as Mazoe and the Lowveld. This study has shown that citriculture can thrive in the cooler areas such as the Eastern Highlands and the Midlands.

Future work should also consider orchard-level flux measurements. Very little has been done in terms of partitioning fluxes within and above the canopy in citrus orchards in this country. Dynamic chamber techniques have been shown to be an affordable method of measuring carbon dioxide and water vapour fluxes. Open-top chambers could be installed in an orchard. They should also be complemented by Bowen Ratio and eddy covariance methods. To get a total view of the whole ecosystem budget, soil chambers may also be useful for determining fluxes of nitrogen within the orchard soil as well as soil respiration. Such measurements can give more realistic predictions of yield and may be useful for commercial citrus growers like Mazoe Citrus Estates who have in the past benefited from the water conservation studies based on sap flow measurements by Dzikiti (personal communication).

REFERENCES

Antigonus Y., Lapidot M., Hadar D., Messika Y., Cohen S. 1998. Ultra-violet absorbing screens serve as optical barriers to protect crops from virus and insect pests. J. Econ. Entomol. 91:1401-1405.

Asseng, S., Turner, N.C., Botwright, Y., Condon, A.G., 2003. Evaluating the impact of a trait for increased specific leaf area on wheat yields using a crop simulation model. J. Agron. 95:10-19.

Assmann, S.M., 1999. The cellular basis of guard cell sensing of rising CO_2. Plant Cell Env.. 22:29-637.

Atwell, B.J. and Newsome, J.C., 1990. Turgor pressure in mechanically impeded lupin roots. Austral. J. Physiol. Plant. 17: 49-56.

Bacon, M.A., 1999. Biochemical control of leaf expansion. Plant Grow. Reg. 29:101-112.

Bacon, M.A., Davies, W.J., Mingo, D., Wilkinson, S., 2003. Root signals. *In* Roots: the hidden half (eds Y. Waisel, A. Ashel and U. Kafkafi). 3rd edn, Marcel Dekker, Inc., USA, PP. 460-471.

Bailey, B.J.1981. The reduction of thermal radiation in glasshouses by thermal screens. J. Agric. Eng. Res., 26:215-224.

Baker, J.M. and van Bavel,C.H.M. 1987. Measurement of mass flow of water in stems of herbaceous plants. Plant Cell Env. 10:777-782.

Ball, J.T., Woodrow, I.E., Berry, J.A., 1987. A model predicting stomatal conductance and its contribution to the control of photosynthesis under different environmental conditions. *In* Progress in Photosynthesis Research (ed. J. Biggins), Martinus Nijhoff, pp. 221-224.

Bevington, K.B. and Castle, W.S., 1985. Annual root growth pattern of young citrus trees in relation to shoot growth, soil temperature and soil water content. J. Am. Soc. Hort. Sci. 110:840-845.

Bhagsari, A.S. and Brown, R.H., 1986. Leaf photosynthesis and its correlations with leaf area. Crop Sci. 26:127-132.

Blum, A., 1996. Crop responses to drought and the interpretation of adaptation. Plant Grow. Reg.. 20:135-148.

Bustan, A., 1996. Carbohydrate availability as a factor limiting citrus productivity. PhD Thesis, Hebrew University of Jerusalem (Hebrew with English summary), submitted.

Castle, W.S. and Krezdorn, A.H.,1979. Anatomy and Morphology of field-sampled citrus fibrous roots as influenced by sampling depth and rootstock. HortScience 14:603-5.

Castle, W.S., 1980. Citrus root systems: their structure, function, growth and relationship to tree performance. *In* Proc. Int. Soc. Citriculture (ed P.R. Cary). pp. 62-9. Griffith, NSW, Australia.

Chaves, M.M., Osorio, J., Pereira, J.S., 2004. Water use efficiency and photosynthesis. *In* WUE in plant biology (ed M.A. Bacon). Blackwell Publishing. pp. 42-66.

Cohen, S. and Fuchs, M., 1999. Measuring and predicting radiometric properties of reflective shade nets and thermal screens. J. Agic. Eng. Res. 73(3):245-255.

Cohen, S., 1984. Light relations of an orange canopy. PhD Thesis; The Hebrew University of Jerusalem. 117 pp.

Cohen, S., Moreshet M., LeGuillou L., Simon, J.C., Cohen, M. 1997. Response of citrus trees to modified radiation regime in semi-arid conditions. J. Ex. Bot. 48(306): 35-44.

Cohen, S., Raveh, E., Grava, A., Goldschmidt, E.E. 2001. Citrus response to radiation load reduction: water use, photosynthesis, and productivity. Proc. Int. Soc. Citriculture, Orlando, FL.

Cowan, I.R. and Farquhar, G.D., 1977. Stomatal function in relation to leaf metabolism and environment. Symp. Soc. Exp. Biol. 31: 471-505.

Cowan, I.R., 1982. Regulation of water use in relation to carbon gain in higher plants. *In* Encyclopedia of Plant Physiology (eds O.L. Lange and J.D. Bewley). Volume 12B, pp. 535-562.

Davies, F.S. and Albrigo, L.G. 1994. Citrus. Redwood Books. Great Britain.

Day, W., 1985. Water vapour measurement and control. *In* Instrumentation for Environmental Physiology (eds B. Marshal and F.I. Woodward). Cambridge University Press, Cambridge. pp. 59-78.

De Jong, T.M. and Grossman, Y.L., 1994. A supply and demand approach to modelling annual reproductive and vegetative growth of deciduous fruit trees. HortScience 29:1435-42.

Dzikiti, S., Steppe, K., Lemeur, R., Milford, J.R., 2006. Water use by Navel orange trees [*Citrus sinensis* (L.) Osbeck] in Zimbabwe. Acta Hort. 707: 135-141.

Dzikiti, S., Steppe, K., Lemeur, R., Milford, J.R., 2007. Whole-tree level water balance and its implications on stomatal oscillations in orange trees [*Citrus sinensis* (L.) Osbeck] under natural climatic conditions. J. Ex. Bot.. 58: 1893 – 1901.

Eissenstadt, D.M. and Duncan, L.W., 1992. Root growth and carbohydrate responses in bearing citrus trees following partial canopy removal. Tree Physiol., 10:245-257.

Ennis, C.A., Lazrus, A.L., Kok, G.L., Zimmerman, P.R., Monson, R.K., 1990. Tellus 42B: 170-182.

Evans, J.R. and von Caemmerer, S., 1996. CO_2 diffusion inside leaves. Plant Physiol. 110:339-346.

Evans, J.R., 1999. Leaf anatomy enables more equal access to light and CO_2 between chloroplasts. New Phytol. 143:93-104.

Faria, T., Garcia-Plazaola, J.I., Abadia, A., Cerasoli, S., Pereira, J.S., Chaves, M.M., 1996. Diurnal changes in photoprotective mechanisms in leaves of cork oak (*Quercus suber* L.) during summer; Tree Physiol. 27:13-25.

Faria, T., Silveiro, D., Breia, E., Cabral, R., Abadia, A., Abadia, J., Pereira, J.S., Chaves, M.M., 1998. Differences in the response carbon assimilation to summer stress (water deficits, high light and temperature) in four Mediterranean tree species. Physiologia plantarum 102: 419-428.

Farquhar, G.D. and Richards, R.A., 1984. Isotopic composition of plant carbon correlates with water-use efficiency of wheat genotypes. Austral. J. Plant Physiol. 11:539-553.

Farquhar, G.D. and Sharkey, T.D., 1982. Stomatal conductance and photosynthesis. Annu. Rev. Plant Physiol. 33:317-345.

Farquhar, G.D. and Wong, S.C., 1984. An empirical model of stomatal conductance. Austral. J. Physiol. Plant. 11:191-210.

Farquhar, G.D., von Caemmerer, S., Berry, J.A., 1980. A biochemical model of photosynthetic CO_2 assimilation in leaves of C_3 species. Planta 149:78-90.

Farrar, J.F. and Williams, J.H.H., 1994. Control of the rate of respiration in roots: compartmentation, demand and the supply of substrate. *In* Compartmentation of Metabolism. (ed. M. Emes). pp. 167-88. London: Butterworths.

Fischler, M., 1985. Fruit size as related to photosynthesis and partition of assimilates in grapefruit trees. PhD Thesis, The Hebrew University of Jerusalem. 121 pp.

Food and Agricultural Organisation (FAO), 2003. WTO Agreement on Agriculture: The Implementation Experience: Developing Country Case Studies (Zimbabwe).

Ghannoum, O., von Caemmerer, S., Conroy, J.P., 2002. The effect of drought on plant water use efficiency of nine NAD-ME and nine NADP-ME Australian C_4 grasses. Func. Plant Biol. 29:1337-1348.

Girton, R.E., 1927. The growth of citrus seedlings as influenced by environmental factors. Univ. California Publ. Agric. Sci. 5:88-117.

Glenn, D.M., Puterka, G.J., Vanderzwet, T., Byers, R.E., Feldhake, C., 1999. Hydrophobic particle films: a new paradigm for suppression of arthropod pests and plant diseases. J. Econ. Entomol. 92:759-771.

Goldschmidt, E.E. and Golomb, A., 1982. The carbohydrate balance of alternate bearing citrus trees and the significance of reserves for flowering and fruiting. J. Am. Soc. Hortic. Sc. 107:206-208.

Goldschmidt, E.E. and Koch, K.E., 1996. Citrus. In Photoassimilate Distribution in Plants and Crops, Eds. E. Zamski and A.A. Schaffer. Marcel Dekker, New York, pp 797-823.

Goldschmidt, E.E., Golomb, A. and Galili, D., 1991. The carbohydrate balance of Citrus source leaves: effects of crop load, girdling and diurnal fluctuations. Alon Hanotea (Hebrew). 46:261-6.

Goldschmidt, E.E.,1999. Carbohydrate supply as a critical for citrus fruit development and productivity. HortScience 34: 1020-1024.

Hall, A.E. and Schulze, E.D., 1980. Stomatal responses to environment and a possible interrelation between stomatal effects on transpiration and CO_2 assimilation. Plant Cell Env. 3:467-474.

Hari, P., Keronen, P., Bäck, J., Altimir, N., Linkosalo, T., Pohja, T., Kulmala, M., Vesala, T., 1999. An improvement of the method for calibrating measurements of CO_2 flux. Plant, Cell, Env. 122: 1297-1301.

Heartspring website. Global Warming & Climate Chaos - Health Tips for Planet Earth. http://heartspring.net/global_warming_greenhouse.html. Date accessed: 2 June 2007.

Holbrook, N. M. and Sinclair, T. R., 1992. Water balance in the arborescent palm, Sabal palmetto: II. Transpiration and stem water storage. Plant Cell Env. 15(4): 401-409.

Hussein, J., 1982. An investigation into methods of irrigation of orange trees. Zim. Agric. J. 79: 73-78.

Incoll, L.D., Long, S.P. and Ashmore, M.R., 1977. S.I. units in publications in Plant Science. Current Advances in Plant Sciences 27:331-43.

Jackson, J.E., 1980. Light interception and utilization by orchard systems. Hort. Rev. 2:208-67.

Jahn, O.L., 1979. Penetration of photosynthetically active radiation as a measurement of canopy density of citrus trees. J. Am. Soc. Hort. Sci. 104:557-560.

Jarvis, A.J. and Davies, W.J., 1998. The coupled response of stomatal conductance to photosynthesis and transpiration. J. Ex. Bot. 49; 399-406.

Jifon, J.L. and Syvertsen, J.P., 2000. Reducing midday irradiance increases net assimilation in citrus leaves. HortScience 35:359 (Abstr.).

Jifon, J.L. and Syvertsen, J.P., 2001. Effects of moderate shade on citrus leaf gas exchange, fruit yield, and quality. Proc. Fla. State Hort. Soc. 114:177-181.

Jones, H.G., 1993. Drought tolerance and water-use efficiency. In Water Deficits: plant responses from cell to community (eds. J.A.C. Smith and H. Griffiths), BIOS Scientific Publishers Ltd, UK.

Jones, H.G., Archer, N., Rotenberg, E., Casa, R., 2003. Radiation measurement for plant ecophysiology. J. Ex. Bot. 54:879-889.

Jones, H.G.,1992. Plants and microclimate. A quantitative approach to environmental plant physiology. Second edition. Cambridge University Press, Cambridge.

Jones, W.W., Embleton, T.W., Coggins, C.W., Jr., 1975. Starch content of roots of 'Kinnow' mandarin trees bearing fruit in alternate years. HortScience 10:514.

Khairi, M.M.A. and Hall, A.E., 1976. Temperature and humidity effects on net photosynthesis and transpiration of citrus. Physiol. Plant. 36:29-34.

Kriedemann, P.E., 1969. 14C distribution in lemon plants. J. Hort. Sci. 44:273-9.

Kriedemann, P.E., 1971. Crop Energetics and horticulture. HortScience 6:432-8.

Kriedemann, P.E. and Barrs, H.D.,1981. Citrus orchard. In: Davies, F.S. and Albrigo, L.G. (eds), Citrus. Redwood Books. Great Britain.

Kriedemann, P.E., 1968. Some photosynthetic characteristics of citrus leaves. Austral. J. Biol. Sci. 21:895-905.

Kurata, K., 1991. View factors involved in radiation exchanges in floating mulches made of non-woven fabrics. J. Agric. Eng. Res. 48, 185-193.

Lambers, H., Chaplain, F.S., Pons, T.L., 1998. Plant Physiological Ecology, Springer, New York.

Lee, J.S. and Bowling, D.J.F., 1995. Influence of the mesophyll on stomatal opening. Austral. J. Physiol. Plant.

Leuning, R., Kelliher, F.M., De Pury D.G.G., Schulze, E.D., 1995. Leaf nitrogen, photosynthesis, conductance and transpiration - scaling from leaves to canopies. Plant Cell Env. 18:1183-1200.

Leuning, R., Tuzet, A.,Perrier, A., 2003. Stomata as part of the soil-plant atmosphere continuum. In: Forests at the Land-Atmosphere Interface (eds M. Mencuccini, J. Grace, J. Moncrieff and K. McNaughton).CAB International, Edinburgh, Scotland.

Levy, Y. and Kaufmann, M.R., 1976. Cycling of leaf conductance in citrus exposed to natural environments and controlled environments. Canadian J. Bot. 54: 2215-2218.

LI-COR, 1996. LI-6262 CO_2/H_2O Analyzer Operating and Instruction Manual. LI-COR Inc., Lincoln, Nebraska, USA.

Loescher, W.H., McCamant, T., Keller, J.D., 1990. Carbohydrate reserves, translocation and storage in woody plant roots. HortScience 25: 274-81.

Long, S.P. and Hällgren, J-E., 1993. Measurement of CO_2 assimilation by plants in the field and the laboratory. In Photosynthesis and production in a changing environment: A field and laboratory manual (eds Hall, D.O., Scurlock, H.R., Bolhàr-Nordenkampf, H.R., Leegood, R.C., Long, S.P.).Chapman and Hall, London, UK.

Long, S.P., 1999. C_4 photosynthesis - environmental responses. In The Biology of C_4 plants (eds Sage, R.F., and Monson, R.K.). Academic Press, San Diego. pp. 215-249.

Lopez-Castaneda, C., Richards, R.A., Farquhar, G.D., Williamson, R.E. 1996. Seed and seedling characteristics contributing to variation in early vigour between wheat and barley. Crop Science. 36: 1257-1266.

Lu, Z., Percy, R.G., Qualset, C.O., Zeiger., E., 1998. Stomatal conductance predicts yields in irrigated Pima cotton an bread wheat grown at high temperatures. J. Ex. Bot. 49:543-560.

McBride, J., 2000. Whitewashing agriculture. Agr. Res. 48:14-17.

McDermitt, D.K., Welles, J.M., Eckles, R.D., 1993. Effects of temperature, pressure and water vapor on gas phase infrared absorption of CO_2. LI-COR, Inc.; Lincoln, NE, USA.

Meinzer, F.C., Clearwater, M.J., Goldstein, G., 2001. Water transport in trees: current perspectives, news insights and some controversies. Env. Exp. Bot. 45:239-262.

Meinzer, F.C., James, S.A., Goldstein, G., Woodruff D., 2003. Whole-tree water transport scales with sapwood capacitance in tropical forest canopy trees. Plant Cell Env. 26:1147-1155.

Mendel, K., 1951. Orange leaf transpiration under orchard conditions. III. Prolonged soil drought and the influence of stocks. Palest. J. Bot. 8:45-53.

Mingo, B., 2003. Regulation of tomato plant growth in relation to soil water availability. PhD thesis, Lancaster University, UK.

Monselise, S.P., 1947. The growth of citrus roots and shoots under different cultural conditions. Palest. J. Bot. 6:43-54.

Monselise, S.P., 1951. Light distribution in Citrus trees. Bull. Res. Coun. Israel. 1: 36-53.

Monteith, J.L., 1993. The exchange of water and carbon by crops in a Mediterranean climate. Irrig. Sci. 14: 85-91.

Mott, K.A., 1988. Do stomata respond to CO_2 concentrations other than intercellular? Plant Physiol. 86: 200-203.

Oppenheimer, J.D., and Mendel, K., 1934. Some experiments on water relations of citrus trees. Hadar. 7: 150-153.

Philips, N., Nagchaudhuri A., Oren R., 2006. Time constant for water transport in loblolly pine trees estimated from time series of evaporative demand and stem sap flow. Trees. 11: 412-419.

Polley, H.W., 2002. Crop physiology and metabolism: Implications of atmospheric and climate change for crop yield and water use efficiency. Crop Sci. 42:131-140.

Raschke, C., 1976. The influence of CO_2 content of the ambient air on stomatal conductance and the CO_2 concentration in leaves. In Carbon Dioxide Enrichment of Greenhouse Crops (eds H.Z. Enoch and B.A. Kimball), Volume 2, CRC Press, USA. Pp. 87-102.

Raveh, E., Cohen, S., Raz, T., Yakir, D., Grava, A., Goldschmidt, E.E., 2003. Increased growth of young citrus trees under reduced radiation in a semi-arid climate. J. Ex. Bot. 54(381): 365-373.

Reuther, W.,1973. Climate and citrus behaviour. In: Gat, E., Erner, Y., Goldschmidt, E.E. The effect of temperature on the citrus crop. WMO, 84: 1-21.

Richards, B.G. and Greacen, E.L., 1986. Mechanical stresses on an expanding cylindrical root analog in antigranulocytes media. Austral. J. Soil Res. 54: 381-387.

Richards, R.A. and Passioura, J.B., 1989. A breeding programme to reduce the diameter of the major xylem vessel in the seminal roots of wheat and its effect on grain-yield in rain fed environments. Austral. J. Agric. Res. 40:943-950.

Richards, R.A., Rebetzke, G.J., Condon, A.G., von Herwaarden, A.F., 2002. Breeding opportunities for increasing the efficiency of water use and crop yield in temperate cereals. Crop Sci. 42: 111-121.

Sakuratani, T., 1981. A heat balance method for measuring water flux in the stem of intact plants. J. Agric. Met. (Japan). 37:9-17.

Schulze, E.D., Cermak, J., Matyssek, R., Penka, M., Zimmermann, R., Vasicek, F., Gries, W., Kucera, J., 1985. Canopy transpiration and water fluxes in the xylem of the trunk of Larix and Picea trees- a comparison of xylem flow, porometer and cuvette measurements. Oecologia 66: 475-483.

Schulze, E.D., Kelliher, F.M., Korner, C., Lloyd, J., Leuning, R., 1994. Relationships between plant nitrogen nutrition, carbon assimilation rate, and maximum stomatal and ecosystem surface conductances for evaporation: A global ecology scaling exercise. Annu. Rev. Ecol. Sys.. 25:629-660.

Sharp R.E., Silk W.K., Hsiao, TC. 1988. Growth of the maize primary root at low water potentials. I. Spatial distribution of expansive growth. Plant Physiol. 87:50–57.

Sharp, R.E., and Davies, W.J., 1985. Solute regulation and growth by roots and shoots of water-stressed maize plants. Planta 147(1):43-49. 1979.

Sharp, R.E., Davies WJ. 1979. Solute regulation and growth by roots and shoots of water-stressed maize plants. Planta 147: 43–49.

Sinclair, T.R. and Allen, I.H. Jr.,1982. Carbon dioxide and water vapor exchange of leaves on field-grown citrus trees. J. Exp. Bot. 33:1166-1175.

Sithole, P., 2005. An evaluation of the effect of canopy microclimate and architecture on the growth and quality of navel orange fruits (*Citrus sinensis* (L.) Osbeck) in Zimbabwe. MSc thesis (submitted). University of Zimbabwe.

Smith, P., 1976. Collapse of 'Murcott' tangerine trees. J. Am. Soc. Hort. Sci. 101: 23-5.

Sperry, J.S., Hacke, U.G., Oren, R., Comstock, J.P., 2002. Water deficits and hydraulic limits to leaf water supply. Plant, Cell and Environment. 25:251-263.

Spiegel-Roy, P. and Goldschmidt, E.E.,1996. Biology of Citrus. Cambridge University Press, Cambridge.

Spollen, W.G., LeNoble, M.E., Samuels, T.D., Bernstein, N., Sharp, R.E., 2000. Abscisic acid accumulation maintains primary root elongation at lower water potential by restricting ethylene production. Plant Physiol. 122: 967-976.

Stanhill, G., 1986. Water use efficiency. Adv. Agron. 39:53-85.

Stanhill, G., Moreshet, S., Fuchs, M., 1976. Effect of increasing foliage and soil reflectivity on the yield and water use efficiency of grain sorghum. Agron J. 68:329-332.

Steduto, P., Hsiao, T.C., Fereres, E., 2007. On the conservative behaviour of biomass water productivity. Irrig. Sci.

Steppe, K., 2004. Diurnal dynamics of water flow through trees: design and validation of a mathematical flow and storage model. PhD Thesis, Ghent University, Belgium.

Steppe, K., Dzikiti, S., Lemeur R., Milford, J.R., 2006b. Stomatal oscillations in orange trees under natural climatic conditions. Annals of Botany 92, 831-835.

Syvertsen, J.P. 1984. Light accumulation in citrus leaves. II. CO_2 assimilation and light, water, and nitrogen use efficiency. J. Amer. Soc. Hort. Sci. 109:812-817.

Syvertsen, J.P. and Albrigo, L.G., 1980. Some effects of grapefruit tree canopy position on microclimate, water relations, fruit yield, and juice quality. J. Am. Soc. Hortic. Sci. 105:454-459.

Syvertsen, J.P. and Lloyd, J. 1994. Citrus. In: Handbook of Environmental Physiology of Fruit Crops. Vol. 2: Sub-Tropical and Tropical Crops. (Eds. B. Schaffer and P.C. Andersen). CRC Press, Boca Raton, FL, pp 65-99.

Syvertsen, J.P., 1981.Hydraulic conductivity of four commercial citrus rootstocks J. Am. Soc. Hort. Sci. 106: 378-381.

Syvertsen, J.P., 1994. Partial shoot removal increases net CO_2 assimilation and alters water relations of Citrus seedlings. Tree Physiol. 14:497-508.

Syvertsen, J.P., Goni, C., Otero, A., 2003. Fruit load and canopy shading affect leaf characteristics and net gas exchange of 'Spring' navel orange trees. Tree Physiol. 23:899-906.

Tanner, C.B., 1981. Transpiration efficiency of potato. J. Agron. 73:49-54.

Tanny, J. and Cohen, S., 2003. The Effect of a Small Shade Net on the Properties of Wind and Selected Boundary Layer Parameters above and within a Citrus Orchard. Biosys Eng. 84(1):57-67.

Tatarinov, F. and Cermak, J., 1999. Daily and seasonal variation of stem radius in oak. Anna. For. Sci. 56:579-590.

Teitel, M. and Segal, I., 1995. Net thermal radiation under shading screens. J. Agric. Eng. Res. 61:19-26.

Teitel, M., Peiper, U., Zvieli, Y., 1996. Shading screens for frost protection. Agric For. Meterol. 81: 273-286.

Turrel, F.M., 1961. Growth of the photosynthetic area of citrus. Bot. Gaz. 122:285-298.

Tyree, M.T. and Zimmerman, M.H., 2002. Xylem structure and the ascent of sap. 2nd ed. Springer-Verlag. Berlin.

van Bavel, M.G., 1999. Dynagage™ installation and operation manual. Dynamax Inc. Texas.

Van de Honert, T.H., 1948. Water transport in plants as a catenary process. Faraday Society Discussions 3:146-153.

von Caemmerer, S. and Farquhar, G.D., 1981. Some relationships between the biochemistry of photosynthesis and the gas exchange of leaves. Planta 153:376-378.

Vu, J.C.V., Yelenosky, G., 1988. Solar irradiance and drought stress effects on the activity and concentration of ribulose bisphosphate carboxylases in 'Valencia' orange leaves. Israel J. Bot. 37:245-256.

Vu, J.C.V., Yelenosky, G., 1989. Non-structural carbohydrate concentrations in leaves of “Valencia” orange subjected to water deficits. Env. Expt. Bot. 29:149-154.

Waggoner, P.E., Boyd Pack A., Reifsnyder, W.E. 1959. The Climate of Shade. The Connecticut Agricultural Experimental Station, New Haven, Bulletin 626.

Wallerstein I., Goren R. and Monselise S.P. 1978. Rapid and slow translocation of 14C [carbon isotope]-sucrose and 14C-assimilates in Citrus and Phaseolus with special reference to ringing effect [Oranges, beans]. J. Hortic. Sci. 53: 203-208.

Webb, A.A.R. and Hetherington, A.M., 1997. Convergence of abscisic acid, CO_2 and extracellular calcium signal transduction pathways in stomatal guard cells. Physiol. Plant. 114:145-161.

Wong, S.C., Cowan, I.R., Farquhar, G.D., 1978. Leaf conductance in relation to assimilation in Eucalyptus paucifora Sieb. Ex Spreng. Influence of irradiance and partial pressure of carbon dioxide. Physiol. Plant. 62:670-674.

Wong, S.C., Cowan, I.R., Farquhar, G.D., 1979. Stomatal conductance correlates with photosynthetic capacity. Nature 282:424-426.

Wong, S.C., Cowan, I.R., Farquhar, G.D., 1985. Leaf conductance in relation to rate of CO_2 assimilation. II. Effects of short-term exposures to different photon flux densities. Plant Physiol. 78:826-829.

Wright, 1977. The relationship between water potential and the levels of abscisic acid and ethylene in excised wheat leaves. Planta 134:183-189.

Zimbabwe International Travel Expo 2007. http://www.zite.co.zw/pages.php?pid=4. Date accessed: 31 May 2007.

Zollner, G.E., Torr, S.J., Ammann, C., Meixner, F.X., 2004. Dispersion of carbon dioxide plumes in African woodland: implications for host-finding by tsetse flies. Physiol. Entomol. 29(4): 381-394.

APPENDICES

Datalogger programs

A1 Datalogger Z5 program

```
;{CR23X}
;Program:  Control and logging data acquisition for UZIM CO2 chamber entered by IVONNE TREBS 27-SEP-2006
;Last edited by ANYWHERE TSOKANKUNKU 02-NOV-2006
;execution time interval 5 sec
;output interval: 1 min


*Table 1 Program
  01: 5        Execution Interval (seconds)


;MEASURE LICOR pressure in sample cell

1:  Volt (SE) (P1)
 1: 1        Reps
 2: 15       5000 mV, Fast Range
 3: 1        SE Channel
 4: 1        Loc [ LIpress   ]
 5: 0.184    Mult
 6: 600      Offset

;MEASURE LICOR temperature in sample cell

2:  Volt (SE) (P1)
 1: 1        Reps
 2: 15       5000 mV, Fast Range
 3: 2        SE Channel
 4: 2        Loc [ LItemp    ]
 5: 0.0122   Mult
 6: 0.0      Offset

;MEASURE LICOR CO2

3:  Volt (SE) (P1)
 1: 1        Reps
 2: 15       5000 mV, Fast Range
 3: 3        SE Channel
 4: 3        Loc [ LICO2     ]
 5: 1.0      Mult
 6: 0.0      Offset

;MEASURE LICOR H2O

4:  Volt (SE) (P1)
 1: 1        Reps
 2: 15       5000 mV, Fast Range
 3: 4        SE Channel
 4: 4        Loc [ LIH2O     ]
 5: 1.0      Mult
 6: 0.0      Offset
```

```
;MEASURE Mass Flow Meter (MFM) signal

5:  Volt (Diff) (P2)
 1: 1        Reps
 2: 15       5000 mV, Fast Range
 3: 7        DIFF Channel
 4: 5        Loc [ MFM       ]
 5: 1.0      Mult
 6: 0.0      Offset

;First turn on power to the probe
6:  Do (P86)
 1: 49       Turn On Switched 12V

7:  Delay w/Opt Excitation (P22)
 1: 3        Ex Channel
 2: 0        Delay W/Ex (units = 0.01 sec)
 3: 100      Delay After Ex (units = 0.01 sec)
 4: 0        mV Excitation

;Measure RH and Temperature mV and multiply readings by 0.1
8:  Volt (SE) (P1)
 1: 2        Reps
 2: 35       5000 mV, 50 Hz Reject, Fast Range
 3: 5        SE Channel
 4: 16       Loc [ HMPRH     ]
 5: 0.1      Mult
 6: 0.0      Offset

;Turn off power to the probe

9:  Do (P86)
 1: 59       Turn Off Switched 12V

; Subtract 40 from temperature to scale to Celsius

10:  Z=X+F (P34)
 1: 17       X Loc [ HMPTEMP   ]
 2: -40      F
 3: 17       Z Loc [ HMPTEMP   ]

; MEASURE leaf temperatures

11:  Thermocouple Temp (SE) (P13)
 1: 1        Reps
 2: 31       10 mV, 50 Hz Reject, Slow Range
 3: 7        SE Channel
 4: 2        Type E (Chromel-Constantan)
 5: 13       Ref Temp (Deg. C) Loc [ pnlTemp   ]
 6: 7        Loc [ Tleaf_1   ]
 7: 1.0      Mult
 8: 0.0      Offset

12:  Thermocouple Temp (SE) (P13)
 1: 1        Reps
 2: 31       10 mV, 50 Hz Reject, Slow Range
 3: 8        SE Channel
 4: 2        Type E (Chromel-Constantan)
 5: 13       Ref Temp (Deg. C) Loc [ pnlTemp   ]
 6: 8        Loc [ Tleaf_2   ]
 7: 1.0      Mult
 8: 0.0      Offset
```

```
13:  Thermocouple Temp (SE) (P13)
 1: 1        Reps
 2: 31       10 mV, 50 Hz Reject, Slow Range
 3: 9        SE Channel
 4: 2        Type E (Chromel-Constantan)
 5: 13       Ref Temp (Deg. C) Loc [ pnlTemp   ]
 6: 9        Loc [ Tleaf_3   ]
 7: 1.0      Mult
 8: 0.0      Offset

14:  Thermocouple Temp (SE) (P13)
 1: 1        Reps
 2: 31       10 mV, 50 Hz Reject, Slow Range
 3: 10       SE Channel
 4: 2        Type E (Chromel-Constantan)
 5: 13       Ref Temp (Deg. C) Loc [ pnlTemp   ]
 6: 10       Loc [ Tleaf_4   ]
 7: 1.0      Mult
 8: 0.0      Offset

15:  Thermocouple Temp (SE) (P13)
 1: 1        Reps
 2: 31       10 mV, 50 Hz Reject, Slow Range
 3: 11       SE Channel
 4: 2        Type E (Chromel-Constantan)
 5: 13       Ref Temp (Deg. C) Loc [ pnlTemp   ]
 6: 11       Loc [ Temp_cham ]
 7: 1.0      Mult
 8: 0.0      Offset

; CM11 S/N 986750 mult 5.01e-6 v/wm-2 (=199.6wm-2/mV) so output=wm-2
16:  Volt (SE) (P1)
 1: 1        Reps
 2: 34       1000 mV, 50 Hz Reject, Slow Range
 3: 12       SE Channel
 4: 15       Loc [ CM11      ]
 5: 199.6    Mult
 6: 0.0      Offset

;sapflow gauge
17:  Volt (Diff) (P2)
 1: 3        Reps
 2: 31       10 mV, 50 Hz Reject, Slow Range
 3: 8        DIFF Channel
 4: 18       Loc [ SAPFL2_1  ]
 5: 0.004    Mult
 6: 0.0      Offset

18:  Volt (Diff) (P2)
 1: 1        Reps
 2: 35       5000 mV, 50 Hz Reject, Fast Range
 3: 11       DIFF Channel
 4: 21       Loc [ SAPFL2_V  ]
 5: 1.0      Mult
 6: 0.0      Offset

19:  Pulse (P3)
 1: 1        Reps
 2: 1        Pulse Channel 1
 3: 1        Low Level AC, All Counts
 4: 22       Loc [ WS_MS     ]
 5: 0.0308   Mult
 6: 0.0      Offset
```

```
20:  Excite-Delay (SE) (P4)
 1: 1        Reps
 2: 15       5000 mV, Fast Range
 3: 23       SE Channel
 4: 4        Excite all reps w/Exchan 4
 5: 2        Delay (units 0.01 sec)
 6: 5000     mV Excitation
 7: 23       Loc [ wd0to360  ]
 8: 0.071    Mult
 9: 0.0      Offset

;par sensor units umols-1m-2uA-1

21:  Volt (SE) (P1)
 1: 1        Reps
 2: 22       50 mV, 60 Hz Reject, Slow Range
 3: 24       SE Channel
 4: 6        Loc [ PAR       ]
 5: -150.83  Mult
 6: 0.0      Offset

; SET HIGH 3-WAY VALVE at begin (0 min) of 6 min interval

22:  If time is (P92)
 1: 0        Minutes (Seconds --) into a
 2: 8        Interval (same units as above)
 3: 30       Then Do

23:  Set Port(s) (P20)
 1: 9999     C8..C5 = nc/nc/nc/nc
 2: 9991     C4..C1 = nc/nc/nc/high

24:  Z=F (P30)
 1: 1        F
 2: 0        Exponent of 10
 3: 12       Z Loc [ Valve     ]

25:  End (P95)

; SET LOW 3-WAY VALVE at mid (3 min) of 6 min interval

26:  If time is (P92)
 1: 4        Minutes (Seconds --) into a
 2: 8        Interval (same units as above)
 3: 30       Then Do

27:  Set Port(s) (P20)
 1: 9999     C8..C5 = nc/nc/nc/nc
 2: 9990     C4..C1 = nc/nc/nc/low

28:  Z=F (P30)
 1: 0        F
 2: 0        Exponent of 10
 3: 12       Z Loc [ Valve     ]

29:  End (P95)

30:  Internal Temperature (P17)
 1: 13       Loc [ pnlTemp   ]

31:  Batt Voltage (P10)
 1: 14       Loc [ Battvolt  ]
```

```
; O U T P U T  T O  F I N A L  S T O R A G E  AND OPTIONALLY TO SOLID STATE STORAGE
MODULE
;  output interval: 1 min

32:  If time is (P92)
 1: 0       Minutes (Seconds --) into a
 2: 1       Interval (same units as above)
 3: 10      Set Output Flag High
;  output time information (output at the END of averaging/sampling interval)

33:  Real Time (P77)^19114
 1: 1111    Year,Day,Hour/Minute,Seconds (midnight = 0000)

34:  Average (P71)^1517
 1: 1       Reps
 2: 1       Loc [ LIpress   ]

35:  Standard Deviation (P82)^28381
 1: 1       Reps
 2: 1       Sample Loc [ LIpress   ]

36:  Average (P71)^10764
 1: 1       Reps
 2: 2       Loc [ LItemp    ]

37:  Standard Deviation (P82)^29402
 1: 1       Reps
 2: 2       Sample Loc [ LItemp    ]

38:  Average (P71)^15703
 1: 1       Reps
 2: 3       Loc [ LICO2     ]

39:  Standard Deviation (P82)^19503
 1: 1       Reps
 2: 3       Sample Loc [ LICO2     ]

40:  Average (P71)^1334
 1: 1       Reps
 2: 4       Loc [ LIH2O     ]

41:  Standard Deviation (P82)^601
 1: 1       Reps
 2: 4       Sample Loc [ LIH2O     ]

42:  Average (P71)^418
 1: 1       Reps
 2: 5       Loc [ MFM       ]

43:  Standard Deviation (P82)^17838
 1: 1       Reps
 2: 5       Sample Loc [ MFM       ]


44:  Average (P71)^12873
 1: 1       Reps
 2: 7       Loc [ Tleaf_1   ]

45:  Standard Deviation (P82)^26262
 1: 1       Reps
 2: 7       Sample Loc [ Tleaf_1   ]
```

46: Average (P71)^32640
1: 1 Reps
2: 8 Loc [Tleaf_2]

47: Standard Deviation (P82)^19003
1: 1 Reps
2: 8 Sample Loc [Tleaf_2]

48: Average (P71)^2151
1: 1 Reps
2: 9 Loc [Tleaf_3]

49: Standard Deviation (P82)^4808
1: 1 Reps
2: 9 Sample Loc [Tleaf_3]

50: Average (P71)^5360
1: 1 Reps
2: 10 Loc [Tleaf_4]

51: Standard Deviation (P82)^9621
1: 1 Reps
2: 10 Sample Loc [Tleaf_4]

52: Average (P71)^12154
1: 1 Reps
2: 11 Loc [Temp_cham]

53: Standard Deviation (P82)^4257
1: 1 Reps
2: 11 Sample Loc [Temp_cham]

54: Sample (P70)^7397
1: 1 Reps
2: 12 Loc [Valve]

55: Sample (P70)^21219
1: 1 Reps
2: 13 Loc [pnlTemp]

56: Sample (P70)^29952
1: 1 Reps
2: 14 Loc [Battvolt]

57: Average (P71)^16431
1: 1 Reps
2: 15 Loc [CM11]

58: Standard Deviation (P82)^9895
1: 1 Reps
2: 15 Sample Loc [CM11]

59: Average (P71)^26980
1: 1 Reps
2: 16 Loc [HMPRH]

60: Standard Deviation (P82)^9075
1: 1 Reps
2: 16 Sample Loc [HMPRH]

61: Average (P71)^9440
1: 1 Reps
2: 17 Loc [HMPTEMP]

62: Standard Deviation (P82)^28358
1: 1 Reps
2: 17 Sample Loc [HMPTEMP]

63: Average (P71)^20800
1: 3 Reps
2: 18 Loc [SAPFL2_1]

64: Standard Deviation (P82)^16966
1: 3 Reps
2: 18 Sample Loc [SAPFL2_1]

65: Average (P71)^15767
1: 1 Reps
2: 21 Loc [SAPFL2_V]

66: Standard Deviation (P82)^4017
1: 1 Reps
2: 21 Sample Loc [SAPFL2_V]

67: Wind Vector (P69)^3695
1: 1 Reps
2: 0 Samples per Sub-Interval
3: 0 S, é1, & å(é1) Polar
4: 22 Wind Speed/East Loc [WS_MS]
5: 23 Wind Direction/North Loc [wd0to360]

68: Average (P71)^17556
1: 1 Reps
2: 22 Loc [WS_MS]

69: Standard Deviation (P82)^1520
1: 1 Reps
2: 22 Sample Loc [WS_MS]

70: Sample (P70)^32742
1: 1 Reps
2: 23 Loc [wd0to360]

71: Histogram (P75)^4046
1: 1 Reps
2: 8 No. of Bins
3: 1 Closed Form
4: 23 Bin Select Value Loc [wd0to360]
5: 0 Frequency Distribution
6: 0 Low Limit
7: 360 High Limit

72: Average (P71)^19553
1: 1 Reps
2: 6 Loc [PAR]

73: Standard Deviation (P82)^24217
1: 1 Reps
2: 6 Sample Loc [PAR]

; S E T O U T P U T F L A G L O W
74: Do (P86)
1: 20 Set Output Flag Low

; O P T I O N A L O U T P U T T O S O L I D S T A T E S T O R A G E M O D U L E

75: Serial Out (P96)
 1: 30   SM192/SM716/CSM1

*Table 2 Program
  02: 0.0000   Execution Interval (seconds)

*Table 3 Subroutines

End Program

-Input Locations-
1 LIpress   1 2 1
2 LItemp   1 2 1
3 LICO2   1 2 1
4 LIH2O   1 2 1
5 MFM   1 2 1
6 PAR   1 2 1
7 Tleaf_1   1 3 1
8 Tleaf_2   1 3 1
9 Tleaf_3   1 3 1
10 Tleaf_4   1 3 1
11 Temp_cham 1 3 1
12 Valve   1 2 2
13 pnlTemp   1 6 1
14 Battvolt 1 1 1
15 CM11   1 2 1
16 HMPRH   5 2 1
17 HMPTEMP   17 3 2
18 SAPFL2_1 13 2 2
19 SAPFL2_2 9 2 1
20 SAPFL2_3 17 2 1
21 SAPFL2_V 1 2 1
22 WS_MS   1 3 1
23 wd0to360 1 3 1
24 _________ 0 0 0
25 _________ 0 0 0
26 _________ 0 0 0
27 _________ 0 0 0
28 _________ 0 0 0

A2 Datalogger Z7 program

```
;{CR23X}
;Datalogger program for logging using 3 dynamax sapflow gages
;Written by Anywhere Tsokankunku 13-11-2006, last edited 30-12-06@

;Datlogger array:
; DIFF Channel    Identifier      inLoc
;                  Battvolt         1
;                  PAneltmp         2
;  1               SAPFL3_1         3
;  2               SAPFL3_2         4
;  3               SAPFL3_3         5
;  4               SAPFL3_V         6
;  5               SAPFL4_1         7
;  6               SAPFL4_2         8
;  7               SAPFL4_3         9
;  8               SAPFL4_V         10
;  9               SAPFL5_1         11
;  10              SAPFL5_2         12
;  11              SAPFL5_3         13
;  12              SAPFL5_V         14

;Output array definitions
;
*Table 1 Program
  01: 5        Execution Interval (seconds)

1:  Batt Voltage (P10)
 1: 1        Loc [ Battvolt  ]

2:  Panel Temperature (P17)
 1: 2        Loc [ PAneltmp  ]


3:  Volt (Diff) (P2)
 1: 3        Reps
 2: 31       10 mV, 50 Hz Reject, Slow Range
 3: 1        DIFF Channel
 4: 3        Loc [ SAPFL3_1  ]
 5: 1        Mult
 6: 0.0      Offset

4:  Volt (Diff) (P2)
 1: 1        Reps
 2: 35       5000 mV, 50 Hz Reject, Fast Range
 3: 4        DIFF Channel
 4: 6        Loc [ SAPFL3_V  ]
 5: .001     Mult
 6: 0.0      Offset

5:  Volt (Diff) (P2)
 1: 1        Reps
 2: 22       50 mV, 60 Hz Reject, Slow Range
 3: 5        DIFF Channel
 4: 7        Loc [ PAR_EXT   ]
 5: -10.78   Mult
 6: 0.0      Offset

;First turn on power to the probe

6:  Do (P86)
 1: 49       Turn On Switched 12V
```

```
7:  Delay w/Opt Excitation (P22)
 1: 1        Ex Channel
 2: 0        Delay W/Ex (units = 0.01 sec)
 3: 100      Delay After Ex (units = 0.01 sec)
 4: 0        mV Excitation

;Measure RH and Temperature mV and multiply readings by 0.1

8:  Volt (SE) (P1)
 1: 2        Reps
 2: 35       5000 mV, 50 Hz Reject, Fast Range
 3: 11       SE Channel
 4: 8        Loc [ HMPRH     ]
 5: 0.1      Mult
 6: 0.0      Offset

;Turn off power to the probe

9:  Do (P86)
 1: 59       Turn Off Switched 12V

; Subtract 40 from temperature to scale to Celsius

10:  Z=X+F (P34)
 1: 9        X Loc [ HMPTEMP    ]
 2: -40      F
 3: 9        Z Loc [ HMPTEMP    ]

; Tipping bucket rain gauge
11:  Pulse (P3)
 1: 1        Reps
 2: 1        Pulse Channel 1
 3: 2        Switch Closure, All Counts
 4: 10       Loc [ TBRaingg  ]
 5: .2       Mult
 6: 0.0      Offset

12:  Volt (Diff) (P2)
 1: 3        Reps
 2: 31       10 mV, 50 Hz Reject, Slow Range
 3: 9        DIFF Channel
 4: 11       Loc [ SAPFL5_1  ]
 5: 1        Mult
 6: 0.0      Offset

13:  Volt (Diff) (P2)
 1: 1        Reps
 2: 35       5000 mV, 50 Hz Reject, Fast Range
 3: 12       DIFF Channel
 4: 14       Loc [ SAPFL5_V  ]
 5: .001     Mult
 6: 0.0      Offset

14:  If time is (P92)
 1: 0        Minutes (Seconds --) into a
 2: 1        Interval (same units as above)
 3: 10       Set Output Flag High
```

```
;   output time information (output at the END of averaging/sampling interval)

15:  Real Time (P77)
 1: 1111     Year,Day,Hour/Minute,Seconds (midnight = 0000)

16:  Sample (P70)
 1: 1        Reps
 2: 1        Loc [ Battvolt  ]


17:  Sample (P70)
 1: 1        Reps
 2: 2        Loc [ PAneltmp  ]

18:  Average (P71)
 1: 3        Reps
 2: 3        Loc [ SAPFL3_1  ]

19:  Standard Deviation (P82)
 1: 3        Reps
 2: 3        Sample Loc [ SAPFL3_1  ]

20:  Average (P71)
 1: 1        Reps
 2: 6        Loc [ SAPFL3_V  ]

21:  Standard Deviation (P82)
 1: 1        Reps
 2: 6        Sample Loc [ SAPFL3_V  ]

22:  Average (P71)
 1: 1        Reps
 2: 7        Loc [ PAR_EXT   ]


23:  Standard Deviation (P82)
 1: 1        Reps
 2: 7        Sample Loc [ PAR_EXT   ]

24:  Average (P71)
 1: 1        Reps
 2: 8        Loc [ HMPRH     ]

25:  Standard Deviation (P82)
 1: 1        Reps
 2: 8        Sample Loc [ HMPRH     ]

26:  Average (P71)
 1: 1        Reps
 2: 9        Loc [ HMPTEMP   ]

27:  Standard Deviation (P82)
 1: 1        Reps
 2: 9        Sample Loc [ HMPTEMP   ]

28:  Totalize (P72)
 1: 1        Reps
 2: 10       Loc [ TBRaingg  ]

29:  Average (P71)
 1: 3        Reps
 2: 11       Loc [ SAPFL5_1  ]
```

30: Standard Deviation (P82)
1: 3 Reps
2: 11 Sample Loc [SAPFL5_1]

31: Average (P71)
1: 1 Reps
2: 14 Loc [SAPFL5_V]

32: Standard Deviation (P82)
1: 1 Reps
2: 14 Sample Loc [SAPFL5_V]

*Table 2 Program
02: 0.0000 Execution Interval (seconds)

*Table 3 Subroutines

End Program

1	[Battvolt]	RW--	1	1	----- ------ ---
2	[PAneltmp]	RW--	1	1	----- ------ ---
3	[SAPFL3_1]	RW--	2	1	Start ------ ---
4	[SAPFL3_2]	RW--	2	1	----- Member ---
5	[SAPFL3_3]	RW--	2	1	----- ------ End
6	[SAPFL3_V]	RW--	2	1	----- ------ ---
7	[PAR_EXT]	RW--	2	1	Start ------ ---
8	[HMPRH]	RW--	2	1	Start ------ ---
9	[HMPTEMP]	RW--	3	2	----- ------ End
10	[TBRaingg]	RW--	1	1	----- ------ ---
11	[SAPFL5_1]	RW--	2	1	Start ------ ---
12	[SAPFL5_2]	RW--	2	1	----- Member ---
13	[SAPFL5_3]	RW--	2	1	----- ------ End
14	[SAPFL5_V]	RW--	2	1	----- ------ ---
15	[_____]	----	0	0	----- ------ ---
16	[_____]	----	0	0	----- ------ ---
17	[_____]	----	0	0	----- ------ ---
18	[_____]	----	0	0	----- ------ ---
19	[_____]	----	0	0	----- ------ ---
20	[_____]	----	0	0	----- ------ ---
21	[_____]	----	0	0	----- ------ ---
22	[_____]	----	0	0	----- ------ ---
23	[_____]	----	0	0	----- ------ ---
24	[_____]	----	0	0	----- ------ ---
25	[_____]	----	0	0	----- ------ ---
26	[_____]	----	0	0	----- ------ ---
27	[_____]	----	0	0	----- ------ ---
28	[_____]	----	0	0	----- ------ ---

A3 Datalogger Z9 program

```
;{CR23X}
;Datalogger program for logging using 4 equitensiometers, 2 dynamax sapflow gages, and 2 dendrometers
;Written by Anywhere Tsokankunku 22-10-2006, edited 11-11-06 changed
;sapflow mult from 1 to 0.004,last edited 15-11-06 changed netrad instruction to include IF condition

;Datlogger array:
; DIFF Channel   Identifier      inLoc
;                Battvolt        1
;                PAneltmp        2
;  1             EQ2_1           3
;  2             EQ2_2           4
;  3             EQ2_3           5
;  4             EQ2_4           6
;  5             Dendro1         7
;  6             Dendro2         8
;  7              SAPFL1_1        9
;  8              SAPFL1_2       10
;  9              SAPFL1_3       11
;  10             SAPFL1_V       12
;  11             soilhflx        13
;  12             Netrad          14

;Output array definitions
;
*Table 1 Program
  01: 1        Execution Interval (seconds)

1:  Batt Voltage (P10)
 1: 1        Loc [ Battvolt  ]

2:  Panel Temperature (P17)
 1: 2        Loc [ PAneltmp  ]

3:  Volt (Diff) (P2)
 1: 1        Reps
 2: 25       5000 mV, 60 Hz Reject, Fast Range
 3: 1        DIFF Channel
 4: 3        Loc [ EQ2_1     ]
 5: 1.0      Mult
 6: 0.0      Offset


4:  Volt (Diff) (P2)
 1: 1        Reps
 2: 25       5000 mV, 60 Hz Reject, Fast Range
 3: 2        DIFF Channel
 4: 4        Loc [ EQ2_2     ]
 5: 1.0      Mult
 6: 0.0      Offset


5:  Volt (Diff) (P2)
 1: 1        Reps
 2: 25       5000 mV, 60 Hz Reject, Fast Range
 3: 3        DIFF Channel
 4: 5        Loc [ EQ2_3     ]
 5: 1.0      Mult
 6: 0.0      Offset
```

```
6:  Volt (Diff) (P2)
 1: 1        Reps
 2: 25       5000 mV, 60 Hz Reject, Fast Range
 3: 4        DIFF Channel
 4: 6        Loc [ EQ2_4     ]
 5: 1.0      Mult
 6: 0.0      Offset

;Dendrometers with values already calibrated in mm

7:  Full Bridge (P6)
 1: 1        Reps
 2: 21       10 mV, 60 Hz Reject, Slow Range
 3: 5        DIFF Channel
 4: 1        Excite all reps w/Exchan 1
 5: 500      mV Excitation
 6: 7        Loc [ Dendro1   ]
 7: 2.09424  Mult
 8: 0.0      Offset

;hukseflux mult =59.8uV/w/m2 = 0.0598mV/W/m2

8:  Volt (Diff) (P2)
 1: 1        Reps
 2: 21       10 mV, 60 Hz Reject, Slow Range
 3: 6        DIFF Channel
 4: 8        Loc [ soilhfl2  ]
 5: 0.0598   Mult
 6: 0.0      Offset
;
;
9:  Volt (Diff) (P2)
 1: 3        Reps
 2: 31       10 mV, 50 Hz Reject, Slow Range
 3: 7        DIFF Channel
 4: 9        Loc [ SAPFL1_1  ]
 5: 0.004    Mult
 6: 0.0      Offset


10:  Volt (Diff) (P2)
 1: 1        Reps
 2: 35       5000 mV, 50 Hz Reject, Fast Range
 3: 10       DIFF Channel
 4: 12       Loc [ SAPFL1_V  ]
 5: 1        Mult
 6: 0.0      Offset

;Measure soil heat flux on smaller range
;mult is 58.7 uV/W/m2 =0.0587mV/W/m2

11:  Volt (Diff) (P2)
 1: 1        Reps
 2: 21       10 mV, 60 Hz Reject, Slow Range
 3: 11       DIFF Channel
 4: 13       Loc [ soilhflx  ]
 5: 0.0587   Mult
 6: 0.0      Offset

; CM11 S/N 986750 mult 5.01e-6 v/wm-2 (=199.6wm-2/mV) so output=wm-2
```

```
12:  Volt (Diff) (P2)
 1: 1        Reps
 2: 34       1000 mV, 50 Hz Reject, Slow Range
 3: 12       DIFF Channel
 4: 14       Loc [ Netrad    ]
 5: 1.0      Mult
 6: 0.0      Offset

13:  If (X<=>F) (P89)
 1: 14       X Loc [ Netrad    ]
 2: 3        >=
 3: 0.0      F
 4: 30       Then Do

14:  Z=X*F (P37)
 1: 14       X Loc [ Netrad    ]
 2: 8.74     F
 3: 14       Z Loc [ Netrad    ]

15:  Z=X*F (P37)
 1: 14       X Loc [ Netrad    ]
 2: 1.045    F
 3: 14       Z Loc [ Netrad    ]


16:  Else (P94)


17:  Z=X*F (P37)
 1: 14       X Loc [ Netrad    ]
 2: 10.76    F
 3: 14       Z Loc [ Netrad    ]

18:  End (P95)

19:  If time is (P92)
 1: 5     -- Minutes (Seconds --) into a
 2: 10    -- Interval (same units as above)
 3: 10       Set Output Flag High
;   output time information (output at the END of averaging/sampling interval)

20:  Real Time (P77)
 1: 1111     Year,Day,Hour/Minute,Seconds (midnight = 0000)


21:  Sample (P70)
 1: 1        Reps
 2: 1        Loc [ Battvolt  ]


22:  Sample (P70)
 1: 1        Reps
 2: 2        Loc [ PAneltmp  ]


23:  Average (P71)
 1: 1        Reps
 2: 3        Loc [ EQ2_1     ]
```

24: Standard Deviation (P82)
1: 1 Reps
2: 3 Sample Loc [EQ2_1]

25: Average (P71)
1: 1 Reps
2: 4 Loc [EQ2_2]

26: Standard Deviation (P82)
1: 1 Reps
2: 4 Sample Loc [EQ2_2]

27: Average (P71)
1: 1 Reps
2: 5 Loc [EQ2_3]

28: Standard Deviation (P82)
1: 1 Reps
2: 5 Sample Loc [EQ2_3]

29: Average (P71)
1: 1 Reps
2: 6 Loc [EQ2_4]

30: Standard Deviation (P82)
1: 1 Reps
2: 6 Sample Loc [EQ2_4]

31: Average (P71)
1: 1 Reps
2: 7 Loc [Dendro1]

32: Standard Deviation (P82)
1: 1 Reps
2: 7 Sample Loc [Dendro1]

33: Average (P71)
1: 1 Reps
2: 8 Loc [soilhfl2]

34: Standard Deviation (P82)
1: 1 Reps
2: 8 Sample Loc [soilhfl2]

35: Average (P71)
1: 3 Reps
2: 9 Loc [SAPFL1_1]

36: Standard Deviation (P82)
1: 3 Reps
2: 9 Sample Loc [SAPFL1_1]

37: Average (P71)
1: 1 Reps
2: 12 Loc [SAPFL1_V]

38: Standard Deviation (P82)
1: 1 Reps
2: 12 Sample Loc [SAPFL1_V]

```
39:  Average (P71)
 1: 1        Reps
 2: 13       Loc [ soilhflx  ]


40:  Standard Deviation (P82)
 1: 1        Reps
 2: 13       Sample Loc [ soilhflx  ]

41:  Average (P71)
 1: 1        Reps
 2: 14       Loc [ Netrad    ]

42:  Standard Deviation (P82)
 1: 1        Reps
 2: 14       Sample Loc [ Netrad    ]

*Table 2 Program
  02: 0.0000    Execution Interval (seconds)

*Table 3 Subroutines

End Program

-Input Locations-
1 Battvolt  1 1 1
2 PAneltmp  1 1 1
3 EQ2_1     1 2 1
4 EQ2_2     1 2 1
5 EQ2_3     1 2 1
6 EQ2_4     1 2 1
7 Dendro1   1 2 1
8 soilhfl2  1 2 1
9 SAPFL1_1  5 2 1
10 SAPFL1_2  9 0 1
11 SAPFL1_3  17 0 1
12 SAPFL1_V  1 2 1
13 soilhflx  5 2 1
14 Netrad    1 6 4
15 cal       1 0 0
16 _________ 0 0 0
17 _________ 0 0 0
18 _________ 0 0 0
19 _________ 0 0 0
20 _________ 0 0 0
21 _________ 0 0 0
22 _________ 0 0 0
23 _________ 0 0 0
24 _________ 0 0 0
25 _________ 0 0 0
26 _________ 0 0 0
27 _________ 0 0 0
28 _________ 0 0 0
```